AFRL-ML-TY-TR-2000-4554

EVALUATION OF SELECTIVE NON-CATALYTIC REDUCTION OF NOx FOR JET ENGINE TEST CELLS

J.W. DILL
G.S. SAMUELSEN

UCI Combustion Laboratory
University of California
Irvine, CA 92697-3550

February 1995

AIR FORCE RESEARCH LABORATORY
MATERIALS & MANUFACTURING DIRECTORATE
AIR EXPEDITIONARY FORCES TECHNOLOGIES DIVISION
139 BARNES DRIVE, STE 2
TYNDALL AFB FL 32403-5323

NOTICES

USING GOVERNMENT DRAWINGS, SPECIFICATIONS, OR OTHER DATA INCLUDED IN THIS DOCUMENT FOR ANY PURPOSE OTHER THAN GOVERNMENT PROCUREMENT DOES NOT IN ANY WAY OBLIGATE THE US GOVERNMENT. THE FACT THAT THE GOVERNMENT FORMULATED OR SUPPLIED THE DRAWINGS, SPECIFICATIONS, OR OTHER DATA DOES NOT LICENSE THE HOLDER OR ANY OTHER PERSON OR CORPORATION; OR CONVEY ANY RIGHTS OR PERMISSION TO MANUFACTURE, USE OR SELL ANY PATENTED INVENTION THAT MAY RELATE TO THEM.

THIS REPORT IS RELEASABLE TO THE NATIONAL TECHNICAL INFORMATION SERVICE
5285 PORT ROYAL RD.
SPRINGFIELD VA 22161
TELEPHONE 703 487-4650; 703 487-4639 (TDD for the hearing-impaired)
E-MAIL orders@ntis.fedworld.gov
http://www.ntis.gov/index.html

AT NTIS, IT WILL BE AVAILABLE TO THE GENERAL PUBLIC, INCLUDING FOREIGN NATIONS.

THIS TECHNICAL REPORT HAS BEEN REVIEWED AND IS APPROVED FOR PUBLICATION.

JOSEPH D. WANDER, Ph.D
Program Manager

THOMAS B. STAUFFER, Ph.D, DR-IV, DAF
Chief, Weapons Systems Logistics Branch

RANDY L. GROSS, Col, USAF, BSC
Chief, Air Expeditionary Forces Technolgies Division

Do not; return copies of this report unless contractual obligations or notice on a specific document requires its return.

REPORT DOCUMENTATION PAGE

Form Approved
OMB No. 0704-0188

1. AGENCY USE ONLY *(Leave blank)*	2. REPORT DATE	3. REPORT TYPE AND DATES COVERED
	15 September 2000	Final, 31 March 1990 - 30 September 1994

4. TITLE AND SUBTITLE
Evaluation of Selective Non-Catalytic Reduction of NOx for Jet Engine Test Cells

5. FUNDING NUMBERS
Contract No : F08635-90-C-0010
JON: 19007057

6. AUTHORS
Dill, J.W., and Samuelsen, G.S.

7. PERFORMING ORGANIZATION NAME(S) AND ADDRESS(ES)
UCI Combustion Laboratory
University of California
Irvine, CA 92697-3550

8. PERFORMING ORGANIZATION REPORT NUMBER
UCI-ARTR-95-11

9. SPONSORING/MONITORING AGENCY NAME(S) AND ADDRESS(ES)
AFRL/MLQL
139 Barnes Drive, Suite 2
Tyndall AFB, FL 32403-5323

10. SPONSORING/MONITORING AGENCY REPORT NUMBER
AFRL-ML-TY-TR-2000-4554

11. SUPPLEMENTARY NOTES
Technical monitor: Dr Joe Wander, AFRL/MLQL, 850-283-6240 [DSN 523-6240]

12a. DISTRIBUTION/AVAILABILITY STATEMENT
Distribution unlimited.

12b. DISTRIBUTION CODE
A

13. ABSTRACT *(Maximum 200 words)*

This research evaluates the use of selective non-catalytic reduction (SNCR) for the removal of oxides of nitrogen (NO_x) in a jet engine test cell (JETC). The plume effluent in the exhaust stream of a TF30-P111+ and a TF33-P9 engine in a jet engine test cell was first characterized. A test stand and five-point sample probe were designed and built to make measurements directly behind the engine nozzle. Data were collected in conjunction with actual engine tests. Temperature, NO_x, carbon monoxide (CO) concentration, and velocity were among the characteristics measured radially and axially in the plume. These parameters were used to determine baseline conditions for the chemical kinetic modeling of SNCR using ammonia, cyanuric acid, urea, and hydrazine with additives of hydrogen, methane, and hydrogen peroxide. The measurements revealed that temperatures are marginal for the application of SNCR in JETCs except at high throttle and afterburner settings on the P111+ engine. The chemicals themselves have limited range of applicability. Additives help to extend their usefulness, mostly by shifting the temperature window down. Urea and hydrogen peroxide yielded the best range of the chemicals tested. However, this combination may reduce NO_x in the entire exhaust stream by up to only 25% at military power on the high- performance P111+ engine. The findings of this work have attractive implications for non-JETC applications operating near the same conditions.

14. SUBJECT TERMS	15. NUMBER OF PAGES
NOx, combustion, air pollution, test cell, TF30, TF33, F-111, KC-135, JETC, SNCR	172
	16. PRICE CODE

17. SECURITY CLASSIFICATION OF REPORT	18. SECURITY CLASSIFICATION OF THIS PAGE	19. SECURITY CLASSIFICATION OF ABSTRACT	20. LIMITATION OF ABSTRACT
UNCLASSIFIED	UNCLASSIFIED	UNCLASSIFIED	UL

NSN 7540-01-280-5500 Computer Generated STANDARD FORM 298 (Rev 2-89)
Prescribed by ANSI Std 239-18
298-102

EXECUTIVE SUMMARY

A. OBJECTIVE:

The objective of this project was to examine the feasibility of applying Selective NonCatalytic Reduction [SNCR] to control NOx emissions from aircraft jet engines during static operation in a jet engine test cell [JETC].

B. BACKGROUND:

Although a JETC is not an actual source of pollutants, its emissions are subject to regulation under Title 1 of the Clean Air Act and it is a potential candidate for imposition of a MACT standard. This project is one of several investigations sponsored by the Air Force to assay the compatibility of individual technologies with the environment inside the JETC. Several technical challenges are indigenous to this proposed application:

- extreme mechanical stresses caused by the thrust generated behind the engine;
- inhomogeneous temperature and concentrations in the turbulent flow field behind the engine and in the augmenter;
- frequent, abrupt changes in the rate of delivery of fuel to the engine;
- intolerance of the testing process to any increase in flow resistance in the JETC; and
- invalidation of the test by any change to the engine's operating environment during testing.

C. SCOPE:

This is a final report. It describes first the design and use of a traversable sampling rake and collection-and-analysis system to characterize the actual emissions and conditions encountered during testing of two kinds of engines in use by the Air Force. These results were then used in a modeling study of the SNCR process as it would be applied to these two engines at various stages of the testing sequence, using combinations of four primary reductants and three additives.

METHODOLOGY:

Chemical emissions from the engines were collected at multiple locations behind operating jet engines using a homemade five-position rake, dried by chilling, and routed through commercial analytical devices. Conventional software was used to model the kinetics of chemical processes occurring at different times after the hypothetical instantaneous mixing of arbitrary amounts of nitrogen oxides and selected amounts of reagents and additives.

TEST DESCRIPTION:

Prototype designs for the exhaust sampling system were evaluated behind an F404 engine at El Toro Marine Station. After additional tuning in the lab, a final design was fabricated and taken into the field at McClellan Air Force Base [MAFB]. Emission measurements from TF30-P111+ and TF33-P9 engines at MAFB were conducted at power settings identified by JETC personnel as "normal" values, used in representative testing procedures. Independent sets of measurements were made at each power setting during several sessions. This sampling was performed at five radial positions simultaneously, and repeated at each of several positions moving away from the engine down the augmenter. Final values for each position and power setting are averages of multiple determinations.

Modeling of kinetics initially assumed uniformity for a 500-msec reaction time [t_{res}], but several conditions were later calculated at 50-msec increments from an initial value of 50 msec to estimate sensitivity to mixing. Four reductants—ammonia, isocyanic acid, urea, and hydrazine—and three additives—hydrogen, methane, and hydrogen peroxide—were introduced in varying amounts and combinations at fixed concentrations of oxygen, water, and carbon, and at each of several fixed values of **[NSR] and **[ACR]. Calculations were performed over the range of temperatures encountered during the engine tests.

RESULTS:

After design adjustment to address observations at El Toro, the rake and sampling system performed satisfactorily. Emissions measured for the two engines at MAFB were consistent with those measured for other military jets, NOx increasing with power level, and CO increasing drastically when the afterburner is activated. Even though modeling results assumed more-ideal conditions than can realistically be assumed in the augmenter, only the P111+ engine attained temperature conditions for which any combination of reductant and additive was predicted to achieve significant removal of NOx. This incompatibility derives primarily from the challenges identified in B, above, and results of calculations for addition of hydrogen peroxide or of hydrogen appear to have significance to SNCR as applied to less-exotic source.

CONCLUSIONS:

The sampling rake performed very well and the design is a reasonable basis for emulation. The emissions data measured for the two engines are intrinsically valuable as data, but indicate no exceptional phenomena. The modeling calculations assumed more-favorable mixing characteristics [*i.e.*, did not take into account large gradients both across and along the axis of the augmenter] than reality, and identified only a few windows in which SNCR could be considered feasible. Thus, it appears that this technology is incompatible with the conditions in a JETC. However, judicious use of additives may enhance performance of SNCR in more-conventional applications.

RECOMMENDATIONS:

The sampling system offers opportunities for both investigation and application in other contexts. Practical reduction of NOx from exhausts passing through a JETC appears infeasible unless a novel concept appears that is effective in extremely inhomogeneous environments. Further examination of the influence of OH-promoting additives on the course of SNCR chemistry may be promising.

PREFACE

This report was prepared by The UCI Combustion Laboratory, University of California, Irvine, CA 92697-3550, under Contract Number F08635-90-C-0100 for the Air Force Research Laboratory, Air Expeditionary Forces Technologies Division (AFRL/MLQ), 139 Barnes Drive, Tyndall AFB, FL 32403-5323.

This is one of two final reports submitted. It describes work performed from 31 March 1990 to 30 September 1994. The Air Force technical program monitors were Maj Wayne P. Chepren and Dr Joe Wander.

We gratefully acknowledge the enthusiastic cooperation of engine-testing facility crews at El Toro Marine Station and McClellan Air Force Base, without whose help this study would not have been possible.

TABLE OF CONTENTS

LIST OF TABLES

LIST OF FIGURES

1.0: INTRODUCTION

1.1 Motivation

Combustion of fossil fuels strongly impacts the quality of everyday life. Electricity, transportation, and heating are only a few of the beneficial products resulting from combustion. Unfortunately, air pollution is another important by-product that is becoming more and more apparent. Oxides of nitrogen (NO_x) are produced by combustion and are released into the atmosphere, where they react to form ozone and other potentially harmful photochemical oxidants. The prevention of photochemical oxidant, better known as smog, has been an important area of research during the past three decades. All sources of combustion (*e.g.*, automobiles, aircraft, boilers, power plants) have been affected by various forms of NO_x control to reduce emissions and improve air quality.

California has led the way in regulating the pollution being produced by combustion sources operating within the state. In 1985, stationary sources accounted for about 57% of the total NO_x emissions (Environmental Protection Agency, 1992). Thus, stationary combustion sources have been a major target for the U.S. Environmental Protection Agency for emissions reduction. Recently, these stationary sources have come to include 250 Air Force jet engine test cells, in which repaired engines are run before reinstallation on the aircraft. By the year 2000, test cells will be required to meet local, state, and federal emission regulations for stationary combustion sources while in operation.

Unlike most stationary sources, a jet engine in a test cell is not a candidate for NO_x control without compromising the engine test. A solution must be found external to the source in the post-combustion region of the flow. Experimental work to date has looked at options such as reburning, selective catalytic reduction, and selective non-

catalytic reduction to reduce NO_x emissions of test cells. Extreme variations in temperature, varying power loads and other test cell dynamics put a high demand on any of these applied technologies.

1.2 Goal and Objectives

One accepted and relatively inexpensive post-combustion control method for use on industrial combustion systems is selective non-catalytic reduction (SNCR). SNCR involves the injection of a reducing chemical into the hot exhaust gases to lower NO_x emissions. The goal of this research was to evaluate the reduction of NO_x emissions from jet engine test cells (JETCs) using SNCR. The following objectives were established to meet this goal:

1) Design, construct, and set up a sampling traverse and sample probe (rake) that can collect gas samples at multiple points in the exhaust stream in a JETC;
2) Analyze the exhaust stream characteristics, including emissions, temperature, and velocity;
3) Evaluate the test cell operating conditions and locations where NO_x reduction using SNCR is possible; and
4) Use computer chemical kinetic models to study the feasibility of SNCR control for a variety of chemicals and additives, and optimize the process.

Chapter 2 discusses the importance and formation of NO_x, reviews the design and dynamics of jet engine test cells, provides the history and chemical background of SNCR, and gives an overview of chemical kinetic modeling. Chapter 3 gives the approach taken to meet the goal of the thesis, and Chapter 4 describes the design and application of the sampling apparatus and the basic modeling strategy. The results and conclusions are discussed in Chapters 5 and 6, respectively.

2.0: Background

Before discussing NO_x prevention, it is appropriate to review the types of NO_x and their formation in combustion systems. A detailed overview of the stationary source in question, the JETC, is provided. The various methods of industrial NO_x control are briefly discussed, followed by the background of the proposed strategy, SNCR. A summary of relevant research and an introduction to chemical kinetic models is also presented.

2.1 Importance and Formation of Nitrogen Oxides

Oxides of nitrogen, collectively known as NO_x, consist of nitric oxide (NO) and nitrogen dioxide (NO_2). All air-breathing combustion sources emit NO_x as a result of the oxidation of fuel-bound and atmospheric nitrogen. When first formed in the combustion process, most of the NO_x exists as NO. This initial concentration of NO is generated by any combination of the following:

1. Thermal NO forms at an exponential rate beginning at 1900°F (2960°F) as nitrogen in the combustion chamber is oxidized. The combustion of clean fuels (fuels not containing nitrogen compounds; *i.e.*, natural gas) forms mostly thermal NO using the atmospheric nitrogen contained in the inlet air. NO formation increases as a function of temperature. The common reaction pathways are known as the Zeldovich mechanism (Zeldovich, 1946):

$$N_2 + O \rightarrow NO + N \qquad (2.1)$$

$$N + O_2 \rightarrow NO + O \qquad (2.2)$$

The energy required to break the triple bond of N_2 in (2.1) is an order of magnitude higher than that needed for reaction (2.2). Once N_2 is in its elemental form (with the resulting NO), oxidation of the nitrogen radical

occurs very quickly (Samuelsen, 1975). Therefore, reaction (2.1) causes the overall mechanism for thermal NO to be slow at lower temperatures. In general, its rate of formation is most sensitive to local flame temperature and less sensitive to local O_2 concentration (EPA Report, 1992).

2. Prompt NO results from reactions that occur early in the combustion process to produce nitrogen in addition to reaction (2.1). This rapid reaction first proposed by Fenimore (1971) occurs near the flame zone in hydrocarbon-rich fuels. In this mechanism nitrogen (N_2) is attacked by HC fragments to subsequently form NO. In systems where gas temperatures are low, this mechanism can account for a significant fraction of the total NO created.
3. Fuel NO comprises a third source of NO resulting from the burning of fuels containing nitrogen (e.g., coal). The loosely-bound nitrogen atom may break its bond with the fuel to combine with other intermediates (*e.g.*, oxygen and hydroxyl radicals) to form NO. The oxidation reactions of fuel nitrogen occur much more rapidly than reaction (2.1). The kinetics of fuel NO are heavily influenced by the local combustion environment (temperature and stoichiometry) and on the initial nitrogen level in the air–fuel mixture (Miller and Bowman, 1989).

Jet engines running on hydrocarbon fuels form NO mostly through the first two mechanisms.

When combustion exhaust is released into the atmosphere, much of the NO is oxidized to NO_2. The increased amounts of NO_2 from the growing number of combustion sources are responsible for the rise of the tropospheric ozone levels through the following reactions:

$$NO_2 + \text{uv-sunlight} \rightarrow NO + O \qquad (2.3)$$

$$O + O_2 + M \rightarrow O_3 + M \qquad (2.4)$$

where M is N_2 or O_2.

The products of these reactions are commonly known as photochemical oxidants. Of equal importance, short-lived, highly reactive hydrocarbon species (also resulting from the combustion of fossil fuels) also form tropospheric O_3 in the presence of NO_x (Prather and Logan, 1994). Increased levels of ozone interfere with breathing (causing coughing and fatigue), slow plant growth, and cause cracking in rubber. Nitrogen dioxide is brown in color and is responsible for the haze sometimes seen in the lower elevations of urban regions. Increased NO_2 levels cause eye irritation and similar respiratory effects as those caused by ozone. As a result, ambient air quality standard exposure limits have been established to prevent these known side-effects: 0.12 ppmv–hour (parts per million by volume for one hour) for ozone and 0.05 ppm annually for NO_2 (Samuelsen, 1980).

Another oxide of nitrogen of growing concern is nitrous oxide (N_2O). N_2O is classified as a greenhouse gas in the troposphere. Its stability allows it to reach the stratosphere, where it supplies the majority of the NO_x in this region (Prather and Logan, 1994). This cyclic sequence is represented by the following reactions (Montgomery, 1988):

$$N_2O + O(\text{'D}) \rightarrow NO + NO \qquad (2.5)$$

$$NO + O_3 \rightarrow NO_2 + O_2 \qquad (2.6)$$

$$NO_2 + O \rightarrow NO + O_2. \qquad (2.7)$$

The combination of these reactions provides the largest natural sink for stratospheric ozone (Montgomery, 1988). Combustion is believed to account for only a small fraction of the N_2O sources, most of them being agricultural or processing related. However, the global mean N_2O concentration is increasing by 0.2 to 0.4% per year (Montgomery, 1988). With the growing use of chemicals and additives aimed at reducing NO, more

N_2O emissions from combustion sources are being observed. Therefore, its emission must be considered when discussing NO_x control possibilities.

2.2 Air Force Jet Engine Test Cells

JETCs provide a uniform environment in which to test an overhauled or repaired engine before it is reinstalled in the aircraft. During a test, the engine is run over its full range of power settings seen during a typical operational cycle. The major diagnostics of the engine are monitored and checked at various points during the test to see that they fall within specifications. Total time on the stand can vary (usually from 2 to 8 hours) depending on the condition of the engine.

Test cells vary from site to site, but a representative configuration is shown in Figure 2.1. The test cell is generally constructed of steel or concrete. The engine is securely mounted on a steel stand located inside either a U- or L-shaped enclosure. The intake air enters through a series of sound-deadening baffles into the front of the cell. The engine exhaust is directed through a large, bell-mouthed opening into a long tube known as an augmenter. The importance of the augmenter is as follows (Johnson and Katz, 1989):

1. The bell-mouthed opening of the augmenter, similar in shape to an ejector pump, draws air into the test cell to ensure equal pressure at the inlet and exit of the engine;
2. Part of the air drawn into the augmenter flows around the engine housing to provide cooling similar to that experienced in the aircraft; and
3. The air drawn into the augmenter dilutes and cools the hot exhaust gases to help prevent damage to the material within the JETC.

To cool the gases further before they are released into the atmosphere, water may be injected into the exhaust stream at various stages downstream of the augmenter mouth.

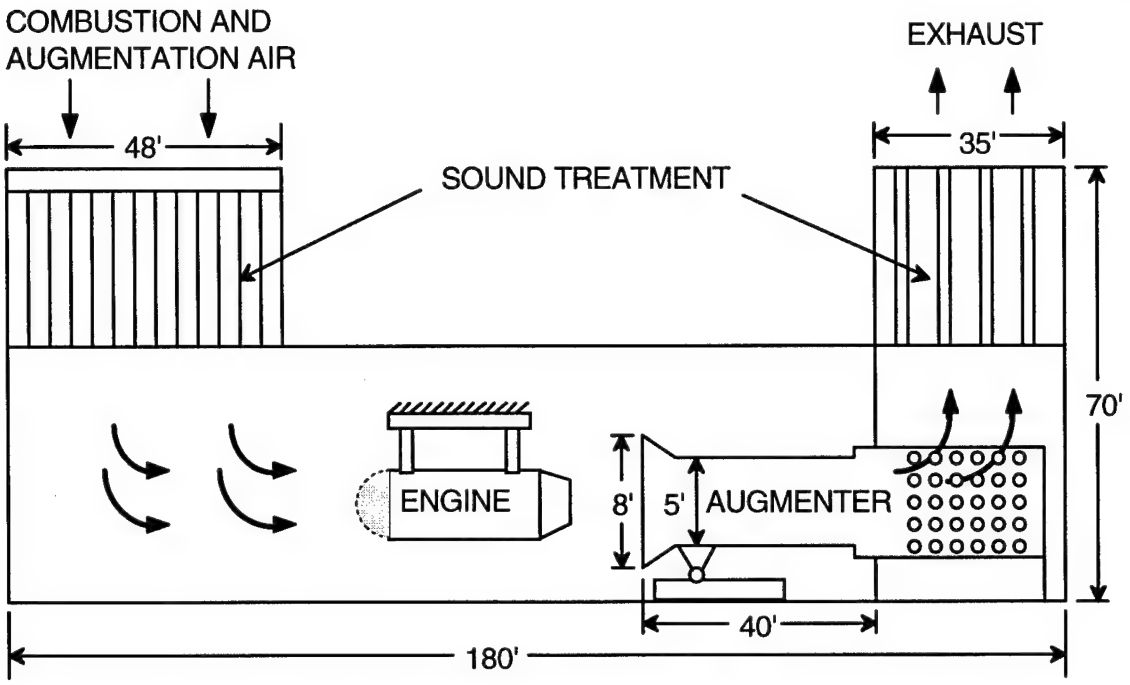

Figure 2.1: Jet Engine Test Cell for TF30 Engines at McClellan Air Force Base (Dimensions Approximate).

The augmenter ends in the blast room where excess cooling water drops out through perforations in the tube, and the exhaust escapes through the building. The construction and large scale of the intake and the exhaust of the cell are very important to prevent adverse pressure gradients within the JETC during testing that could affect the trim of the engine.

Many features are unique to JETCs. At full military power (full power, no afterburner) and full afterburner loads, a typical test cell can process as much as 600 pounds of air per second (Johnson and Katz, 1989). Compared with other stationary sources, JETCs spend much of their operating time in transition from one power extreme to the other, causing high fluctuations of emission levels, flow rates, and temperatures. Since the engines are there only temporarily, modification to the source of the emissions is unfeasible. Work with various fuel additives (*i.e.*, cerium) has been performed, mostly in the prevention of soot. For NO_x levels to be reduced by any substantial amount, a post-combustion control system must be considered.

2.3 Post-Combustion NO_x Control Strategies

The nature of the JETC does not allow for in-flame control techniques such as modification of the combustion equipment. Post-combustion control is the most likely candidate for reduction in this environment. Exhaust reburning, selective catalytic reduction, and selective non-catalytic reduction are three methods of post-combustion control of NO_x currently under development and experimentation by the Air Force for use in JETCs (Bergman et al., 1991; Ham et al., 1989; Johnson and Katz, 1989; and Nelson *et al.*, 1989).

In a reburner arrangement, a second reaction zone is created downstream of the primary combustion zone (for a JETC, inside the augmenter tube or the blast room) where a hydrocarbon fuel is injected into the exhaust stream (Wendt, 1973). The secondary reaction creates hydrocarbon radicals, which reduce NO_x to N_2 and H_2O via a complex series of reactions. Studies conducted have shown that NO_x reductions in excess of 50% can be achieved using natural gas as the secondary (reburner) fuel (Johnson and Katz, 1989 and Lanier, *et al.*, 1986).

Reburning achieves two goals: NO_x levels are reduced and raw fuel in the exhaust stream burns out. The fuel-rich region created initiates NO destruction through the reaction

$$CH + NO \rightarrow HCN + O. \qquad (2.8)$$

HCN is only an intermediary by-product that leads to the formation of a partially equilibrated pool of NH_i species (Lanier, *et al.*, 1986). These amine radicals either react with NO to form N_2 (via the reverse Zeldovich mechanism, reaction (2.2)), or oxidize to form additional NO (Chen, *et al.*, 1986). Non-hydrocarbon fuels (*e.g.*, CO and H_2) are not as effective in forming these radicals. Optimum reburning conditions have been shown to be most effective when at least 400 msec. residence time (time for the reaction to occur) is available and when the oxygen concentration entering the reburner section is

low (Chen et al., 1986). However, high requirements of the secondary fuel (based upon a fixed flow rate) make this an expensive option for a JETC. A solution proposed by Johnson and Katz (1989) is to only use the reburner at loads greater than 50% thrust to cut fuel costs, thus requiring a control system to monitor the intermittent use. The challenge again is the wide range of operation parameters for the test cell.

Selective catalytic reduction (SCR) uses a combination of chemical injection with a catalytic bed to condition the exhaust gas exiting the primary combustion zone. Ammonia or urea is injected into the gas stream, where it mixes with the exhaust products. The basis of the SCR lies in the reaction of the amine radical with NO, generally stated as

$$NH_2 + NO \rightarrow N_2 + H_2O \qquad (2.9)$$

Just downstream of the injection, the entire flow passes through a catalyst bed which lowers the activation energy required to complete reaction (2.9). Research has shown the catalyst reduces temperatures needed for this process by up to 200 to 425°C (392 to 797°F) while retaining reductions in NO by up to 80% (Ham et al., 1989). Larger catalyst beds are needed to facilitate the both the quantity of the gas processed and the slow reaction rates of NH_3 at these temperatures. Catalyst lifetimes are limited depending on the fuels burned and the extremities of the temperatures seen. The maintenance of the catalyst and the initial capital costs make SCR an expensive, but effective, process (Table 2.1).

Table 2.1: Post-Combustion NO_x Control Costs (Parkinson, 1994).

Technology	% NO_x Removal	Capital Cost ($/kW)
Gas Reburning	60	30
SCR	80	80
SNCR	50	15

Selective non-catalytic reduction (SNCR), like SCR, uses chemical injection into the hot exhaust gases to reduce nitric oxide to harmless molecular nitrogen and water. Unlike SCR, SNCR does not incorporate expensive catalysts, relying only on the high temperatures of the exhaust flows for the activation energies needed to initiate the necessary reactions. Typical temperatures range from 1300°F to 2200°F with 50% to 85% NO_x reduction possible. Although not always as effective as SCR, SNCR's relatively low cost and ease of installation have made it a popular retrofit option in many industrial applications.

2.4 The Proposal: Selective Non-Catalytic Reduction

Many selective non-catalytic reduction systems have been installed in areas of Europe and Japan, and an increasing number of successful new systems have been constructed in the United States (Jones, *et al.*, 1989; Jones, *et al.*, 1991). A typical configuration is shown in Figure 2.2. The SNCR section provides the conditions needed for the process to be effective. These conditions consist of sustained high temperatures (usually between 1600 to 2100°F), adequate mixing, and sufficient residence times for the

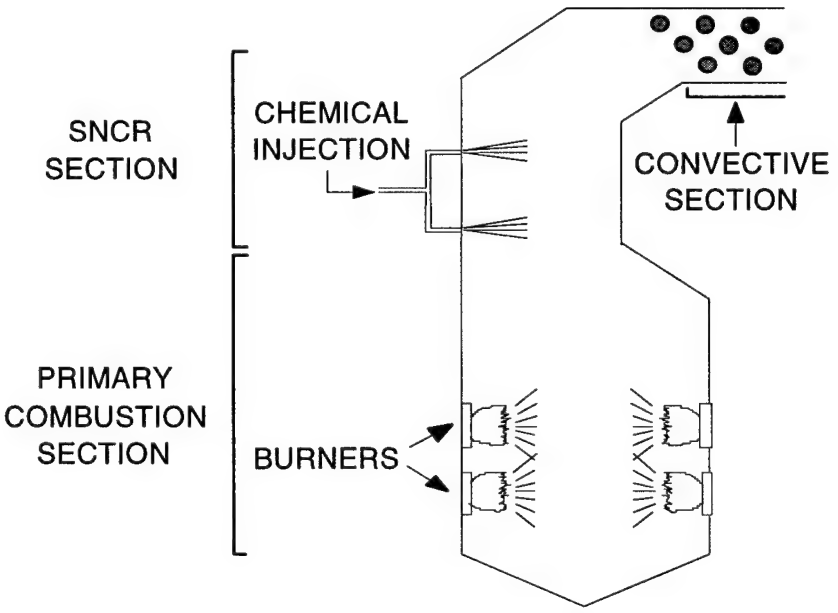

Figure 2.2: Furnace Equipped with SNCR System.

reactions to occur. Each combustion system is unique in each of these categories, resulting in finely-tuned systems for optimal performance. As a result, the type(s) of chemicals used to initiate the reduction process are also tailored to the specific initial emission levels of the primary combustion source and the final emissions levels required of the source. Determination of the best chemical combination (in terms of its cost-effectiveness, storage hazards, by-products created, etc.) plays a large role in the success of the process.

This work looks at SNCR and how it may be applied to reduce NO_x emissions in a JETC environment. The remaining sections of this chapter will a) provide a further understanding of the chemical processes and characteristics of the better-known SNCR chemicals and additives, and b) give further background on the theories and structure of chemical kinetics.

2.4.1 The History and Characteristics of Thermal $DeNO_x$

The birth of SNCR is credited to Lyon and his work with ammonia (NH_3) at Exxon Research and Engineering in the early 1970s. In his patent (Lyon, 1975), Lyon observed that by adding ammonia in the proper environment, NO levels were reduced significantly. The process was deemed *Thermal $DeNO_x$* by Exxon. He also showed that the use of additives such as hydrogen could help the reduction process by allowing the reactions to occur at lower temperatures (up to 300°F lower in the original patent). The effective temperature range of ammonia was shown to be 1700°F to 2000°F, with the optimum occurring at about 1800°F.

The homogeneous gas-phase decomposition of ammonia at high temperatures involves complex intermediate chain branching reactions as shown in Figure 2.3. The creation of hydroxyl (OH) radicals is important to generate amine (NH_2) radicals from ammonia (or any other NH_i-producing chemical). Until sufficient energies have been

reached, injected ammonia escapes from the SNCR section unreacted (known as ammonia slip). Once temperatures reach the start of the effective temperature window (~1600°F), the following overall reaction is initiated:

$$NO + NH_3 + O_2 + H_2O + (H_2) \rightarrow N_2 + H_2O. \qquad (2.10)$$

Note the selectivity of the process—only NO is reduced and not NO_2. However, NO_2 and N_2O may be produced in certain cases, such as conversion of NO into either NO_2 or N_2O. This must be watched carefully since conversions from one oxide of nitrogen to another cannot be considered a reduction in total NO_x.

At temperatures above the useful temperature window (greater than 2200°F), ammonia begins producing NO_x via the reaction

$$NH_3 + O_2 \rightarrow NO + H_2O, \qquad (2.11)$$

thus defeating the $DeNO_x$ process. Temperature, however, is only one of many parameters that greatly affect the efficiency of the process. Other important factors include the following:

- Normalized Stoichiometric Ratio (NSR), defined as the molar ratio of NH_i-producing compound being injected divided by initial NO;

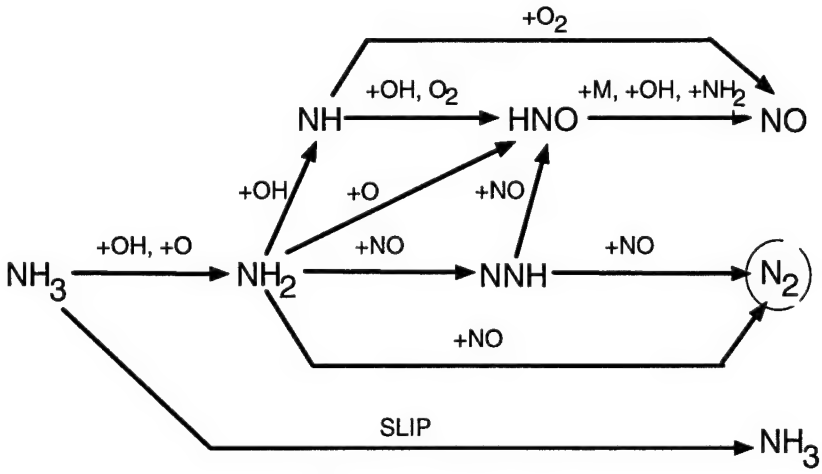

Figure 2.3: Reaction Path Diagram for the Thermal $DeNO_x$ Process (Miller and Bowman, 1989)

- Initial NO (NO_i) concentration;
- Additive–Chemical Ratio (ACR) equals the molar ratio of additive (*e.g.*, hydrogen or methane) divided by the SNCR chemical injected;
- Residence time (t_{res}) available; and
- Mixing and thermal gradients (°/sec.).

All of the above parameters are interrelated; that is, changing one condition affects the optimum range of the others. Efficiency, optimum NO reduction temperature, and chemical slip are all affected by any changes in one or more of these parameters. Other parameters that are less critical, but essential, when considering SNCR have the following features:

- Excess O_2 is required in the combustion products (greater than 4%: Muzio, *et al.*, 1977);
- Increasing water concentration in the exhaust stream slightly inhibits the NO reduction possible by increasing the optimum temperature window.

A brief overview of each of these topics follows.

Temperature is the most sensitive parameter for NO reduction of any of the above listed. Figure 2.4 shows typical NO reduction profiles for varying NH_3 injection. As the threshold energy is reached, NO reduction levels begin to rise sharply to a peak. At higher temperatures, reaction (2.11) becomes more dominant and NO reduction levels fall. Depending on the chemical injected, the initial NO reduction seen at the lower end of the temperature window changes only the form of the pollutant, transforming NO into either NO_2 or N_2O. The effective range of the window for reducing NO is only about 200°F for this condition. Temperature windows play an important role in practical systems, where the inevitable temperature gradients create control challenges with varying primary combustion loads.

The amount of NO reduction is a function of the initial NO in the reaction. The research of Muzio, *et al.*, (1976) showed that as initial NO levels rise, the percent of reduction also increases. However, for a constant NSR level, the needed ammonia levels also rise, giving way to more unwanted ammonia slip. The addition of ammonia (higher NSR) shows the same trend of increased NO reduction levels. Higher emissions of ammonia result, and the optimum temperature range shifts upward. To reduce slip emissions, reduction may be sacrificed for lower slip values or a "clean-up" chemical addition downstream (*i.e.*, H_2O_2) may be used (Sowa, *et al.*, 1992).

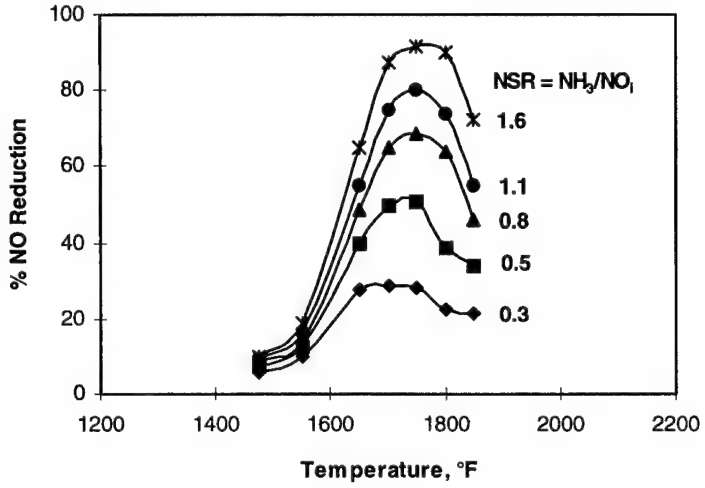

Figure 2.4: Effect of Temperature on NO Reduction. (Muzio et al., 1976)

Other additives besides hydrogen and hydrogen peroxide may be used with beneficial effects. Pilot-scale experiments adding CO with ammonia show a shift in the temperature window to lower temperatures while consuming the CO added (Teixeira, *et al.*, 1991 and Sowa, *et al.*, 1992). Hydrocarbons (*i.e.*, CH_4, C_2H_6, C_4H_{10}) have also been tried and produce similar shifts in temperature (Wenli, *et al.*, 1990).

The physical and thermal constraints of the area available for SNCR determine the residence time available. Reaction rates of the chemicals involved, the dynamics of the

flow, and the injection temperature determine the residence times needed for the NO reduction to be completed. Making these two times coincide with one another could prove challenging in itself. Thermal gradients inside the SNCR section are fairly straightforward to quantify, but measurements to determine the degree of mixing of the injected chemical and hot exhaust streams are not as easy. Each combustion system is different and must be characterized separately to tailor the SNCR system to the particular application.

2.4.2 Other Chemicals

As discussed earlier, SNCR depends on the generation of the NH_2 radical to initiate the reduction process. Several chemicals have been used to generate the necessary pool of radicals. Among these, cyanuric acid and urea have been most popular. These chemicals generally demonstrate the same characteristics as ammonia, but each has its own specific properties resulting from a slight variation in the radical pools created.

The injection of cyanuric acid ($(HOCN)_3$) into the exhaust flow is a relatively recent technology commonly known as *RAPRENO$_x$* (Perry and Siebers, 1986, Perry, 1988, and Perry, 1989). The process involves heating the solid cyanuric acid past its sublimation point (~300°C/572°F), producing isocyanic acid:

$$(HOCN)_3 \rightarrow 3(HNCO) \qquad (2.12)$$

HNCO is then injected into the gas stream to reduce NO. To make the necessary NH_2 radicals, Perry and Siebers (1986) have proposed the following mechanism:

$$HNCO \rightarrow NH + CO \qquad (2.13)$$

$$NH + NO \rightarrow H + N_2O \qquad (2.14)$$

$$H + HNCO \rightarrow NH_2 + CO \qquad (2.15)$$

The original patent reported optimal temperatures around 1000°F, much less than ammonia. However, it was later discovered that the iron reactor acted as a catalyst to the

reaction which lowered the NO reduction temperature. More-recent tests show optimal temperatures centered around 1700°F (Siebers and Cayton, 1990).

Urea injection was developed in 1976 by Muzio, *et al.*, in a program sponsored by the Electric Power Research Institute (EPRI). Urea ($(NH_2)_2CO$) can be injected as a powder or dissolved in a hydroxylic solvent into an air-rich (Arand, *et al.*, 1980) or fuel-rich (Arand, *et al.*, 1982) environment. The current understanding of the complex chemistry believes the following simplified reaction path to be correct:

$$(NH_2)_2CO \rightarrow NH_3 + HNCO \qquad (2.16)$$

Thus, urea injection uses both ammonia and isocyanic acid to create the necessary radical pool. Experiments show reductions occurring between 1600°F and 1900°F.

Other chemicals with lesser understood reaction pathways have been explored for their ability to selectively reduce NO. Hydrazine and mono-, di-, and trimethylamine are four such chemicals (Turchan, 1988; Muzio, *et al.*, 1977; and Ham, *et al.*, 1989). All four of these chemicals react to form the radical species (*i.e.*, NH_2, NH, or N) necessary for reduction. Ham, *et al.*, (1989) showed very little NO reduction using hydrazine (N_2H_4) under the conditions tested. However, unpublished data exist that shows excellent NO reduction using hydrazine hydrate at low temperatures (Muzio, 1994). Methylamine (CH_3NH_2), dimethylamine ($(CH_3)_2NH$), and trimethylamine ($(CH_3)_3NH$) have demonstrated two temperatures of effectiveness—950 and 1550°F (Muzio, *et al.*, 1977). At 950°F, significantly high levels of cyanide (HCN) were recorded (~150 ppm). Studies using methylamines have been limited to experiments only, due to the toxicity of the chemicals and the potentially hazardous by-products that make it an impractical chemical for SNCR.

2.4.3 Summary of Relevant SNCR Research

Much research has been performed on a variety of SNCR chemicals and additives in systems ranging from laboratory reactors to full-scale plants. The research mentioned in the text has shown that good NO reduction can be accomplished under the proper conditions. The following table (2.2) summarizes and highlights the chemicals and trends noted previously in this chapter to demonstrate the varied conditions for which similar NO removals can be achieved. In all cases, NO was reported and plotted to give the reduction values listed. Most researchers in this table who measured NO_2 stated its concentration was negligible or within 5% of the NO reading and thus discarded. N_2O levels are listed in the comments section for those who reported it.

2.5 Kinetic Models

With the advance of workstation and high-speed personal computers, modeling of elementary chemical reactions in flowing system is becoming commonplace as a means to complement experimental work. Computer models have greatly reduced experimental time and costs by being able to run several cases quickly to better define the optimum conditions. Software such as Sandia National Lab's Chemkin-II (Kee, *et al.*, 1990) and SENKIN (Lutz, *et al.*, 1990) packages not only allow users to model flows under a myriad of conditions (*e.g.*, constant pressure, constant temperature, plug flow, etc.), but it also can perform sensitivity analysis to help determine key reactions in a particular process.

The software solves the various reactions defined in the form of the Arrhenius rate equation. In the case of the Zeldovich mechanism (reactions 2.1 and 2.2), the rate equations describing the NO formation rates are as follows:

Table 2.2: Relevant Research

Investigators	Chemical / Additive	NO / NSR, ACR / Optimum Temp.	Reactor Type: Initial Conditions Comments
Jodal, *et al.* (1990)	Ammonia	NO_i = 400 ppm NO Reduction = 91% 1.6 1223K (1742°F)	Pilot reactor: H_2O = 7% Final NH_3 concentrations of < 10 ppm obtained. Higher NSR yields higher ammonia slip. Less than 5% NO reduction at 1073K.
Jodal, *et al.* (1990)	Ammonia / Propane	NO_i = 400 ppm NO Reduction = 60% 1.6, 0.069 1073K (1472°F)	Pilot reactor: H_2O = 7% 39% NO reduction observed at 1023K. Reduced NO reduction. Optimum temperature shifted down 150K..
Jodal, *et al.* (1990)	Ammonia / Dimetyl-amine	NO_i = 400 ppm NO Reduction = 79% 1.6, 0.206 1223K (1742°F)	Pilot reactor: H_2O = 7% 26% NO reduction observed at 1023K. Increased emissions of HCN observed (as much as 200 ppm). No temperature shift.
Wenli, *et al.* (1990)	Ammonia	NO_i = 507 ppm NO Reduction = 85% 1.64, 1238K (1770°F)	Isothermal plug-flow reactor: H_2O = 0–0.2%, t_{res} = 0.07–0.14 sec. Significant reduction begins around 1100K.
Wenli, *et al.* (1990)	Ammonia / Methane	NO_i = 507 ppm NO Reduction = 77% 1.64, 0.416 1190K (1684°F)	Isothermal plug-flow reactor: H_2O = 0–0.2%, t_{res} = 0.07–0.14 sec. Increasing CH_4 concentration lowers optimum temperature with somewhat lessened NO reduction levels.
Teixeira, *et al.* (1991)	Ammonia / Carbon Monoxide	NO_i = 125 ppm NO Reduction = 40% 2.0, 2.0 1033K (1400°F)	Pilot-scale facility: t_{res} = 0.5 sec., -450°F/sec., 500 ppm CO_i. NO produced at T>1160K. At optimum, CO_f = 465 ppm and $NH_{3,f}$ = 135 ppm. At CO_i = 0 ppm, NO reduction = 53%.
Sowa, *et al.* (1992)	Ammonia / Hydrogen Peroxide	NO_i = 8.14 ppm NO Reduction = 98% 9.93, 3.7 1122K (1560°F)	Kinetic modeling study using Miller and Bowman (1989) mechanism to study reduction of NH_3 slip: CO_i = 1.24 ppm, t_{res} = 0.5 sec., $NH_{3,f}$ = 25 ppm
Siebers and Cayton (1990)	Cyanuric Acid	NO_i = 330 ppm NO Reduction = 95% 1.42 1190K (1682°F)	Quartz flow reactor with simulated diesel exhaust: H_2O = 5.2%, CO = 260 ppm, t_{res} ~ 0.63 sec.
Cayton and Siebers (1990)	Cyanuric Acid / Hydrogen	NO_i = 330 ppm NO Reduction = 90% 1.42, 1.28 1250K (1790°F)	Quartz flow reactor with simulated diesel exhaust: CO = 0 ppm, t_{res} ~ 1 sec. N_2O levels reach 200ppm at optimum. When H_2 = 0 ppm, NO reduction = 55% at 1350K.
Jodal, *et al.* (1990)	Urea	NO_i = 400 ppm NO Reduction = 88% 1.6 1273K (1832°F)	Pilot reactor: H_2O = 7% Final NH_3 < 10 ppm. Optimum temperature shifted up 50K. Significant N_2O (71 ppm) and CO production observed.
Teixeira, *et al.* (1991)	Urea	NO_i = 125 ppm NO Reduction = 55% 2.0 1263K (1814°F)	Pilot-scale facility: t_{res} = 0.5 sec., -450°F/sec. gradient. NH_3 slip = 39 ppm. N_2O increases by 20 ppm.

$$\frac{d[\mathrm{NO}]}{dt} = k_1[\mathrm{N_2}][\mathrm{O}] \qquad (2.17)$$

$$\frac{d[\mathrm{NO}]}{dt} = k_2[\mathrm{N}][\mathrm{O_2}] \qquad (2.18)$$

where $k_i = AT^{\beta}\exp(-E/RT)$: k_i is the equilibrium rate constant for each reaction, A and E are empirically-determined constants, R is the universal gas constant, and T is temperature in degrees Kelvin.

In the discussion on thermal NO, reaction (2.1) was determined to be very slow (or rate limiting) compared with reaction (2.2). Thus, the rate equation can be rewritten as

$$\frac{d[\mathrm{NO}]}{dt} = 2k_1[\mathrm{N_2}][\mathrm{O}]$$

or

$$\frac{d[\mathrm{NO}]}{dt} = AT^{\beta}\exp\left(\frac{-E}{RT}\right)[\mathrm{N_2}][\mathrm{O}] \qquad (2.19)$$

In equation (2.19), constants A, β, and E are specified with each reaction to define its forward rate of reaction. Therefore, equation (2.19) is dependent on time, temperature, and N_2 and O concentrations to determine NO. Temperature has the largest effect on NO formation rate due to its exponential power.

Many experimental data exist over a wide range of operating parameters, applying SNCR in bench-top reactors, pilot-scale facilities, and full-scale demonstrations. The information learned about the various reactions involved through these research studies and shock tube studies have helped in the development of chemical kinetic models. Past studies have shown that these chemical kinetic models are capable of predicting experimental results for SNCR processes with a fair degree of accuracy (Sowa, *et al.*, 1992, and Dill and Sowa, 1992). Dill's thesis uses computer chemical kinetic models to predict the SNCR efficiency for several chemical and additive combinations "injected" into a simulated JETC environment to evaluate its feasibility.

The most heavily documented SNCR chemical is ammonia (Miller, *et al.*, 1981; Kimball–Linne and Hanson, 1986; Lyon, 1987; Miller and Bowman, 1989). The Miller

and Bowman (1989) chemical kinetic model has been the most accepted published model to date. In their paper, they provided two reaction mechanisms: the first comprised 73 elementary reactions for ammonia oxidation involving species made up of N, H, and O atoms. The second reaction mechanism involved 234 elementary reactions that describe C_1 and C_2 hydrocarbon oxidation as well as nitrogen chemistry.

Also introduced in Miller and Bowman's 1989 paper were the reactions for cyanuric acid based upon the work of Perry and Siebers. In a 1991 paper, Miller and Bowman proposed an updated mechanism for cyanuric acid based upon the experiments performed by Siebers and Cayton (Cayton and Siebers, 1989, and Siebers and Cayton, 1990). The model built upon the 1989 mechanism by making some necessary changes to reproduce the dependence of NO removal on the concentrations of O_2, CO and H_2O.

Recently, Bowman has updated the 1991 model with new reaction rates based upon more current shock-tube experiments (Bowman, 1994). This model incorporates reactions for both $DeNO_x$ and $RAPRENO_x$ processes, meaning that urea can also be modeled. The result is a model with 123 elemental reactions that, according to Bowman, shows generally good agreement between the trends of experiments and the model calculations.

3.0: APPROACH

Chapter 1.0 stated the goal of this project: to evaluate the reduction of NO_x emissions from jet engine test cells using selective non-catalytic reduction. The approach to meeting the research goal was divided into five tasks:

1) Design, construct, and set up a sampling traverse, consisting of an *x-y-z* traverse and sample probe (rake), that can collect gas samples at multiple points in the exhaust stream in the JETC. The sample traverse needs to be capable of taking measurements axially in the exhaust flow between the engine and the augmenter mouth. Construction of the probe needs to withstand extreme temperatures (up to 3000°F) as well as the force of the turbulent flows in the exhaust (up to 25,000 pounds of thrust).
2) Characterize the plume of an afterburning and a non-afterburning engine at normal jet engine test cell operating conditions.
3) Analyze the exhaust stream characteristics including emissions, temperature, and velocity. Perform several tests for each engine to allow a mean set of temperature values to be generated.
4) Evaluate the test cell emissions map created for locations where NO_x reduction using SNCR is possible.
5) Use computer kinetic models to study the feasibility of SNCR control and optimize the process. The subtasks in the evaluation include a) the "injection" of ammonia, isocyanic acid, urea, and hydrazine for baseline calculations and b) the "co-injection" of additives with the select chemicals.

The next chapter (Chapter 4) discusses Task 1 and the approach to Task 5. Chapter 5 addresses the remaining tasks, and Chapter 6 summarizes the findings.

4.0: EXPERIMENT

This chapter is divided into two major sections. The first discusses the design and construction of the sampling traverse and the emissions instrumentation used. The second chapter discusses the basic approach to the design of the SNCR modeling grid.

4.1 Plume Characterization

The first part of this research consisted of collecting and analyzing exhaust samples for species composition, temperature, and velocity. An actual JETC was used to provide realistic data sets which map out the exhaust characteristics of the engines being tested under normal operation profiles. Two engines were tested using a multi-point sampling probe and a single-point pitot probe to measure the exhaust samples and velocity, respectively. A traverse was constructed to hold the probe securely and allow for three-dimensional movement within the flow. A combination of both on- and off-line instrumentation analyzed the gas flows for their composition and characteristics. Due to the hostile environment the design of the probe and sampling system was conducted following established UC Irvine Combustion Laboratory protocol in lieu of conventional guidelines (*e.g.*, International Civil Aviation Organization, 1993).

4.1.1 Preliminary Tests

To insure as few problems as possible during the actual testing period, preliminary testing was performed in a JETC located at El Toro Marine Corps Air Station, California. A General Electric F404 turbofan engine with afterburner (17,000 pounds thrust) was used to examine the following issues:

- The structural integrity needed for the sampling probe to withstand high-temperature flows seen at full afterburner conditions,

- The possible designs for a probe-holding device that would provide the greatest amount of rigidity, and
- The approximate temperatures and velocities to be expected.

After several initial attempts, a successful run through full afterburner was accomplished. The probe used was fabricated from 0.75-inch stainless steel pipe enclosing a 0.31-inch pitot probe. The entire fabricated section of the probe was water-cooled, however the exposed tip of the pitot probe was not. The probe was mounted to a square base made of 2-inch-by-6-inch box tubing and 4-inch-by-0.5-inch steel plate bolted to the frame rails of the test stand behind the engine tailpipe. This testing proved invaluable to the development and success of the final sampling traverse and probe configuration.

4.1.2 The Engines

McClellan Air Force Base (MAFB) in Sacramento, California, was chosen as the site for the emissions gathering. McClellan AFB serves as a depot for the repair of F-111 and KC-135 aircraft. Both aircraft use Pratt and Whitney engines as their power plants. The TF30-P111+ model is an afterburning engine used in the F-111 fighter. This turbofan ducts all of its bypass fan air through the engine. The afterburner (AB) section sprays fuel into the hot exhaust gases behind the turbine where it ignites and produces additional thrust. It develops 25,000 pounds of thrust while consuming almost 54,000 pounds of fuel per hour at full afterburner. The nozzle is of a converging-diverging configuration consisting of an inner and outer nozzle. The inner nozzle is controlled while the outer nozzle works on aerodynamic effects. The inner nozzle radius is 13 inches through military power (full power, no afterburner) and 18 inches at full afterburner.

A typical run schedule for an engine mounted in the test cell is intended to check critical specifications (*i.e.*, speeds, temperatures, pressures) and trim the engine as necessary. For example, a complete test for a TF30-P100 series engine consists of two different run schedules as shown in Figure 4.1. The different power settings and checks are defined as follows:

- Flight idle is the minimum power setting;
- The 80% and 90% power settings are based upon the turbine shaft speed;
- Military minus 10 inches and Military minus 6 inches powers are based upon engine pressure ratio;
- Military power is full power without afterburner;
- Zone 1 through Zone 5 afterburner represent the five fuel spray-bars as they are activated in the augmenter section of the engine (behind the turbine) with Zone 5 denoting full afterburner power; and
- Scavenge involves a short burst of power before shutdown.

The TF33-P9 non-afterburning engine is used on the KC-135 transport. Its 17,000 pounds of thrust are developed mostly by its high-bypass turbofan that is ducted outside the engine casing through a cowling. Instead of concentrating on power as does the P111+, the focus of the P9 is on fuel economy, using only 9500 pounds of fuel per hour at military power. The radius of the exhaust nozzle on this engine is fixed at 12 inches. Its power settings are similar to the non-afterburning positions of the P111+ engine, with the addition of two powers:

- Data-set power is used to collect necessary information for proper engine evaluation, and
- Part power is a typical cruising speed.

Preliminary Run

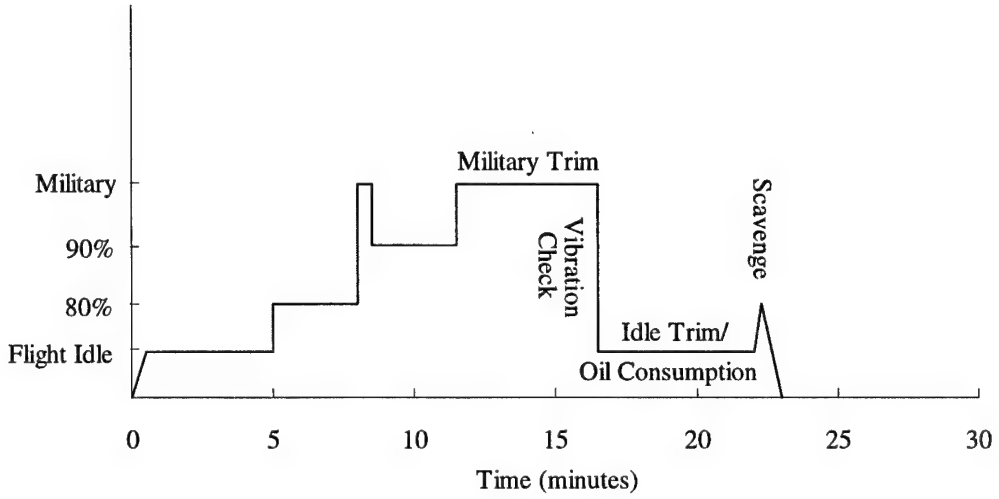

Performance Run

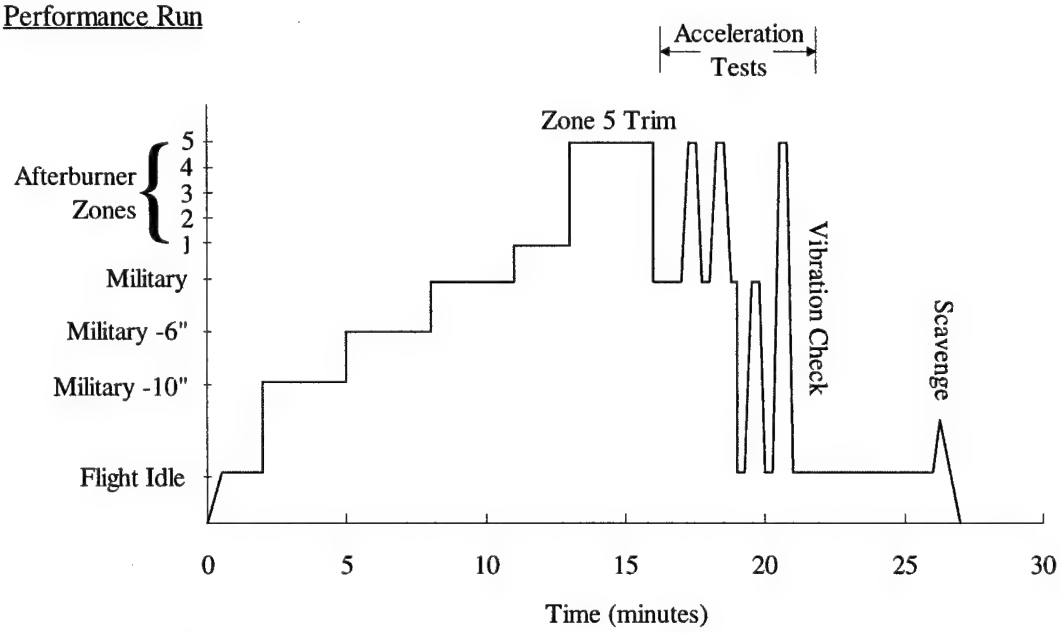

Figure 4.1: Typical TF30-P111+ Preliminary and Performance Run Schedules at McClellan AFB

Typical MAFB runs call for extended periods of running at each of these positions with occasional cool-down periods at flight idle. Typical engine run throttle positions and characteristics for both engines are noted in Table 4.1.

4.1.3 Sample Probes

Based upon the preliminary tests, the sample probe was designed from 0.75-inch stainless steel (SS) pipe in a reverse double triangle configuration [shown in Figure 4.2]. The probe was constructed using threaded lengths of pipe and threaded fittings throughout. The modular design allowed for ease of assembly and the replacement of parts such as probe tips in the field, if necessary. However, the joints along the vertical leg and the reverse triangle were welded after final assembly for added strength and rigidity. The five sampling probes were equally spaced approximately 3.5 inches apart to map a radial emissions profile from the engine centerline to the edge of the flow field based upon the dimensions of the MAFB test cells. Radial points were measured from the engine centerline (z = 0.0 inches) to the edge of the flow field (z = -14.75 inches). Radial uniformity of the flow field was assumed for these tests.

Table 4.1: Typical Engine Speeds and Fuel Flow Rates

	TF30-P111+				TF33-P9		
Throttle Setting	Turbine (%)	Turbine (RPM)	Fan (RPM)	Fuel (lb/hr)	Turbine (%)	Turbine (RPM)	Fuel (lb/hr)
Flight Idle	66.1%	10100	4300	1152	58.6%	5706	1790
80% Power	79.9%	12300	6700	3104	--	--	--
Military -10" Power	89.1%	13700	8500	6543	--	--	--
90% Power	90.3%	13800	8700	7077	90.1%	8774	4848
Data-Set Power	--	--	--	--	92.2%	8974	5049
Military -6" Power	91.1%	14000	8800	7403	95.3%	9274	6993
Part Power	--	--	--	--	96.4%	9381	7206
Military Power	94.6%	14500	9500	9402	100.0%	9733	8773
Zone 1 Afterburner	94.6%	14500	9400	13944	--	--	--
Full Afterburner	94.1%	14400	9300	53788	--	--	--

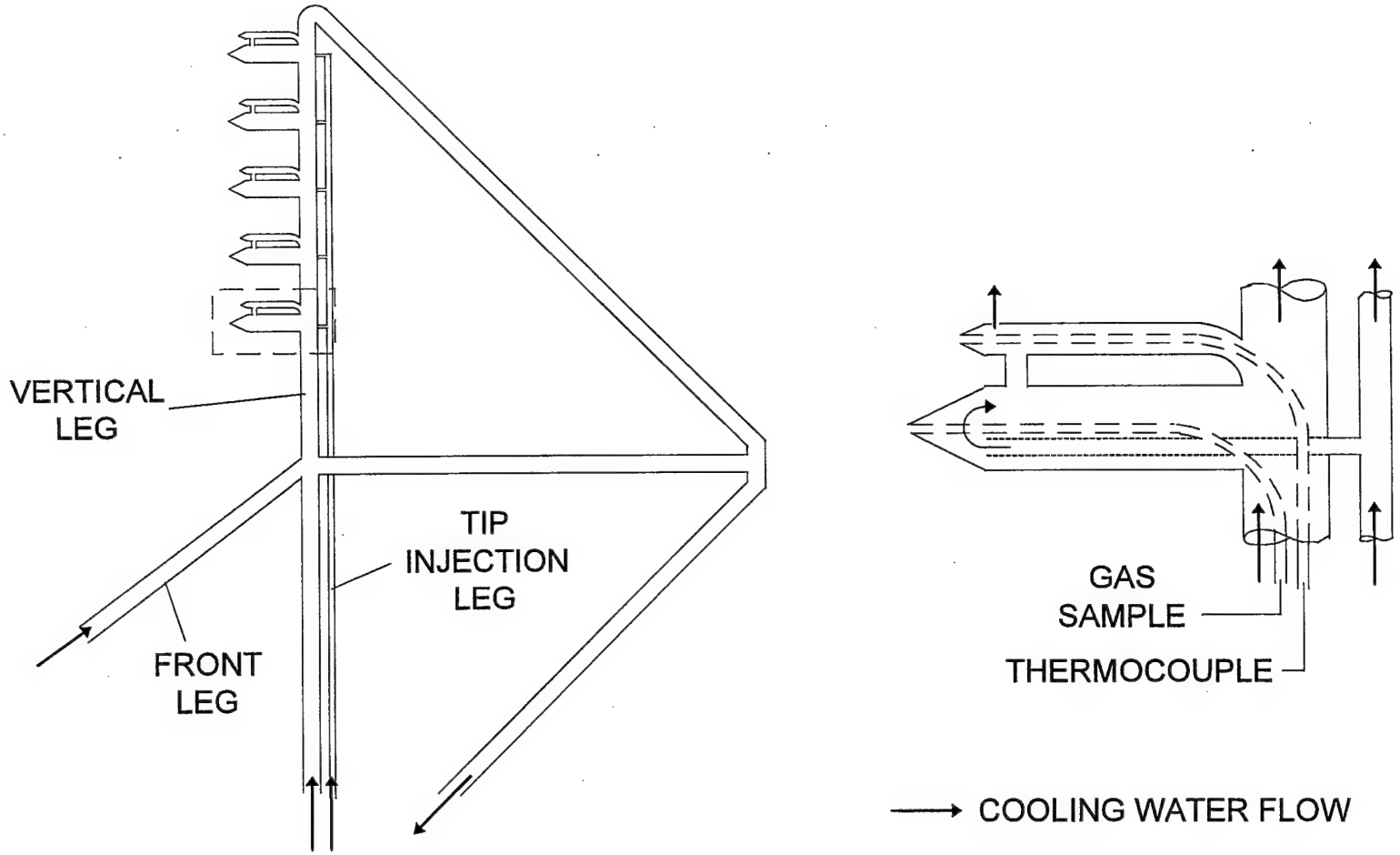

Figure 4.2: The Five-Point Sample Probe.

In the initial tests at El Toro, a shock wave was noticed extending from the blunt face of the water-cooled section. To counter this, a conscious effort was made to reduce the shock formed. The tailpipe of the P111+ engine has a converging-diverging nozzle which implies that the flow exiting the tailpipe, at least during afterburner conditions, will be greater than the speed of sound. To lessen the effects of the shock on the probe and its measurements, conical-shaped probe tips were machined at the same angle as the shock wave. The shock cone angle was determined according to the following formula:

$$\text{Cone angle} = \sin^{-1}(1/M) \qquad (4.1)$$

where the cone angle is measured from the direction of the flow to the shock wave and M is the Mach number of the flow.

Thus, the Mach number of the flow determines the optimum angle for the probe tip. Based on the velocities observed for the F404 engine, a Mach number of two was assumed, thus a cone angle of 30° was taken

Each axial station used two probe tips as shown in the expanded section of Figure 4.2. Gas samples were drawn in continuously through 0.125-inch SS tubing inside the larger 0.75-inch probe tip. A Type-R, open-junction thermocouple was also run through 0.125-inch SS tubing in a 0.325-inch probe tip located on top of the larger tip. All ten 0.125-inch tubing lengths were run inside the main vertical leg of the probe until exiting via a manifold at the base of the sample probe.

The entire sample probe was water cooled to retain the integrity of the structure during afterburner operation. Referring again to Figure 4.2, water enters the probe through the front leg, the vertical leg, and the tip injector leg. The bulk of the cooling water flows through the front and vertical legs. The tip injection leg has a 0.325-inch feed line running up the back of the vertical leg. A 0.25-inch tube directs the water from this leg into the front of the large probe tip to keep water circulating in this closed cooling system. The short piece of tubing connecting the small and large probe acts as a support

as well as a second cooling leg for the small probe. A 0.125-inch hole was drilled near the tip of the small probe, creating an open system to circulate the cooling water through it. The bulk of the water exits via the rear vertical leg. Total flow was kept constant at approximately 30 to 40 gallons per minute by diverting part of the high-pressure water used for cooling the augmenter.

A Dwyer 0.31-inch pitot probe was used to make centerline velocity measurements. By knowing the velocity, residence time of the flow can be predicted in the augmenter section. The vertical leg of the pitot probe is run inside 0.75-inch SS pipe that triangulates backwards in a fashion similar to the sample probe while the tip of the probe is left exposed. Its design permits easy replacement of the pitot probe if necessary. The assembly is attached to the main probe using bolt-on clamps to allow for its removal during extended testing. The thermocouples on the main sampling probe are used to determine the flow temperature for velocity corrections.

4.1.4 The Traverse

The traverse was designed with strength and rigidity in mind as well as flexibility of probe positioning. The frame was constructed from 3-inch box tubing extending 100 inches in length by 50 inches in width by 48 inches in height (Figures 4.3 and 4.4). A fully-welded carriage rides on top of the frame, allowing the probe to have three-dimensional movement. The carriage sits well below the hot flows of the jet exhaust. Total weight of the traverse was about 800 pounds.

The sample probe bolts to a smaller *y*-traverse via three sets of choke blocks. Initial vertical centering of the probe is accomplished by loosening the blocks. The *y*-traverse and the carriage use *T*-rails and pillow blocks for horizontal centering and axial positioning of the probe in the flow. Axial capability of the carriage is 70 inches. Once in place, the traverse was held fixed by a series of clamping plates along unistrut runners.

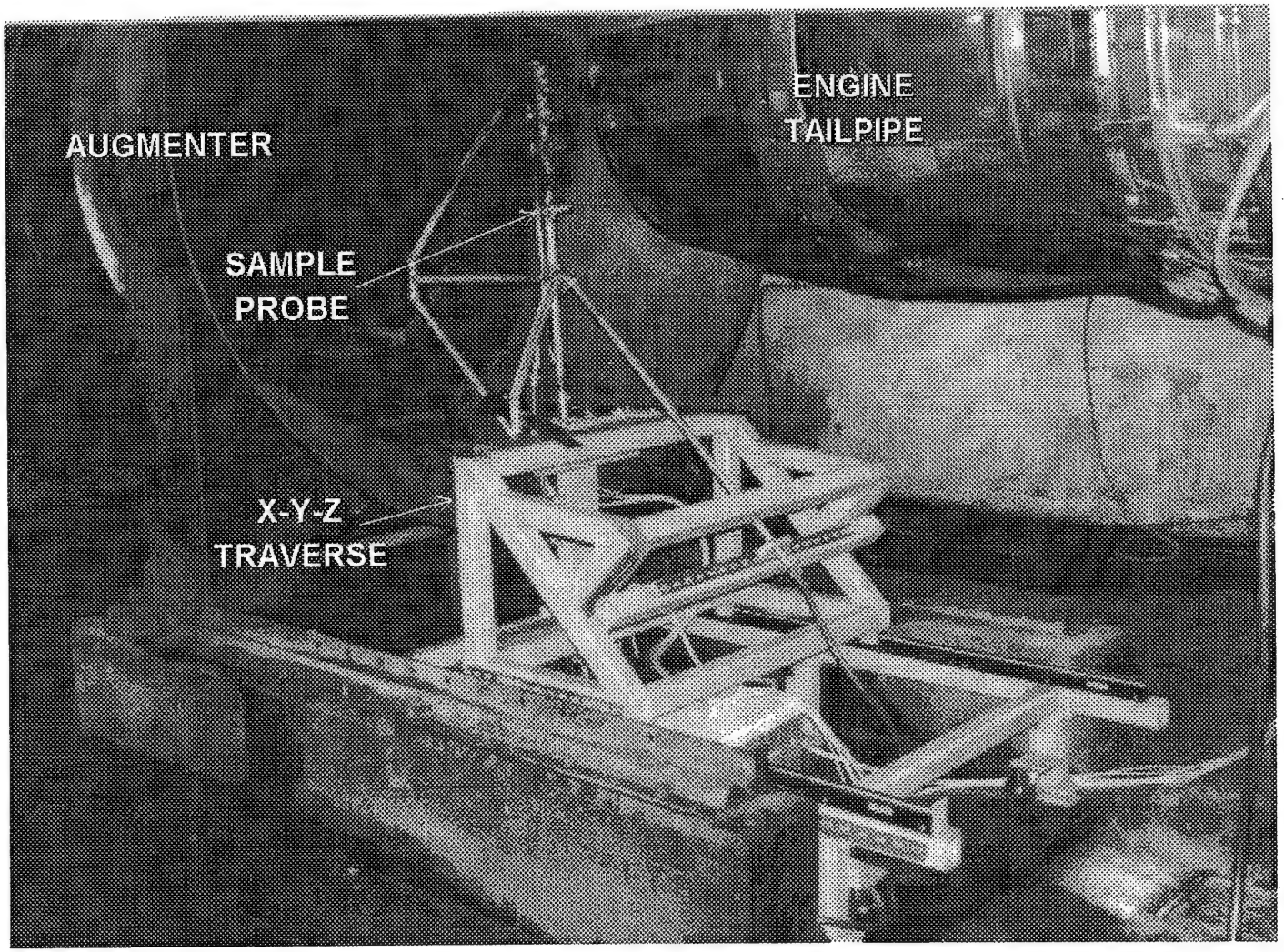

Figure 4.3: The Sample Probe, Traverse, and JETC Orientation

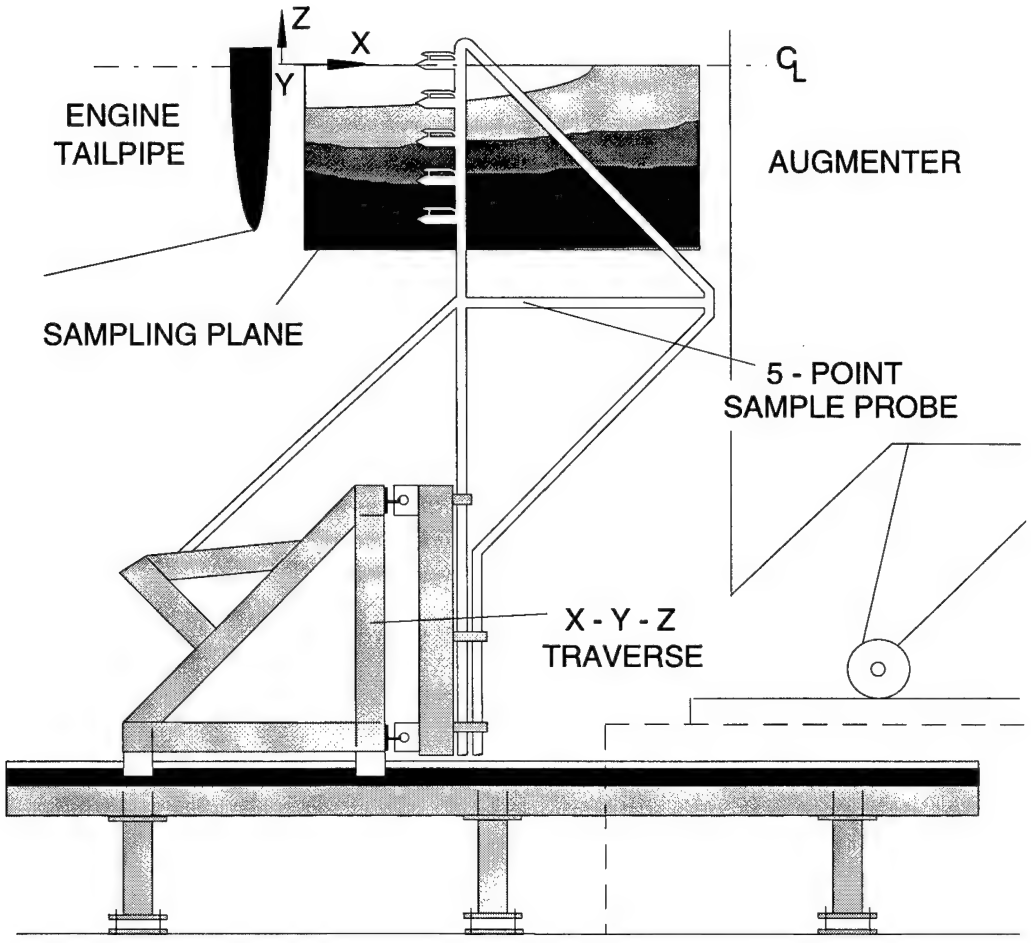

Figure 4.4: The Traverse and Sampling Plane.

The sampling traverse was built on casters to allow the assembly to be moved between test cells. Once in place, the stand was leveled and bolted to stand-off plates which were mounted to the floor of the test cell. This created a test stand that was both secure and vibration-free.

4.1.5 Experimental Monitoring and Protocol

The nature of the sample probe design allowed for quick quenching of the sample flow. To ensure a "dry" sample, a PVC water drop-out in an ice bath was used immediately following the exit of the sample lines from the sample probe. Teflon™ 0.25-inch tubing at ambient temperature carried the sample to a series of pumps, valves

and analyzers known collectively as the sampling system (Figure 4.5). Two pumps using stainless steel bellows delivered the gas to a manifold of valves that allowed one sample leg to be analyzed while the other four legs were directed into a dump line. A Magnahelic pressure gauge was used to measure the differential pressure from the pitot probe.

The gas species of major concern for this testing include NO, NO_x, carbon monoxide (CO), carbon dioxide (CO_2), and oxygen (O_2). Unburned hydrocarbons (HC) were also monitored. NO and NO_x were measured using a Horiba CLA-120 chemiluminescent analyzer calibrated on a 488-ppm NO span gas in nitrogen. A Horiba PIR 2000 nondispersive infrared (NDIR) analyzer measured CO concentrations calibrated on a 102-ppm span bottle. Both instruments were calibrated at the beginning of each engine run. The calibration held to within $\pm$ 5% during the course of each run. A Horiba MEXA-544GE analyzer was used to measure CO_2, O_2, HC, and high CO concentrations. The unit was spanned on a bottle containing 13% CO_2, 848 ppm HC, and 1.8% CO. Room air was used to calibrate O_2 concentration (20.91%).

A Hewlett-Packard 5890 Series II gas chromatograph (GC) equipped with a HaySep DB packed column and a thermal conductivity detector was used to measure O_2 and CO_2 concentrations. Samples were collected in Teflon™ sample bags for later measurements using the chromatograph. An automated valve with a sample loop in the GC allowed for accurate dispensing of the sample. Calibration was performed using a span gas of 19.2 percent O_2, 4.6 percent CO_2, and a balance of N_2. The GC served as the primary source of CO_2 and O_2 measurements while the MEXA provided a redundant check. Table 4.2 summarizes the characteristics of each instrument.

Calibration of the instruments was performed before the beginning of each run. Measurements were made over an entire engine run, holding the probe position fixed. Once a condition was reached, 30 seconds were allowed for the condition and the instruments to stabilize before readings were taken. Testing was performed in parallel

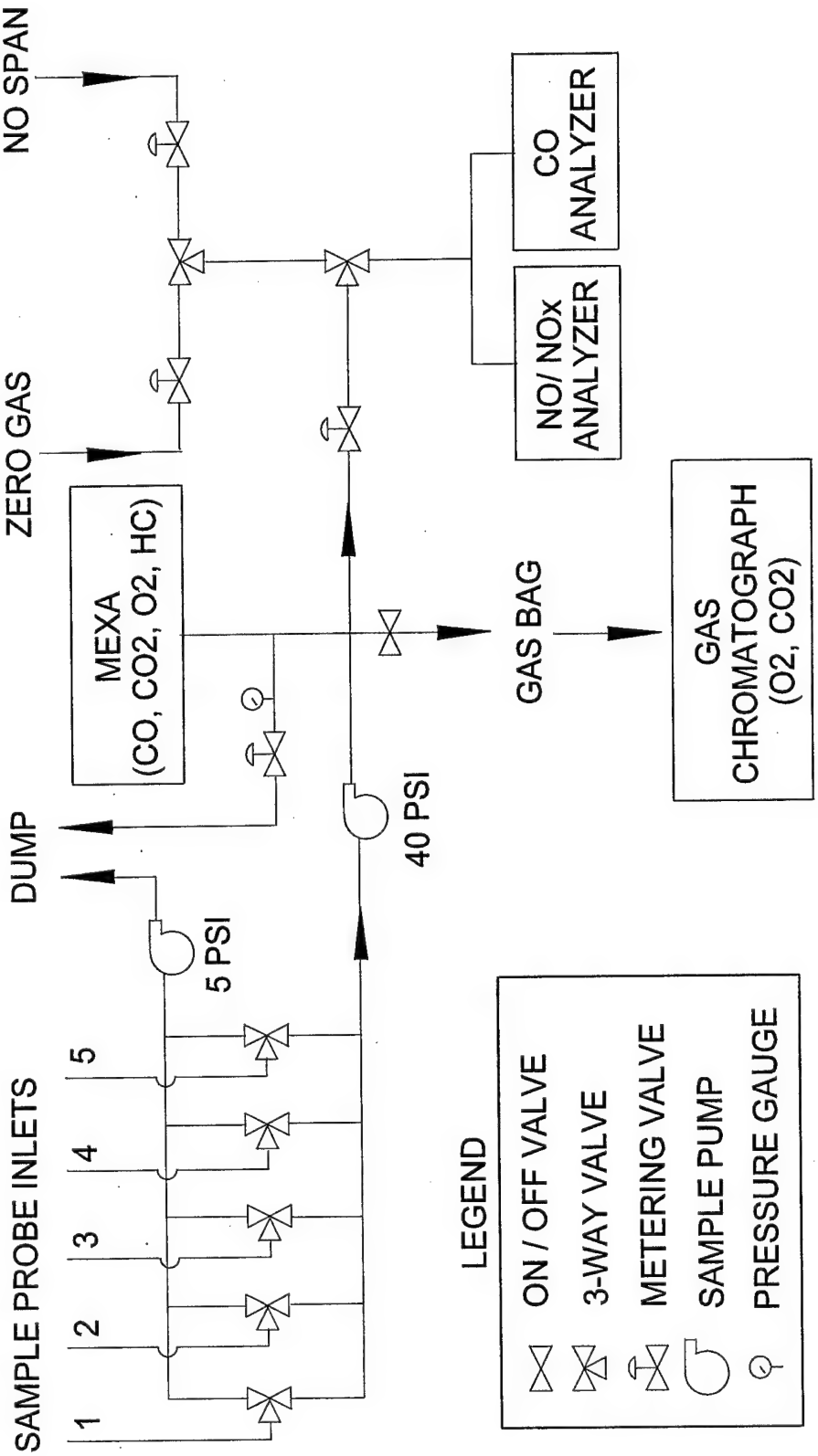

Figure 4.5: Schematic of Sampling System and Diagnostics.

Table 4.2: Emissions Instrumentation

Analyzer	Species Measured	Method	Range	Accuracy
Horiba CLA-120	NO, NO_x	chemiluminescence	0 – 500 ppm	± 5 ppm
Horiba PIR-2000	CO	NDIR	0 – 3000 ppm	± 30 ppm
Horiba MEXA-544GE	CO	NDIR	0 – 10.00%	± 0.04%
	CO_2	NDIR	0 – 20.00%	± 0.1%
	HC	NDIR	0 – 10,000 ppm	± 20 ppm
	O_2	Galvanic Battery	0 – 25%	± 0.4%
HP 5890 Series II Gas Chromatograph	O_2	Thermal Conductivity	~4 – 22%	± 5% of value
	CO_2	Thermal Conductivity	~2 – 15%	± 5% of value

with normal test cell activities. The points measured at each downstream position were taken during the course of one engine testing cycle. Therefore, the data in the following results reflect the collection of many data points from many different engines. Data taken at similar power conditions for each engine were averaged to get a final emissions value at each sample point.

A sampling grid was created for this experiment based on the radial profile of the sampling probe and the extremities of x-traverse. For the P111+ engine, samples were taken at the exit of the exhaust nozzle (x = 0.0 inches), at the furthest downstream point allowed by the augmenter (x = 21.5 inches), and at a point halfway between (x = 10.75 inches). The augmenter on the P9 test stand was located further back from the exhaust exit allowing for sampling at x equals 36.5 inches away from the exhaust exit as well as at x equals 0.0 inches.

Measured values were generally repeatable from engine to engine. However, mass balances were not completed on the measurement results. Several sources of error exist in attempting a mass balance on the engines:

- The measured data must be spatially averaged from several different engines in varying conditions to complete the mass balance. A mass-weighted averaging approach cannot be used due to lack of necessary data.
- Different day-to-day ambient inlet temperatures and pressures alter the performance of each engine during the run,
- The fuel used for the tests is a blend of JP-4, -5, and -8 that varies in composition (all serviced aircraft have their tanks drained and are combined into the JETC tank),
- Each engine is trimmed differently to meet the given ranges at each power band, thus resulting in slight engine-to-engine variation,
- Airflow into the engine is not measured. It must be extracted from curves using the fan speed to calculate the available air,
- Fuel flow to the engine was monitored using a bulk flow reading for which calibration curves were not available,

For these reasons, mass balances were not completed.

4.2 SNCR Modeling

4.2.1 Mechanisms

As discussed in the background, kinetic modeling has come a long way in helping researchers help to predict the reduction possibilities and trends seen with SNCR. While not completely accurate in their predictions, these models allow researchers to perform many otherwise costly experiments without ever entering the laboratory. Many chemicals have been tried experimentally, but only the most popular candidates for industrial applications have been heavily documented. When several sources of "good" data are available, kinetic modelers can develop chemical kinetic mechanisms geared towards that particular application. Ammonia and cyanuric acid are such chemicals that have had

chemical kinetic mechanisms tailored specifically for their SNCR applications (Miller and Bowman 1989 and 1991, Bowman 1994). Bowman's (1994) model is the most current understanding of these two chemical processes to date, and thus it will be used in the modeling of ammonia, cyanuric acid, and urea. The mechanism is currently in print, but a listing of the reactions and their rates is provided in Appendix A.

Hydrazine has been a chemical of moderate interest. Although no work has been done specifically to model the pure hydrazine process, reaction constants have been published for N_2H_4 and related reactions (Miller et al., 1983). A hybrid reaction set was compiled from Miller and Bowman's (1989) mechanism and Miller's (1983) reaction rates for hydrazine by Muzio, *et al*,. at Fossil Energy Research Corp. for comparison with their experimental data. The hydrazine mechanism is presented in detail in Appendix B for reference.

The necessary reaction rates are available also to perform tests using modifiers to the SNCR process. Hydrogen, methane, and hydrogen peroxide were used as additives with the above chemicals to extend their useful ranges. Since the current Bowman (1994) mechanism does not contain the hydrocarbon chemistry necessary to support methane reactions, the C_iH_j reactions were taken from the original mechanism (Miller and Bowman, 1989). This hybrid mechanism was used only in the case for which methane was the modifier.

4.2.2 Basic Strategy

From the results of the test-cell emissions sampling, a general range of parameters were established. Initial variable parameters included NO, temperature, CO, normalized stoichiometric ratio (NSR), and (where applicable) the additive-to-chemical ratio (ACR). Carbon dioxide and oxygen concentrations were held fixed based upon the experimental results. Water concentration in the flow was determined through the use of the NASA Equilibrium code assuming complete combustion of the original reactants. Conditions of

the most-promising combinations will be applied to the specific JETC conditions to test their feasibility.

Chemkin-II, distributed by Sandia National Laboratories, was used to model the effects of SNCR on the exhaust stream. This software package of Fortran subroutines models the homogeneous, gas-phase kinetics of a given system. A Chemkin interpreter uses the reaction mechanism given and extracts the necessary information from the Thermodynamic Database (Kee, *et al.*, 1987) to create a linking file. This file contains all of the essential information on the elements, species, and reactions contained in the mechanism. The user inputs the specific conditions to be modeled, and the linking file defines the basis of the subroutines needed to solve the given problem. Here, a plug-flow, isothermal system was assumed.

5.0: RESULTS

5.1 Plume Characterization

A two-dimensional sampling plane was defined radially from centerline (radial distance, z = 0 inches) to the extent of the flow and from the exit of the exhaust (axial distance, x = 0 inches) to the mouth of the augmenter (Figure 4.4). For the P111+ contour plots, linear interpolation with a second-order smoothing of the data was used to generate the contours seen in Figures 5.1 through 5.6. The data set was derived from averages of experimentally measured data. A typical data field was based on the sampling points indicated by open circles in the plots. In all cases, radial uniformity of the flow was assumed.

5.1.1 NO/ NO_x Emissions

The plots shown for NO and NO_x (Figures 5.1 and 5.2, respectively) show similar trends. Strong gradients towards the exhaust plume centerline (z = 0.0 inches) are seen through military power. The slight positive slope shows some signs of dilution from the ambient room air towards the centerline, but the effects are not considered significant enough within the resolution of the curve fitting. Table 5.1 shows that the area-weighted NO_x concentrations increase from 7.4 to 137 ppm (parts per million) as the power increases through military power. However, peak NO_x values exceed 300 ppm along the centerline in Figure 5.2f.

Zone 1 afterburner experiences a dip in the point NO and NO_x emissions made evident in Figures 5.1g and 5.2g, respectively. Since the reaction in the afterburner is closer to atmospheric pressure, it acts as a reburner, breaking down NO from the combustor. However, nitrogen dioxide (NO_2) concentrations rise significantly relative to NO, suggesting oxidation of nitric oxide in the hot gas stream. When an area-weighted average of the NO_x values is taken (see Table 5.1) the result is a steady increase

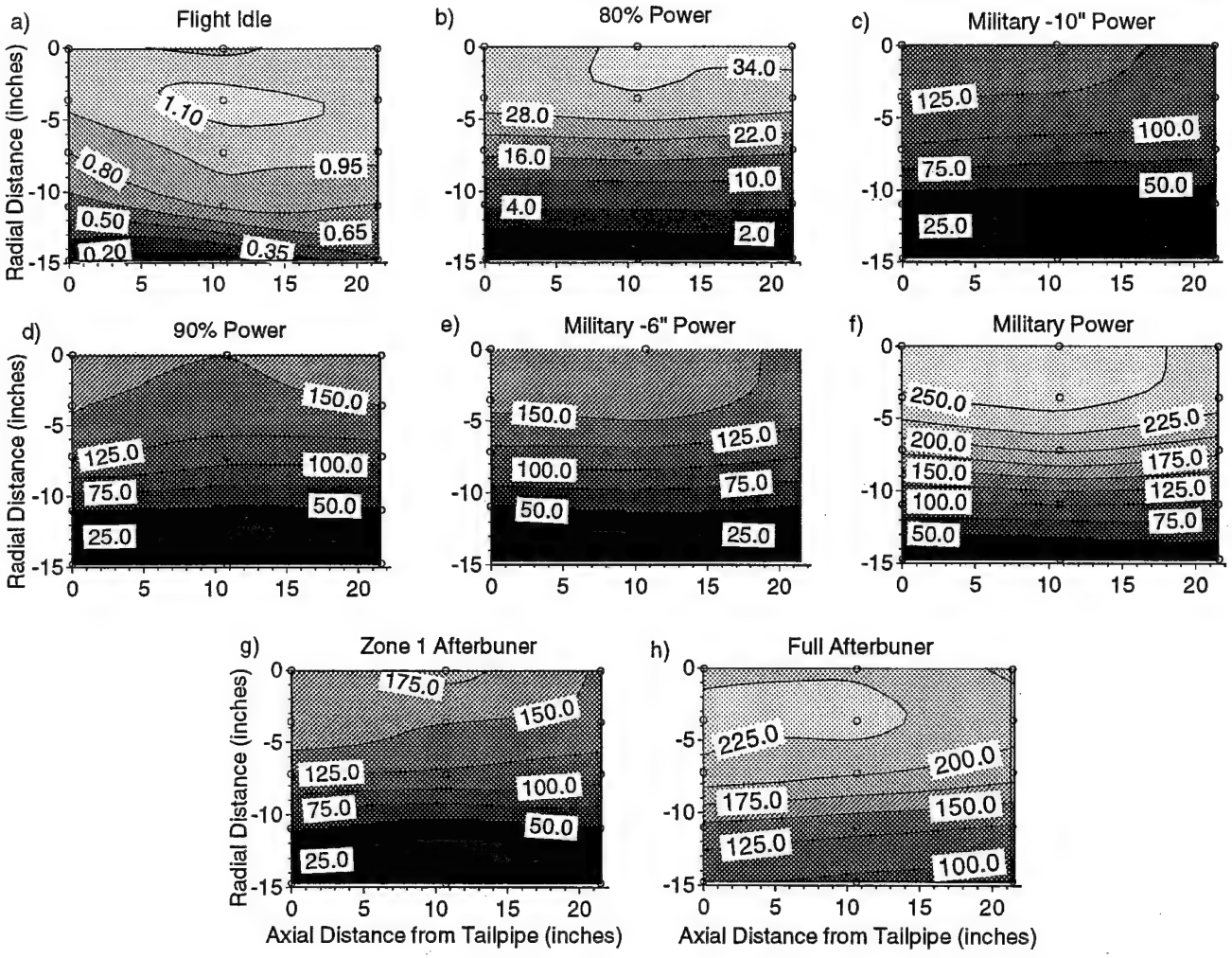

Figure 5.1: TF30-P111+ Contour Plots Showing Exhaust NO Concentration (ppm).

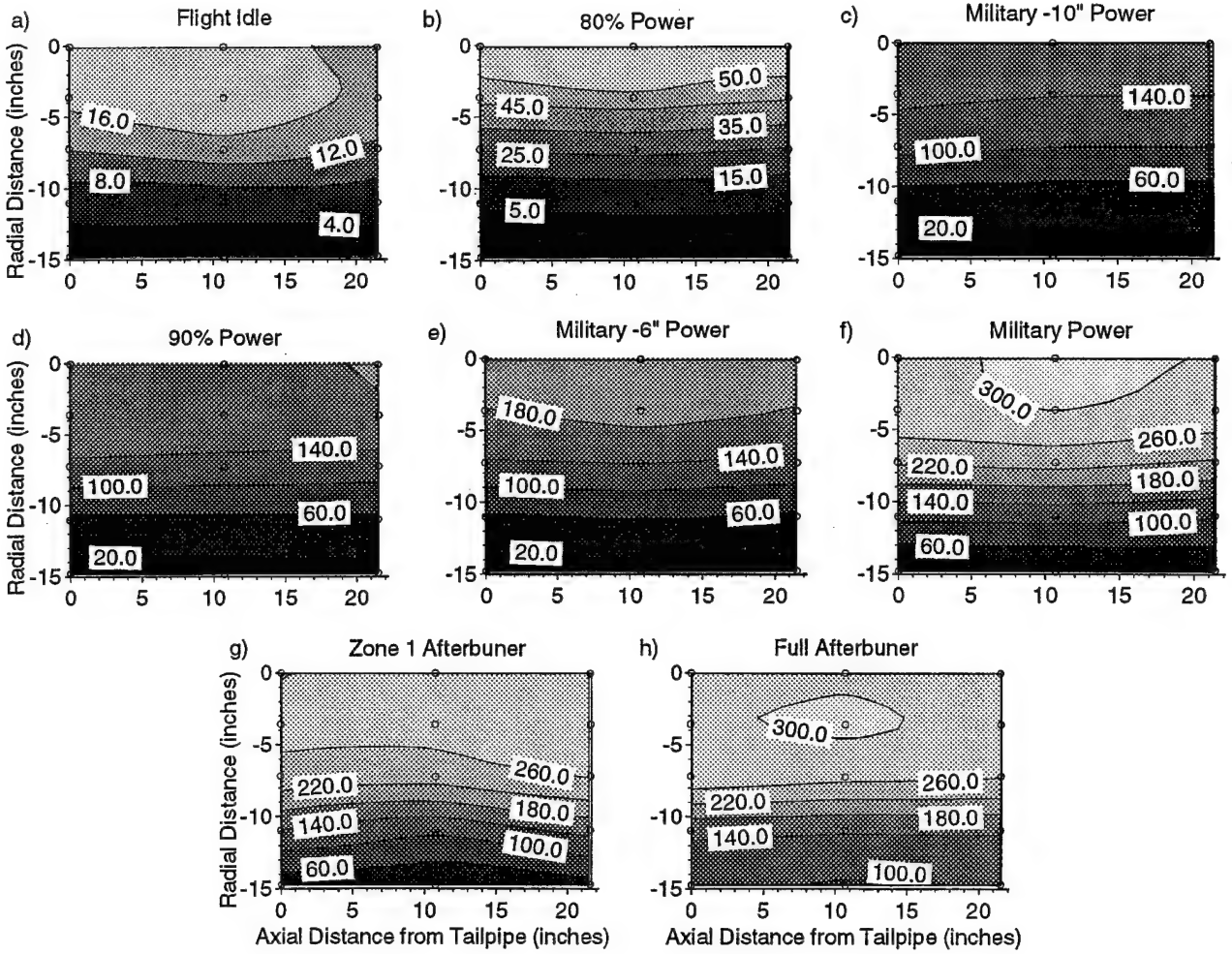

Figure 5.2: TF30-P111+ Contour Plots Showing Exhaust NOx Concentration (ppm).

in the NO_x levels through full afterburner. At full afterburner, the NO_x values at the edge of the flow field (z = -14.75 inches) are seen in Figure 5.2h to be much higher than at the lower throttle settings. This occurs as a result of the inner nozzle opening, causing a spreading of the flow field.

Table 5.1 also shows the scaled indexes for NO and NO_x. These values are calculated as an emissions index (see Appendix D) and divided through by the highest value for comparison purposes. The NO_x index climbs until it reaches its peak at military power. Afterburner levels drop off significantly due to the increased fuel flow rates with little change in emissions output. The scaled indexes also indicate the significance of NO_2 in the plume. Nitrogen dioxide appears to make up from 2% to 50% of the total NO_x seen in the exhaust with peak levels occurring at Zone 1 afterburner. Conversion of NO to NO_2 in the sample probe was minimized by rapid convective sample quenching at the probe tips, and by a design that ensured that the probe tip was thoroughly and completely cooled.

The P9 engine shows similar NO and NO_x trends to the P111+ through its power band. Figures 5.3 and 5.4 show that NO_2 makes up 10 to 30 percent of the total NO_x. One difference seen here is the peak point values at each power setting occur towards the wall of the nozzle located at radial position z equals -12 inches. Unlike the P111+, the P9

Table 5.1. TF30-P111+ Exhaust Characteristics

	Area-Weighted Average				Scaled	
Throttle Setting	NO (ppm)	NO_x (ppm)	CO (ppm)	Temp. (°F)	NO Index (lb/k-lb fuel)	NO_x Index (lb/k-lb fuel)
Flight Idle	0.8	7.4	242	328	0.01	0.14
80% Power	9.9	14.6	88.4	353	0.20	0.29
Military -10" Power	52.0	60.7	61.2	547	0.62	0.72
90% Power	67.9	75.6	73.1	594	0.72	0.79
Miliatry -6" Power	71.6	79.8	63.3	599	0.74	0.81
Military Power	125.2	137.2	74.6	723	0.92	1.00
Zone 1 AB	77.7	173.1	1121.0	1264	0.37	0.87
Full Afterburner	153.0	182.7	66376.3	2792	0.11	0.13

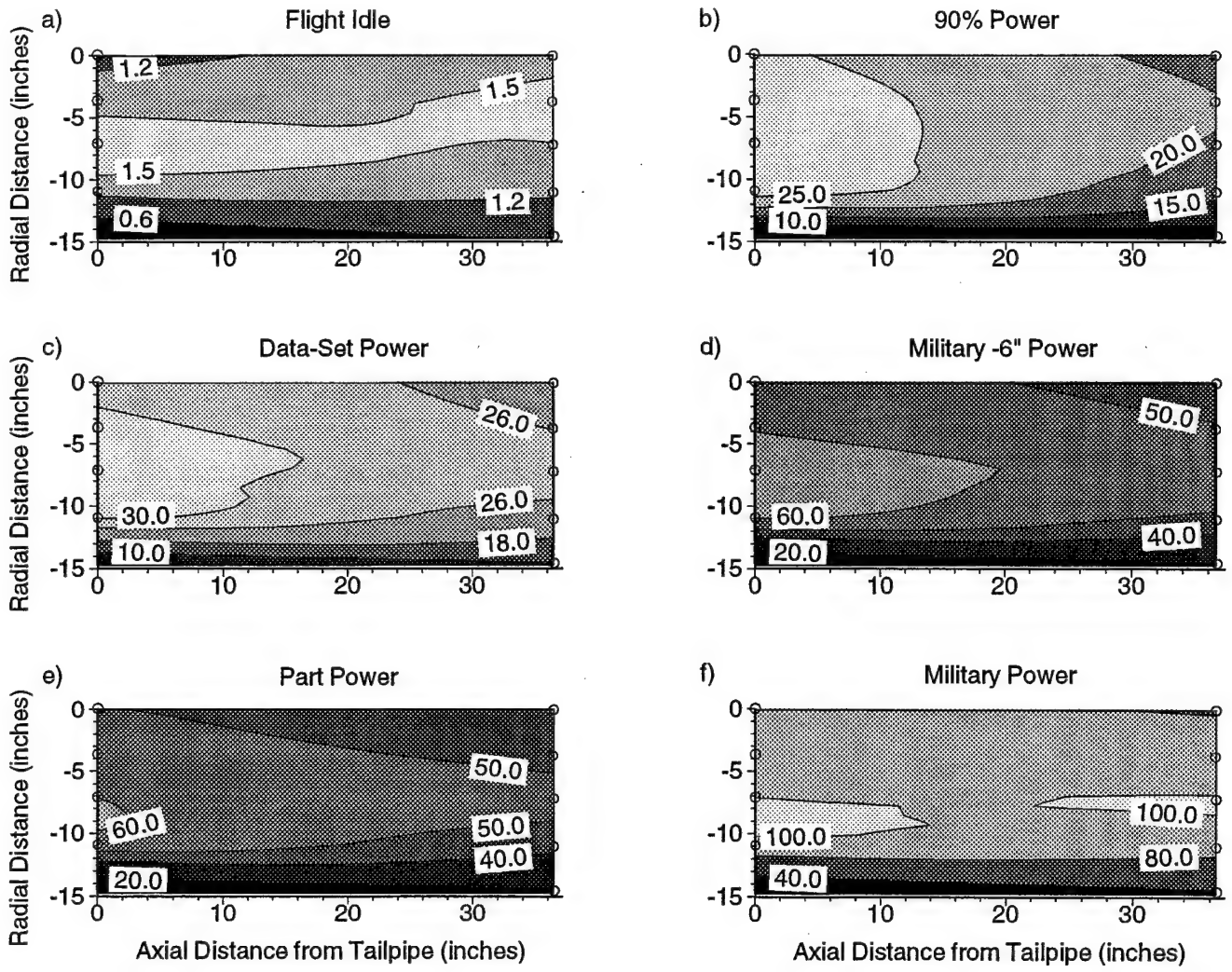

Figure 5.3: TF33-P9 Contour Plots Showing Exhaust NO Concentration (ppm).

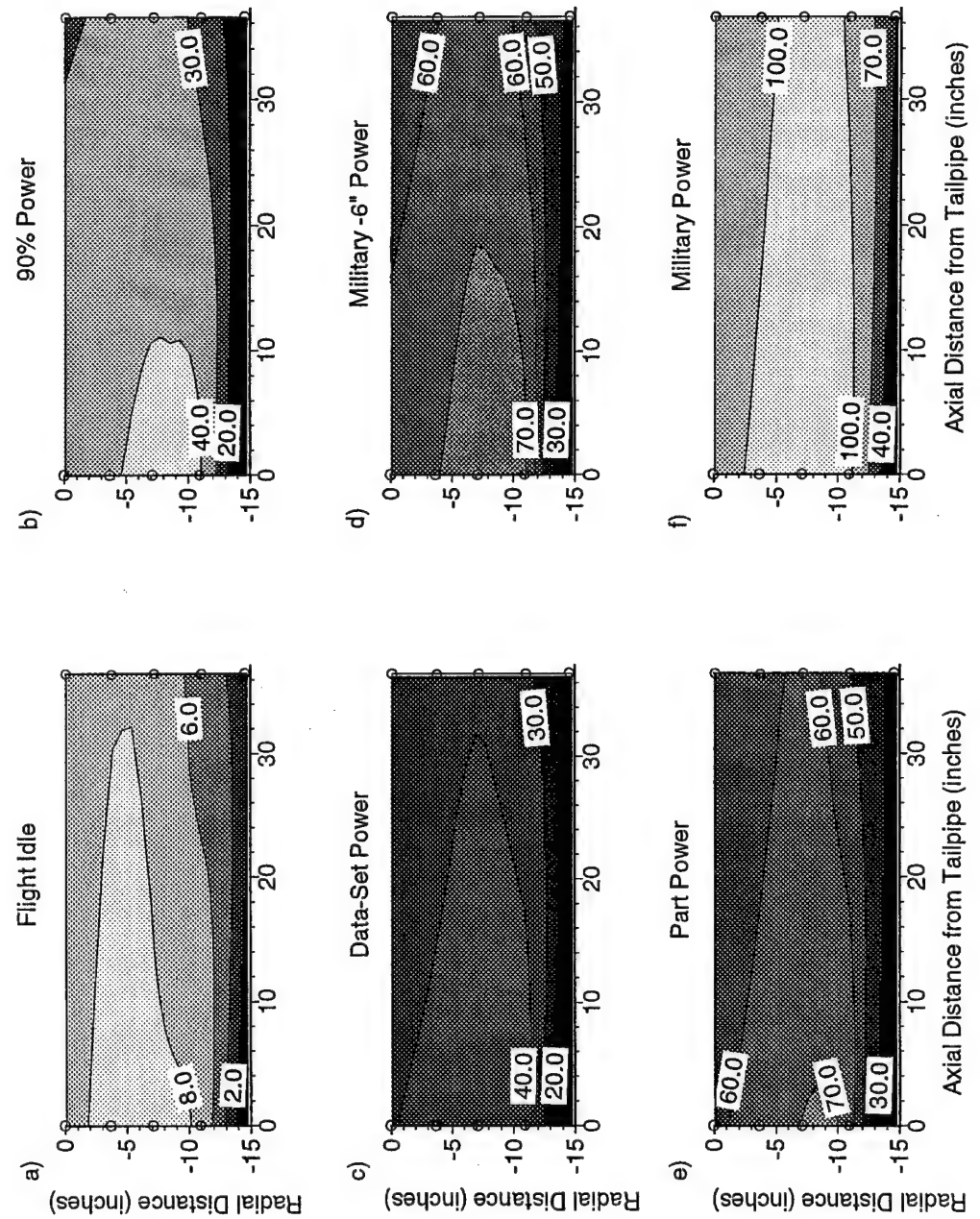

Figure 5.4: TF33-P9 Contour Plots Showing Exhaust NOx Concentration (ppm).

Directs most of the bypass fan air around the engine case, leaving only the exhaust products in the center of the plume. The degree of dilution and mixing that occurs before the converging nozzle results in the distribution of points seen at the exit plane.

The P9 exhaust stream does show signs of dilution over the sampling area, but the degree of dilution is not significant. Table 5.2 shows a 80% jump in the area-weighted NO_x emissions from part power to military power. However, the 88 ppm NO_x produced at peak power is less than half as much as for the P111+ engine.

5.1.2 CO Emissions

The carbon monoxide data illustrated in Figure 5.5 (P111+) and in Table 5.2 (P9) show that as engine speed increases towards military power, CO concentrations decrease. Abnormalities in the midpoint contours seen in Figures 5.5d-f have very little deviation (about 5 ppm, or 6% error) and cannot be considered significant within the resolution of the plots. Overall, the levels of CO are relatively low (under 80 ppm) for powers above idle through military power on both engines. The distribution of CO across the P9 plume are generally similar to the gradients in the P111+ plume.

As the P111+ is accelerated into afterburner, the radial spray bars in the afterburner section begin introducing fuel into the hot exhaust stream. The fuel ignites to produce additional thrust. This inefficient burning process is reflected in the high CO

Table 5.2. TF33-P9 Exhaust Characteristics

	Area-Weighted Average			
Throttle Setting	NO (ppm)	NO_x (ppm)	CO (ppm)	Temp. (°F)
Flight Idle	1.2	5.7	644.9	390
90% Power	15.8	26.2	118.0	543
Data-Set Power	22.0	31.2	107.0	578
Part-Power	41.1	48.8	80.0	666
Military -6" Power	44.5	52.0	88.7	578
Military Power	81.8	87.7	77.9	818

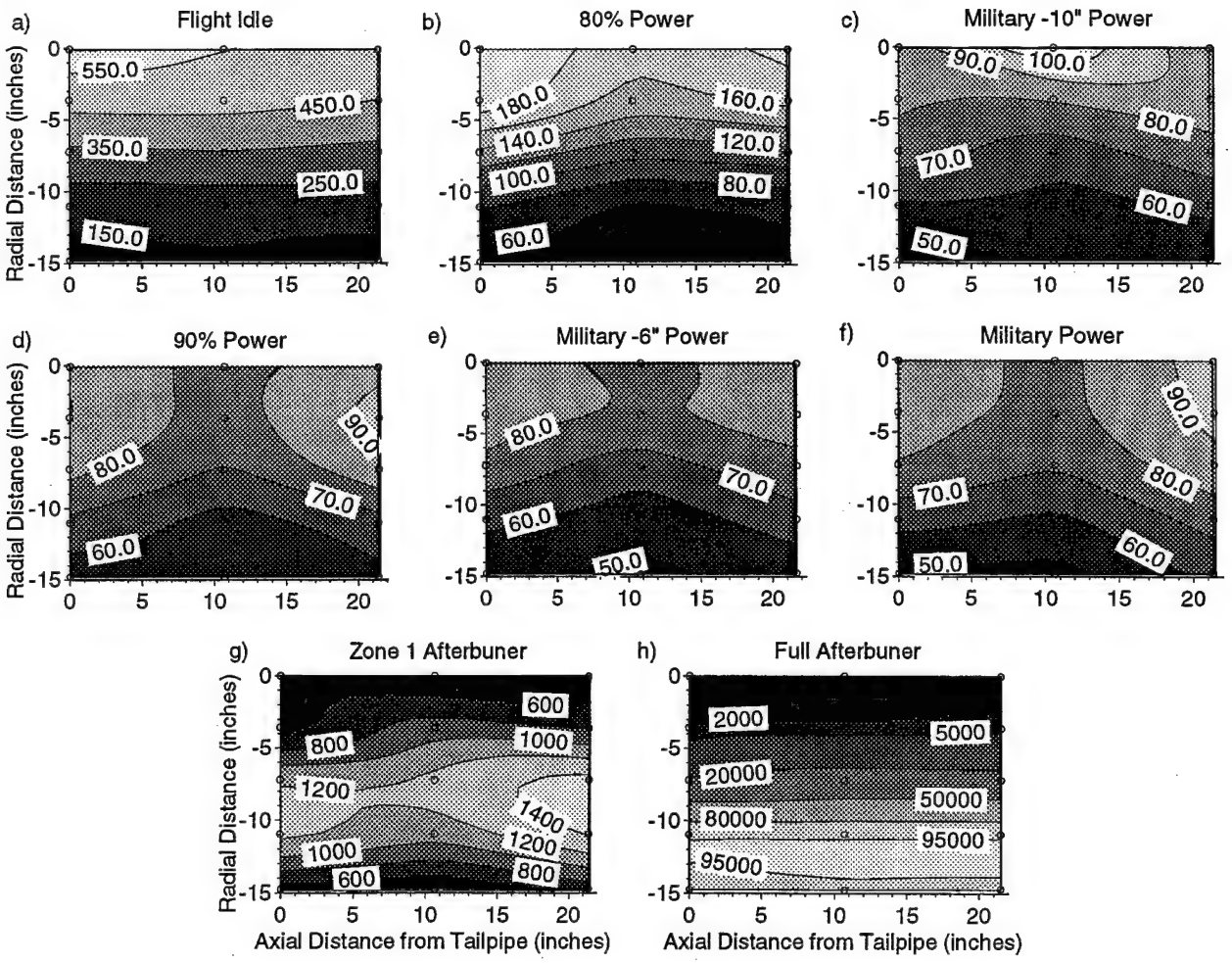

Figure 5.5: TF30-P111+ Contour Plots Showing Exhaust CO Concentration (ppm).

measurements seen in the afterburner power band. Also, a shift in the peak CO readings to the boundary of the exhaust flow occurs due to the geometry of the spray bars. At full afterburner, CO levels are above 9% (90,000 ppm) at the radial extents, whereas the centerline values are below 1000 ppm.

5.1.3 Temperature Profiles

Temperature profiles show a slight dilution effect as the flow proceeds downstream (Figure 5.6). The temperatures increase steadily from 328°F to 723°F through military power, with peak values appearing along the centerline. With the almost 600% increase in fuel consumption from military to full afterburner, temperatures climb above 2800°F. Figure 5.6g shows that as the afterburner ignites, the temperature peaks are shifted radially outward in the flow. Spray bar geometry and the opening of the nozzle, which is closed during the non-afterburning stages, help to create this temperature shift. The hot spot in this plot corresponds to the peak CO concentration in Figure 5.5g. However, the parabolic shapes of the temperature profiles cannot be confirmed within resolution of the sample grid and the contour plot interpolation.

Unlike the P111+, the TF33-P9 engine plume exhibits an even temperature distribution across its nozzle's radius. Peak temperatures at full power are less than 900°F, much lower than the hotter-burning P111+. However, the P9's area-weighted average temperature at military power is 95°F higher than at military power on the P111+ (compare Tables 5.2 and 5.1, respectively).

5.1.4 Run-Time NO and NO_x

Based upon the emissions at each position, the approximate weight of NO and NO_x was calculated using the method shown in Appendix D and multiplied by the fuel consumed. Both NO and NO_x values were then divided through by the highest value to produce the scaled values found in Table 5.3. Military power is seen to be the largest

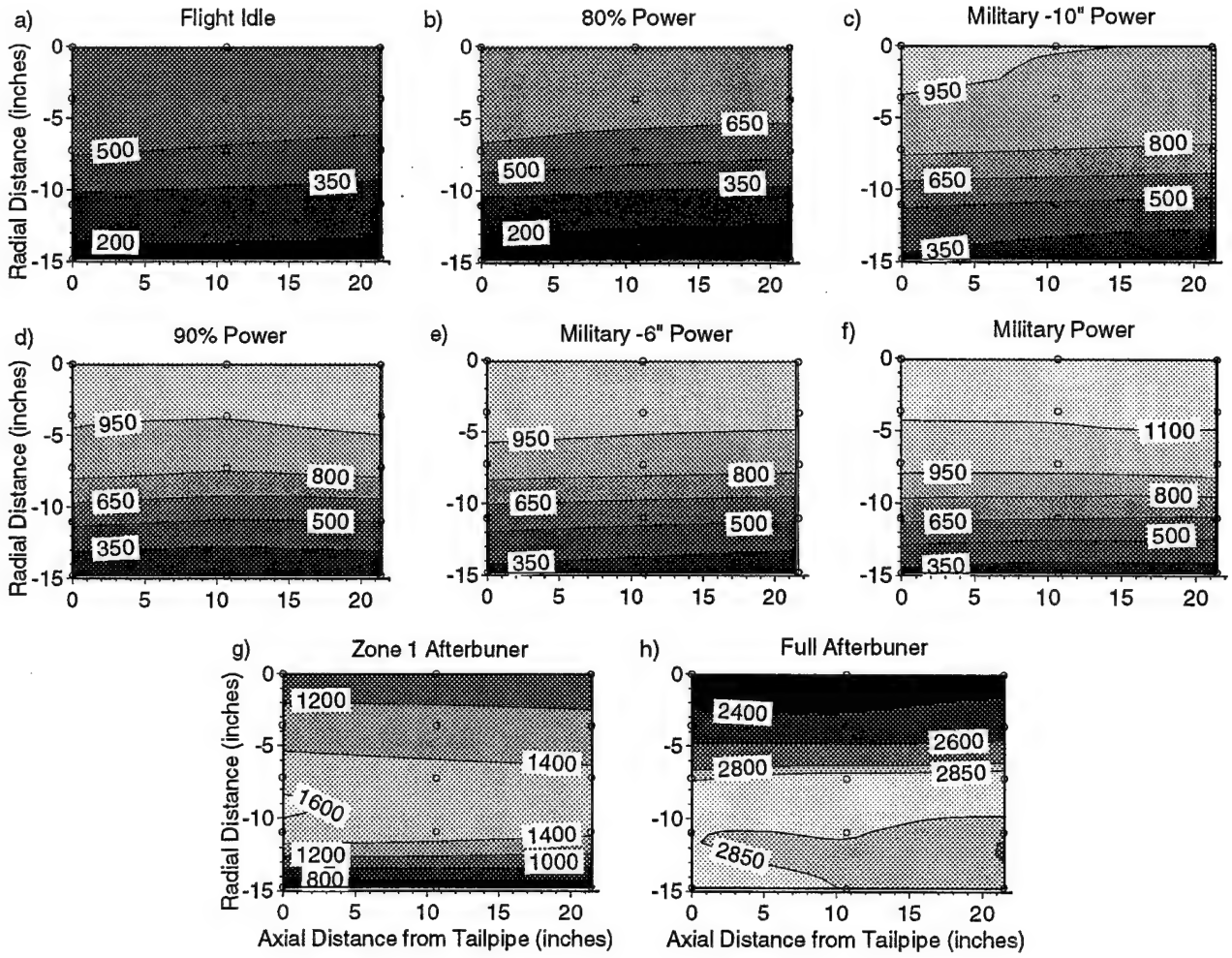

Figure 5.6: TF30-P111+ Contour Plots Showing Exhaust Temperature (F).

Table 5.3. Scaled NO/ NO_x Production per TF30-P111+ Run

	Run Time (min.)	Fuel Usage (lb.)	Scaled NO (lb NO/lb NO)	Scaled NO_x (lb NO_x/lb NO_x)
Flight Idle	17	326	0.01	0.06
80% Power	3	155	0.03	0.05
Military -10" Power	3	327	0.15	0.18
90% Power	3	354	0.19	0.20
Miliatry -6" Power	3	370	0.19	0.21
Military Power	10.25	1606	0.92	1.00
Zone 1 Afterburner	2	465	0.08	0.19
Zone 5 Afterburner	3.5	3138	0.08	0.09
Totals	44.75	6741	1.65	1.98

offender, producing 50% of the total NO_x and 46% of the NO emitted from the JETC during a full testing period. The next highest offenders produce only one quarter of military power NO_x values. Over 95% of the total NO_x emitted is produced between Military -10 inches power and full afterburner settings. Seventy-five percent of all NO and NO_x emissions are produced from military power to full afterburner. This shows that an applied NO_x control system should focus on the higher power settings.

5.1.5 Emissions Summary

The exhaust streams of two engines, one afterburning (TF30-P111+) and one non-afterburning (TF33-P9), were characterized inside a jet engine test cell to determine both exhaust emissions and temperatures at several radial and axial locations. The area of interest lay between the engine nozzle and the mouth of the augmenter. The important general results pertaining to the application of SNCR were the following:

- Power setting of the engine makes a significant impact on the NO and NO_x produced;
- Dilution is noticeable but not significant in the exhaust free stream between the tailpipe exit and the augmenter;

- NO_2 makes up from 2% to 50% of the total NO_x flow field; and
- Carbon monoxide decreases with increasing power for the non-afterburning settings.

The afterburning P111+ engine had the additional characteristics:

- NO_2 at Zone 1 AB makes up a significant fraction (up to 50%) of the NO_x emissions here;
- Peak temperatures range from 1100°F at military power to over 2800°F at full afterburner;
- Levels of CO increase dramatically (peak values in excess of 10%) in the afterburner regions, due to inefficient burning;
- A scaled index for NO_x reveals military power is the highest polluter during a typical engine run. Power settings between Military -10 inches and Zone 1 AB comprise 95% of the total NO_x produced.

The non-afterburning, high-bypass TF33-P9 engine exhaust characteristics were different in the following ways:

- Peak NO_x values reach 117 ppm at military power, almost a third less than for the P111+ at full power; and
- Peak temperatures at military throttle are almost 200°F less than at military power for the P111+.

The results are promising for at least a few of the higher power settings of the P111+. The high amounts of CO emitted from this engine might add to the attraction of the SNCR application. The TF33-P9 had lower peak temperatures and lower CO concentrations than the P111+ at full power, making the application of SNCR more challenging for this engine.

5.2 SNCR Modeling

The results from the JETC experimental work defined the ranges for the conditions considered in the SNCR modeling. A general test matrix of conditions was determined to define the reduction characteristics of different chemicals and additives modeled. Once the attractive chemical combinations are identified, some actual JETC conditions are modeled to demonstrate the potential NO_x reduction.

5.2.1 Test Matrix

Section 5.1.5 discussed the major points of the emissions data collected. Based upon the temperatures seen in traditional SNCR applications (Section 2.4), full military power and Zone 1 afterburner settings on the P111+ engine were chosen to be the focus of the initial chemical kinetic modeling. Table 5.4 lists the exhaust gas composition for each of these power settings. An initial range of parameters was determined to span as many of these data as possible without having to track each point individually. This allows the points around the one of interest to be scanned also to give a more general picture of the trends occurring.

During the engine tests, local centerline velocities of 2000 to 2500 feet per second were measured. These represent a localized velocity centered at the peak temperature of the flow. We were unable to measure bulk velocity for the entire flow. Johnson and Katz (1989) estimated bulk velocities in the augmenter tube to be about 80 feet per second. This calculates to about 0.5 seconds residence time based upon the dimensions of the MAFB augmenter tube. Therefore, this value will serve as a best-case scenario for residence time and should allow sufficient time for the reactions to stabilize.

Chemical injection ratios were chosen based upon previous areas of interest in literature. The Chemkin solver was set up to simulate isothermal conditions where the reactants are perfectly mixed. The parameters and ranges were as follows:

$NO_{initial}$	=	100, 200 ppm
$CO_{initial}$	=	100, 1300 ppm
Temperature	=	800 – 1700°F (100° increments)
Residence Time	=	0.5 seconds
Chemical/NO (NSR)	=	1, 3
Additive/Chemical (ACR)	=	1, 3.

To limit the number of variables in performing the numerical calculations, three fixed values were taken:

$O_{2,\ initial}$	=	18%
$CO_{2,\ initial}$	=	4%
$H_2O_{initial}$	=	3.5%.

Water concentration was determined by the NASA Equilibrium code for the initial conditions being simulated. This initial search served to determine what other throttle settings should be evaluated.

The following subsections discuss the numerical results of the different combinations of NO_x-reducing chemicals and additives "injected" over the range of parameters. The NO_x-reducing chemicals include ammonia, cyanuric acid, urea, and

Table 5.4: JETC Conditions for SNCR Modeling

	Position inches	Temperature °F	NO ppm	NO_2* ppm	CO ppm	CO_2 %	O_2 %
Military Power	0.00	1107	246.7	36.6	89.4	2.4	16.64
	-3.63	1123	249.4	38	89.4	3.65	16.71
	-7.31	1019	180	47.3	84.1	1.8	17.57
	-11.00	680	92.3	13.9	69.6	0.89	19.29
	-14.75	326	11.4	2.6	54.2	0.16	20.53
Zone 1 Afterburner	0.00	1173	161.3	96.8	471.4	3.61	16.68
	-3.63	1218	172	99.1	473.5	4.14	16.25
	-7.31	1602	129.7	120.1	1239.7	4.38	14.31
	-11.00	1623	48.4	87.4	1326.7	3.78	15.71
	-14.75	772	5	30.5	529.8	1.23	19.42

*NO_2 is assumed to be the difference of the measured NO_x and NO concentrations.

hydrazine. Additives modeled include hydrogen, methane, and hydrogen peroxide. For simplicity, only NO_x reduction is reported graphically in the text. A complete set of plots showing all Chemkin results, including final concentrations of NO_2, N_2O, CO, chemical slip, and additive slip, are located in Appendix E. The plots depict the final concentrations at the end residence time (0.5 seconds) for the fixed (*e.g.*, O_2, CO_2, and H_2O concentrations) and variable conditions indicated.

5.2.2 Chemical Injection Only

Ammonia (NH_3): The NO_x results for the ammonia case are plotted in Figure 5.7. The *y*-axis, "% NO_x Reduction," is defined as

$$\%\ NO_x\ \text{Reduction} = 100 \times \left[1 - \left(\frac{NO_f + NO_{2,f} + N_2O_f}{NO_i} \right) \right] \qquad (5.1)$$

where 100% reduction is the best achievable goal, subscript *I* indicates initial concentrations and subscript *f* indicates final concentrations.

By looking at reduction as a function of total NO_x, the results take into account conversions from NO into NO_2 and from NO into N_2O. These represent only internal changes in the form of NO_x, and no change in the total NO_x concentration.

The first observation is that NO_x reduction increases as increasing amounts of NH_3 are injected. Peak levels of reduction in the cases considered were above 55%, some being as high as 85% NO_x reduction. However, not all of the ammonia reacts at the optimum temperature, resulting in unwanted slip. The increase in ammonia also results in a broader temperature window (defined here as the temperature range for which NO_x reduction exceeds 50%). The largest temperature window spans over 225°F (Figure 5.6, case 4). Optimum temperatures ranged from 1300 to 1600°F, with temperature windows beginning as low as 1275°F for high initial CO levels (Figure 5.7, cases 6 and 7). At lower levels of initial NO, slightly decreased levels of NO_x reduction are evident.

The addition of CO shifts the reduction window to lower temperatures, but optimal NO_x reduction decreases by 5 to 15% and the temperature window narrows. Increased CO also causes a steep drop in peak NO_x reduction at the high end of the temperature window. Since ammonia levels go to zero at the upper end of the temperature window, conversion of ammonia into NO via the alternate mechanistic pathway is evident. When CO_i equals 1300 ppm, final levels of total NO_x exceed initial levels at temperatures between 1460–1650°F (indicated by negative reduction values). In all numerical cases shown in Figure 5.7, CO levels decrease sharply from the initial concentration of CO to sub-10 ppm levels by 1500°F.

As expected, ammonia reduction coincides with the onset of NO_x reduction. At the middle of the temperature window, NH_3 can reach levels below 10 ppm under the proper conditions. In the cases where the initial CO concentration equals 100 ppm, NH_3 is almost depleted at the optimum NO_x reduction temperature. High levels of CO demonstrate the ability to shift the temperature window so that ammonia levels can be as high as 150 ppm (50% of the initial concentration) at the optimum temperature (Figure 5.7, case 6).

For NO_x reduction temperatures on the low-temperature side, levels of NO_2 and N_2O rise slightly due to low-temperature NO conversion. This is most noticeable in the higher NH_3 injection cases (where NSR = 3). NO_2 and N_2O also rise with increased CO at these lower temperatures. Peak concentrations of NO_2 and N_2O do not exceed 30 ppm at any time for any of the cases shown in Figure 5.7 and are less than 10 ppm whenever initial CO concentrations equal 100 ppm.

Cyanuric Acid ($(HOCN)_3$ or CA): Cyanuric acid has much different performance characteristics from those of ammonia over the range presented in Figure 5.8. Recall that cyanuric acid breaks down to isocyanic acid (HNCO) before reacting with NO, so it is actually HNCO that is modeled here (see Section 2.4.2). Reduction levels for CA are much lower than for ammonia, with only two conditions having greater than 50%

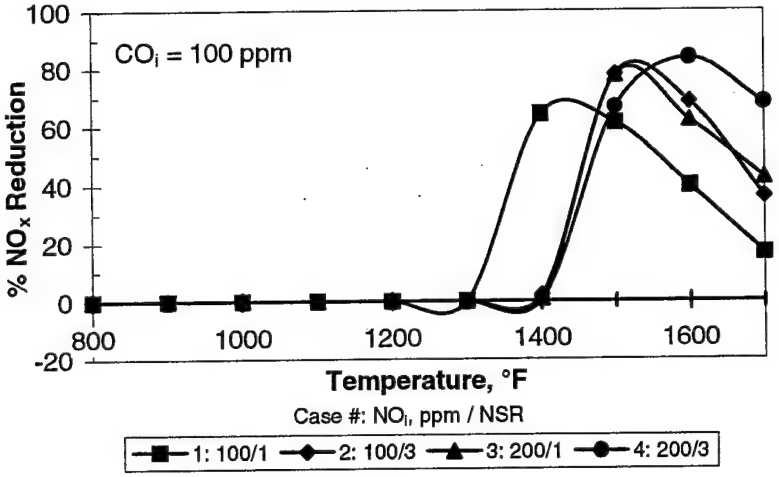

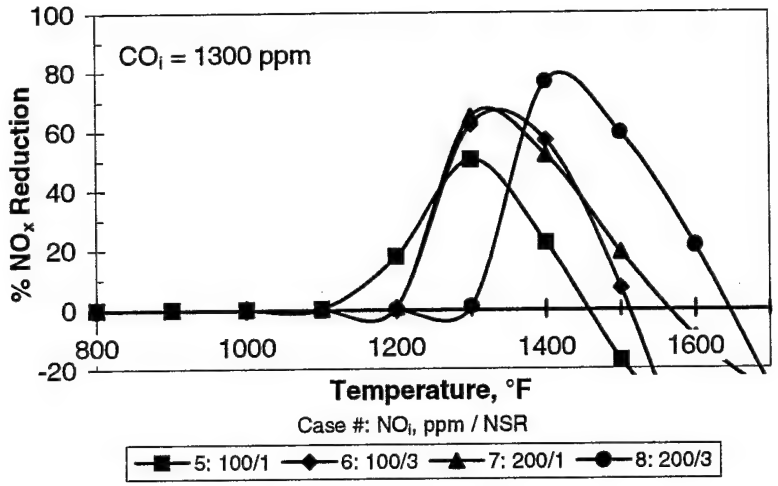

Figure 5.7: Effective NO_x Reduction using Ammonia.

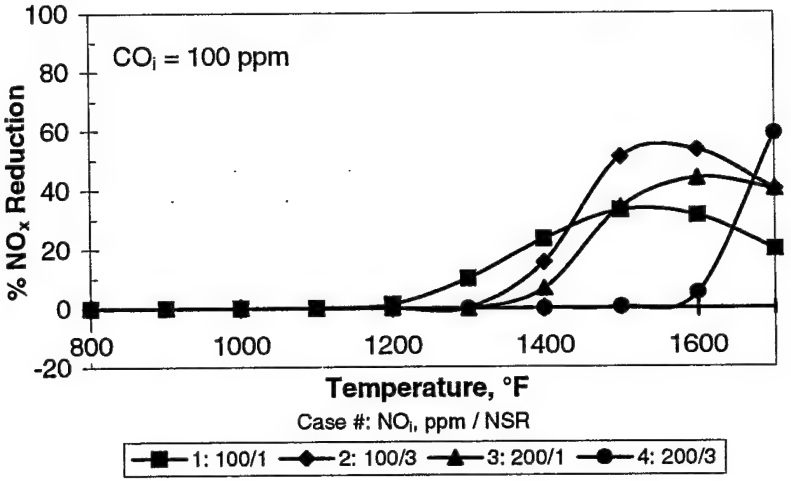

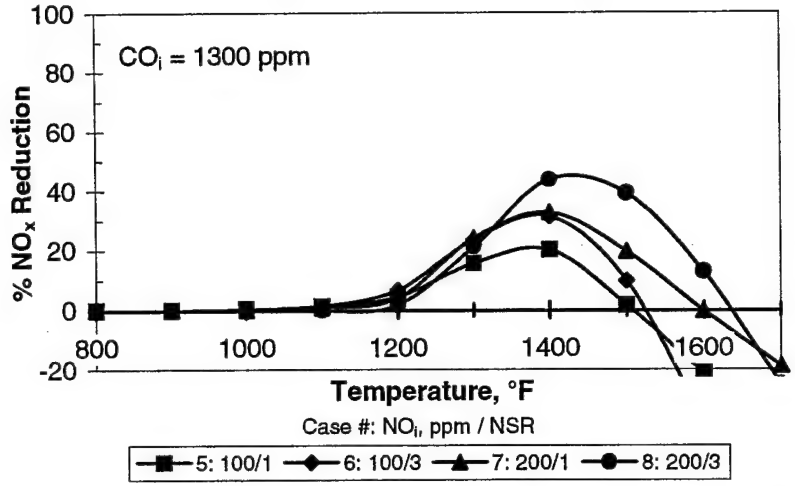

Figure 5.8: Effective NO_x Reduction using Cyanuric Acid.

reduction. These low levels of NO_x reduction are the result of high NO_2 and N_2O concentrations, reaching as high as 60 and 100 ppm, respectively, for cases 5 and 8 in Figure 5.8. The conversion of NO into NO_2 at low temperatures is more prevalent at higher initial CO concentrations. Nitrous oxide concentrations also rise when initial CO is increased from 100 ppm to 1300 ppm.

HNCO slip levels tend to be higher than NH_3 slip levels at higher process temperatures. At the optimum temperature, 25 to 50% of the injected HNCO remains. Increasing the NSR significantly increases the reduction abilities of CA at the cost of a 100 to 200% increase in HNCO slip at the optimum temperature (up to 150 ppm for Case 8 in Figure 5.8).

Urea ($(NH_2)_2CO$): Urea is modeled as a co-injection of equal amounts of NH_3 and HNCO as discussed in Section 2.4.2. The Chemkin simulation shows that NH_3 generates radicals quicker than HNCO, which results in higher HNCO slip levels at a given temperature. In the cases where NSR equals one, NH_3 and HNCO levels at the optimum temperature are less than 5 ppm and 75 ppm, respectively. At an NSR value of three, slip levels of both chemicals are much higher (both concentrations are well over 100 ppm in Figure 5.9, cases 2/6 and 4/8).

The increase in initial urea concentration results in only a slight change in NO_x reduction (less than 10% either way) The temperature windows available with urea injection are less than or equal to those of ammonia, ranging from 125 to 225°F. Again, the NO_x reduction values are hindered by the increased amount of N_2O present at the final time as the condition temperatures increase.

N_2O levels are similar to those seen for cyanuric acid with peak levels being slightly lower (less than 85 ppm for the worst case; Figure 5.9, case 8). The N_2O curve remains flat and at a sustained level throughout the range. The production of N_2O and NO_2 is more affected by increasing the initial CO concentration and/or increasing the NSR than by changing the process temperature. N_2O levels for urea remain below 40

ppm for cases where initial NO, initial CO, and NSR levels are high (Figure 5.9, case 8; 85 ppm N_2O). NO_2 levels remain below 50 ppm in all cases.

Hydrazine (N_2H_4): Hydrazine demonstrates the highest potentials for NO_x reduction (92%) and N_2O production (160 ppm) of the four chemicals tested (Figure 5.10, cases 4 and 8, respectively). In all cases, N_2O levels peak when temperature is 1300°F, resulting in the "saddles" seen in the NO_x reduction curves. The low initial CO cases demonstrate a broad temperature window (225°F to over 300°F). When the initial CO concentration is raised, it shifts the temperature windows as with the other chemicals. However, its presence severely hinders the NO_x reduction process. Not only are the temperature windows much broader (300°F to over 550°F), many cases have a peak of maximum reduction that will plateau for several hundred degrees, a characteristic not seen by the other chemicals. NO_2 levels are also low, never exceeding 15 ppm over the range.

Another concern when using hydrazine, besides its high N_2O production, is the creation of NH_3. At an NSR value of three, ammonia concentrations can reach as high as 460 ppm at temperatures just below the temperature window (Figure 5.10, case 8). Ammonia levels are significantly less (less than 125 ppm) at low NSR levels, accompanied by a shifted temperature window with slightly lower reduction levels. For an NSR of one, ammonia concentrations reach about two-thirds of the initial NO levels while peak N_2O levels are half of the initial NO concentrations. Ammonia levels are further retarded at high CO levels. Previous research has demonstrated that it is possible to control high ammonia exhaust levels through post-process clean-up using additional chemical injection (*e.g.*, methane) downstream of the initial injection (Sowa, 1992). However, it is not possible to scrub out N_2O in the exhaust products with either chemicals or water.

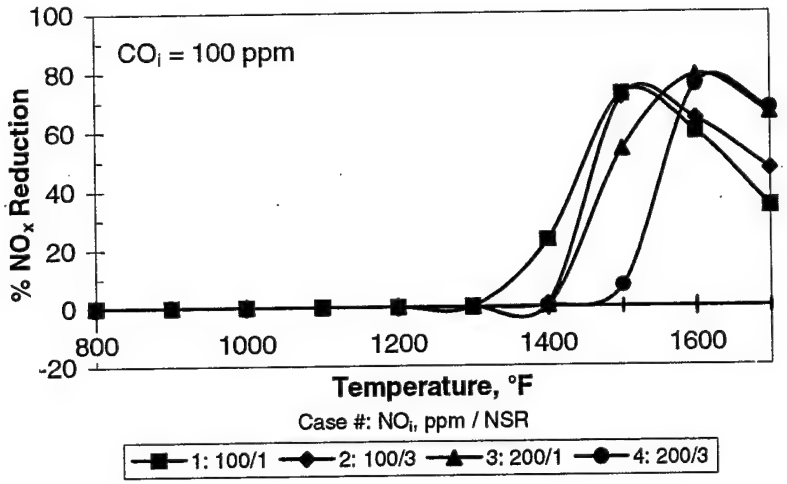

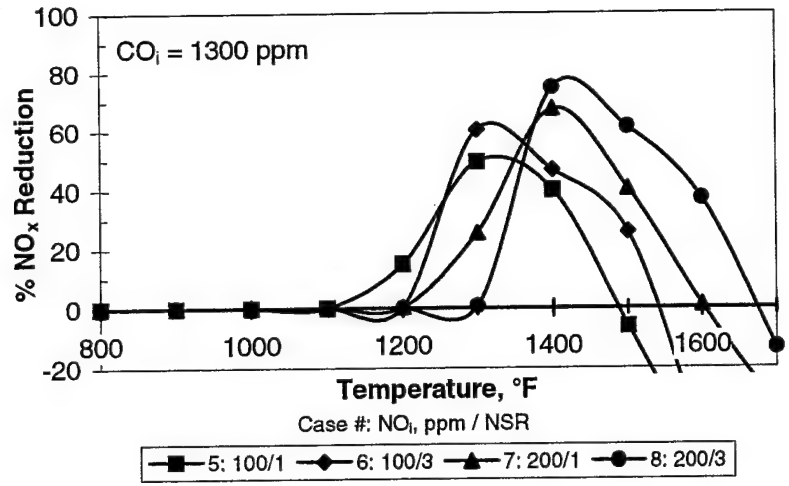

Figure 5.9: Effective NO_x Reduction using Urea.

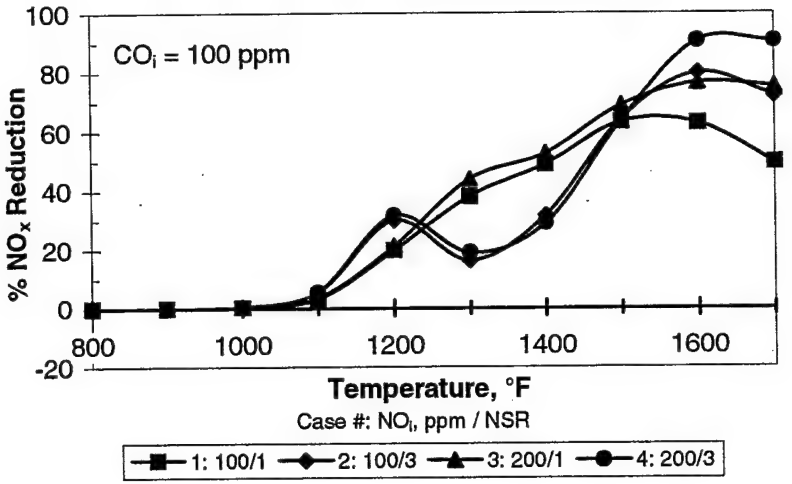

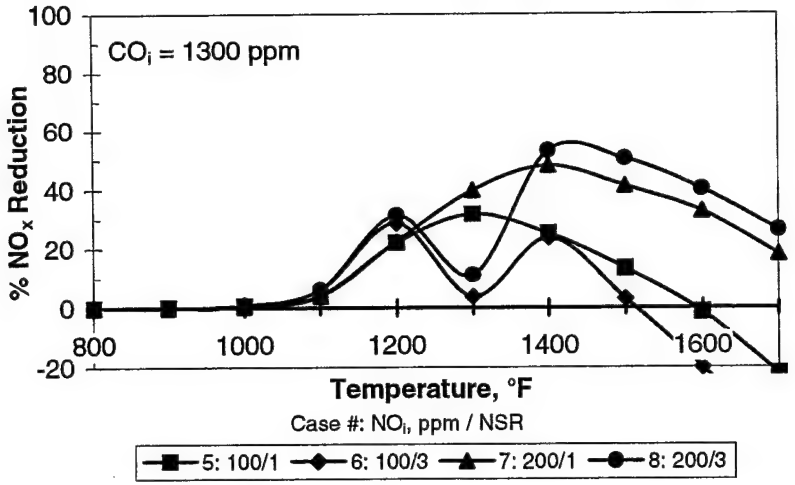

Figure 5.10: Effective NO_x Reduction using Hydrazine.

5.2.3 The Effect of Additives

As described in Chapter 2.4.2, additives are used to enhance the reducing characteristics of SNCR chemicals. Usually, additives are sought that will shift the temperature window down while maintaining optimal reductions. To help evaluate which additives are better than others, the following criteria were used to establish a comparison of the co-injection of additive and chemical versus the injection of the chemical only (baseline cases 1–8):

- NO_x reductions should be close to or greater than the chemical-only levels;
- Additive injection should shift down and/or broaden the temperature window;
- The resulting chemical slip should be no more than that for baseline processes; and
- Emissions of NO_2 and N_2O should be kept to a minimum.

To simplify the evaluation, only the cases with initial NO concentrations of 200 ppm are considered since this is where the greatest chemical slip occurs. (NO_i = 100 ppm and 200 ppm cases are included in Appendix E.) This section examines the additives hydrogen, methane, and hydrogen peroxide as modifiers to the baseline chemicals.

Hydrogen (H_2): The NO_x reduction plots for hydrogen addition are shown in Figures 5.11–5.14. In general, H_2 shifts the temperature windows down by 50°F to 200°F. Most conditions see small changes (both positive and negative) in peak NO_x reductions, usually ranging from 0% to 10% in either direction.

Figure 5.11 shows that hydrogen addition with ammonia increases the amount of reduction by as much as 10% and that it can shift the beginning of the temperature window down by 350°F (Figure 5.11, case 11). The resulting temperature windows are narrower than those of the baseline cases, extending no more than 250°F. The low NSR

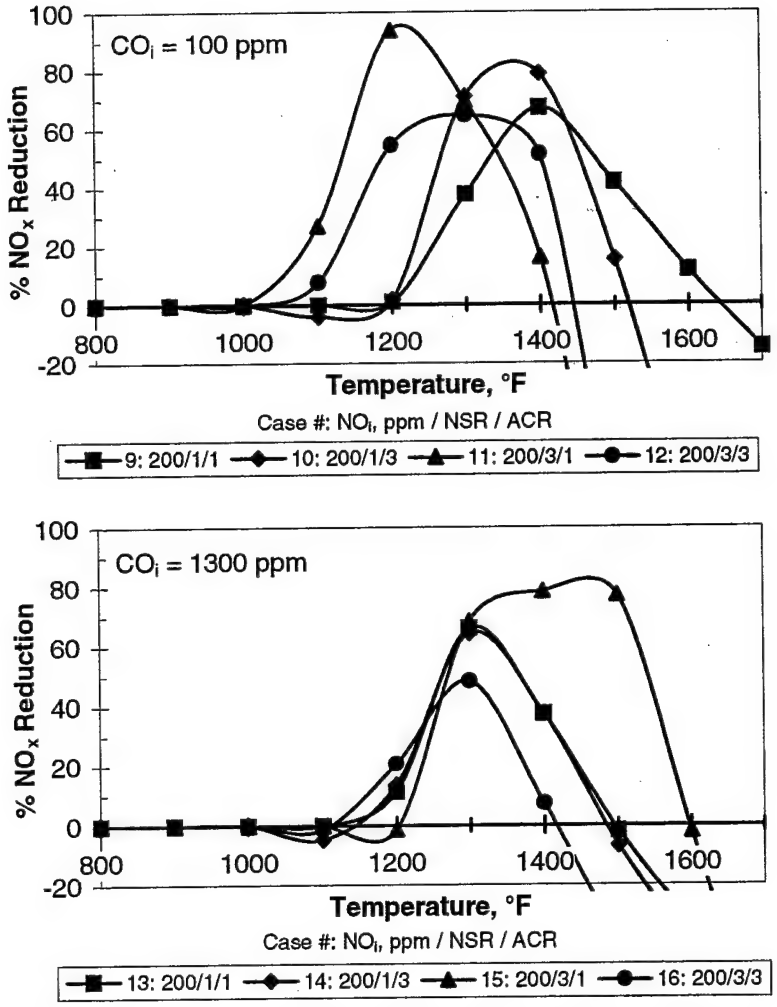

Figure 5.11: Effective NO_x Reduction using Ammonia with Hydrogen Additive.

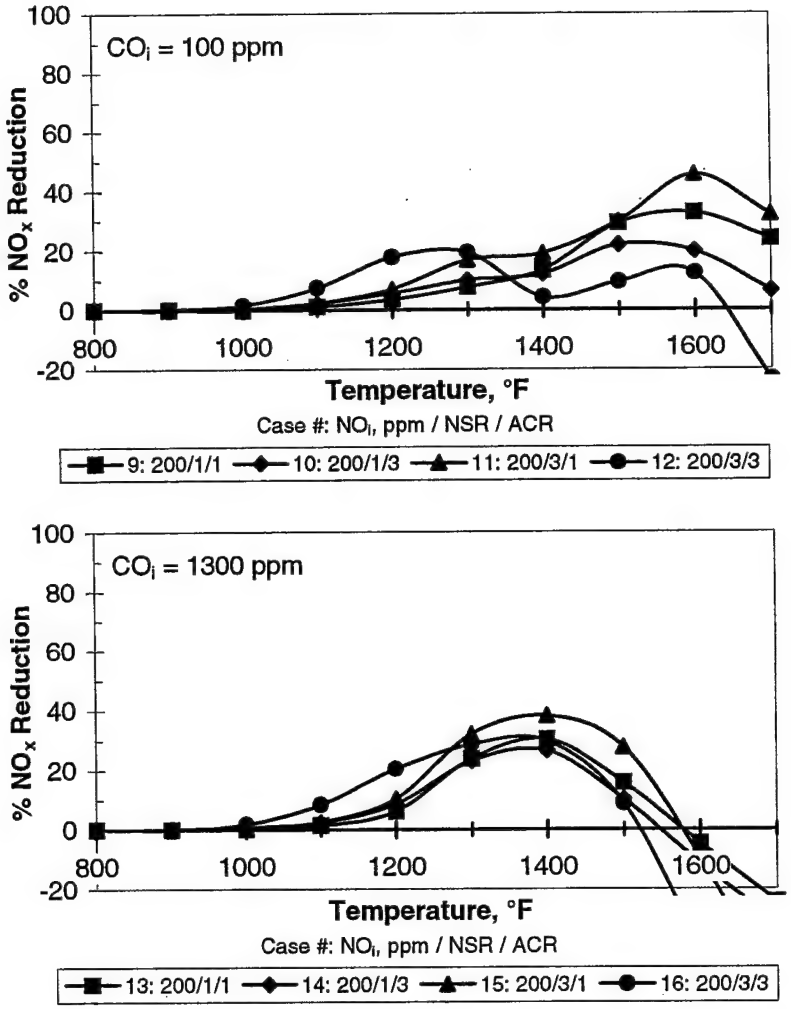

Figure 5.12: Effective NO_x Reduction using Cyanuric Acid with Hydrogen Additive.

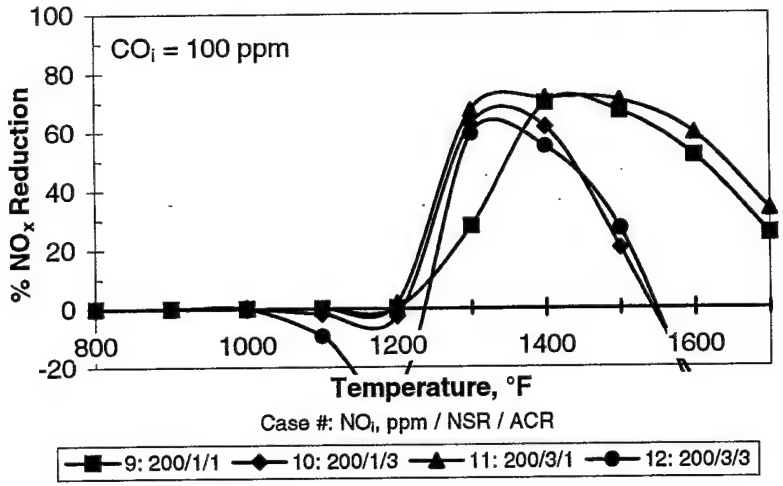

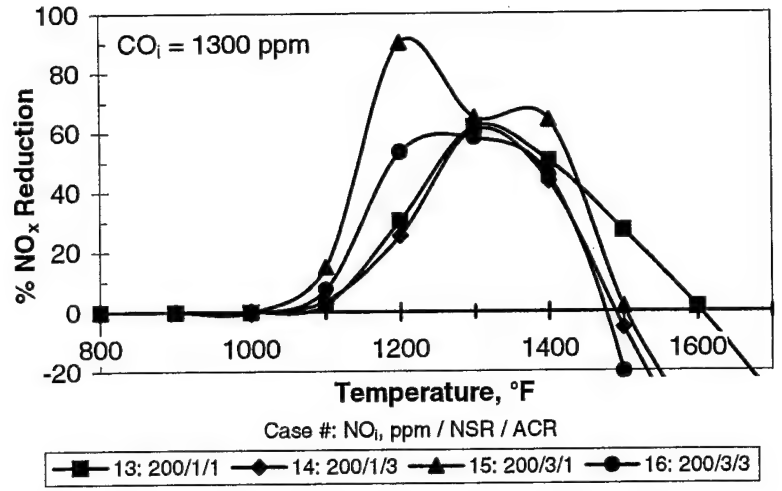

Figure 5.13: Effective NO_x Reduction using Urea with Hydrogen Additive.

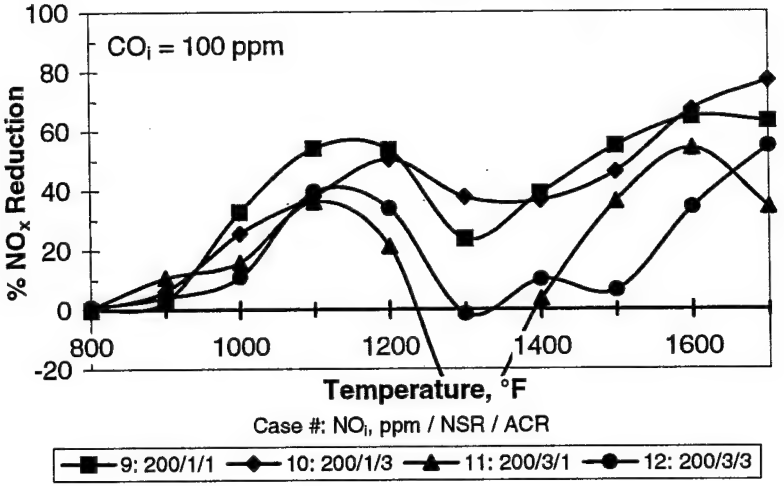

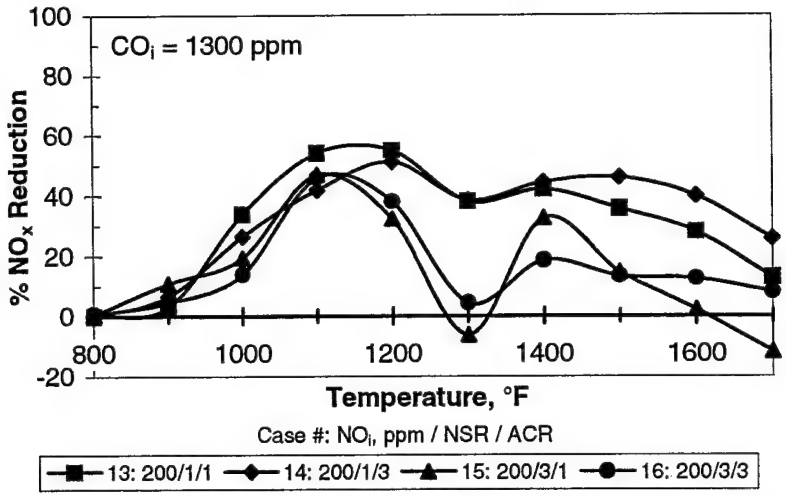

Figure 5.14: Effective NO_x Reduction using Hydrazine with Hydrogen Additive.

cases (9/13 and 10/14 in Figure 5.11) have ammonia slip levels similar to the baseline cases at the beginning of the temperature window. However, NO_2 and N_2O levels are higher than the baseline conditions, reaching as high as 70 ppm (case 14) and 40 ppm (case 15), respectively. The main point to note in Figure 5.11 is this: the hottest temperatures seen at both engine power settings (1100°F for military power and 1600°F for Zone 1 AB) are out of the applicable temperature windows for these conditions using NH_3 and H_2 (cases 9–12 for military power and cases 13–16 for Zone 1 AB).

Figure 5.12 shows that adding hydrogen to cyanuric acid brings the NO_x reduction levels down further. The maximum reduction possible for these combinations is 45%, but most fall below 25% NO_x reduction. Even so, peak NO_x reductions are centered at about 1600°F for the low-CO case and 1400°F for the high-CO case, making applications to the JETC conditions difficult. H_2 does little to shift the temperature window for NO_x reduction. However, NO_2 and N_2O form at much lower temperatures than for the baseline, chemical-only injection.

In Figure 5.13, coaddition of urea and hydrogen achieves high NO_x reductions (60% to 90%) and low, broad temperature windows extending up to 375°F (*e.g.*, Figure 5.13, case 11). Unlike the previous two chemicals, hydrogen addition results in a range of up to 200°F where optimal reduction levels are sustained, shown again by case 11, where NSR equals three. However, high NSR causes high slip levels of HNCO and NH_3 and produces copious amounts of N_2O (*e.g.*, case 12/16 where N2O ≈ 150 ppm).

Hydrogen addition with hydrazine extends NO_x reduction to temperatures below 1000°F in all cases (Figure 5.14). A "saddle" is seen centered at 1300°F in the NO_x reduction curve that is more distinctive than for the baseline case. The peak N_2O concentration that coincides with this saddle remains unchanged (as does NO_2) from the baseline cases. The appearance of a second, low-temperature window as well as the lower NO_x reduction levels account for its prominence. The high-NSR cases are relatively uninteresting due to the low NO_x reduction and high slip values.

Methane (CH_4): The addition of methane to the flow does not promote the SNCR reduction process as hydrogen does for ammonia, cyanuric acid, and urea (Figures 5.15–18). NO_x reduction levels are lower in most cases than those seen for hydrogen addition. Instead of converting nitric oxide into nitrogen, methane promotes conversion into NO_2 at lower temperatures. This is especially evident for HNCO, for which conversion nears 100% in the high-ACR cases (Figure 5.16, cases 19/23 and 20/24). Also, more N_2O is formed using methane versus hydrogen (about 50% more). Thus, the potential of the broad reduction curves noted in some cases is lost by the lower reduction levels resulting from the conversion of one oxide of nitrogen into another.

The model also shows that CO is produced at low temperatures for NH_3, HNCO, and urea. This trend is not observed for hydrogen addition or for any of the chemical-only injections. Methane generates more necessary radicals for CO production as the initial NSR and ACR are increased, creating several hundred parts per million of new CO at these conditions.

Peak NO_x-reduction levels using hydrazine remain fairly immune to injected methane (Figure 5.18). The formation of N_2O at 1300°F hinders the NO_x reduction process severely, and results in a slight shift upward in the optimum temperature window. Unlike the case during hydrogen addition, the NO_x reduction curves remain fairly consistent with the baseline case. The only noticeable change is that NO_2, N_2O, and NH_3 emissions remain high over several hundred degrees of temperature range versus the sharp peaks of the baseline case. The bottom line is that methane as an additive does not perform favorably for the conditions tested.

Hydrogen Peroxide (H_2O_2): Hydrogen peroxide addition severely alters the shapes of the NO_x reduction curves from the baseline conditions due to the abundance of OH radicals generated. The most noticeable aspect seen when comparing Figures 5.19 through 5.22 is the relatively flat NO_x reduction curve for ammonia, urea, and hydrazine

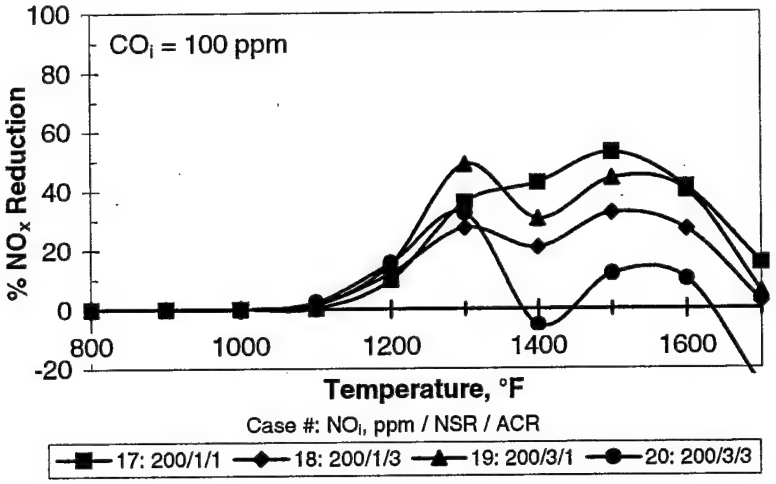

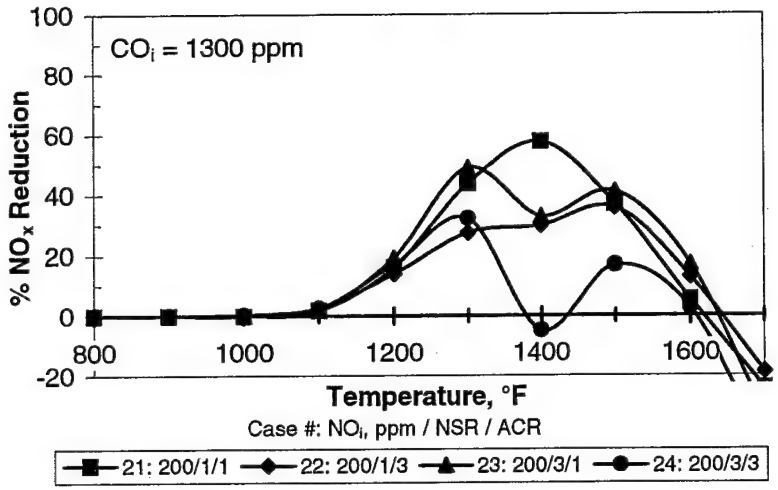

Figure 5.15: Effective NO_x Reduction using Ammonia with Methane Additive.

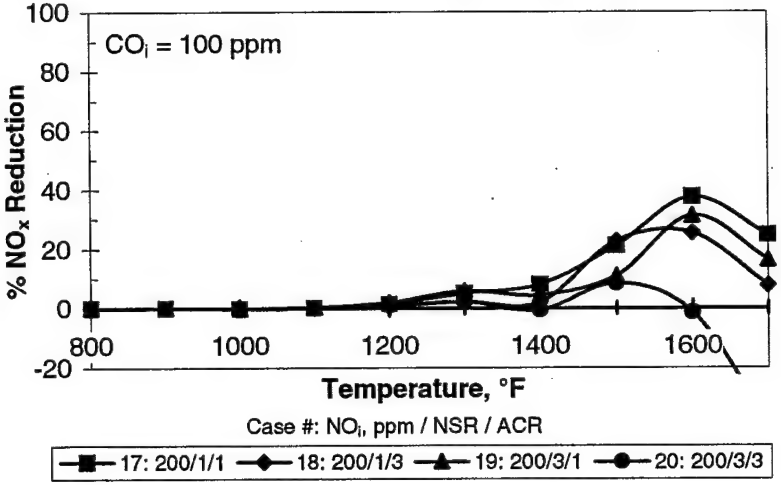

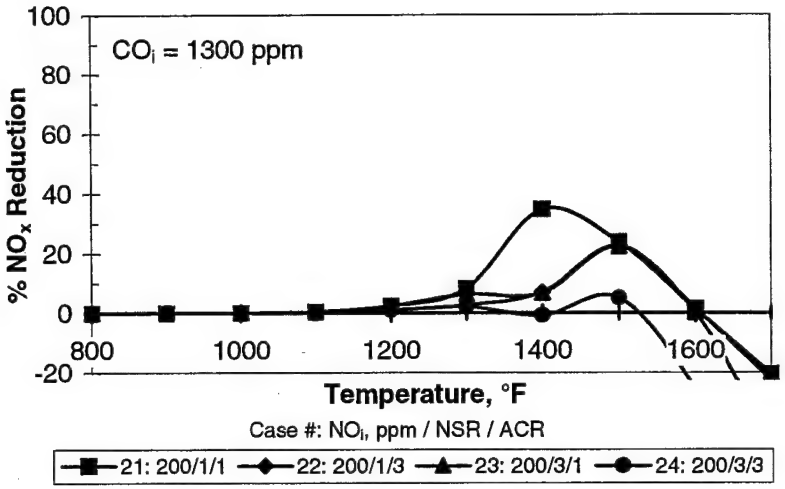

Figure 5.16: Effective NO_x Reduction using Cyanuric Acid with Methane Additive.

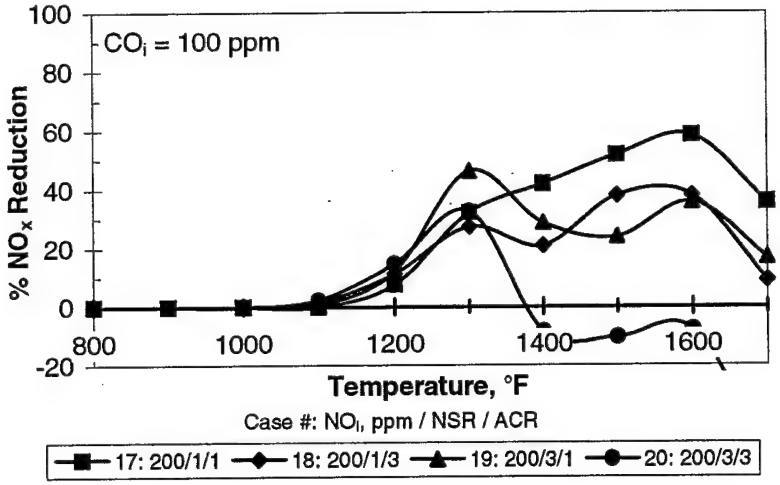

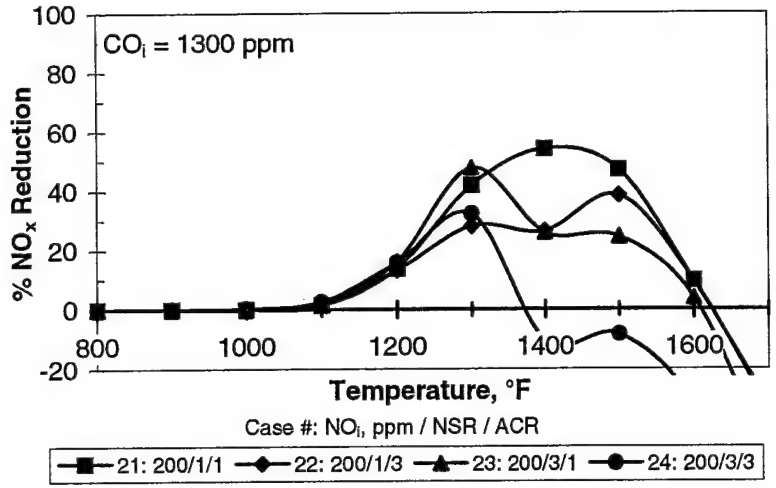

Figure 5.17: Effective NO_x Reduction using Urea with Methane Additive.

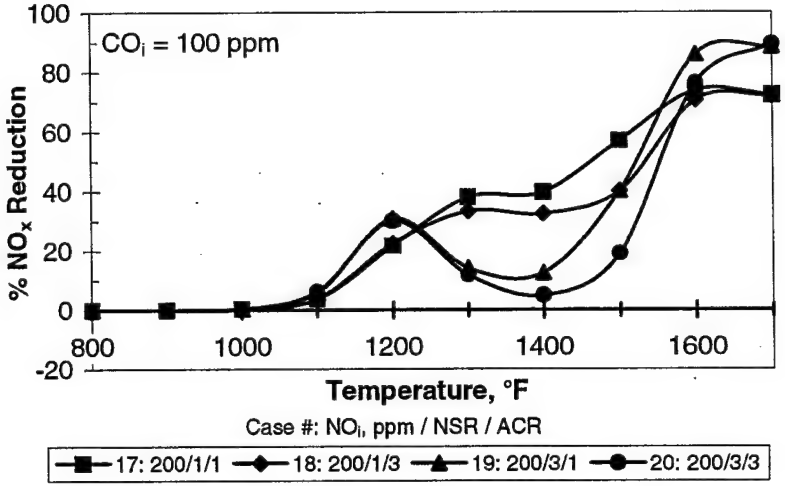

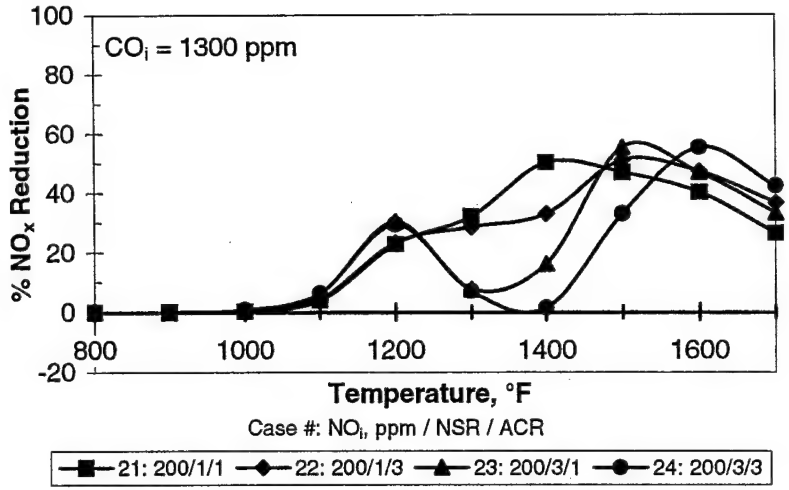

Figure 5.18: Effective NO_x Reduction using Hydrazine with Methane Additive.

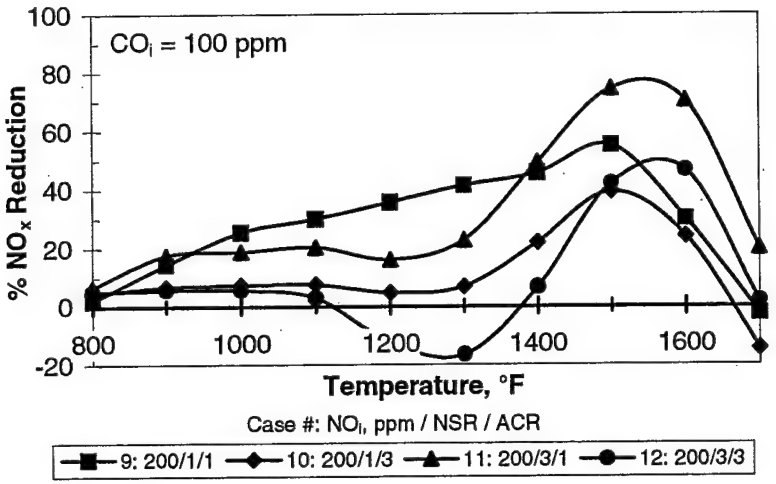

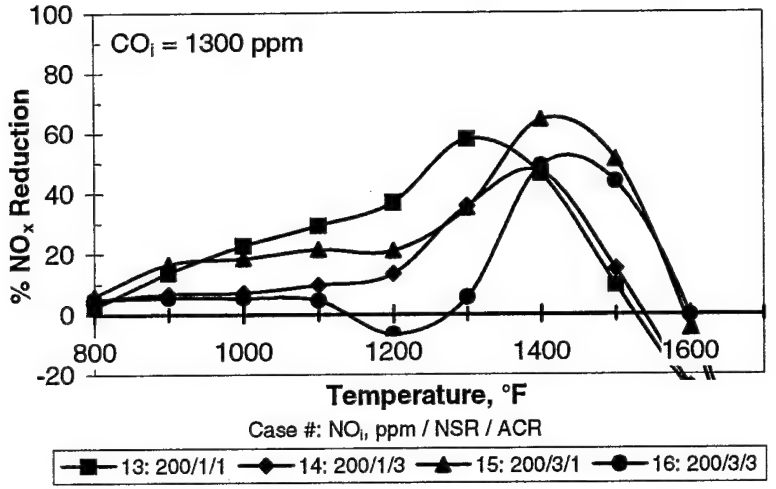

Figure 5.19: Effective NO_x Reduction using Ammonia with Hydrogen Peroxide Additive.

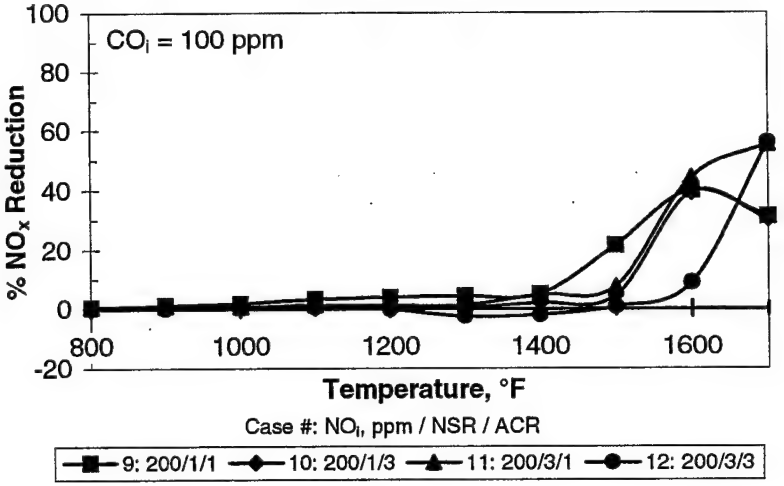

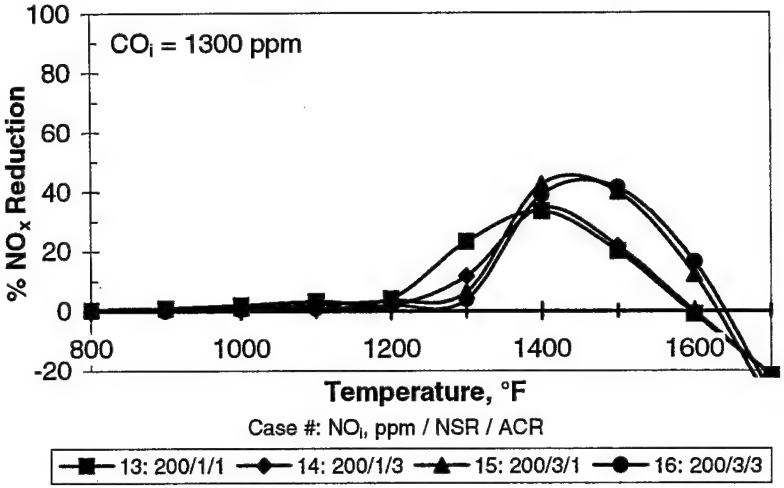

Figure 5.20: Effective NO_x Reduction using Cyanuric Acid with Hydrogen Peroxide Additive.

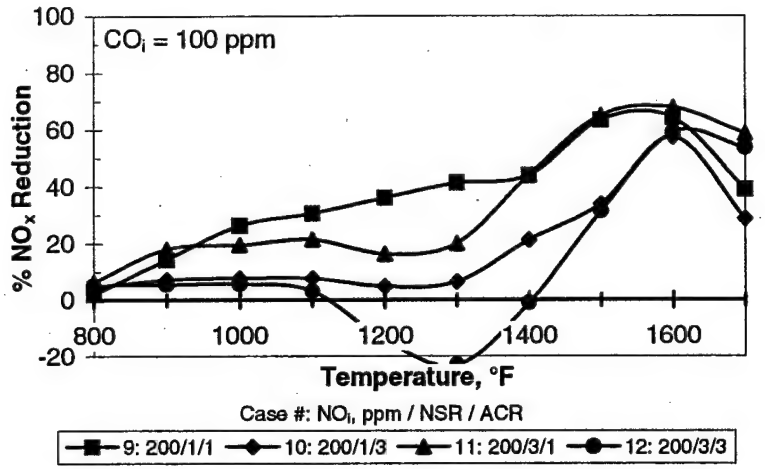

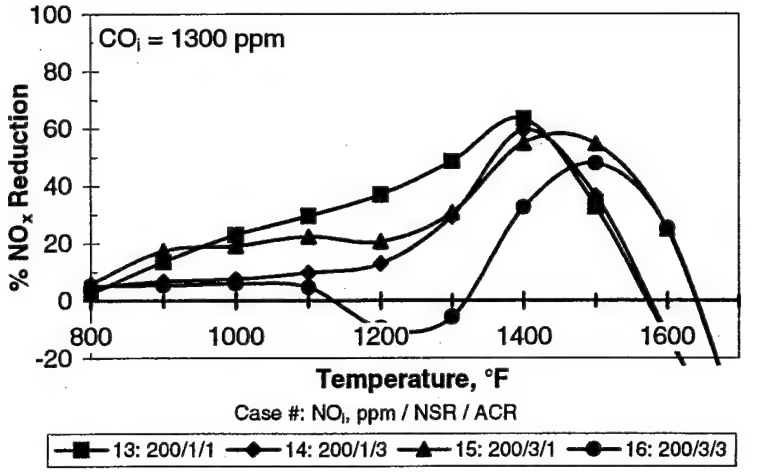

Figure 5.21: Effective NO_x Reduction using Urea with Hydrogen Peroxide Additive.

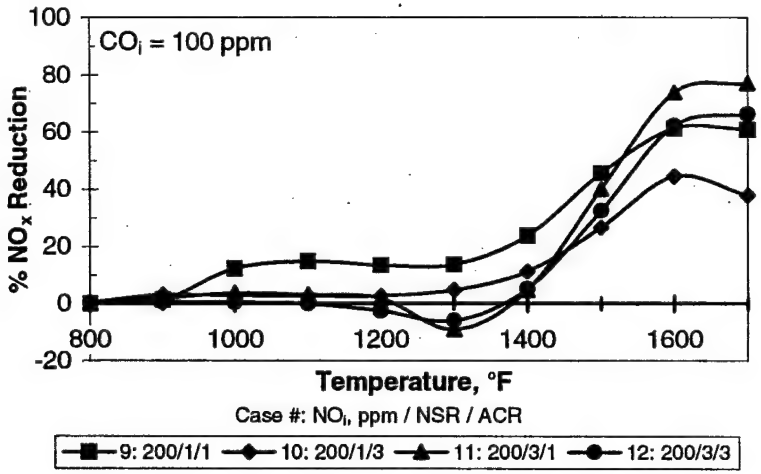

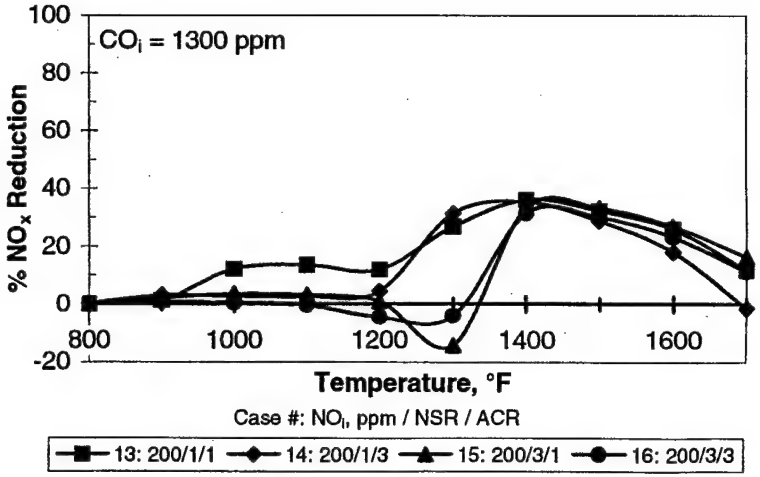

Figure 5.22: Effective NO_x Reduction using Hydrazine with Hydrogen Peroxide Additive.

when NSR equals one. Ammonia and urea in particular have windows of NO_x reduction that remain over 30% for a range of 500°F of more (Figures 5.19 and 5.21, case 9). The significance of this in relation to a JETC is the ability of one condition to reduce NO_x over a steep radial temperature gradient and/or in a non-isothermal system where downstream temperature varies.

NO_x reduction levels suffer noticeably (as does the temperature window) when more H_2O_2 is initially added to the systems. Again, this is due mostly to the NO-to-NO_2 and NO-to-N_2O conversions that are strongly promoted as additive concentrations increase. Reduction levels are suppressed further from low-temperature NO_2 conversion and remain this way through the mid-temperature range due to N_2O conversion. For ammonia and urea, N_2O levels are still much higher than initial levels (Figures 5.19 and 5.21, cases 25 and 29). For these cases, N_2O is less than 55 ppm, but this increases to as much as 175 ppm at high NSRs and ACRs. Hydrazine also demonstrates significant increases in N_2O and NO_2 concentrations from baseline emissions levels. This severely affects the total NO_x reduction.

In addition to N_2O, chemical slip remains a concern. NH_3 concentrations for SNCR using ammonia or urea drop to just below 25% of the initial concentration at the low-temperature end of the temperature window. Though these levels are still high, ammonia emissions for all four chemicals using H_2O_2 are cut significantly, resulting in much lower levels at temperatures between 1100° and 1300°F. However, urea has the additional concern of HNCO slip, which is higher at lower temperatures. Comparable slip levels from HNCO are not achieved until temperatures are above the optimum NO_x reduction temperature.

5.2.4 Application to JETC Conditions

The preceding SNCR analyses have demonstrated several conditions that could be applied to JETC conditions. The injection of only the baseline chemicals gave good

reducing properties, but the temperature windows were too narrow and not conducive to the gradients seen radially across the plume. The use of additives helped to extend this range by lowering the optimal temperature window and extending its range tremendously. Optimal conditions were usually located around unity values of the NSR and ACR.

Recall that the JETC conditions and measured emission levels to be used are listed in Table 5.4. Using these data points, the chemical kinetic model was run again using a finer grid for the chemical and additive ratios (NSR and ACR = 0.3, 0.6, 0.9, 1.2, 1.5). NSR and ACR are held constant throughout the modeled injection grid, thus implying different flow rates at each point of injection. Both hydrogen and hydrogen peroxide displayed good performances as additives to ammonia, urea, and hydrazine for the cases run in the previous section. These combinations and the baseline cases were run in the extended model with the JETC conditions.

NO_x reduction levels using hydrogen for the JETC conditions were surprisingly low. Modeled results show its poor performance to be due to the conversion of initial NO_2 concentration (now present in the gas stream) into NO. Therefore, the three best strategies all use hydrogen peroxide with ammonia, urea, and hydrazine. The results are described below.

Tables 5.5 through 5.7 show a sample of optimal conditions possible for SNCR application in a JETC assuming 0.5 seconds residence time. Since NO and NO_2 were both measured initially, Equation 5.1 was modified as shown in Equation 5.2:

$$\%\ NO_x\ \text{Reduction} = 100 \times \left[1 - \left(\frac{NO_f + NO_{2,f} + N_2O_f}{NO_i + NO_{2,i}} \right) \right] \qquad (5.2)$$

where 100% reduction is the best achievable goal, subscript *i* indicates initial concentrations and subscript *f* indicates final concentrations.

The combinations include hydrogen peroxide coupled with ammonia, urea, and hydrazine. All three combinations were able to reduce total NO_x for the conditions in the

Table 5.5: SNCR Model Predictions of Ammonia with H_2O_2 Addition (NSR = 0.9, ACR = 0.6, H_2O = 3.5%, t_{res} = 0.5 sec.)

	Position inches	% NO_x* Reduction	NO ppm	NO_2 ppm	N_2O ppm	NH_3 ppm	H_2O_2 ppm
Military Power	0.00	33.9	62.8	99.1	25.7	99.0	0.5
	-3.63	33.9	64.8	99.0	25.8	98.7	0.2
	-7.31	22.9	60.6	98.5	16.1	93.4	9.5
	-11.00	0.0	92.2	14.0	0.0	83.0	49.7
	-14.75	0.0	11.4	2.6	0.0	10.3	6.2
Zone 1 Afterburner	0.00	21.5	72.0	109.0	21.4	65.5	0.0
	-3.63	22.6	84.0	105.0	20.8	67.9	0.0
	-7.31	0.1	241.0	4.7	4.0	0.0	0.0
	-11.00	-14.3	152.0	2.2	1.0	0.0	0.0
	-14.75	-0.1	4.7	30.8	0.0	4.5	2.7

Table 5.6: SNCR Model Predictions of Urea with H_2O_2 Addition (NSR = 1.2, ACR = 0.3, H_2O = 3.5%, t_{res} = 0.5 sec.)

	Position inches	% NO_x* Reduction	NO ppm	NO_2 ppm	N_2O ppm	NH_3 ppm	HNCO ppm	H_2O_2 ppm
Military Power	0.00	39.0	82.0	68.7	22.2	173.0	285.0	0.7
	-3.63	39.2	82.6	69.0	22.8	173.0	288.0	0.2
	-7.31	23.9	87.8	72.7	12.4	154.0	211.0	11.6
	-11.00	0.1	92.2	13.9	0.0	111.0	111.0	33.2
	-14.75	0.0	11.4	2.6	0.0	13.7	13.7	4.1
Zone 1 Afterburner	0.00	23.8	79.4	94.7	22.4	115.0	186.0	0.0
	-3.63	24.9	88.2	92.8	22.6	121.0	198.0	0.0
	-7.31	14.2	176.0	6.8	31.8	0.1	1.8	0.0
	-11.00	-21.4	153.0	3.2	8.8	0.0	0.5	0.0
	-14.75	0.1	4.8	30.6	0.0	6.0	6.0	1.8

Table 5.7: SNCR Model Predictions of Hydrazine with H_2O_2 Addition (NSR = 0.6, ACR = 1.2, H_2O = 3.5%, t_{res} = 0.5 sec.)

	Position inches	% NO_x* Reduction	NO ppm	NO_2 ppm	N_2O ppm	NH_3 ppm	N_2H_4 ppm	H_2O_2 ppm
Military Power	0.00	19.0	11.7	131.0	87.1	36.3	24.3	1.2
	-3.63	18.9	8.1	133.0	91.8	40.4	21.7	0.4
	-7.31	11.1	55.3	112.0	34.7	10.8	42.8	23.5
	-11.00	0.0	92.3	13.9	0.0	0.0	55.3	66.4
	-14.75	0.0	11.4	2.6	0.0	0.0	6.8	8.2
Zone 1 Afterburner	0.00	14.8	6.3	143.0	70.4	35.3	8.3	0.0
	-3.63	16.1	4.5	139.0	84.1	46.2	3.9	0.0
	-7.31	18.0	181.0	6.0	17.9	0.0	0.0	0.0
	-11.00	0.7	128.0	2.6	4.3	0.0	0.0	0.0
	-14.75	-0.1	4.8	30.7	0.0	3.0	3.6	0.0

*NO_x Reduction is determined using Equation 5.2.

core of the flow (up to 7.3 inch radius). This reduction resulted in a substantial increase in the NO_2 concentration from the baseline JETC case. The outer extents of the flow field had very little reduction, and in the case of ammonia and urea, NO was produced. Significant N_2O and elevated NO_2 form in all cases when temperatures are sufficient for reduction; ammonia had the lowest of the three. Ammonia and urea have very similar highest NO_x reductions available (between 14 and 39%), but have very high chemical and additive slips (especially urea, where slips range from 111 to 285 ppm for the core flow). Hydrazine has a much lower reduction, but has by far the lowest values for slip (less than 55 ppm in all cases). Area-weighted averaging of the flow shows that for the best case (urea with hydrogen peroxide), NO_x experiences a 23% reduction at military power and only a 5% reduction at Zone 1 afterburner over uncontrolled levels.

In the test cell, it is unlikely that the flow will remain isothermal for 0.5 seconds. Therefore, the speed of the process is also an issue. For these same conditions, the effect of residence time was studied at 0.05-second intervals. From 0.05 to 0.10 seconds, chemical kinetics makes the most significant change. Extending the time, especially in low-temperature cases, allows the reactions to move toward equilibrium. Tables 5.8 through 5.10 list the final concentrations at the same conditions modeled after 0.15 seconds. As expected, NO_x reduction and N_2O emissions decrease while slip values increase. Urea has the highest NO_x reduction levels (centerline values ranging from 23% to 34%), but it has the highest slip levels. N_2O never exceeds 37 ppm and NO_2 remains under 100 ppm for the modeled urea conditions. Ammonia with hydrazine achieves nearly the same NO_x reduction, but has more resulting NO_2 and N_2O emissions.

Table 5.8: SNCR Model Predictions of Ammonia with H_2O_2 Addition (NSR = 0.9, ACR = 0.6, H_2O = 3.5%, t_{res} = 0.15 sec.)

	Position inches	% NO_x* Reduction	NO ppm	NO_2 ppm	N_2O ppm	NH_3 ppm	H_2O_2 ppm
Military Power	0.00	29.6	75.8	104	19.8	117	8.2
	-3.63	30.9	74	103	21.4	112	5.4
	-7.31	14.7	95	91.8	7.1	121	34.2
	-11.00	0	92.3	13.9	0	83.1	49.8
	-14.75	0	11.4	2.6	0	10.3	6.2
Zone 1 Afterburner	0.00	20.6	73.2	111	20.5	68.2	0.6
	-3.63	22.2	84.8	106	20.1	70.3	0
	-7.31	0	240	5.3	4.7	0	0
	-11.00	-14.2	151	2.8	1.2	0	0
	-14.75	0.1	4.9	30.5	0	4.5	2.7

Table 5.9: SNCR Model Predictions of Urea with H_2O_2 Addition (NSR = 1.2, ACR = 0.3, H_2O = 3.5%, t_{res} = 0.15 sec.)

	Position inches	% NO_x* Reduction	NO ppm	NO_2 ppm	N_2O ppm	NH_3 ppm	HNCO ppm	H_2O_2 ppm
Military Power	0.00	32.3	104.0	72.0	16.1	196.0	288.0	10.3
	-3.63	34.3	98.6	71.9	18.1	190.0	290.0	7.1
	-7.31	12.9	126.0	66.9	5.2	183.0	214.0	32.6
	-11.00	0.0	92.3	13.9	0.0	111.0	111.0	33.2
	-14.75	0.0	11.4	2.6	0.0	13.7	13.7	4.1
Zone 1 Afterburner	0.00	23.0	81.3	95.8	21.4	118.0	186.0	0.9
	-3.63	24.6	89.0	93.2	22.2	123.0	198.0	0.1
	-7.31	10.7	181.0	5.9	36.4	0.2	5.5	0.0
	-11.00	-22.7	153.0	3.3	10.3	0.1	1.7	0.0
	-14.75	0.1	5.0	30.5	0.0	6.0	6.0	1.8

Table 5.10: SNCR Model Predictions of Hydrazine with H_2O_2 Addition (NSR = 0.6, ACR = 1.2, H_2O = 3.5%, t_{res} = 0.15 sec.)

	Position inches	% NO_x* Reduction	NO ppm	NO_2 ppm	N_2O ppm	NH_3 ppm	N_2H_4 ppm	H_2O_2 ppm
Military Power	0.00	14.0	59.1	128.0	56.9	49.2	20.9	20.1
	-3.63	15.1	46.1	132.0	65.5	42.6	13.9	24.4
	-7.31	4.1	116.0	90.9	11.1	72.0	65.4	3.2
	-11.00	0.0	92.3	13.9	0.0	55.4	66.4	0.0
	-14.75	0.0	11.4	2.6	0.0	6.8	8.2	0.0
Zone 1 Afterburner	0.00	12.8	19.4	148.0	57.5	16.4	1.3	25.6
	-3.63	14.0	17.9	148.0	67.3	13.1	0.1	32.6
	-7.31	15.3	181.0	5.8	25.0	0.0	0.0	0.0
	-11.00	-1.4	128.0	3.4	6.3	0.0	0.0	0.0
	-14.75	0.1	5.0	30.5	0.0	3.0	3.6	0.0

*NO_x Reduction is determined using Equation 5.2.

6.0: SUMMARY, CONCLUSIONS, AND RECOMMENDATIONS

6.1 Summary

The goal of this project was to evaluate selective non-catalytic reduction of NO_x for jet engine test cells. This was accomplished by building a sample probe capable of withstanding the 3000°F peak temperatures and up to 25,000 pounds of thrust in the exhaust stream directly behind a jet engine. The exhaust flows from two engines were characterized for NO_x, temperature, velocity, and other exhaust constituents over the range of operating conditions for the test cell. The results were analyzed and used in a modeling feasibility study of the application of SNCR to this environment.

6.1.1 JETC Emissions Summary

The overall focus of this program was on NO_x and its possible reduction. Knowing the exhaust effluent characteristics of the target engines was necessary for the optimization of a NO_x control strategy. It was therefore essential, as a first step, to characterize the entire plume. Two engines, the TF30-P111+ and the TF33-P9, were selected to obtain data from jet engines currently in use by the U.S. Air Force. The general engine exhaust flow field characteristics can be summarized as follows:

- The power setting of the engine makes a significant impact on the emissions of NO and NO_x;
- Dilution is noticeable but not significant in the exhaust free stream between the tailpipe exit and the augmenter; and
- NO_2 constitutes 2% to 50% of the total NO_x flow field.

Specific details about the high performance, afterburning P111+ engine from the data collected were as follows:

- At the Zone 1 (or initial) afterburner setting, NO and NO_x emissions are less than those at full military power (no afterburner) possibly due to reburning and/or dilution effects. However, NO_2 appears to make up a significant fraction (up to 50%) of the total NO_x emissions;
- Peak temperatures range from 1100°F at military power to over 2800°F at full afterburner. Peak afterburner temperatures shift radially outward due to the AB spray-bar geometry;
- Levels of CO increase dramatically (peak values in excess of 10%) in the afterburner regions due to inefficient burning. Peak CO concentrations shift radially outward with the peak afterburner temperatures; and
- A scaled index for NO_x shows military power as the highest polluter during a typical engine run. Power settings between Military -10 inches and Zone 1 afterburner comprise 90% of the total NO_x produced.

The non-afterburning, high-bypass TF33-P9 engine exhaust characteristics differed in the following ways:

- The combination of a narrow exhaust nozzle and only a small fraction of fan bypass air in the turbine exhaust creates an evener distribution of emissions and temperatures at the exhaust exit;
- The area-weighted NO_x value for the P9 is 88 ppm at full military power, less than half of the P111+ value at military power; and
- Peak average temperatures at military throttle are almost 200°F less than those for the P111+.

The results demonstrate few throttle settings with sufficient temperatures for traditional SNCR application. Of the two engines, only the TF30-P111+ engine has

temperatures extending into SNCR ranges. This engine emits the bulk of its emissions between 90% power and Zone 5 afterburner. However, when the boundaries of the SNCR process are considered, the extreme throttle settings have temperatures outside of the SNCR temperature window. Military power and Zone 1 afterburner were chosen as the most applicable conditions for evaluation.

6.1.2 SNCR Evaluation Summary

Based upon the findings of the JETC activity, a test matrix was designed to cover as much of the area of interest as possible. Four chemicals were chosen based upon their performance in literature and the availability of kinetic mechanisms to describe the processes. Ammonia, cyanuric acid, urea, and hydrazine were tested and compared to establish a base condition. Hydrogen, methane, and hydrogen peroxide were then added in various amounts to observe their effects on the reduction process. From this, the best conditions were selected to model the data from Military and Zone 1 afterburner settings.

The total NO_x reduction (accounting for NO, NO_2, and N_2O) was plotted as a function of temperatures for a 0.5-second residence time. Ammonia was used to establish the general SNCR characteristics for the range of parameters with the following results:

- NO_x levels are reduced in excess of 55% (85% maximum), with peak levels falling between the temperatures of 1300°F and 1600°F;
- NO_x reduction increases as increasing amounts of ammonia are injected, with the tradeoff of increased ammonia slip;
- Much of the NO is converted into NO_2 and N_2O at lower temperatures, thus hindering NO_x reduction; and
- Carbon monoxide lowers the temperature window for optimal NO reduction, but also results in a steep drop in reduction at the high end of the temperature

window as well as increased production of NO_2 and N_2O (up to 30 ppm maximum for each).

The other chemicals offered the following deviations:

- Cyanuric acid does not perform as well as ammonia. Lower NO_x reductions (less than 50%), higher NO_2 and N_2O levels, and higher slip values account for this;
- Urea has NO_x reduction peaks resembling ammonia. Optimal temperatures are slightly higher than ammonia, and N_2O levels are similar to those for cyanuric acid; and
- Hydrazine features the highest potentials for NO_x reduction (92% at 1600°F) and N_2O production (160 ppm). Temperature windows are much broader, extending 300°F to over 500°F.

The use of additives affected the SNCR process in the following ways:

- Hydrogen addition shifts the temperature window down by 50°F to 200°F. Ammonia cases have narrower temperature windows with NO_x reduction peaks sometimes 10% higher than baseline levels. Hydrogen is not beneficial to the cyanuric acid process, but urea has lower, broader temperature windows at sustained reduction levels greater than 70%. Hydrogen extends the NO_x reduction potential of hydrazine below 1000°F;
- Methane promotes NO_2 conversion at lower temperatures for ammonia, cyanuric acid, and urea, thus lowering NO_x reduction levels further from baseline and hydrogen cases. Significant rises in CO were also observed. Hydrazine is relatively unaffected by methane; and
- NO_x reductions for hydrogen peroxide remain at similar temperatures as those of the baseline conditions. However, the effective temperature range is extended below 1000°F for ammonia, urea, and hydrazine, albeit at low

overall NO_x reductions. NO_2 and N_2O levels are still much higher than baseline levels.

Hydrogen and hydrogen peroxide were chosen as the modifiers for ammonia, urea, and hydrazine to model SNCR application at the power settings considered. Combinations of the three chemicals and H_2O_2 gave the best NO_x reductions, and the results are as follows:

- At a residence time of 0.5 seconds, ammonia and urea with hydrogen peroxide demonstrate NO_x reducing abilities of 23% to 39% for the central core of the exhaust flow (7.3-inch radius from centerline). Hydrazine achieves only 11% to 19% NO_x reduction in the core flow at military and Zone 1 afterburner powers;
- Ammonia and urea demonstrate N_2O levels less than 32 ppm for all conditions, but both have high levels of chemical slip (especially urea) for the conditions tested;
- An area-weighted average of the best combination (urea with hydrogen peroxide) shows overall NOx reductions for the entire flow of 23% for military power and only 5% for Zone 1 AB;
- Ammonia and urea show high slip values (greater than 125 ppm at the core) while hydrazine has much lower slip values (less than 55 ppm) due to low NSR; and
- For t_{res} of 0.15 seconds, NO_x reduction and N_2O emissions decrease slightly while slip values increase accordingly.

6.2 Conclusions

Significant conclusions that can be drawn from this project are the following:

- Measurements can be made in the exhaust plane of a jet engine operating over its complete range of power settings. The success of the sampling system requires:
  - A sample probe able to withstand the forces and temperatures in a jet engine exhaust stream; and
  - A traverse to position the sample probe spatially in the flow.
- Temperatures and other exhaust plume factors are marginal for the application of SNCR, even at high power settings. The low temperatures of the TF33-P9 engine at full power make SNCR application unfeasible. The TF30-P111+ engine has sufficient temperatures at full military and afterburner powers, but other factors such as strong radial temperatures and high CO concentrations in the afterburner limit the application. Even when optimized (assuming the ideal conditions of the chemical kinetic model), SNCR is capable of only small reductions in the total NO_x concentration;
- Hydrogen peroxide may stretch the SNCR chemical over many conditions that would otherwise be unsuitable with only the baseline chemicals. This may allow a chemical combination greater flexibility in its application to a practical system, in which gases are not always isothermal and well-mixed;
- Experimental studies are required to verify the conclusions resulting from the chemical kinetic model predictions. Although a useful tool to the researcher, chemical kinetics models are not wholly accurate over the entire range of variables and should be verified with experimental results; and
- These findings have attractive implications for non-JETC applications (*e.g.*, power plants, boilers, furnaces) that operate near the conditions studied but

more favorable in terms of effluent temperatures and pressures. There are many applications suited for SNCR that will benefit from this investigation.

6.3 Recommendations

The lingering challenge with the application of SNCR to a JETC is the low temperatures over a majority of the operating range. One possible method for increasing the temperatures is the implementation of a reburner upstream of the SNCR injection point and far enough downstream from the engine exhaust exit to not affect its operation. Methane would be the most obvious choice for a fuel due to its availability as natural gas. The main challenges with using two technologies (reburning and SNCR) are the physical constraints of the test cell, the available residence time of the hot exhaust flow, and the effects of the upstream control system on the downstream system. This could be modeled using a combination of further computer modeling and bench-top experiments.

This research could easily be applied to such other forms of combustion as boilers and power plants, to which SNCR is commonly applied. Hydrogen peroxide with ammonia or urea have shown some very interesting traits, such as the extended temperature windows, that are desirable for most systems that must deal with thermal gradients. This study is an excellent springboard for extended research using bench-top reactors and modeling for a variety of practical applications. In addition, the incorporation of a two-dimensional computational fluid dynamics code would facilitate handling the two-phase flow and high-temperature chemical kinetics.

7.0: REFERENCES

1. Arand J.K., *et al.*, "Urea Reduction of NO_x in Combustion Effluents," U.S. Patent 4,208,386 (1980).

2. Arand J.K., *et al.*, "Urea Reduction of NO_x in Fuel Rich Combustion Effluents," U.S. Patent 4,325,924 (1982).

3. Berman, E., Dong, J., and Lichtin, N.N., *Photopromoted and Thermal Decomposition of Nitric Oxide by Metal Oxides*, Air Force Report ESL-TR-91-32, September 1991.

4. Bowman, C.T., "Mechanisms and Modeling of Gas-Phase Aftertreatment Methods for NO Removal from Combustion Products," in *Physical and Chemical Aspects of Combustion. A Tribute to Irvin Glassman*, Dryer, F.L., and Sawyer, R.F., (Eds), Gordon and Breach, Amsterdam, 1997, pp. 29–68.

5. Caton, J.A., and Siebers, D.L., "Comparison of Nitric Oxide Removal by Cyanuric Acid and by Ammonia," *Combust. Sci. Technol.*, **65**, 277 (1989).

6. Caton, J.A., and Siebers, D.L., "Effects of Hydrogen Addition on the Removal of Nitric Oxide by Cyanuric Acid," *Twenty-Third Symposium (International) on Combustion*, The Combustion Institute, Pittsburgh, 1990, pp. 225–230.

7. Chen, S.L., McCarthy, J.M., Clark, W.D., Heap, M.P., Seeker, W.R., and Pershing, D.W., "Bench and Pilot Scale Process Evaluation of Reburning for In-Furnace NO_x Reduction," *Twenty-First Symposium (International) on Combustion*, The Combustion Institute, Pittsburgh, 1986, pp. 1159–1169.

8. Dean, A.M., Hardy, J.E., and Lyon, R.K., "Kinetics and Mechanism of NH_3 Oxidation," *Nineteenth Symposium (International) on Combustion*, The Combustion Institute, Pittsburgh, 1982, pp. 92–105.

9. Dill, J.W., and Sowa, W.A., "Nitric Oxide Reduction Using Ammonia Injection: Numerical Modeling Comparisons," Paper No. 92-89, Fall Meeting of the Western States Section of the Combustion Institute, October 1992.

10. Environmental Protection Agency, "Summary of NO_x Control Tecnologies and their Availability and Extent of Application," EPA-450/3-92-004, U.S. Environmental Protection Agency, February 1992.

11. Exxon Research and Engineering Co., "Thermal $DeNO_x$ Process," advertisement pamphlet (1989).

13. Ham, D.O., Moniz, G.A., and Katz, C.B., "A New Low-Temperature SNR Process for Post-Combustion NO_x Control," AIChE Summer National Meeting: Removal of Gaseous Contaminants During Coal Utilization, August, 1990.

14. International Civil Aviation Organization, "Environmental Protection, Annex 16: Volume II, Aircraft Engine Emissions, Second Edition," International Standards and Recommended Practices, 1993.

15. Jodal, M., Nielsen, C., Hulgaard, T., and Dam–Johansen, K., "Pilot-Scale Experiments with Ammonia and Urea as Reductants in Selective Non-Catalytic Reduction of Nitric Oxide," *Twenty-Third Symposium (International) on Combustion*, The Combustion Institute, Pittsburgh, 1990, pp. 237–243.

16. Johnson, S.A., and Katz, C.B., *Feasibility of Reburning for Controlling NO_x Emissions from Air Force Jet Engine Test Cells*, Air Force Report ESL-TR-89-33, June 1989.

17. Jones, D.G., Muzio, L.J., Stocker, E., *et al.*, "Two-Stage $DeNO_x$ Process Test Data for 3330 TPD MSW Incineration Plant," 82nd APCA Annual Meeting and Exhibition, June 1989.

18. Jones, D.G., *et al.*, "Preliminary Test Results: High Energy Urea Injection $DeNO_x$ on a 215 MW Utility Boiler," EPRI–EPA Joint Symposium on Stationary Combustion NO_x Control, 1991.

19. Kee, R.J., Rupley, F.M., and Miller, J.A., "Chemkin-II: A Fortran Chemical Kinetics Package for the Analysis of Gas-Phase Chemical Kinetics," SAND89-8009 • UC-401, Sandia National Laboratories, December 1990.

20. Kee, R.J., Rupley, F.M., and Miller, J.A., "The Chemkin Thermodynamic Database," SAND87-8215, Sandia National Laboratories, 1987.

21. Kimball–Linne, M.A., and Hanson, R.K., "Combustion-Driven Flow Reactor Studies of Thermal $DeNO_x$ Reaction Kinetics," *Combust. Flame*, **64**, 337 (1986).

22. Lanier, W.S., Mulholland, J.A., and Beard, J.T., "Reburning Thermal and Chemical Processes in a Two-Dimensional Pilot-Scale System," *Twenty-First Symposium (International) on Combustion*, The Combustion Institute, Pittsburgh, 1986, pp. 1171–1179.

23. Lutz, A.E., Kee, R.J., and Miller, J.A., "SENKIN: A Fortran Program for Predicting Homogeneous Gas Phase Chemical Kinetics with Sensitivity Analysis," SAND87-8248 • UC-401, Sandia National Laboratories, July 1990.

24. Lyon, R.K., "Method for the Reduction of the Concentration of NO in Combustion Effluents Using Ammonia," U.S. Patent 3,900,554 (1975).

25. Lyon, R.K., "Kinetics and Mechanism of Thermal DeNO$_x$: A Review," *ACS Div. Fuel Chemistry*, **32**[*4*], 433 (1987).

26. Miller, J.A., Branch, M.C., and Kee, R.J., "A Chemical Kinetic Model for the Selective Reduction of Nitric Oxide by Ammonia," *Comb. Flame*, **43**, 81 (1981).

27. Miller, J.A., Smooke, M.D., Green, R.M., and Kee, R.J., "Kinetic Modeling of the Oxidation of Ammonia in Flames," *Combust. Sci. Technol.*, **34**, 149 (1983).

28. Miller, J.A., and Bowman, C.T., "Mechanism and Modeling of Nitrogen Chemistry in Combustion," *Prog. Energy Combust. Sci.*, **15**, 287 (1989).

29. Miller, J.A., and Bowman, C.T., "Kinetic Modeling of the Reduction of Nitric Oxide in Combustion Products by Isocyanic Acid," *Int. J. Chem. Kinetics*, **23**, 289 (1991).

30. Montgomery, T.A., "Infrared Analysis of N_2O in Combustion Products," University of California, Irvine, Masters Thesis (1988).

31. Muzio, L.J., and Arand, J.K., "Homogeneous Gas Phase Decomposition of Oxides of Nitrogen," EPRI Report FP-253, Electric Power Research Institute (1976).

32. Muzio, L.J., Arand, J.K., and Teixeira, D.P., "Gas Phase Decomposition of Nitric Oxide in Combustion Products," *Sixteenth Symposium (International) on Combustion*, The Combustion Institute, Pittsburgh, 1976, pp. 199–207.

33. Muzio, L.J., personal communication, September 1994.

34. Nelson, B.W., Nelson, S.G., Higgins, M.O., and Brandum, P.A., *A New Catalyst for NO_x Control*, ESL-TR-89-11, Air Force Engineering and Services Center, Tyndall AFB FL, 1989.

35. Perry, R.A., and Siebers, D.L., "Rapid Reduction of Nitrogen Oxides in Exhaust Gas Streams," *Nature*, **324**, 657 (1986).

36. Perry, R.A., "NO Reduction Using Sublimation of Cyanuric Acid," U.S. Patent 4,731,231 (1988).

37. Perry, R.A., "System for NO Reduction Using Sublimation of Cyanuric Acid," U.S. Patent 4,800,068 (1989).

38. Prather, M.J., and Logan, J.A., "Combustion's Impact on the Global Atmosphere," Paper No. 5009-108, Twenty-fifth Symposium (International) on Combustion, The Combustion Institute, August 1994.

39. Samuelsen, G.S., *in* Pitts, J.N. Jr., and Metcalf, R.L.(eds), *Advances in Environmental Science and Technology Vol. 5*, John Wiley and Sons, Inc., New York, N.Y., 1975 pp. 219–323.

40. Samuelsen, G.S., *in* Rau, J.G., and Wooten, D.C.(eds), *Environmental Impact Analysis Handbook*, McGraw–Hill, 1980, pp. 3-1 to 3-47.

41. Siebers, D.L., and Caton, J.A., "Removal of Nitric Oxide from Exhaust Gas with Cyanuric Acid," *Comb. Flame*, **79**, 31 (1990).

42. Society of Automotive Engineers, "Procedure for the Calculation of Basic Emission Parameters for Aircraft Turbine Engines," *AIR* 1533, Society of Automotive Engineers, April 1982.

43. Sowa, W.A., Dill, J.W., Pohl, J.H., and Yang, S–C., "Thermal DeNOx: Process Definition and Enhancement," Paper No. 92-41, Spring Meeting of the Western States Section of the Combustion Institute, March 1992.

44. Teixeira, D.P., Muzio, L.J., and Montgomery, T.A., "Effect of Trace Combustion Species on SNCR Performance," Paper No. 20, AFRC/JFRC International Conference on Environmental Control of Combustion Processes, October 1991.

45. Teixeira, D.P., *et al.*, " Selective Noncatalytic Reduction (SNCR) Field Evaluation in Utility Natural Gas-Fired Boilers," GRI Report GRI-92/0083 (1992).

46. Turchan, O.C., "Method of Reducing the Oxides of Nitrogen in Fossil Fuels Combustion and Combustion Effluents Using Hydrazine and/or Hydrazine Compounds," U.S. Patent 4,761,270 (1988).

47. Wendt, J.O.L., Sternling, C.V., and Matovich, M.A., "Reduction of Sulfur Trioxide and Nitrogen Oxides by Secondary Fuel Injection," *Fourteenth Symposium (International) on Combustion*, The Combustion Institute, Pittsburgh, 1973, pp. 897–904.

48. Wenli, D., Dam–Johansen, K., and Ostergaard, K., "Widening the Temperature Range of the Thermal DeNO$_x$ Process. An Experimental Investigation," *Twenty-Third Symposium (International) on Combustion*, The Combustion Institute, Pittsburgh, 1990, pp. 297–303.

49. Zeldovich, J., The Oxidation of Nitrogen in Combustion and Explosions, *Acta Physicochemica*, **21**, 577 (1946).

APPENDIX A: Bowman Mechanism (1994)

REACTIONS CONSIDERED			(k = A T**b exp(-E/RT)) A	b	E
1. H2+O2=OH+OH			1.70E+13	0.0	47780.0
2. O+H2=OH+H			5.08E+04	2.7	6290.0
3. OH+H2=H2O+H			2.14E+08	1.5	3450.0
4. OH+O=O2+H			3.26E+11	0.4	-2210.0
5. OH+OH=O+H2O			3.57E+04	2.4	-2112.0
6. 2H+M=H2+M			1.00E+18	-1.0	0.0
H2	Enhanced by	0.000E+00			
H2O	Enhanced by	0.000E+00			
7. 2H+H2=2H2			9.20E+16	-0.6	0.0
8. 2H+H2O=H2+H2O			6.00E+19	-1.2	0.0
9. H+O+M=OH+M			6.20E+16	-0.6	0.0
H2O	Enhanced by	5.000E+00			
10. H+OH+M=H2O+M			1.60E+22	-2.0	0.0
H2O	Enhanced by	5.000E+00			
11. H+O2+M=HO2+M			2.50E+18	-1.0	0.0
O2	Enhanced by	2.200E+00			
H2	Enhanced by	0.000E+00			
N2	Enhanced by	0.000E+00			
12. H+O2+N2=HO2+N2			6.50E+19	-1.4	0.0
13. H+O2+H2O=HO2+H2O			1.60E+16	0.0	-1500.0
14. 2O+M=O2+M			1.89E+13	0.0	-1788.0
15. H+HO2=H2+O2			1.25E+13	0.0	0.0
16. H+HO2=OH+OH			1.40E+14	0.0	1073.0
17. O+HO2=O2+OH			1.40E+13	0.0	1073.0
18. OH+HO2=H2O+O2			2.60E+13	0.0	-220.0
19. HO2+HO2=H2O2+O2			2.00E+12	0.0	0.0
20. H2O2+M=OH+OH+M			1.30E+17	0.0	45500.0
21. H2O2+H=HO2+H2			1.60E+12	0.0	3800.0
22. H2O2+O=HO2+OH			6.30E+03	2.9	2770.0
23. H2O2+OH=H2O+HO2			1.00E+13	0.0	1800.0
24. CO+O+M=CO2+M			6.17E+14	0.0	3000.0
25. CO+OH=CO2+H			4.76E+07	1.2	70.0
26. CO+O2=CO2+O			2.50E+12	0.0	47688.0
27. HO2+CO=CO2+OH			1.57E+14	0.0	23770.0
28. HCO+H=CO+H2			1.19E+13	0.2	0.0
29. HCO+O=CO+OH			3.00E+13	0.0	0.0
30. HCO+O=CO2+H			3.00E+13	0.0	0.0
31. HCO+O2=HO2+CO			3.30E+13	-0.4	0.0
32. HCO+OH=H2O+CO			1.00E+14	0.0	0.0
33. HCO+M=H+CO+M			2.50E+14	0.0	16802.0
CO	Enhanced by	1.900E+00			
H2	Enhanced by	1.900E+00			
CO2	Enhanced by	3.000E+00			
H2O	Enhanced by	5.000E+00			
34. NH3+H=NH2+H2			5.40E+05	2.4	9918.0
35. NH3+O=NH2+OH			9.40E+06	1.9	6461.0
36. NH3+OH=NH2+H2O			2.04E+06	2.0	566.0
37. NH3+HO2=NH2+H2O2			3.00E+11	0.0	22000.0
38. NH2+H=NH+H2			4.00E+13	0.0	3650.0
39. NH2+O=HNO+H			4.50E+13	0.0	0.0
40. NH2+O=NH+OH			7.00E+12	0.0	0.0
41. NH2+O=NO+H2			5.00E+12	0.0	0.0
42. NH2+OH=NH+H2O			4.00E+06	2.0	1000.0
43. NH2+O2=HNO+OH			4.50E+12	0.0	25000.0
44. NH2+O2=H2NO+O			1.10E+18	-1.3	33600.0
45. NH2+HO2=H2NO+OH			2.50E+13	0.0	0.0
46. NH2+NO=NNH+OH			2.80E+13	-0.6	0.0
47. NH2+NO=N2+H2O			1.30E+16	-1.2	0.0
Declared duplicate reaction...					
48. NH2+NO=N2+H2O			********	-0.6	0.0
Declared duplicate reaction...					
49. NH2+NO2=N2O+H2O			2.84E+18	-2.2	0.0
50. NH2+NH2=N2H2+H2			5.00E+11	0.0	0.0
51. NH2+NH2=NH+NH3			5.00E+13	0.0	10000.0

REACTIONS CONSIDERED			A	(k = A T**b exp(-E/RT)) b	E
52. NH2+NH=N2H2+H			1.50E+15	-0.5	0.0
53. NH2+N=N2+H+H			7.20E+13	0.0	0.0
54. NH+H=N+H2			3.20E+13	0.0	328.0
55. NH+O=NO+H			9.20E+13	0.0	0.0
56. NH+OH=HNO+H			2.00E+13	0.0	0.0
57. NH+OH=N+H2O			5.00E+11	0.5	2000.0
58. NH+O2=HNO+O			4.61E+05	2.0	6500.0
59. NH+O2=NO+OH			1.28E+06	1.5	100.0
60. NH+NO=N2O+H			2.94E+14	-0.4	0.0
Declared duplicate reaction...					
61. NH+NO=N2O+H			********	-0.2	0.0
Declared duplicate reaction...					
62. NH+NO=N2+OH			2.16E+13	-0.2	0.0
63. NH+NO2=N2O+OH			1.00E+13	0.0	0.0
64. NH+NH=N2+2H			2.50E+13	0.0	0.0
65. NH+N=N2+H			3.00E+13	0.0	0.0
66. NH+H2O=HNO+H2			2.00E+13	0.0	13850.0
67. HNO+M=H+NO+M			1.50E+16	0.0	48680.0
H2O	Enhanced by	1.000E+01			
O2	Enhanced by	2.000E+00			
N2	Enhanced by	2.000E+00			
H2	Enhanced by	2.000E+00			
68. HNO+H=H2+NO			5.00E+12	0.0	0.0
69. HNO+O=NO+OH			1.00E+13	0.0	0.0
70. HNO+OH=NO+H2O			3.60E+13	0.0	0.0
71. HNO+O2=NO+HO2			1.00E+13	0.0	25000.0
72. HNO+NO=N2O+OH			2.00E+12	0.0	26000.0
73. HNO+NH2=NH3+NO			2.00E+13	0.0	1000.0
74. HNO+HNO=N2O+H2O			3.95E+12	0.0	5000.0
75. H2NO+M=HNO+H+M			5.00E+16	0.0	50000.0
76. NNH=N2+H			1.00E+09	0.0	0.0
77. NNH+H=N2+H2			1.00E+14	0.0	0.0
78. NNH+O=N2O+H			1.00E+14	0.0	0.0
79. NNH+OH=N2+H2O			5.00E+13	0.0	0.0
80. NNH+NO=N2+HNO			5.00E+13	0.0	0.0
81. NNH+NH2=N2+NH3			5.00E+13	0.0	0.0
82. NNH+NH=N2+NH2			5.00E+13	0.0	0.0
83. N2H2+M=NNH+H+M			5.00E+16	0.0	50000.0
H2O	Enhanced by	1.500E+01			
O2	Enhanced by	2.000E+00			
N2	Enhanced by	2.000E+00			
H2	Enhanced by	2.000E+00			
84. N2H2+H=NNH+H2			5.00E+13	0.0	1000.0
85. N2H2+O=NH2+NO			1.00E+13	0.0	0.0
86. N2H2+O=NNH+OH			2.00E+13	0.0	1000.0
87. N2H2+OH=NNH+H2O			1.00E+13	0.0	1000.0
88. N2H2+NO=N2O+NH2			3.00E+12	0.0	0.0
89. N2H2+NH2=NH3+NNH			1.00E+13	0.0	1000.0
90. N2H2+NH=NNH+NH2			1.00E+13	0.0	1000.0
91. N+NO=N2+O			2.50E+13	0.0	328.0
92. N+O2=NO+O			6.40E+09	1.0	6280.0
93. N+OH=NO+H			3.80E+13	0.0	0.0
94. NO+HO2=NO2+OH			2.11E+12	0.0	-479.0
95. NO+O+M=NO2+M			7.60E+19	-1.4	0.0
H2O	Enhanced by	5.000E+00			
N2	Enhanced by	1.600E+00			
96. NO2+H=NO+OH			3.50E+14	0.0	1500.0
97. NO2+O=NO+O2			4.00E+12	0.0	-178.0
98. N2O(+M)=N2+O(+M)			1.30E+11	0.0	59615.0
Low pressure limit: 0.69000E+24 -0.25000E+01 0.64995E+05					
H2O	Enhanced by	5.000E+00			
N2	Enhanced by	1.600E+00			
99. N2O+H=N2+OH			7.60E+13	0.0	15200.0
100. N2O+O=N2+O2			1.40E+12	0.0	10810.0
101. N2O+O=2NO			2.90E+13	0.0	23150.0
102. N2O+OH=N2+HO2			2.00E+11	0.0	5445.0
103. NCO+M=N+CO+M			3.10E+16	-0.5	48000.0
104. NCO+H=NH+CO			5.00E+13	0.0	0.0
105. NCO+O=NO+CO			4.70E+13	0.0	0.0

REACTIONS CONSIDERED	(k = A T**b exp(-E/RT)) A	b	E
106. NCO+OH=NO+CO+H	5.00E+12	0.0	15000.0
107. NCO+O2=NO+CO2	2.00E+12	0.0	20000.0
108. NCO+N=N2+CO	2.00E+13	0.0	0.0
109. NCO+NO=N2O+CO	1.90E+17	-1.5	743.0
110. NCO+NO=N2+CO2	1.40E+18	-1.7	763.0
Declared duplicate reaction...			
111. NCO+NO=N2+CO2	********	-1.5	743.0
Declared duplicate reaction...			
112. NCO+NO2=N2O+CO2	5.80E+14	-0.7	0.0
113. HNCO+M=NH+CO+M	4.50E+15	0.0	83600.0
114. HNCO+H=NH2+CO	2.25E+07	1.7	3800.0
115. HNCO+H=H2+NCO	1.05E+05	2.5	13300.0
116. HNCO+O=NH+CO2	9.80E+07	1.4	8525.0
117. HNCO+O=HNO+CO	1.49E+08	1.6	44015.0
118. HNCO+O=NCO+OH	2.20E+06	2.1	11425.0
119. HNCO+OH=NCO+H2O	4.65E+12	0.0	6850.0
120. HNCO+OH=NH2+CO2	1.55E+12	0.0	6850.0
121. HNCO+HO2=NCO+H2O2	3.00E+11	0.0	29000.0
122. HNCO+NH2=NH3+NCO	1.00E+12	0.0	6955.0
123. HNCO+NH=NCO+NH2	3.00E+13	0.0	23700.0

APPENDIX B: Hydrazine Mechanism (Miller, 1983 and Miller and Bowman, 1989)

	REACTIONS CONSIDERED			(k = A T**b exp(-E/RT)) A	b	E
1.	CO+O+M=CO2+M			6.17E+14	0.0	3000.0
2.	CO+OH=CO2+H			1.51E+07	1.3	-758.0
3.	CO+O2=CO2+O			1.60E+13	0.0	41000.0
4.	HO2+CO=CO2+OH			5.80E+13	0.0	22934.0
5.	H2+O2=2OH			1.70E+13	0.0	47780.0
6.	OH+H2=H2O+H			1.17E+09	1.3	3626.0
7.	O+OH=O2+H			4.00E+14	-0.5	0.0
8.	O+H2=OH+H			5.06E+04	2.7	6290.0
9.	H+O2+M=HO2+M			3.61E+17	-0.7	0.0
	H2O	Enhanced by	1.860E+01			
	CO2	Enhanced by	4.200E+00			
	H2	Enhanced by	2.860E+00			
	CO	Enhanced by	2.110E+00			
	N2	Enhanced by	1.260E+00			
10.	OH+HO2=H2O+O2			7.50E+12	0.0	0.0
11.	H+HO2=2OH			1.40E+14	0.0	1073.0
12.	O+HO2=O2+OH			1.40E+13	0.0	1073.0
13.	2OH=O+H2O			6.00E+08	1.3	0.0
14.	H+H+M=H2+M			1.00E+18	-1.0	0.0
	H2	Enhanced by	0.000E+00			
	H2O	Enhanced by	0.000E+00			
	CO2	Enhanced by	0.000E+00			
15.	H+H+H2=H2+H2			9.20E+16	-0.6	0.0
16.	H+H+H2O=H2+H2O			6.00E+19	-1.2	0.0
17.	H+H+CO2=H2+CO2			5.49E+20	-2.0	0.0
18.	H+OH+M=H2O+M			1.60E+22	-2.0	0.0
	H2O	Enhanced by	5.000E+00			
19.	H+O+M=OH+M			6.20E+16	-0.6	0.0
	H2O	Enhanced by	5.000E+00			
20.	O+O+M=O2+M			1.89E+13	0.0	-1788.0
21.	H+HO2=H2+O2			1.25E+13	0.0	0.0
22.	HO2+HO2=H2O2+O2			2.00E+12	0.0	0.0
23.	H2O2+M=OH+OH+M			1.30E+17	0.0	45500.0
24.	H2O2+H=HO2+H2			1.60E+12	0.0	3800.0
25.	H2O2+OH=H2O+HO2			1.00E+13	0.0	1800.0
26.	HCNO+H=HCN+OH			1.00E+14	0.0	12000.0
27.	CO2+N=NO+CO			1.90E+11	0.0	3400.0
28.	HCN+OH=CN+H2O			1.45E+13	0.0	10929.0
29.	OH+HCN=HOCN+H			5.85E+04	2.4	12500.0
30.	OH+HCN=HNCO+H			1.98E-03	4.0	1000.0
31.	OH+HCN=NH2+CO			7.83E-04	4.0	4000.0
32.	HOCN+H=HNCO+H			1.00E+13	0.0	0.0
33.	HCN+O=NCO+H			1.38E+04	2.6	4980.0
34.	HCN+O=NH+CO			3.45E+03	2.6	4980.0
35.	HCN+O=CN+OH			2.70E+09	1.6	26600.0
36.	CN+H2=HCN+H			2.95E+05	2.5	2237.0
37.	CN+O=CO+N			1.80E+13	0.0	0.0
38.	CN+O2=NCO+O			5.60E+12	0.0	0.0
39.	CN+OH=NCO+H			6.00E+13	0.0	0.0
40.	CN+HCN=C2N2+H			2.00E+13	0.0	0.0
41.	CN+NO2=NCO+NO			3.00E+13	0.0	0.0
42.	CN+N2O=NCO+N2			1.00E+13	0.0	0.0
43.	C2N2+O=NCO+CN			4.57E+12	0.0	8880.0
44.	C2N2+OH=HOCN+CN			1.86E+11	0.0	2900.0
45.	HO2+NO=NO2+OH			2.11E+12	0.0	-479.0
46.	NO2+H=NO+OH			3.50E+14	0.0	1500.0
47.	NO2+O=NO+O2			1.00E+13	0.0	600.0
48.	NO2+M=NO+O+M			1.10E+16	0.0	66000.0
49.	NCO+H=NH+CO			5.00E+13	0.0	0.0
50.	NCO+O=NO+CO			2.00E+13	0.0	0.0
51.	NCO+N=N2+CO			2.00E+13	0.0	0.0
52.	NCO+OH=NO+CO+H			1.00E+13	0.0	0.0
53.	NCO+M=N+CO+M			3.10E+16	-0.5	48000.0
54.	NCO+NO=N2O+CO			1.00E+13	0.0	-390.0

	REACTIONS CONSIDERED			(k = A T**b exp(-E/RT)) A	b	E
55.	NCO+H2=HNCO+H			8.58E+12	0.0	9000.0
56.	HNCO+H=NH2+CO			2.00E+13	0.0	3000.0
57.	NH+O2=HNO+O			1.00E+13	0.0	12000.0
58.	NH+O2=NO+OH			7.60E+10	0.0	1530.0
59.	NH+NO=N2O+H			2.40E+15	-0.8	0.0
60.	N2O+OH=N2+HO2			2.00E+12	0.0	10000.0
61.	N2O+H=N2+OH			7.60E+13	0.0	15200.0
62.	N2O+M=N2+O+M			1.60E+14	0.0	51600.0
63.	N2O+O=N2+O2			1.00E+14	0.0	28200.0
64.	N2O+O=NO+NO			1.00E+14	0.0	28200.0
65.	NH+OH=HNO+H			2.00E+13	0.0	0.0
66.	NH+OH=N+H2O			5.00E+11	0.5	2000.0
67.	NH+N=N2+H			3.00E+13	0.0	0.0
68.	NH+H=N+H2			1.00E+14	0.0	0.0
69.	NH2+O=HNO+H			6.63E+14	-0.5	0.0
70.	NH2+O=NH+OH			6.75E+12	0.0	0.0
71.	NH2+OH=NH+H2O			4.00E+06	2.0	1000.0
72.	NH2+H=NH+H2			6.92E+13	0.0	3650.0
73.	NH2+NO=NNH+OH			6.40E+15	-1.2	0.0
74.	NH2+NO=N2+H2O			6.20E+15	-1.2	0.0
75.	NH3+OH=NH2+H2O			2.04E+06	2.0	566.0
76.	NH3+H=NH2+H2			6.36E+05	2.4	10171.0
77.	NH3+O=NH2+OH			2.10E+13	0.0	9000.0
78.	NNH=N2+H			1.00E+04	0.0	0.0
79.	NNH+NO=N2+HNO			5.00E+13	0.0	0.0
80.	NNH+H=N2+H2			1.00E+14	0.0	0.0
81.	NNH+OH=N2+H2O			5.00E+13	0.0	0.0
82.	NNH+NH2=N2+NH3			5.00E+13	0.0	0.0
83.	NNH+NH=N2+NH2			5.00E+13	0.0	0.0
84.	NNH+O=N2O+H			1.00E+14	0.0	0.0
85.	HNO+M=H+NO+M			1.50E+16	0.0	48680.0
	H2O	Enhanced by	1.000E+01			
	O2	Enhanced by	2.000E+00			
	N2	Enhanced by	2.000E+00			
	H2	Enhanced by	2.000E+00			
86.	HNO+OH=NO+H2O			3.60E+13	0.0	0.0
87.	HNO+H=H2+NO			5.00E+12	0.0	0.0
88.	HNO+NH2=NH3+NO			2.00E+13	0.0	1000.0
89.	N+NO=N2+O			3.27E+12	0.3	0.0
90.	N+O2=NO+O			6.40E+09	1.0	6280.0
91.	N+OH=NO+H			3.80E+13	0.0	0.0
92.	HNCO+M=NH+CO+M			1.14E+16	0.0	86800.0
93.	NH+HNCO=NH2+NCO			3.00E+13	0.0	23700.0
94.	NH2+HNCO=NH3+NCO			5.00E+12	0.0	6200.0
95.	OH+HNCO=NCO+H2O			2.65E+12	0.0	5540.0
96.	O+HNCO=NH+CO2			3.25E+12	0.0	10300.0
97.	N2H3+O=N2H2+OH			5.00E+12	0.0	5000.0
98.	N2H3+O=NH2+HNO			1.00E+13	0.0	0.0
99.	N2H3+OH=N2H2+H2O			1.00E+13	0.0	1000.0
100.	N2H3+H=NH2+NH2			1.60E+11	0.0	0.0
101.	N2H3+M=N2H2+H+M			3.50E+15	0.0	46000.0
102.	N2H3+NH=NH2+N2H2			2.00E+13	0.0	0.0
103.	N2H2+M=NNH+H+M			5.00E+16	0.0	50000.0
104.	N2H2+O=NNH+OH			2.00E+13	0.0	1000.0
105.	N2H2+O=NO+NH2			1.00E+13	0.0	0.0
106.	N2H2+NO=N2O+NH2			3.00E+12	0.0	0.0
107.	NH+NH2=N2H2+H			5.00E+13	0.0	0.0
108.	N2H2+OH=NNH+H2O			1.00E+13	0.0	1000.0
109.	N2H2+H=NNH+H2			5.00E+13	0.0	1000.0
110.	N2H2+NH=NNH+NH2			1.00E+13	0.0	1000.0
111.	N2H2+NH2=NH3+NNH			1.00E+13	0.0	1000.0
112.	NH2+NH2+M=N2H4+M			3.00E+20	-1.0	0.0
113.	H+N2H4=H2+N2H3			1.00E+13	0.0	2500.0
114.	NH2+N2H4=NH3+N2H3			3.90E+12	0.0	1500.0
115.	O+N2H4=N2H2+H2O			8.50E+13	0.0	1200.0
116.	OH+N2H4=N2H3+H2O			5.00E+12	0.0	1000.0
117.	N2H3+OH=NH3+HNO			1.00E+12	0.0	15000.0

APPENDIX C: JETC Exhaust Data

Appendix C lists the average exhaust emission point values used to create Figures 6-11. These were found by averaging the various data taken from different engines at similar throttle positions and sampling points. The probe column shows the measurements made (0.0 inches is centerline, -14.75 inches is the outer edge of the sampling area). NO, NO_x, CO, and HC emission values are tabulated in parts per million (ppm). The values of O_2 and CO_2 measured with the gas chromatograph (GC) are listed in percents. MEXA O_2 values are also listed as a redundant measurement of the GC. The pitot probe readings were taken at the centerline of the flow to help determine the residence time for SNCR applications at the various throttle settings.

ENGINE EXHAUST VALUES (CONT.)

Engine: TF30-P111+
Axial Position: 0.0"

Throttle Setting	Probe inches	NO ppm	NO_x ppm	CO ppm	Temp °F	HC ppm	GC		MEXA	Pitot
							O_2 %	CO_2 %	O_2 %	ft/sec
Flight Idle	0.00	1.0	16.1	493.4	599	11	20.00	1.09	17.78	887
Average	-3.63	1.0	17.1	434.7	613	8	20.22	1.09	17.97	
	-7.31	0.8	12.0	306.8	532	6	20.89	1.30	18.63	
	-11.00	0.6	5.1	168.9	291	2	21.32	0.93	19.43	
	-14.75	0.2	2.0	90.8	159	1	22.03	0.36	19.93	
80% Power	0.00	32.2	51.4	206.2	782	6	18.86	2.08	17.62	1361
Average	-3.63	32.2	49.3	196.4	758	4	19.07	1.94	17.86	
	-7.31	16.8	24.9	134.4	648	2	20.50	1.10	19.17	
	-11.00	3.2	4.6	78.8	286	2	21.65	0.24	20.41	
	-14.75	0.2	0.7	52.5	126	2	22.05	0.14	20.64	
Military -10" Power	0.00	129.9	150.2	85.0	952	0	18.26	3.12	17.40	1996
Average	-3.63	130.3	151.9	82.3	960	0	18.21	3.17	17.46	
	-7.31	97.4	112.3	75.3	845	0	19.14	2.20	18.24	
	-11.00	31.8	36.6	58.6	499	0	20.97	0.83	19.95	
	-14.75	2.7	3.7	41.1	305	0	22.13	0.11	20.75	
90% Power	0.00	154.8	177.9	88.5	979	2	18.17	2.17	16.87	2019
Average	-3.63	153.0	177.5	91.1	974	0	18.06	2.18	17.01	
	-7.31	134.5	133.6	83.2	881	0	18.53	1.47	17.86	
	-11.00	43.2	49.1	67.4	524	0	19.29	0.54	19.66	
	-14.75	4.6	6.4	54.2	217	0	21.78	0.14	20.55	

ENGINE EXHAUST VALUES (CONT.)

Engine: TF30-P111+
Axial Position: 0.0"

Throttle Setting	Probe inches	NO ppm	NO_x ppm	CO ppm	Temp °F	HC ppm	GC O_2 %	GC CO_2 %	MEXA O_2 %	Pitot ft/sec
Military -6" Power Average	0.00	158.0	182.3	85.0	999	0	17.94	2.90	17.36	2068
	-3.63	159.9	184.1	86.7	1016	0	17.74	2.96	17.39	
	-7.31	120.7	139.1	77.1	904	0	18.94	2.21	18.20	
	-11.00	43.7	51.0	62.1	561	0	20.87	0.95	19.91	
	-14.75	4.7	6.1	52.5	323	0	22.12	0.20	20.65	
Military Power Average	0.00	246.7	283.3	89.4	1107	0	17.96	2.40	16.64	2172
	-3.63	249.4	287.4	89.4	1123	0	16.64	3.65	16.71	
	-7.31	180.0	227.3	84.1	1019	0	19.02	1.80	17.57	
	-11.00	92.3	106.2	69.6	680	0	20.94	0.89	19.29	
	-14.75	11.4	14.0	54.2	326	0	21.17	0.16	20.53	
Zone 1 Afterburner Average	0.00	161.3	258.1	471.4	1173	70	16.68	3.61	16.68	2688
	-3.63	172.0	271.1	473.5	1218	52	16.93	4.14	16.25	
	-7.31	129.7	249.8	1239.7	1602	26	14.28	4.38	14.31	
	-11.00	48.4	135.8	1326.7	1623	70	16.54	3.78	15.71	
	-14.75	5.0	35.5	529.8	772	44	20.48	1.23	19.42	
Full Afterburner Average	0.00	220.6	285.8	1079.4	2287	12	10.75	7.28	11.46	2748
	-3.63	231.4	299.0	837.0	2445	16	9.23	8.30	9.61	
	-7.31	222.9	297.8	16839	2905	98	2.95	12.14	5.47	
	-11.00	139.8	139.8	103450	2840	340	0.00	9.07	3.84	
	-14.75	104.2	111.5	86900	2883	130	0.00	9.46	3.60	

ENGINE EXHAUST VALUES (CONT.)

Engine: TF30-P111+
Axial Position: 10.75"

Throttle Setting	Probe inches	NO ppm	NO_x ppm	CO ppm	Temp °F	HC ppm	GC		MEXA	Pitot
							O_2 %	CO_2 %	O_2 %	ft/sec
Flight Idle	0.00	2.0	15.9	559.0	536	24			17.19	210
Average	-3.63	2.7	15.7	494.6		22			17.67	
	-7.31	3.7	12.6	347.1		20			18.37	
	-11.00	0.7	3.7	197.4	269	16			19.26	
	-14.75	0.0	2.1	141.5		14			19.82	
80% Power	0.00	34.6	53.5	164.5	751	10	18.55	2.32	18.21	1122
Average	-3.63	35.0	51.4	153.8	743	10	17.97	2.10	18.28	
	-7.31	18.2	27.2	104.8	583	8	19.25	1.22	18.93	
	-11.00	3.3	5.6	52.0	257	6	21.47	0.28	19.83	
	-14.75	0.5	1.2	44.2	112	8	20.87	0.07	20.25	
Military -10" Power	0.00	130.4	148.8	108.7	929					
	-3.63	127.2	144.8	79.7						
	-7.31	87.7	102.1	63.9						
	-11.00	29.5	34.4	56.0						
	-14.75	3.8	5.3	53.4						
90% Power	0.00	149.7	174.7	75.7	968	10	17.33	2.99	17.72	2070
Average	-3.63	144.4	172.8	75.7	966	8	17.45	2.49	17.60	
	-7.31	110.5	127.6	69.2	840	6	19.07	1.82	18.15	
	-11.00	41.0	48.2	54.7	479	4	20.75	0.65	19.26	
	-14.75	5.1	7.3	50.7	189	6	21.29	0.15	20.02	

ENGINE EXHAUST VALUES (CONT.)

Engine: TF30-P111+
Axial Position: 10.75"

Throttle Setting	Probe inches	NO ppm	NO_x ppm	CO ppm	Temp °F	HC ppm	GC		MEXA	Pitot
							O_2 %	CO_2 %	O_2 %	ft/sec
Military -6" Power	0.00	166.1	201.8	77.1	989					
	-3.63	169.5	199.0	79.7						
	-7.31	120.5	143.5	63.9						
	-11.00	52.6	60.6	53.4						
	-14.75	7.5	10.0	48.1						
Military Power Average	0.00	268.0	313.9	76.2	1123	10	18.58	3.06	17.22	2502
	-3.63	264.0	309.1	77.1	1124	6	18.21	3.83	17.17	
	-7.31	200.2	235.6	68.3	1026	8	19.11	2.46	17.58	
	-11.00	98.0	112.7	57.7	657	6	21.69	1.03	18.81	
	-14.75	14.6	19.8	46.4	271	4	22.62	0.25	19.97	
Zone 1 Afterburner Average	0.00	185.4	285.3	398.7	1176					2613
	-3.63	149.7	273.2	918.6						
	-7.31	125.2	242.5	1303.6						
	-11.00	26.4	98.4	1106.5						
	-14.75	4.5	26.6	417.8						
Full Afterburner Average	0.00	221.9	295.1	1112.1	1163	20	12.43	6.34	13.13	
	-3.63	237.1	309.0	691.9	2414	14	10.26	7.93	11.42	
	-7.31	207.3	279.8	25600	2960	54	2.09	11.91	7.98	
	-11.00	128.4	131.9	102000	2844	256		8.03	5.95	
	-14.75	94.4	95.3	93300		146		9.26	5.23	

ENGINE EXHAUST VALUES (CONT.)

Engine: TF30-P111+
Axial Position: 21.5"

Throttle Setting	Probe inches	NO ppm	NO_x ppm	CO ppm	Temp °F	HC ppm	GC		MEXA	Pitot
							O_2 %	CO_2 %	O_2 %	ft/sec
Flight Idle	0.00	2.0	15.0	509.8	561	21	20.17	1.34	17.92	868
Average	-3.63	1.3	14.1	453.9	591	18	20.22	1.74	18.11	
	-7.31	1.5	10.3	321.8	483	14	21.05	0.85	18.60	
	-11.00	0.4	4.2	198.2	254	11	21.72	0.43	19.21	
	-14.75	0.3	2.1	121.6	164	9	21.98	0.19	19.54	
80% Power	0.00	35.6	53.6	192.5	714	6	19.92	2.08	17.61	1360
Average	-3.63	32.6	47.8	174.2	744	6	19.41	1.76	17.87	
	-7.31	16.1	23.1	117.1	553	3	20.60	0.94	18.97	
	-11.00	3.6	4.9	64.8	231	2	21.09	0.26	19.66	
	-14.75	1.0	1.6	59.9	109	4	21.82	0.11	20.25	
Military -10" Power	0.00	120.9	147.5	82.3	896	6	18.10	2.52	17.16	1987
Average	-3.63	118.3	144.6	84.5	935	6	18.38	2.44	17.25	
	-7.31	83.0	102.1	77.6	798	4	19.34	1.69	18.07	
	-11.00	29.3	35.1	62.3	451	3	20.72	0.59	19.35	
	-14.75	7.8	9.3	53.4	212	2	21.21	0.16	19.96	
90% Power	0.00	159.8	183.1	109.5	966	4	18.16	2.67	16.85	2059
Average	-3.63	153.8	179.4	94.0	980	3	18.34	2.59	17.00	
	-7.31	111.2	125.3	88.7	880	2	19.55	1.79	17.94	
	-11.00	42.9	51.0	64.9	488	2	21.29	0.73	19.29	
	-14.75	12.2	9.4	58.0	202	3	21.45	0.23	20.03	

ENGINE EXHAUST VALUES (CONT.)

Engine: TF30-P111+
Axial Position: 21.5"

Throttle Setting	Probe inches	NO ppm	NO_x ppm	CO ppm	Temp °F	HC ppm	GC		MEXA	Pitot
							O_2 %	CO_2 %	O_2 %	ft/sec
Military -6" Power	0.00	150.7	185.8	85.0	949	5			17.09	2114
Average	-3.63	149.7	183.7	83.4	989	5	18.53	2.55	17.11	
	-7.31	108.6	131.9	78.1	864	3	19.15	1.72	17.91	
	-11.00	41.9	49.6	65.5	505	2			19.24	
	-14.75	14.8	13.0	66.7	236	4	22.20	0.23	19.98	
Military Power	0.00	247.0	295.9	94.6	1031	4	17.39	2.89	16.51	2171
Average	-3.63	246.6	288.8	92.9	1122	3	18.30	2.89	16.58	
	-7.31	187.3	217.3	86.7	1063	3	18.81	2.70	17.43	
	-11.00	90.5	99.2	74.4	634	4	20.56	1.30	18.89	
	-14.75	29.3	27.5	63.2	279	3	21.36	0.35	19.82	
Zone 1 Afterburner	0.00	146.8	266.1	430.1	928	176	18.20	2.04	16.55	2510
Average	-3.63	115.6	205.5	316.3	1205	87	17.11	4.04	16.14	
	-7.31	60.1	128.4	602.7	1472	63	17.51	2.79	15.02	
	-11.00	137.1	243.3	581.9	1515	89	18.65	2.24	15.72	
	-14.75	140.0	269.0	301.6	777	81	21.80	0.71	18.09	
Full Afterburner	0.00	195.2	277.8	828.8	2356	33	13.86	4.37	11.62	2812
Average	-3.63	121.0	222.9	1918.0	2460	22	11.64	5.20	10.01	
	-7.31	99.8	184.0	22834	2974	71	2.08	12.01	5.80	
	-11.00	119.4	200.8	102400	2785	268	0.00	8.26	4.47	
	-14.75	105.0	217.2	92700	2814	162	0.00	8.26	4.11	

ENGINE EXHAUST VALUES (CONT.)

Engine: TF33-P9
Axial position: 0.0"

Throttle Setting	Probe inches	NO ppm	NO_x ppm	CO ppm	Temp °F	HC ppm	GC O_2 %	GC CO_2 %	MEXA O_2 %	Pitot ft/sec
Flight Idle	0	1.1	7.6	754.1	504	84			19.17	170
Average	-3.63	1.35	8.4	848.7	451	93			19.13	
	-7.31	1.70	8.6	725.2		118			19.06	
	-11	1.40	8.2	644.5	472	93			19.14	
90% Power	0	25.9	36.0	81.0	640	29			18.74	1157
Average	-3.63	27.70	38.5	78.4	627	27			18.58	
	-7.31	28.50	43.9	98.2		27			18.38	
	-11	30.50	45.9	95.5	654	25			18.34	
Dataset Power	0.00	28.5	39.6	77.1	646	22			18.74	1166
	-3.63	31.2	42.5	63.9	630	22			18.58	
	-7.31	31.7	47.6	92.9		24			18.38	
	-11.00	34.1	49.0	95.5	655	20			18.34	
Military -6" Power	0.00	55.0	63.7	53.4	749	36			18.29	1469
	-3.63	59.0	68.9	50.7	760	32			18.17	
	-7.31	66.1	77.4	53.4		32			17.93	
	-11.00	67.5	79.7	53.4	754	26			17.77	
Part Power	0	50.4	58.4	50.7	740	31			18.35	1449
Average	-3.63	54.45	63.4	48.1	755	30			18.23	
	-7.31	60.85	71.3	57.3		29			17.98	
	-11	61.30	72.5	61.3	747	27			17.87	
Military Power	0.00	85.5	94.5	50.7	851	30			17.96	1654
	-3.63	90.9	102.6	48.1	854	26			17.81	
	-7.31	101.0	112.0	50.7		26			17.53	
	-11.00	105.7	117.7	50.7	867	26			17.34	

ENGINE EXHAUST VALUES (CONT.)

Engine: TF33-P9
Axial position: 36.5"

Throttle Setting	Probe inches	NO ppm	NO_x ppm	CO ppm	Temp °F	HC ppm	GC O_2 %	GC CO_2 %	MEXA O_2 %	Pitot ft/sec
Flight Idle	0	1.4	7.6	845.8	474	108	19.59	1.33	20.29	147
Average	-3.63	1.63	8.0	901.7	468	114	19.85	1.40	20.23	
	-7.31	1.50	7.9	890.2	477	107	19.21	1.32	20.30	
	-11	1.30	4.9	582.1	391	80	20.46	0.87	20.69	
	-14.75	0.70	3.2	344.4	253	61	20.90	0.45	20.75	
90% Power	0.00	18.4	29.0	129.9	603	28			19.78	1124
	3.63	20.5	31.1	116.7	607	28			19.66	
	7.31	19.8	35.2	143.2	611	28			19.52	
	11.00	17.2	28.1	127.3	595	26			19.84	
	14.75	6.8	11.2	77.1	354	24			20.56	
Dataset Power	0.00	24.7	33.5	106.1		30			19.70	1244
	3.63	25.6	35.5	108.7	647	28			19.51	
	7.31	28.7	40.3	129.9	642	28			19.27	
	11.00	24.2	34.6	108.7	633	28			19.54	
	14.75	9.4	14.1	79.7	383	26			20.38	
Part Power	0	44.4	52.0	83.7	721	38	19.71	2.36	19.37	1479
Average	-3.63	46.80	55.1	81.0	725	26	19.74	2.30	19.41	
	-7.31	54.25	63.8	82.3	733	28	19.92	2.32	18.99	
	-11	45.00	53.5	82.3	723	25	20.09	2.01	19.26	
	-14.75	18.30	22.5	73.2	473	24	21.11	0.90	20.18	

ENGINE EXHAUST VALUES (CONT.)

Engine: TF33-P9
Axial position: 36.5"

Throttle Setting	Probe inches	NO ppm	NO_x ppm	CO ppm	Temp °F	HC ppm	GC		MEXA	Pitot
							O_2 %	CO_2 %	O_2 %	ft/sec
Military -6" Power	0.00	46.1	55.2	85.0		18	18.68	1.58	19.17	1445
	3.63	50.2	59.2	85.0	647	18	18.47	1.45	19.10	
	7.31	58.1	66.9	95.5	642	36	18.57	2.76	18.83	
	11.00	49.9	57.9	92.9	633	32	18.94	2.45	18.98	
	14.75	18.7	23.2	77.1	383	30	20.24	1.00	20.13	
Military Power	0.00	78.5	86.5	82.3	870	28	19.86	2.39	18.84	1760
	3.63	90.1	93.9	79.7	888	26	19.42	3.10	18.70	
	7.31	103.1	108.6	82.3	877	22	19.07	2.28	18.38	
	11.00	94.5	102.5	79.7	897	22	18.35	2.21	18.36	
	14.75	35.3	39.3	69.2	594	20	20.32	0.89	19.82	

APPENDIX D: Calculations

To reduce the two-dimensional flow seen in the sample plane, the following procedure was used. Assuming radial uniformity, the values at each spatial location were averaged. These averages were used as the values for each annulus as shown below (the spacing between probes is 3.68 inches). Each of the five values were multiplied by the area of its annulus, the resulting values were added together, and the sum was divided by the total area, which resulted in the desired area-weighted average.

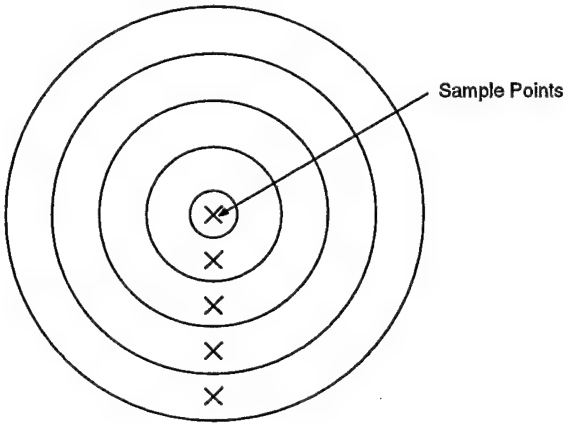

To standardize NO and NO_x values further, an index was calculated using the area-weighted averages to form an NO/NO_x production index (Society of Automotive Engineers, 1982). This index is similar to a conventional emissions index. The emissions index nomenclature is not used, however, due to the fact that rigorous data validation through the use of mass balances was not completed for the reasons described in the report. The intention of this calculation was to find the relative pollution levels for each of the throttle positions using area-weighting.

The formulas used to calculate the NO and NO_x indexes are the following:

$$\text{NO Index} = \left(\frac{[NO]}{[CO]+[CO_2]+[HC]}\right)*\left(\frac{1000*M_{NO_2}}{M_C+\alpha M_H}\right)*\left(1+T*\left(\frac{X}{m}\right)\right)$$

$$\text{NO}_x\text{ Index} = \left(\frac{[NO_x]}{[CO]+[CO_2]+[HC]}\right)*\left(\frac{1000*M_{NO_2}}{M_C+\alpha M_H}\right)*\left(1+T*\left(\frac{X}{m}\right)\right)$$

where

$[x]$	=	mole fraction of species x (*e.g.*, *NO*, *CO*, etc.) in exhaust
M_x	=	atomic weight of species x
α	=	(atomic) hydrogen-carbon ratio of fuel = n/m
T	=	mole fraction of carbon dioxide in dry inlet air = 0.00032
X	=	moles of dry air per mole of fuel
m, n	=	molecular constants for fuel, C_mH_n

Sample Calculation

The following conditions exist for the TF30-P111+ engine at military power assuming JP-8 fuel ($C_{10.9}H_{20.9}$):

NO	=	104.7 ppm
CO	=	74.6 ppm
CO_2	=	13651 ppm
HC	=	5 ppm
Total airflow	=	257 lb/sec
Fuel flow rate	=	9402 lb/hr
M_C	=	12.011
M_H	=	1.008
M_{NO2}	=	46.005
M_{air}	=	28.965
M_{fuel}	=	151.700

Solving for the variables in the NO Index equation, we find:

α = 20.9/10.9 = 1.917

$$X = \left(\frac{151.7}{28.965}\right)*\left(\frac{\text{airflow lb / sec}}{\text{fuelflow lb / hr}}\right)*(3600\text{ sec / hr}) = 18225*\left(\frac{\text{airflow lb / sec}}{\text{fuelflow lb / hr}}\right)$$

Therefore,

$$\textbf{NO Index} = \left(\frac{[104.7]}{[74.6]+[13651]+[5]}\right)*\left(\frac{1000*46.005}{12.011+1.917*1.008}\right)*\left(1+0.00032*\left(\frac{18225*\left(\frac{257}{9402}\right)}{10.9}\right)\right)$$

$$= \textbf{25.5 lb NO/k-lb fuel}$$

These index values were used with fuel flow rates and estimated run time to produce emissions values for further evaluation. The actual numbers were divided through by the highest value to normalized the numbers. These numbers revealed the conditions that produce the most NO/NO_x during normal JETC operation.

APPENDIX E: SNCR Data Plots

This appendix shows the detailed plots from the NOx Reduction curves presented in Figures 5.7 through 5.22. The detailed plots show the NOx Reduction (%) and the Output Emission Levels (ppm) as a function of temperature. The left-hand axis (% NOx Reduction) is associated with the NOx Reduction curve (solid line with filled circles). All other curves are plotted against the right-hand axis (Output Levels, ppm) over the range 0 to 500 ppm. At lower temperatures, some output levels are above 500 ppm. These date, however, are not plotted to (1) maintain uniformity of the plots or (2) provide unambiguous resolution for levels below 100 ppm.

Figures 1 through 8 plot the results of chemical-only injection (*i.e.*, ammonia, cyanuric acid, urea, and hydrazine). The remaining figures show the effects of hydrogen, methane, and hydrogen peroxide as modifiers to these chemicals. A List of Figures for easy reference within this appendix follows.

LIST OF FIGURES

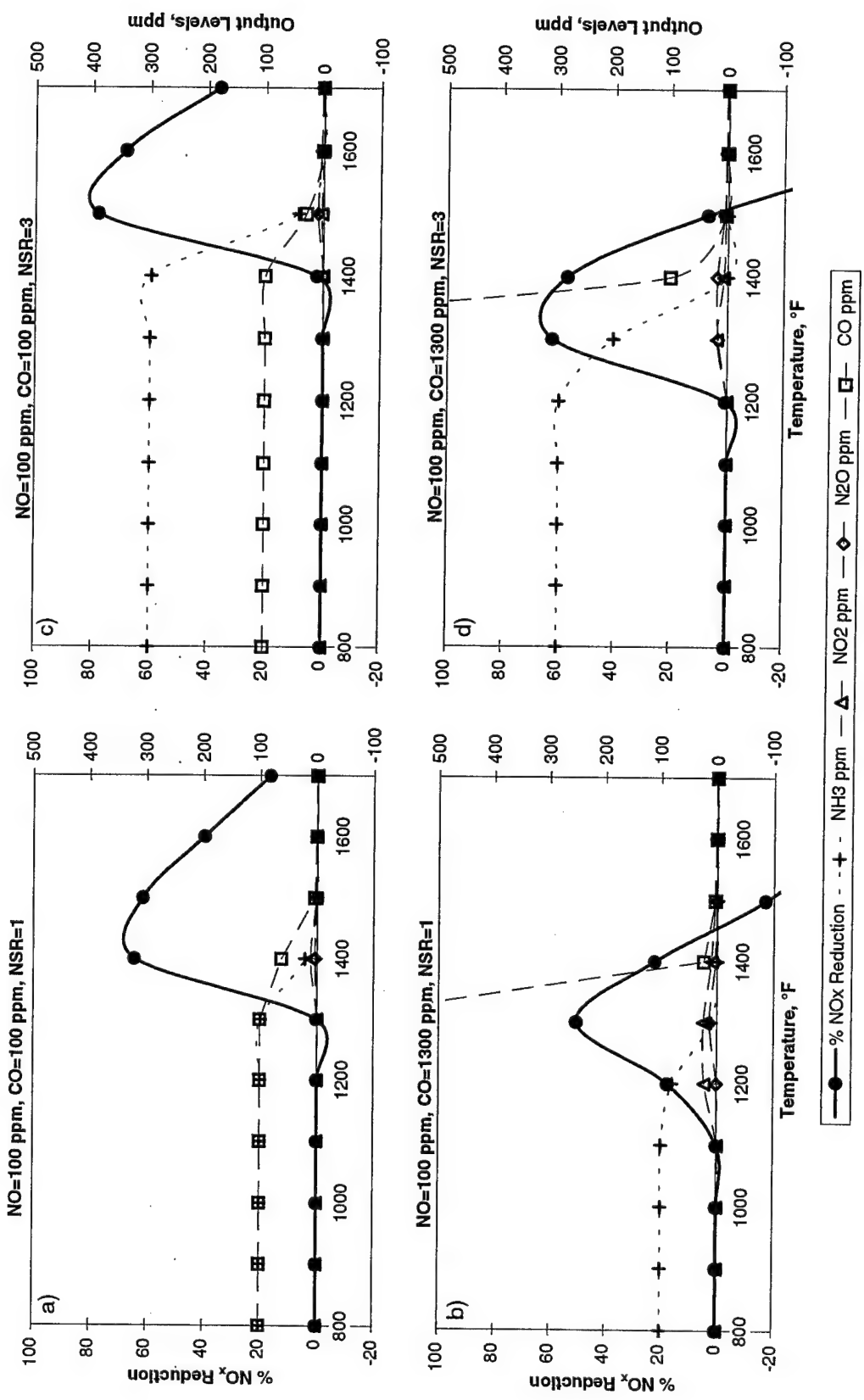

Figure E-1: Chemkin Modeling Results using Ammonia.

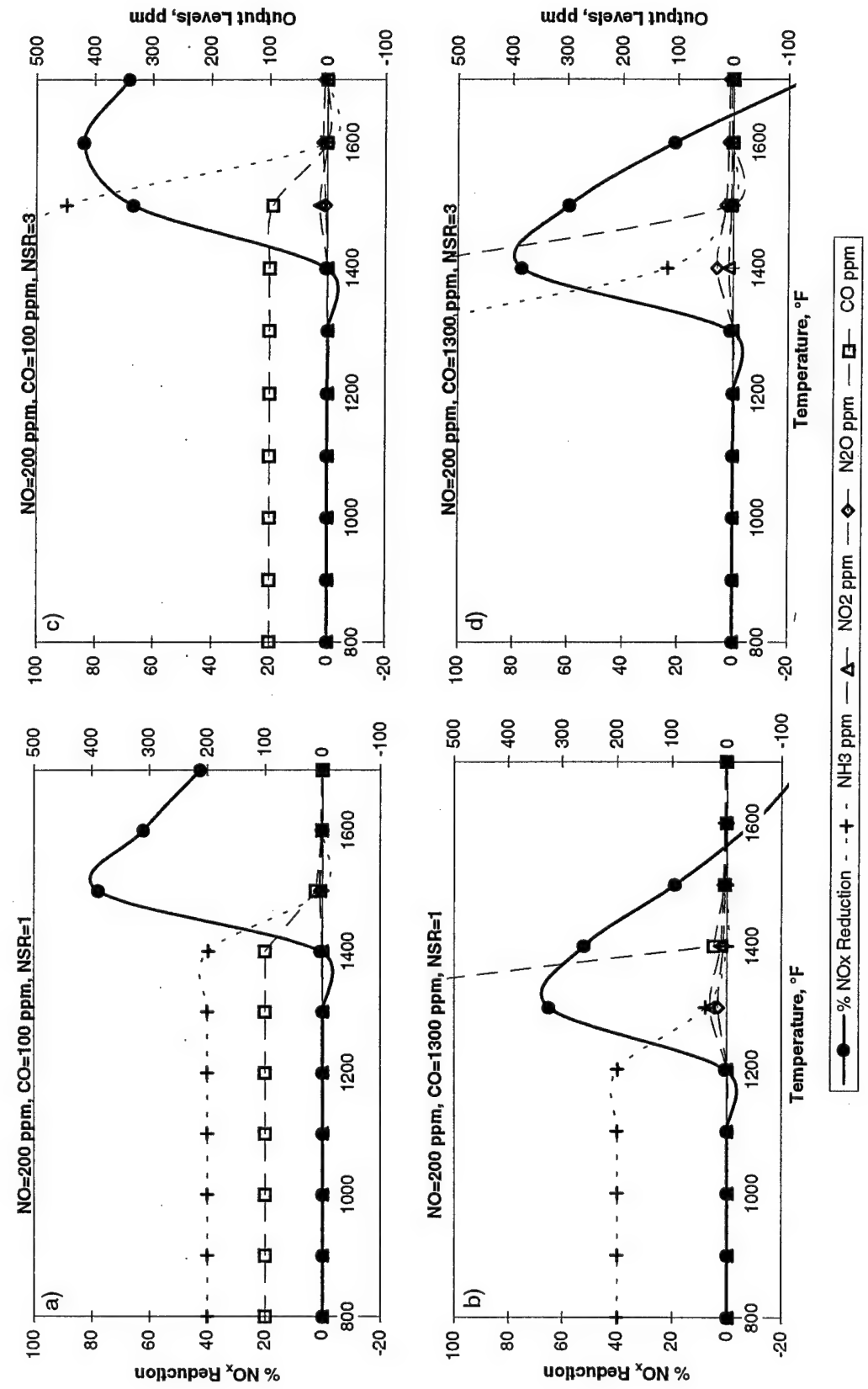

Figure E-2: Chemkin Modeling Results using Ammonia.

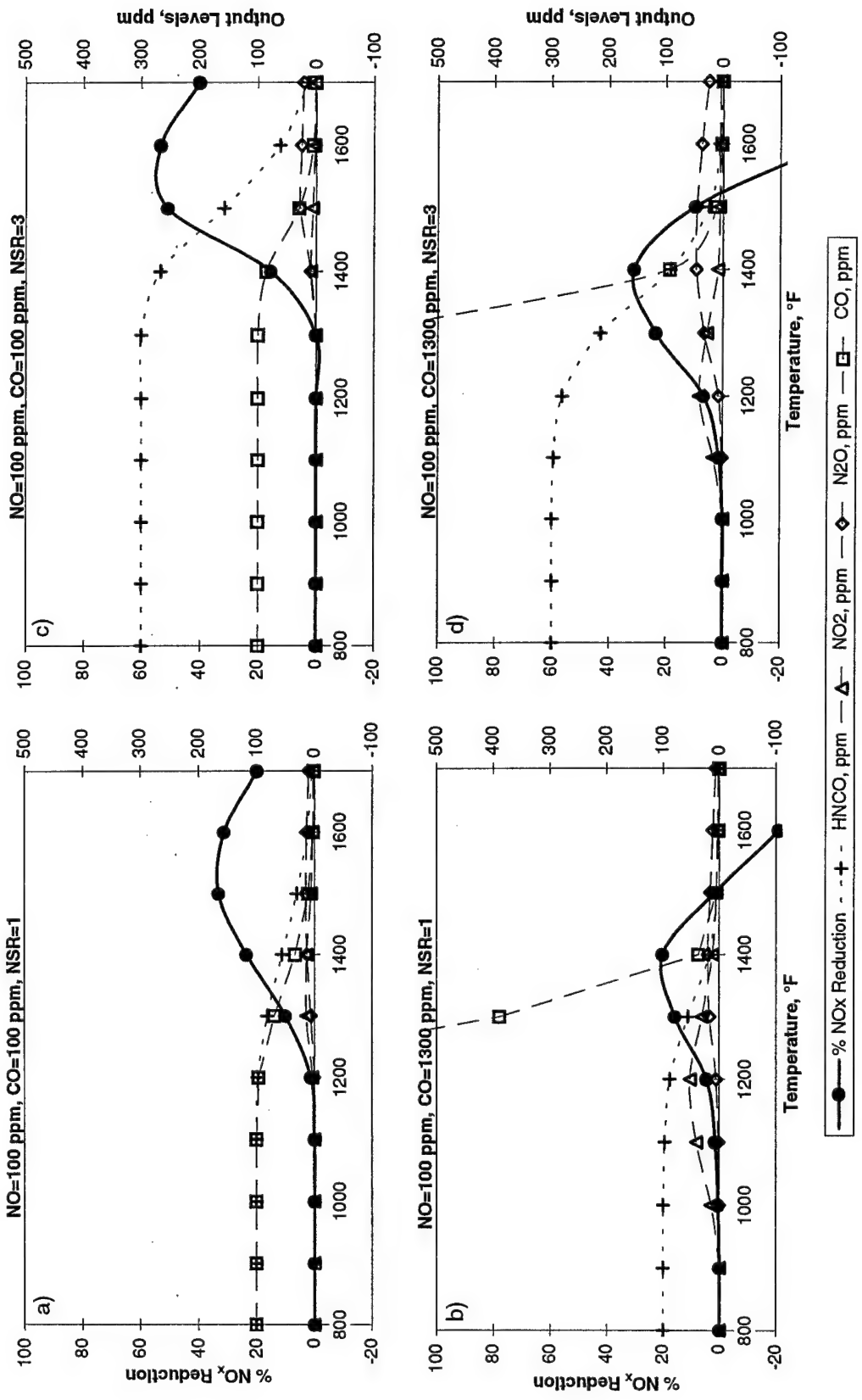

Figure E-3: Chemkin Modeling Results using Cyanuric Acid.

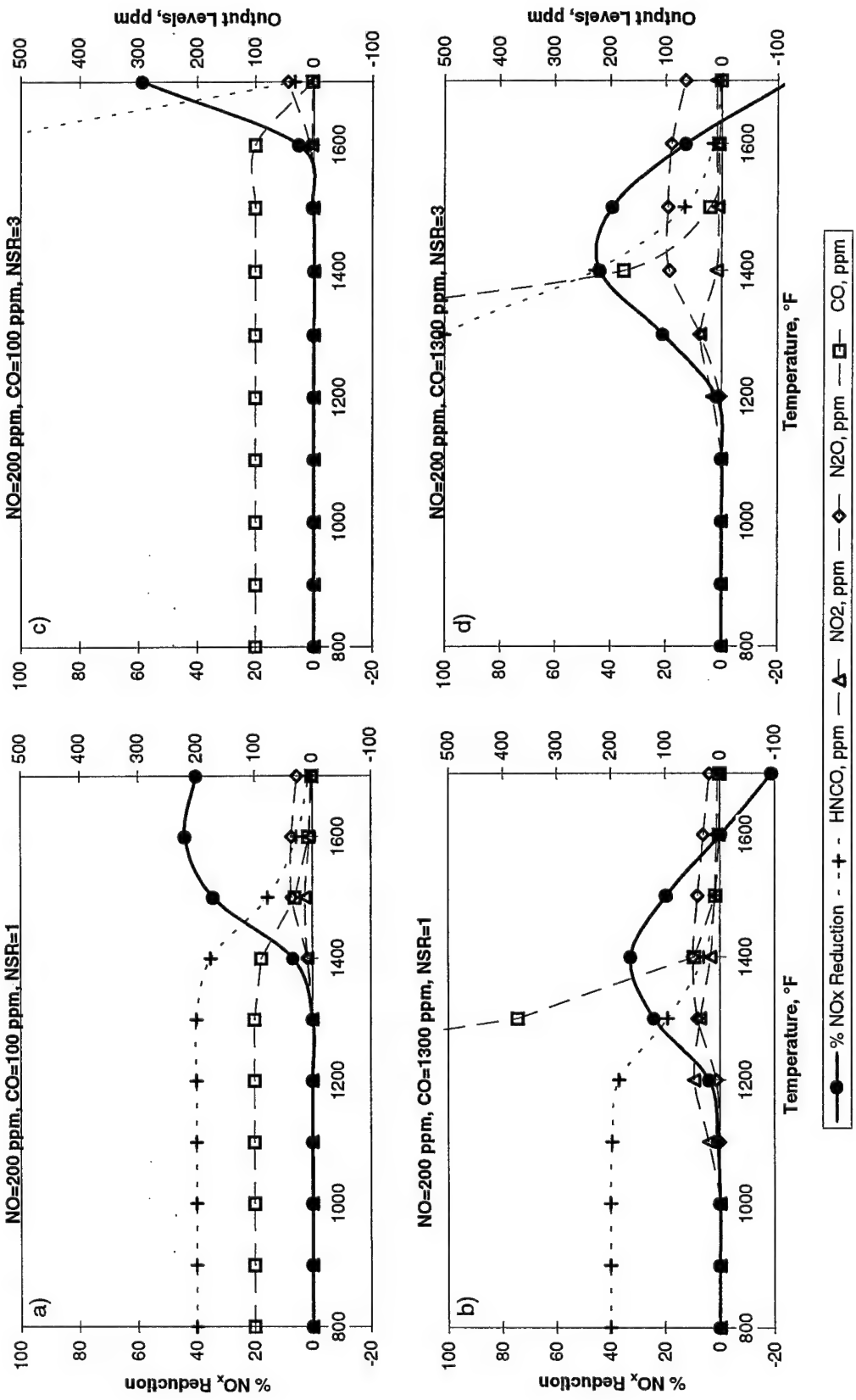

Figure E-4: Chemkin Modeling Results using Cyanuric Acid.

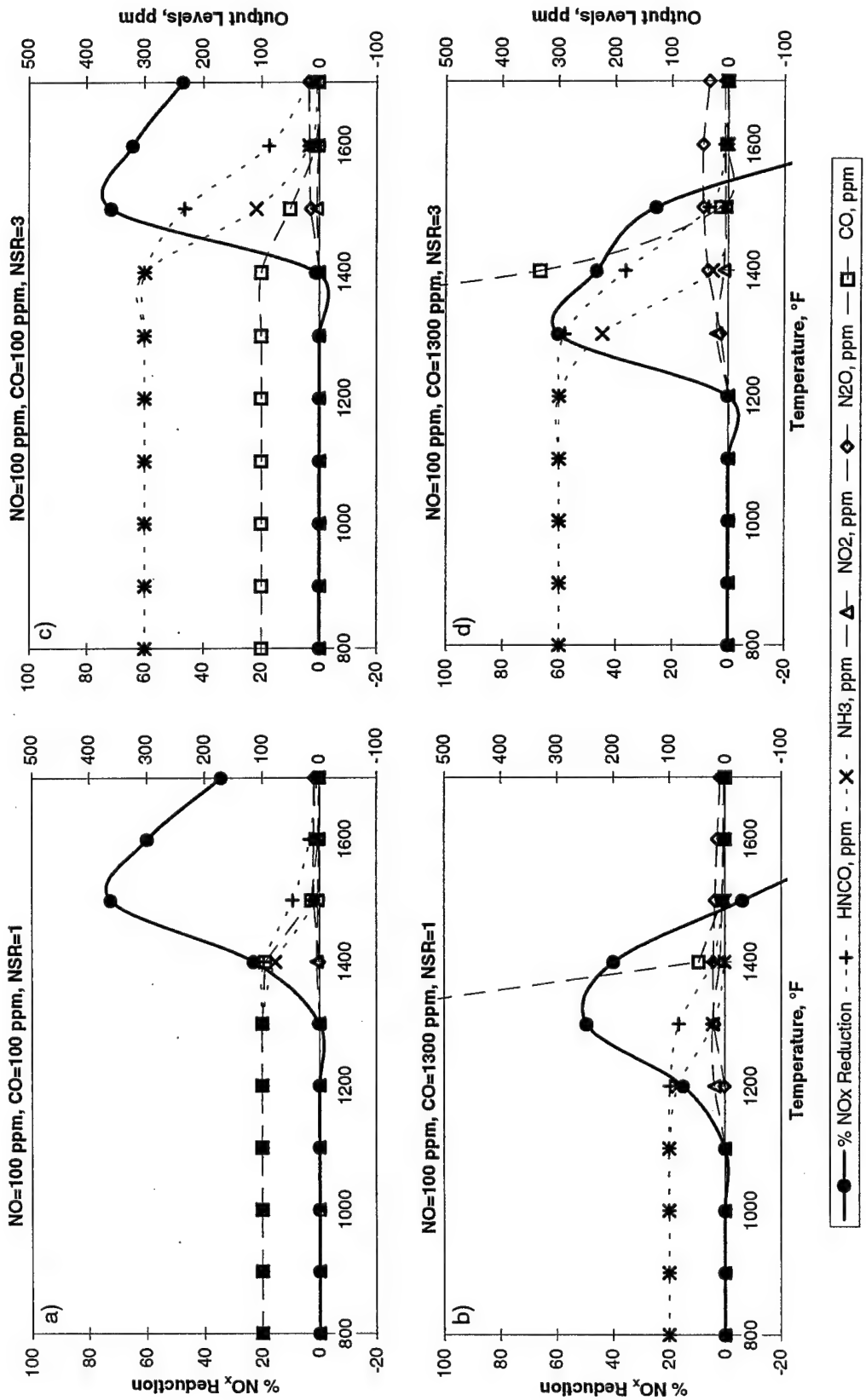

Figure E-5: Chemkin Modeling Results using Urea.

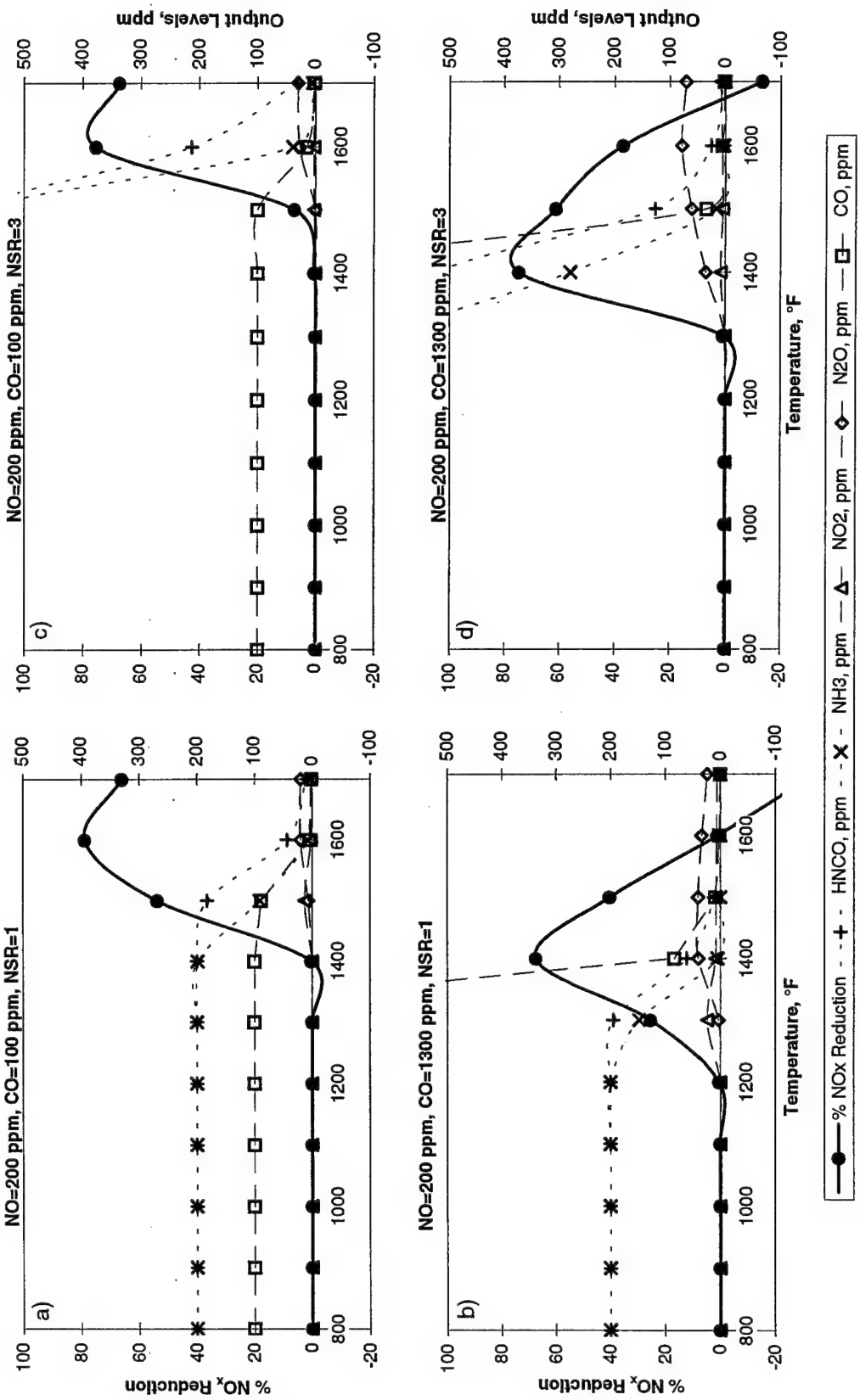

Figure E-6: Chemkin Modeling Results using Urea.

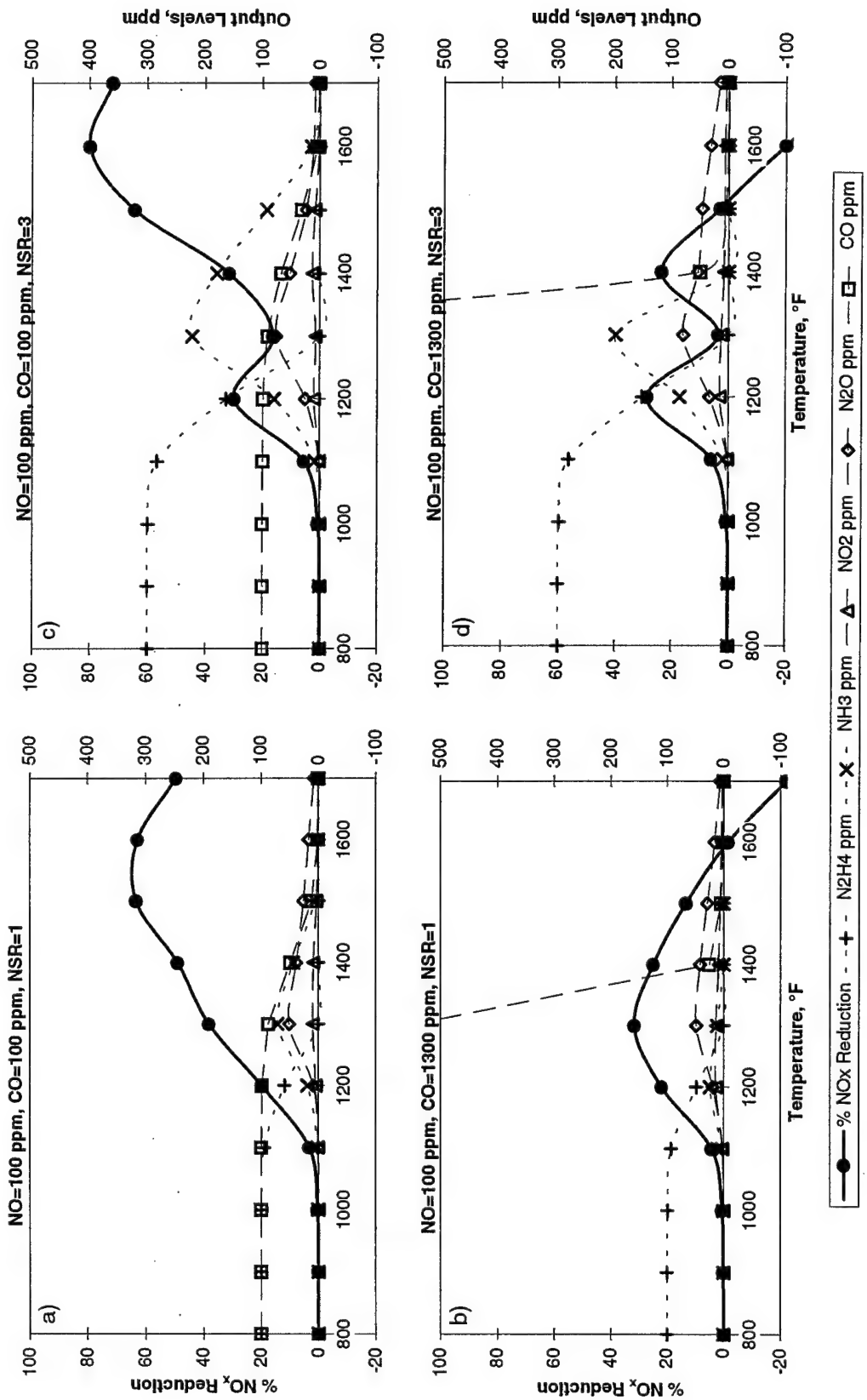

Figure E-7: Chemkin Modeling Results using Hydrazine.

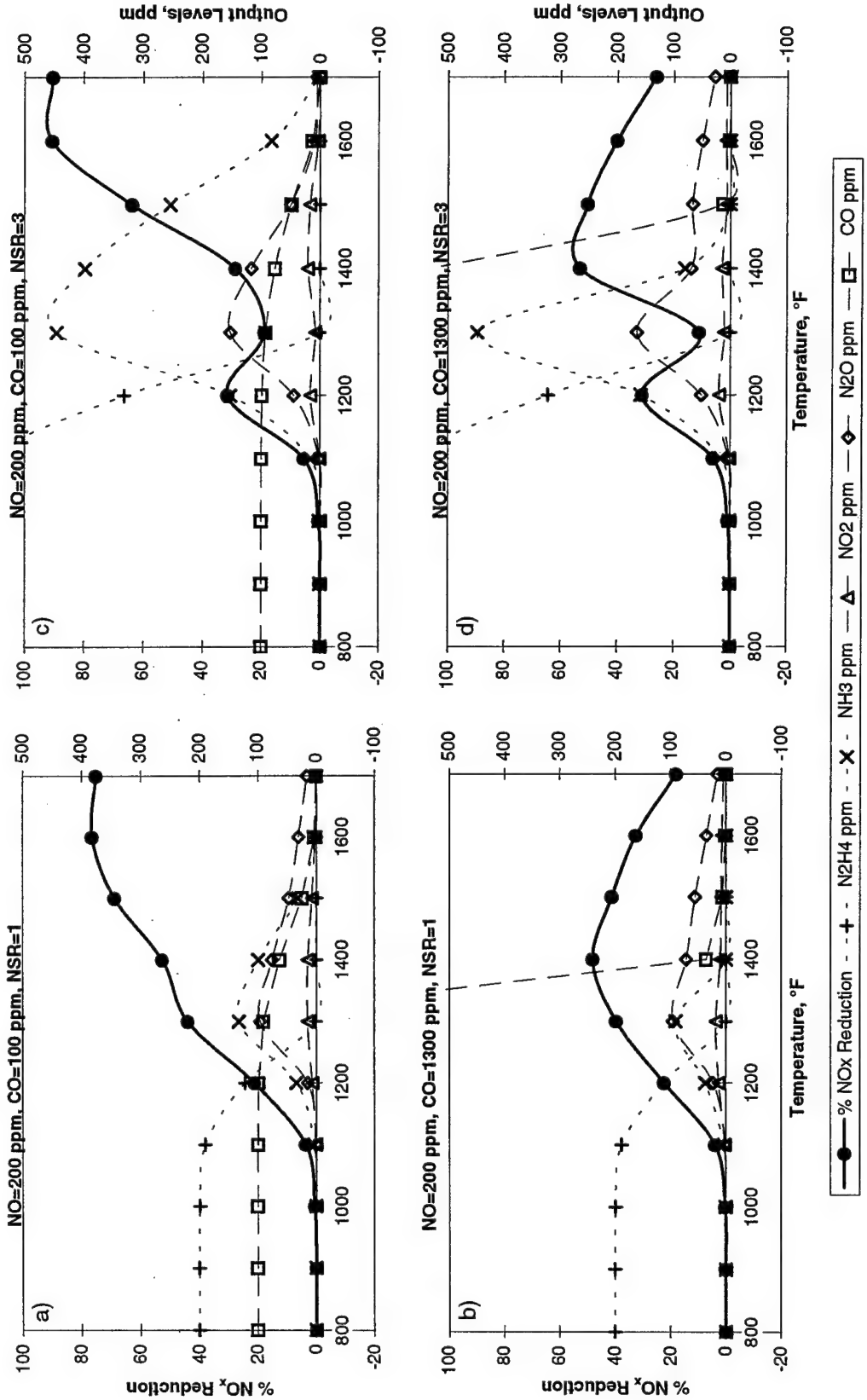

Figure E-8: Chemkin Modeling Results using Hydrazine.

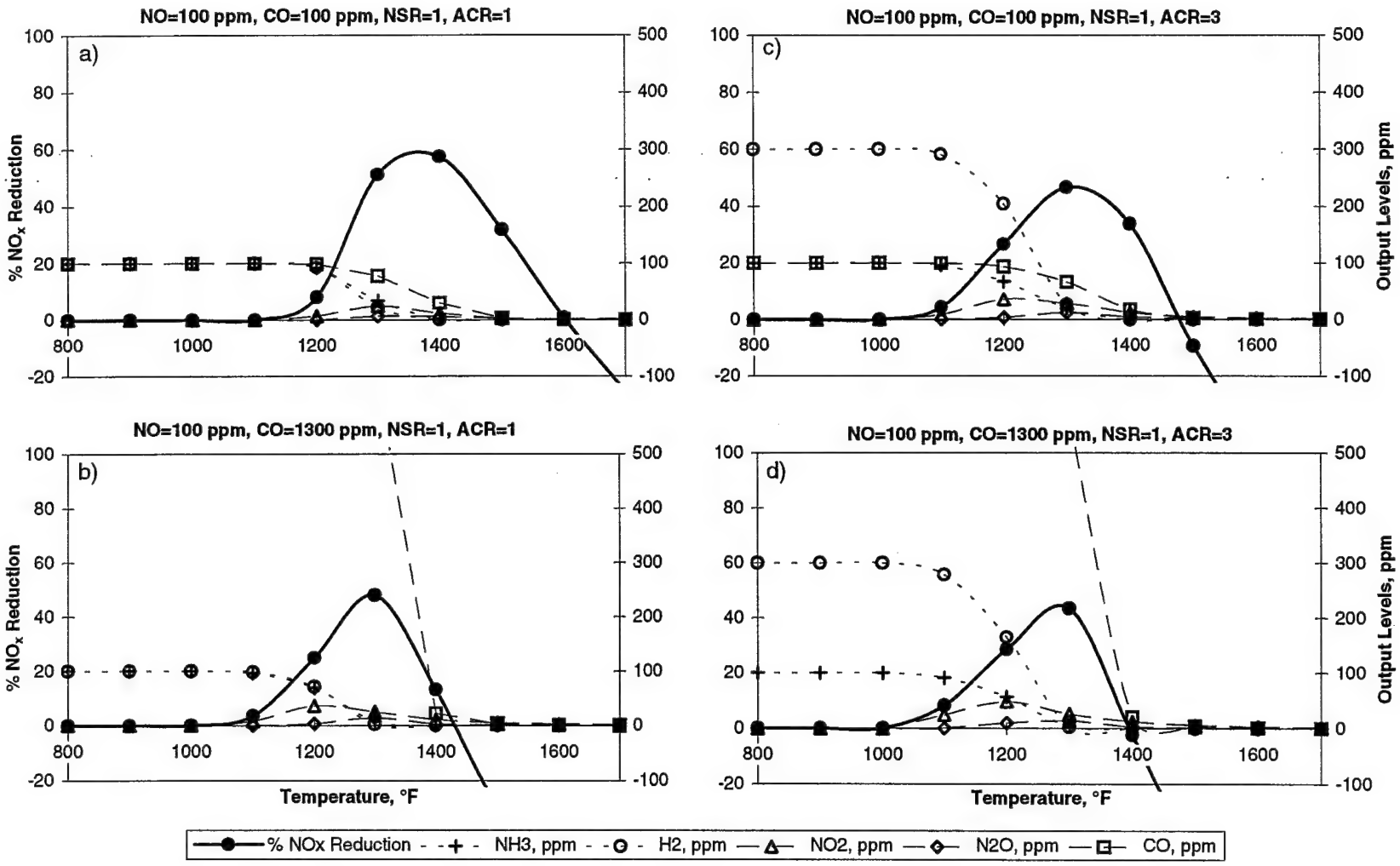

Figure E-9: Chemkin Modeling Results using Ammonia with Hydrogen Additive.

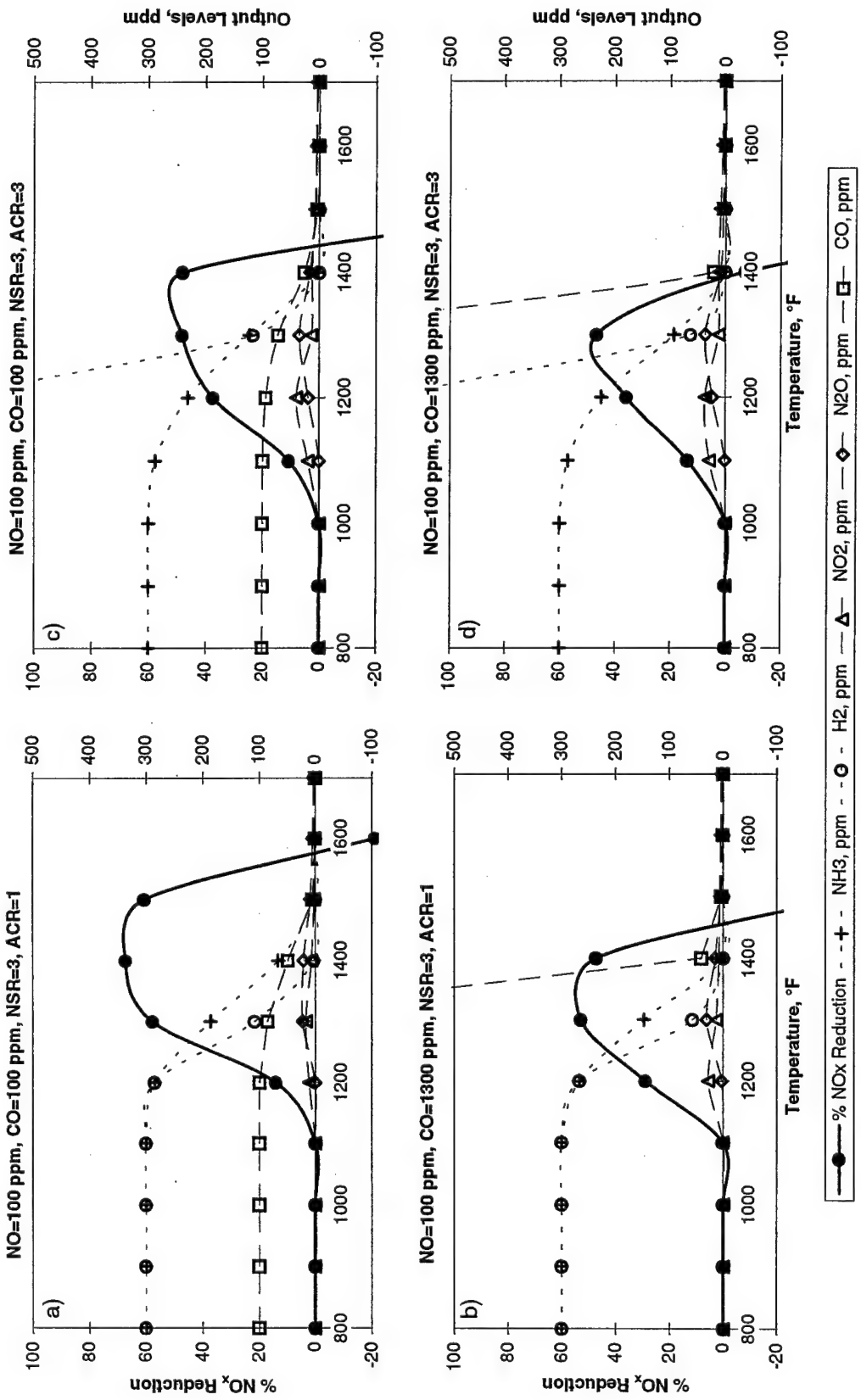

Figure E-10: Chemkin Modeling Results using Ammonia with Hydrogen Additive.

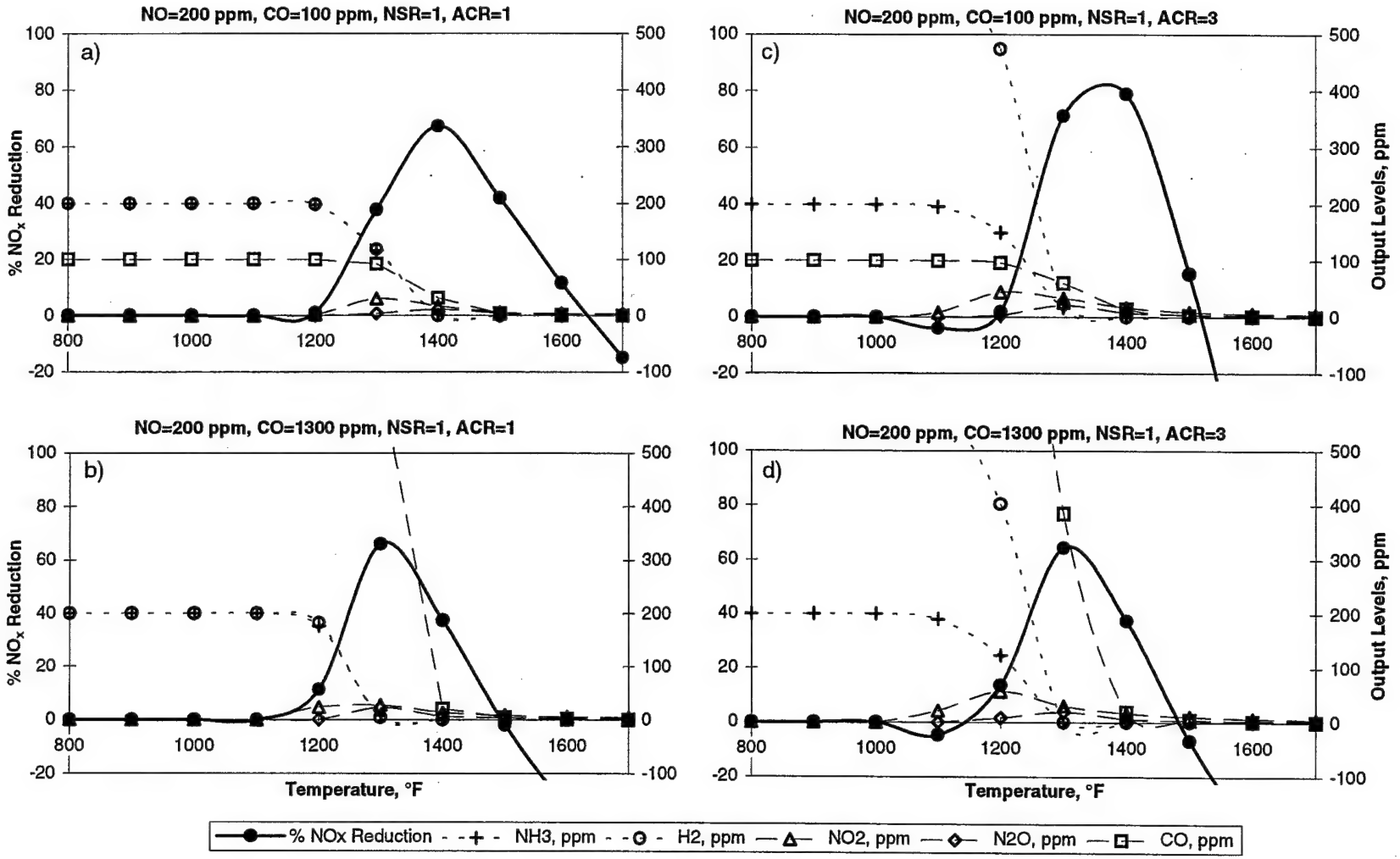

Figure E-11: Chemkin Modeling Results using Ammonia with Hydrogen Additive.

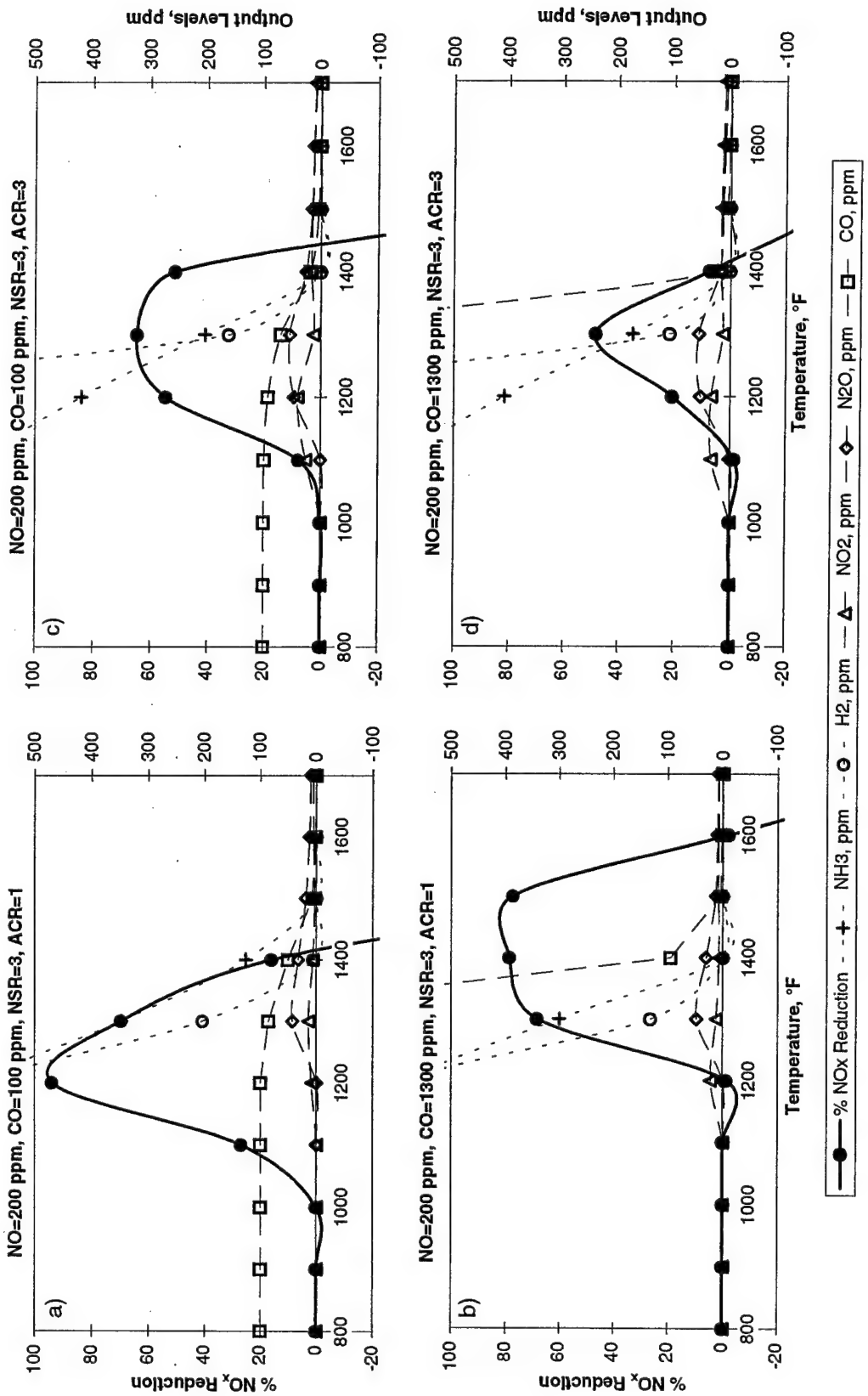

Figure E-12: Chemkin Modeling Results using Ammonia with Hydrogen Additive.

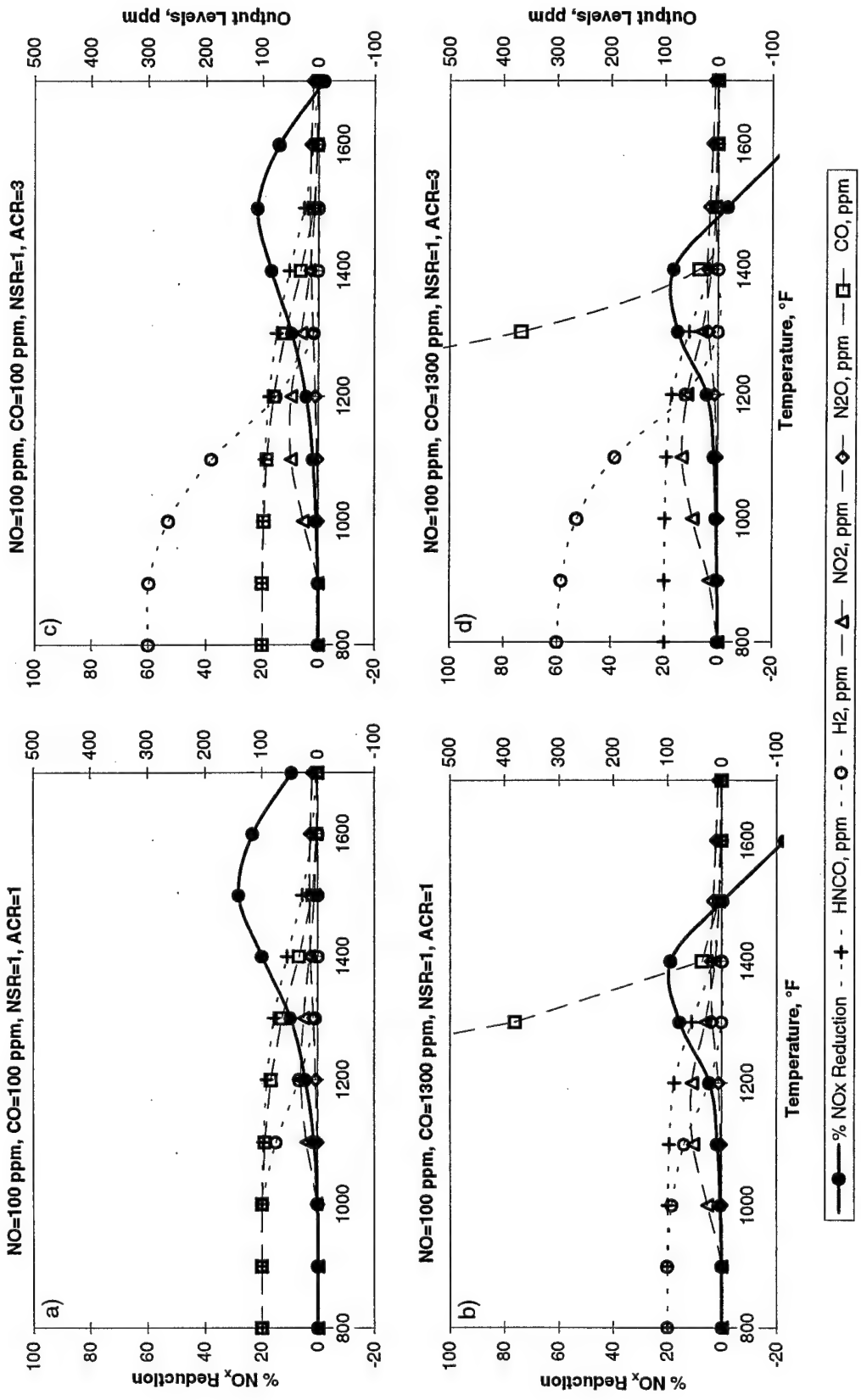

Figure E-13: Chemkin Modeling Results using Cyanuric Acid with Hydrogen Additive.

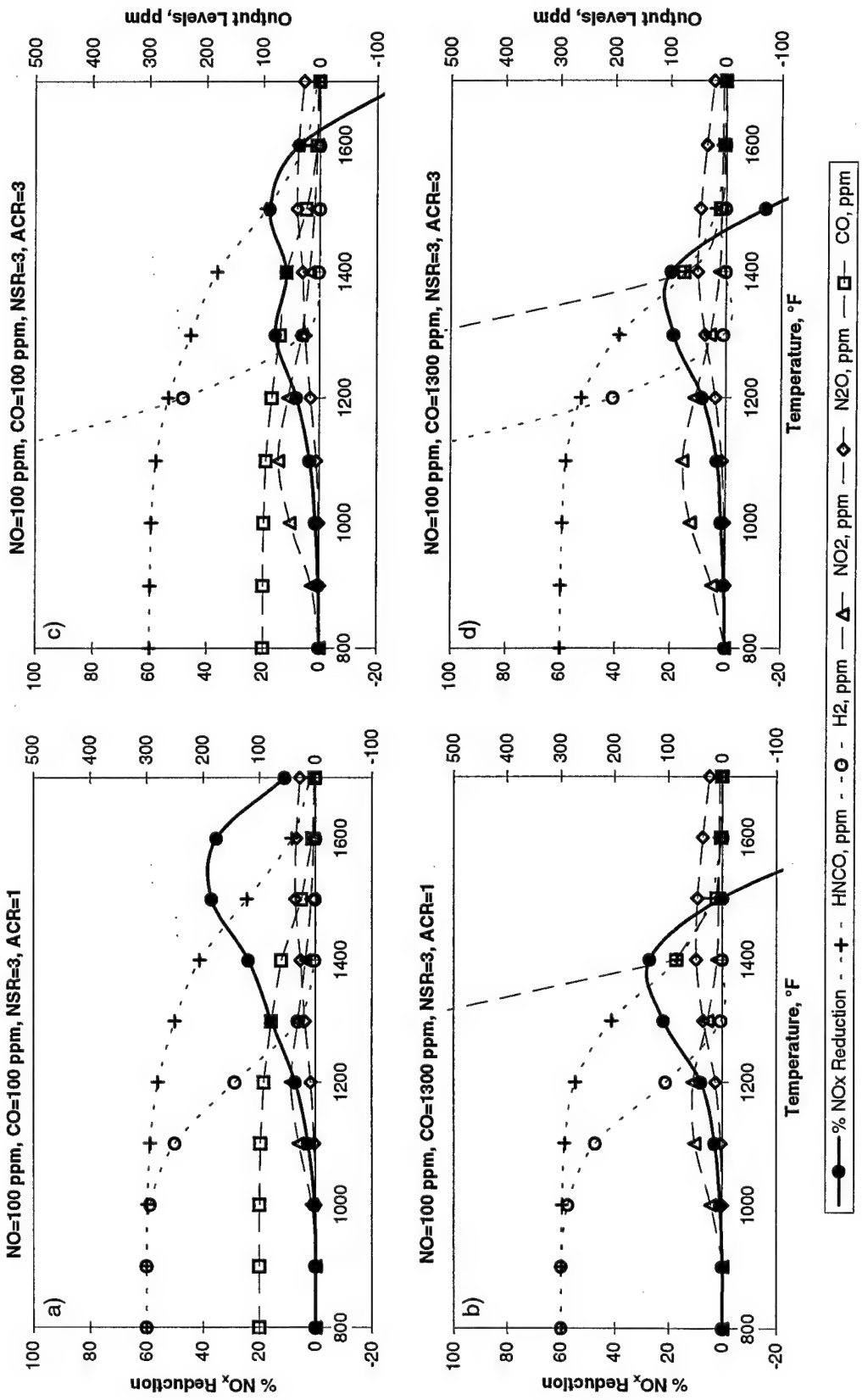

Figure E-14: Chemkin Modeling Results using Cyanuric Acid with Hydrogen Additive.

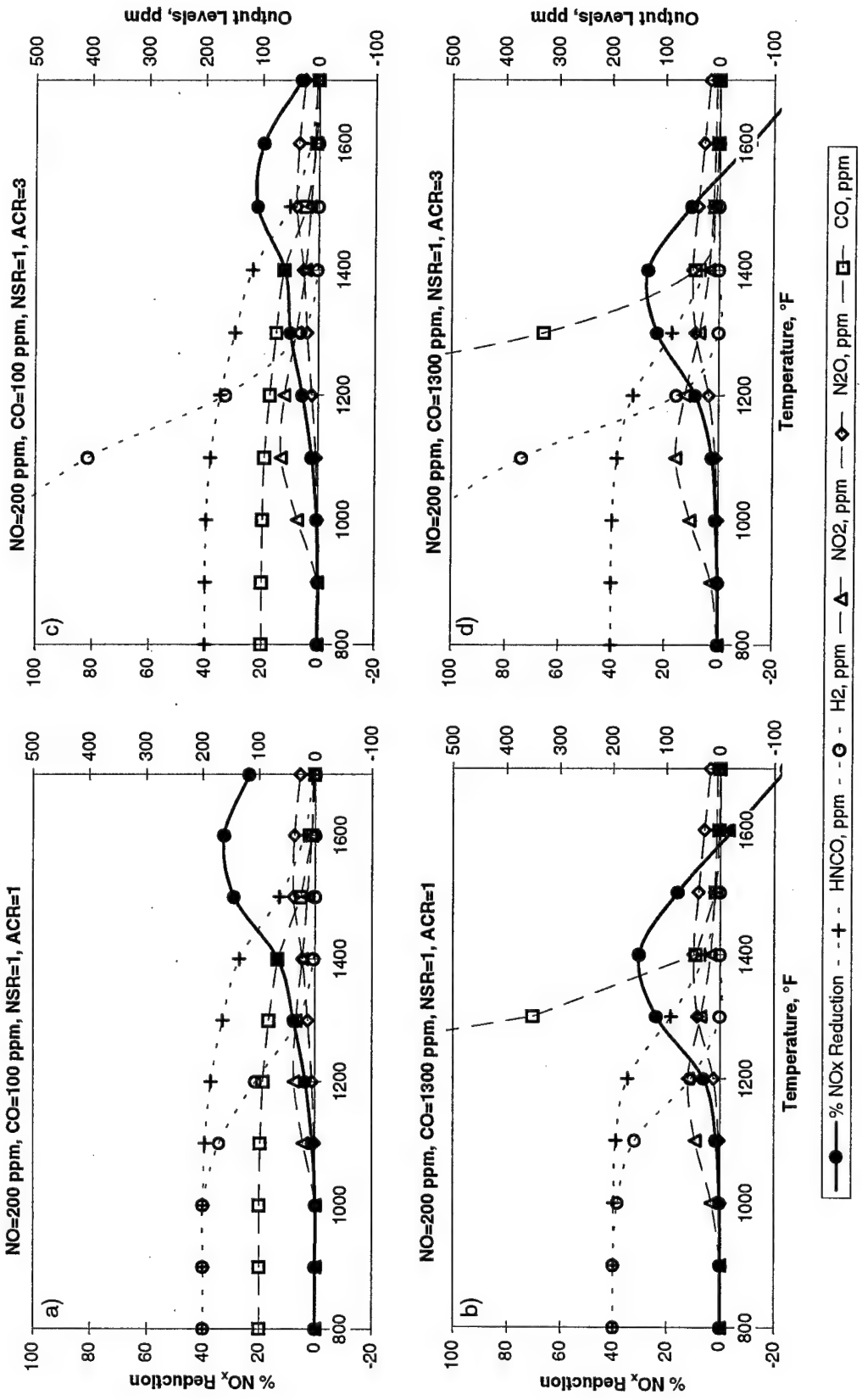

Figure E-15: Chemkin Modeling Results using Cyanuric Acid with Hydrogen Additive.

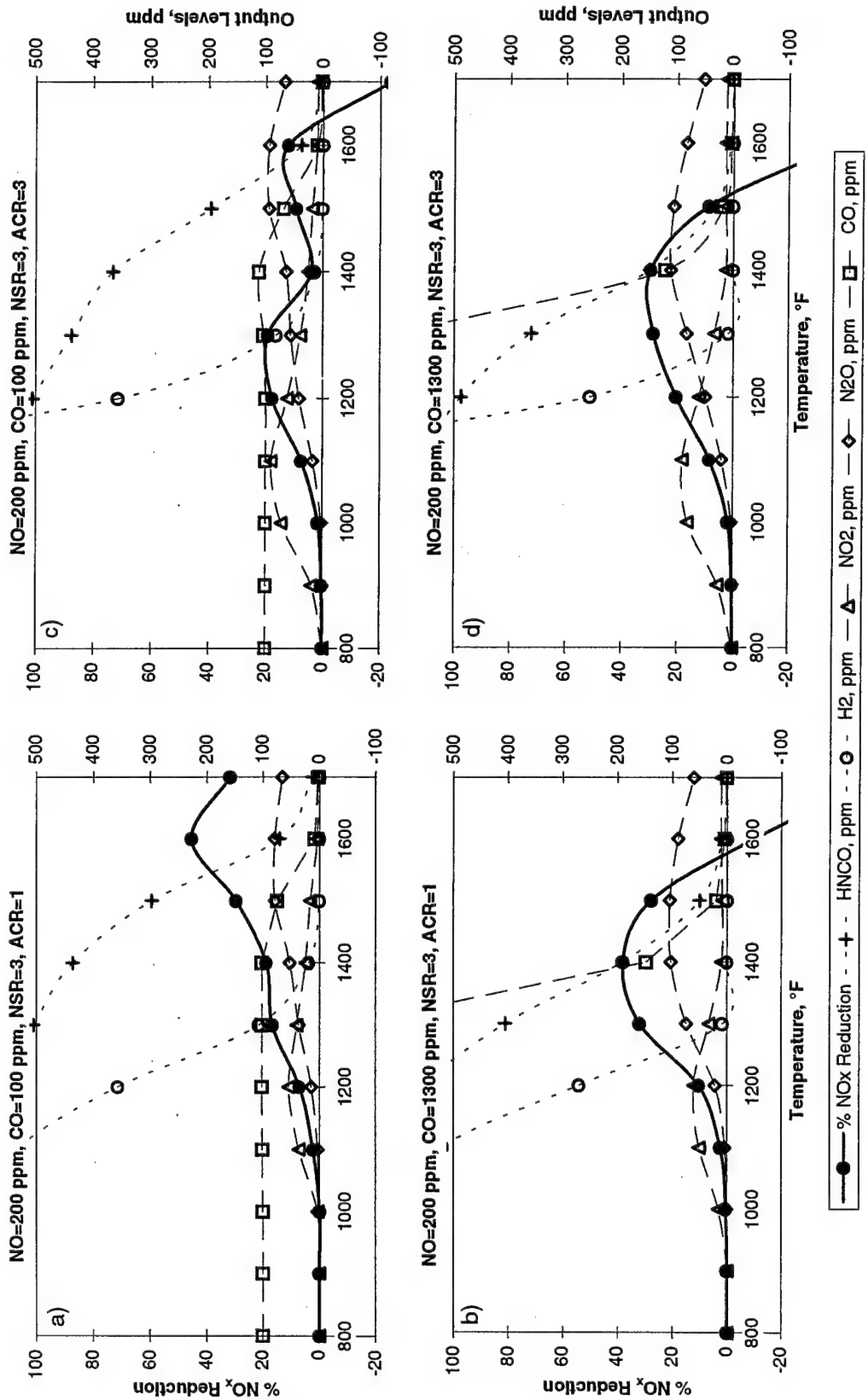

Figure E-16: Chemkin Modeling Results using Cyanuric Acid with Hydrogen Additive.

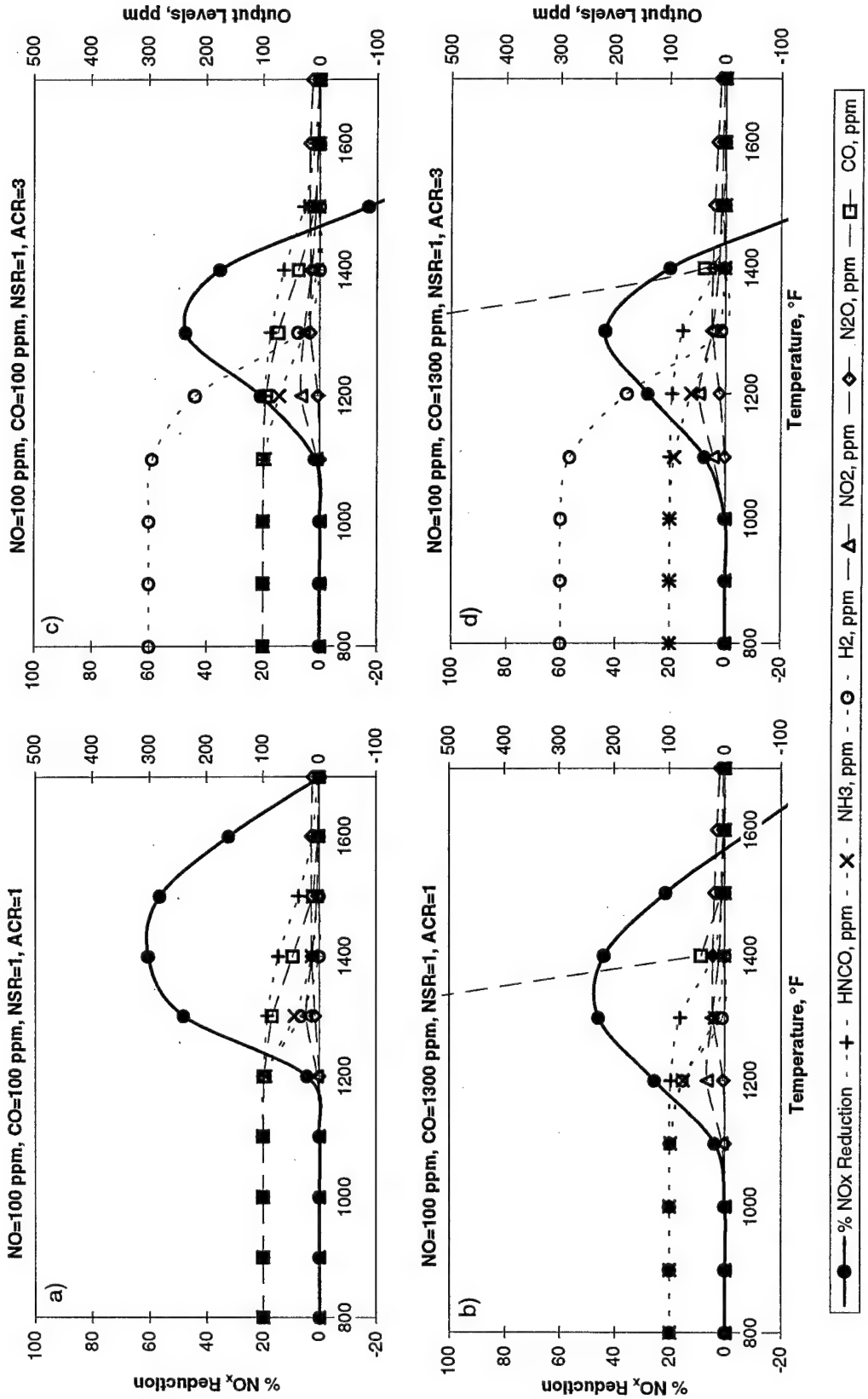

Figure E-17: Chemkin Modeling Results using Urea with Hydrogen Additive.

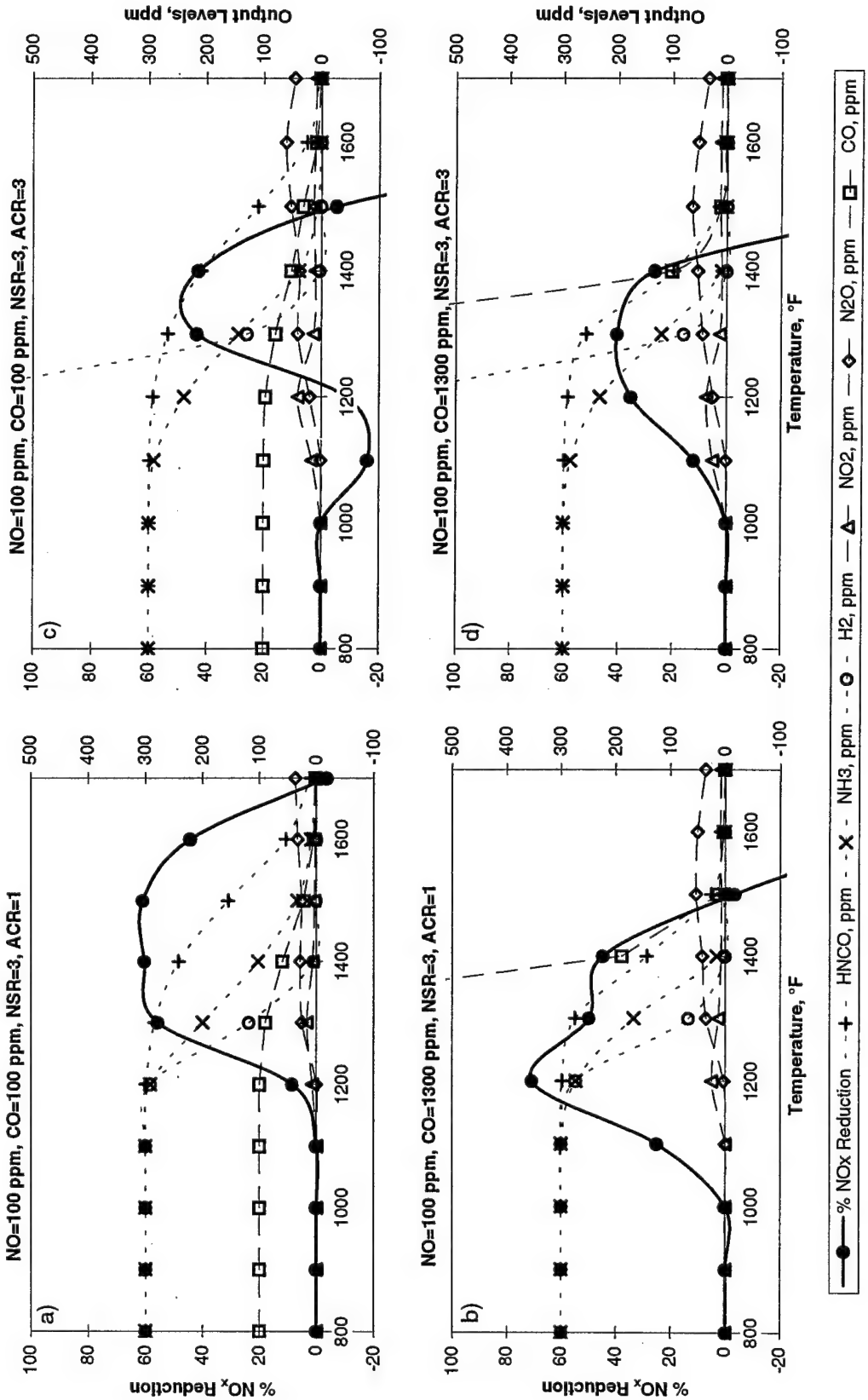

Figure E-18: Chemkin Modeling Results using Urea with Hydrogen Additive.

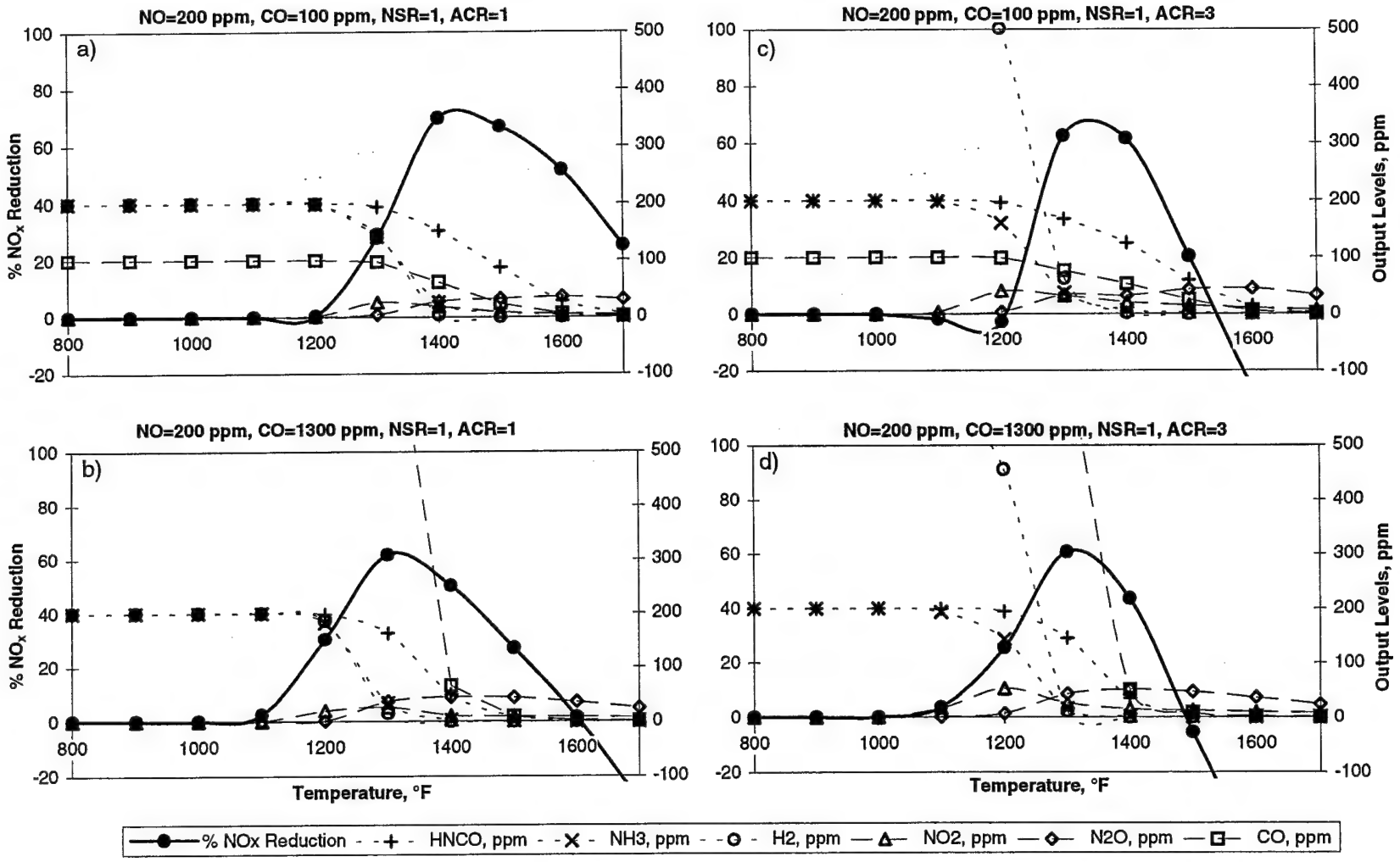

Figure E-19: Chemkin Modeling Results using Urea with Hydrogen Additive.

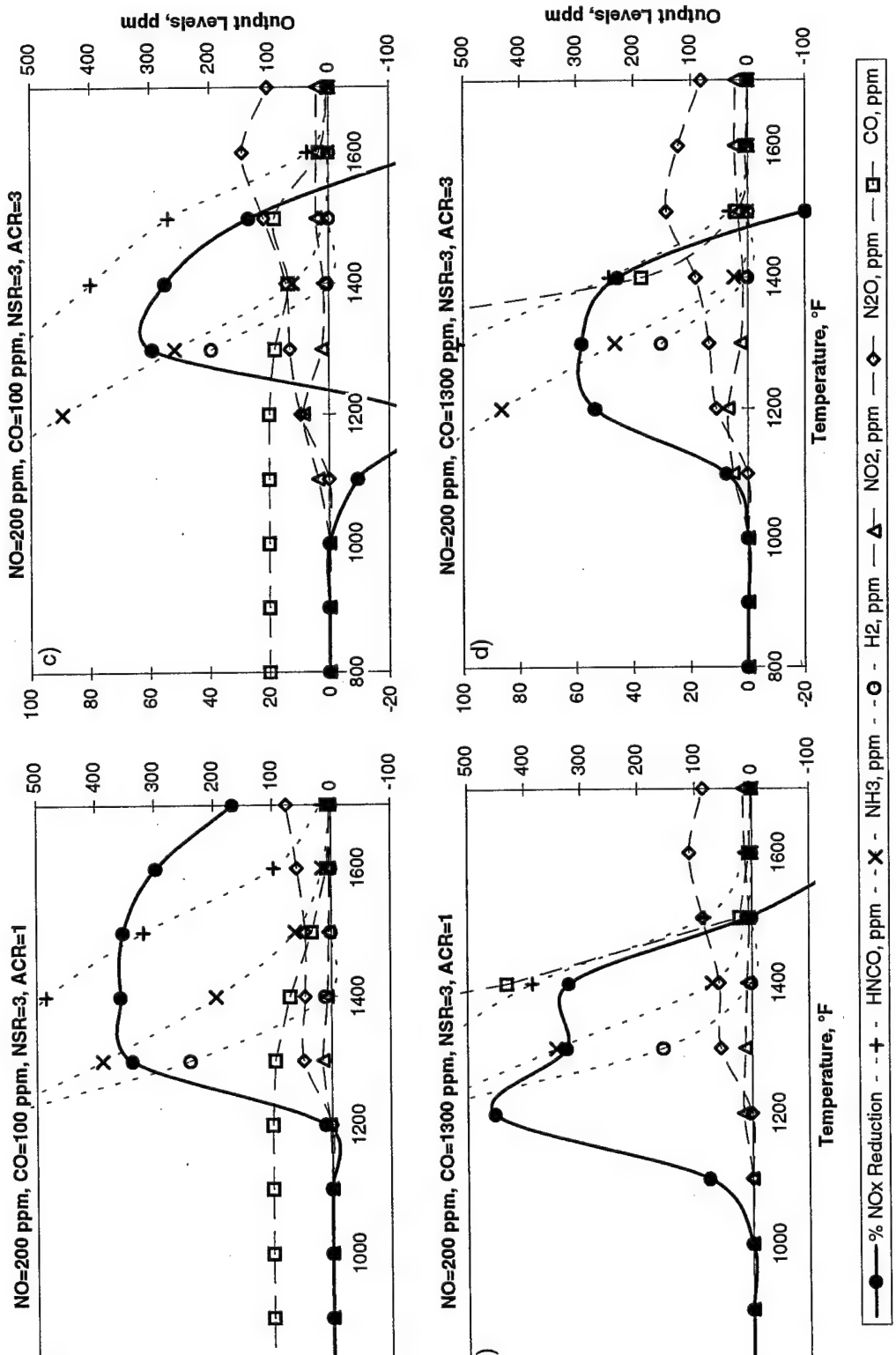

Figure E-20: Chemkin Modeling Results using Urea with Hydrogen Additive.

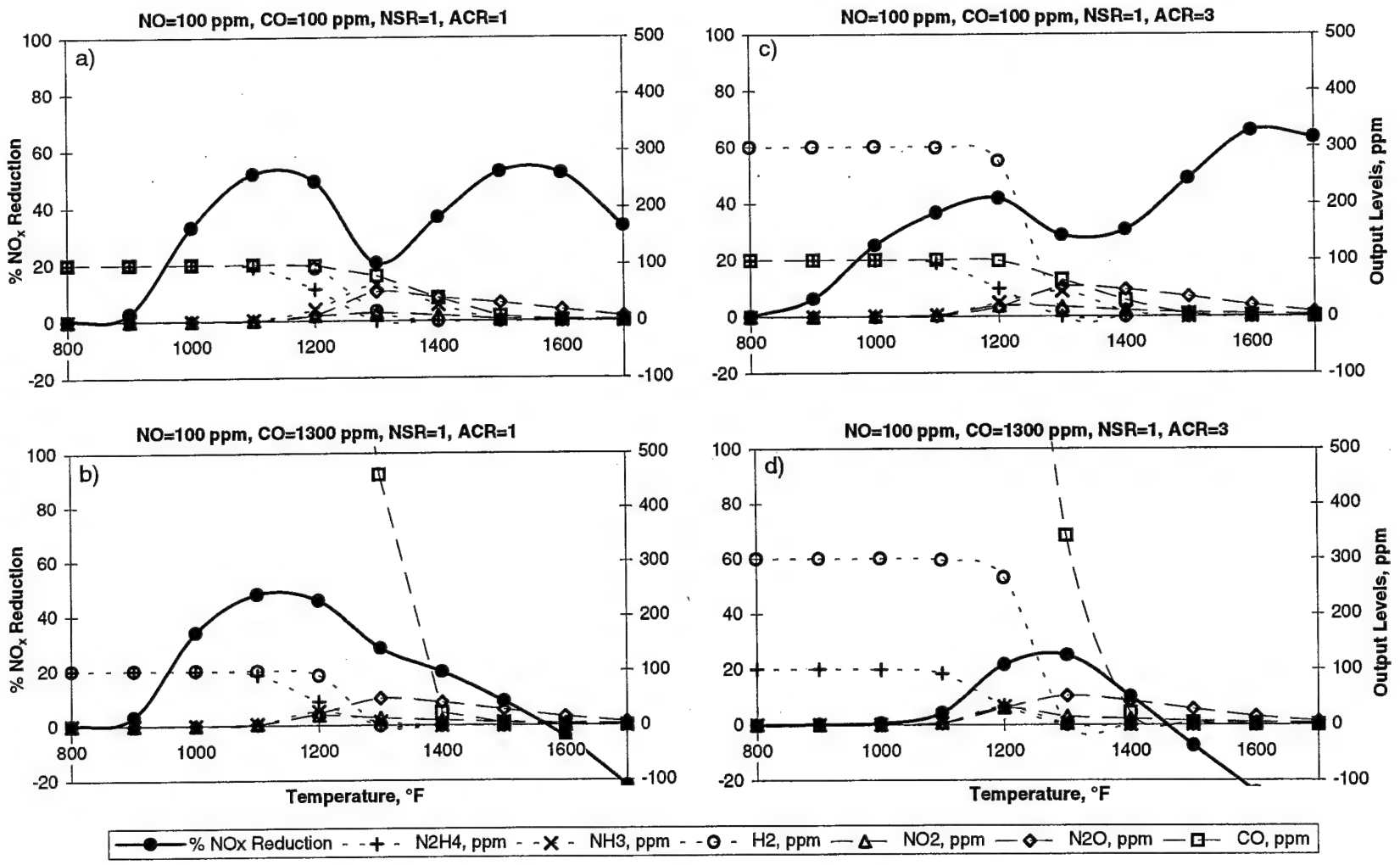

Figure E-21: Chemkin Modeling Results using Hydrazine with Hydrogen Additive.

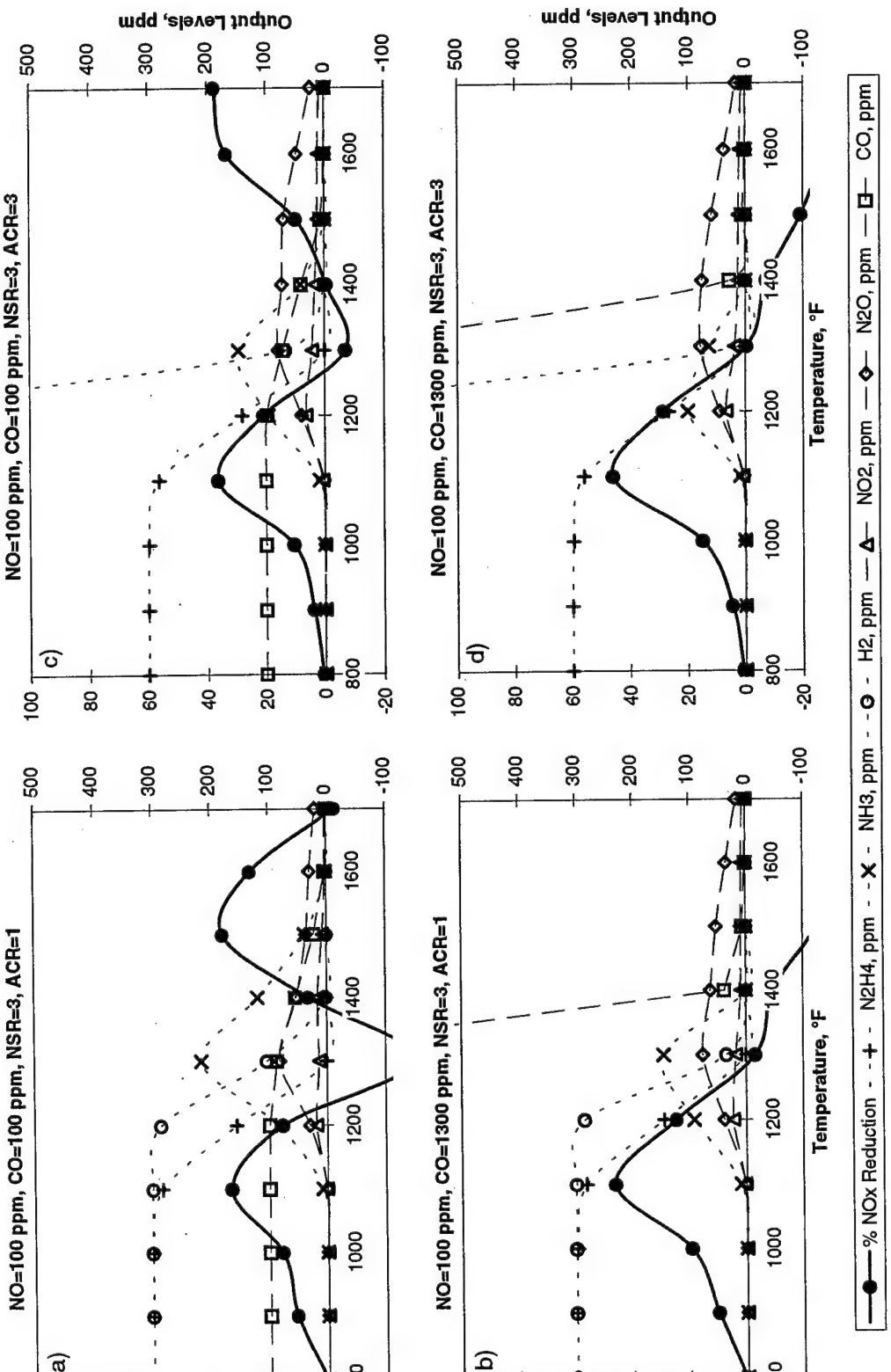

Figure E-22: Chemkin Modeling Results using Hydrazine with Hydrogen Additive.

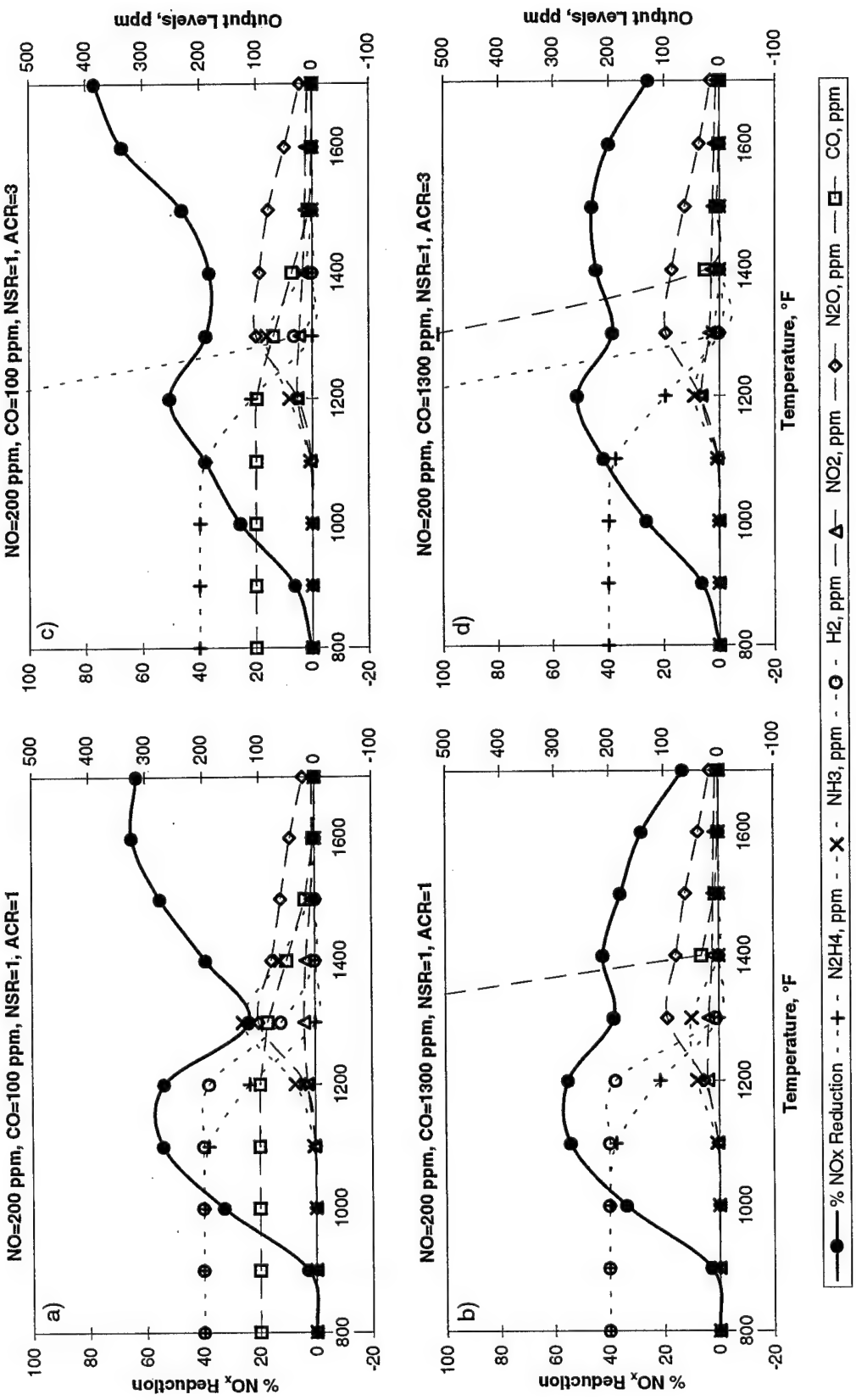

Figure E-23: Chemkin Modeling Results using Hydrazine with Hydrogen Additive.

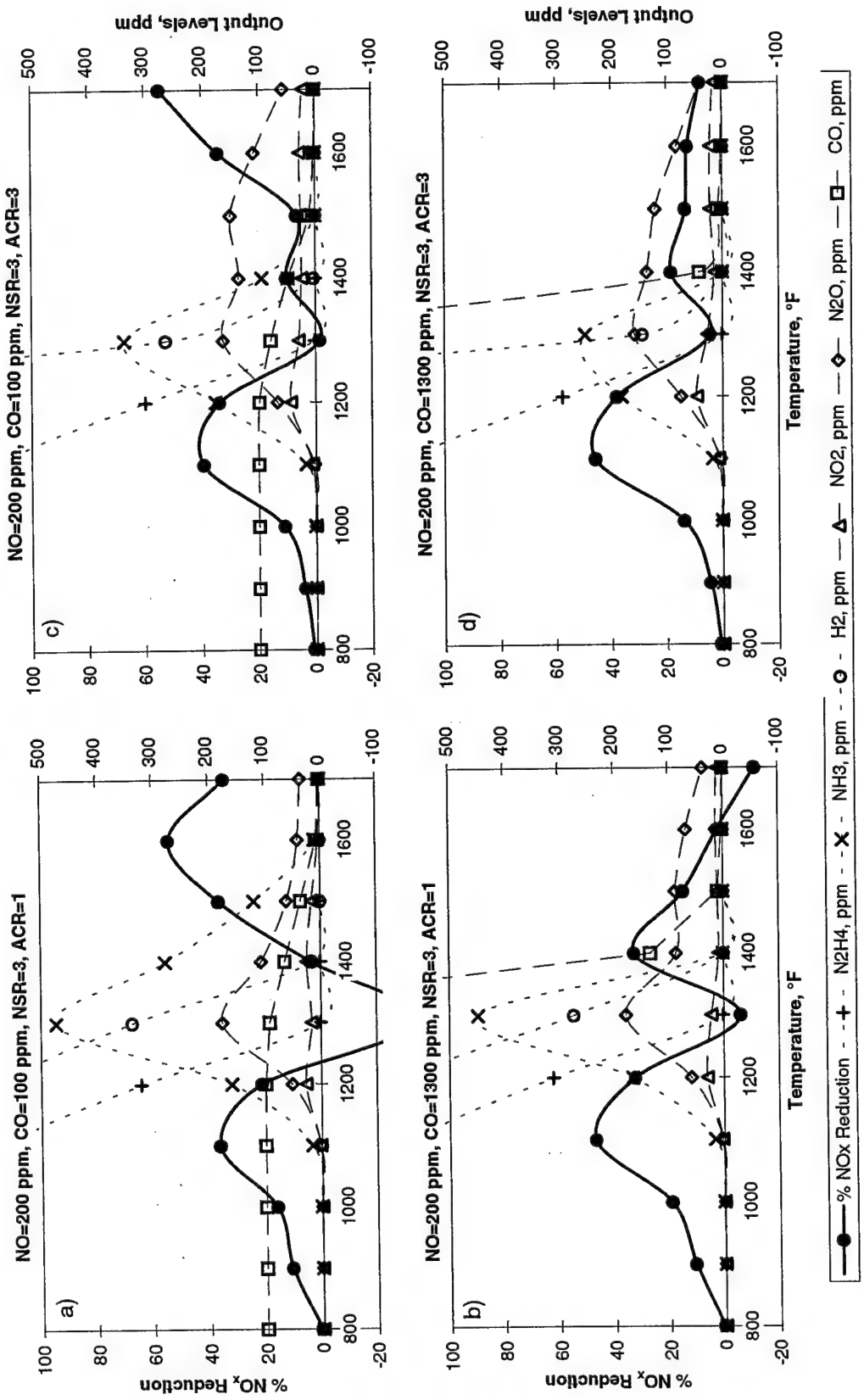

Figure E-24: Chemkin Modeling Results using Hydrazine with Hydrogen Additive.

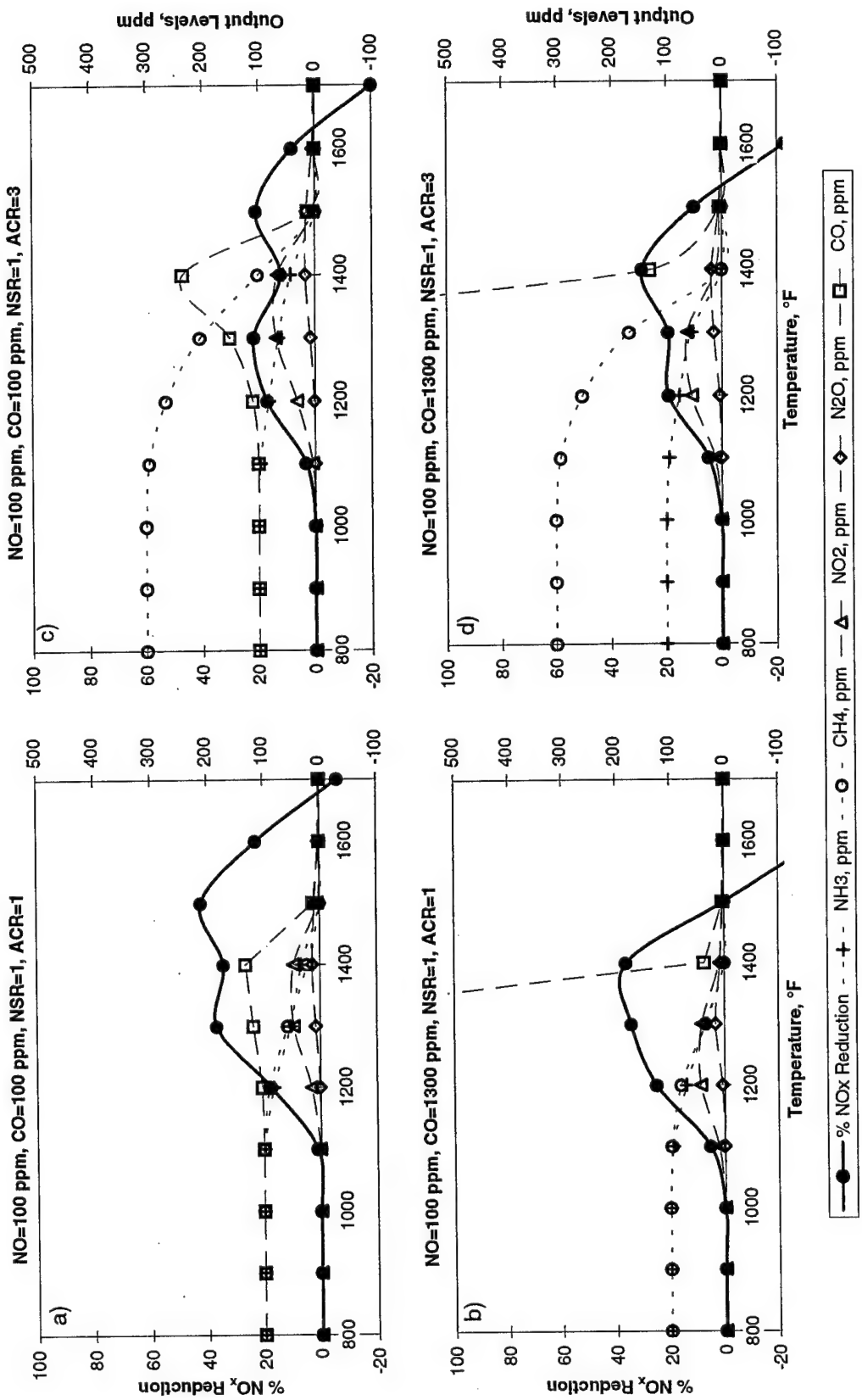

Figure E-25: Chemkin Modeling Results using Ammonia with Methane Additive.

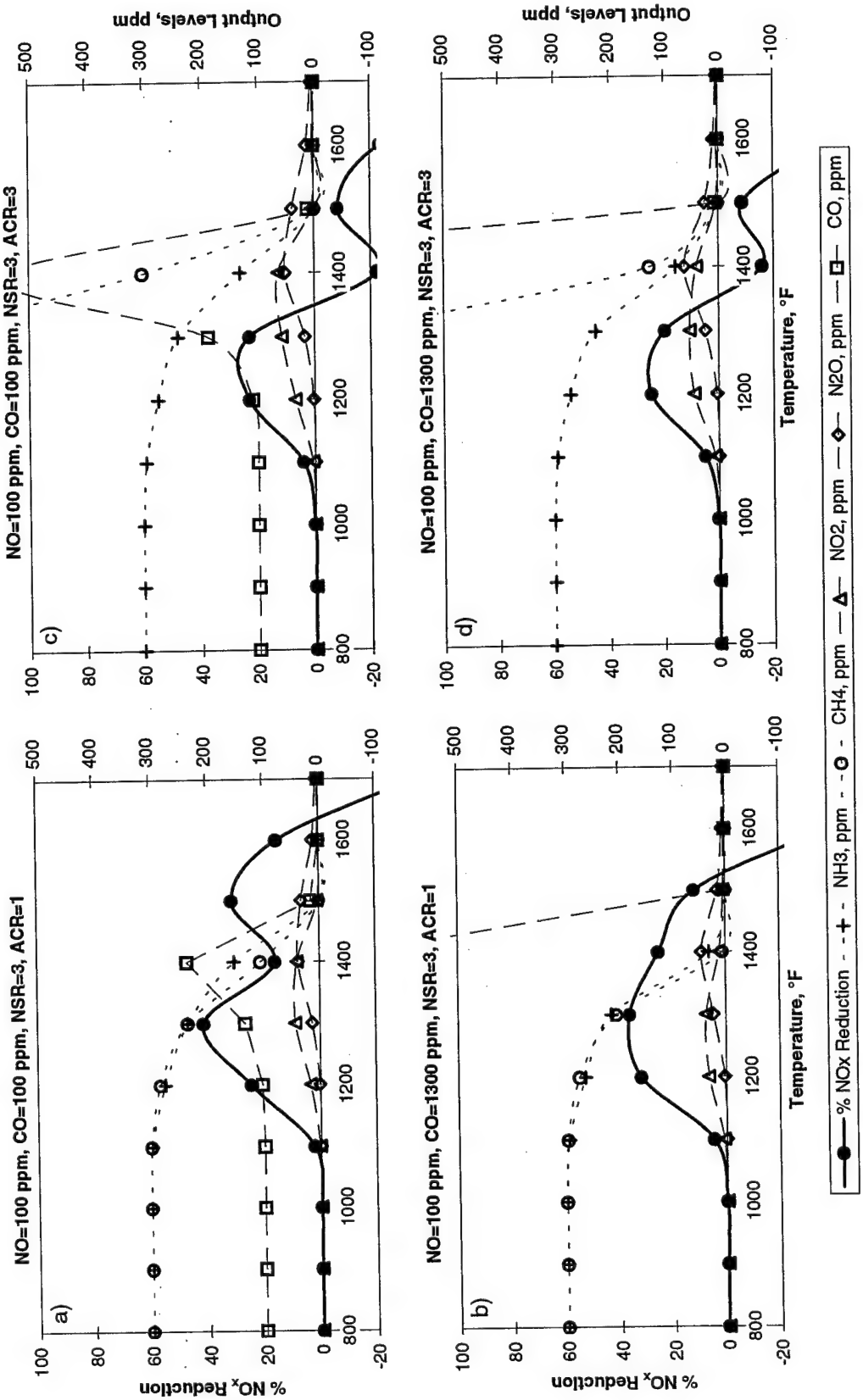

Figure E-26: Chemkin Modeling Results using Ammonia with Methane Additive.

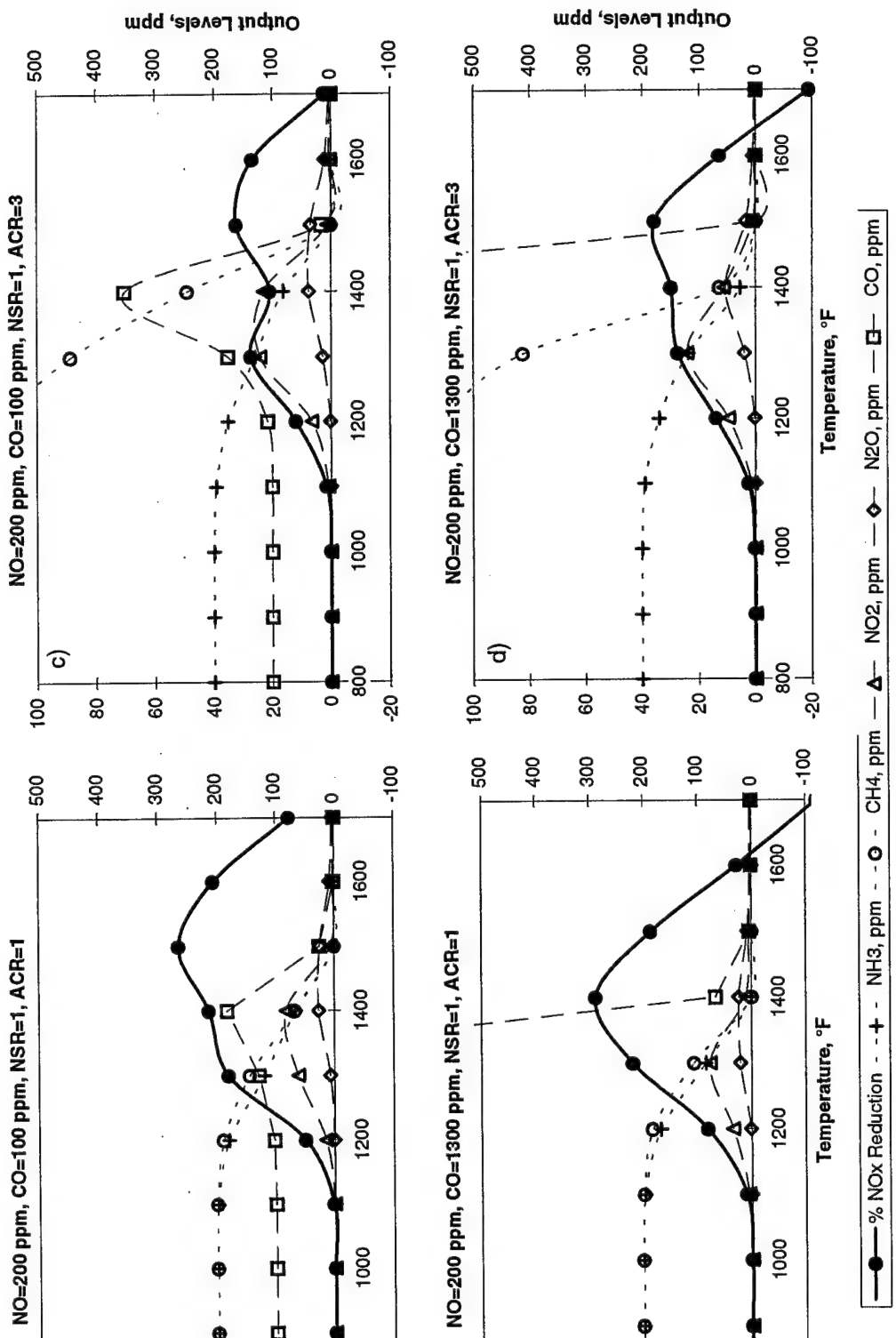

Figure E-27: Chemkin Modeling Results using Ammonia with Methane Additive.

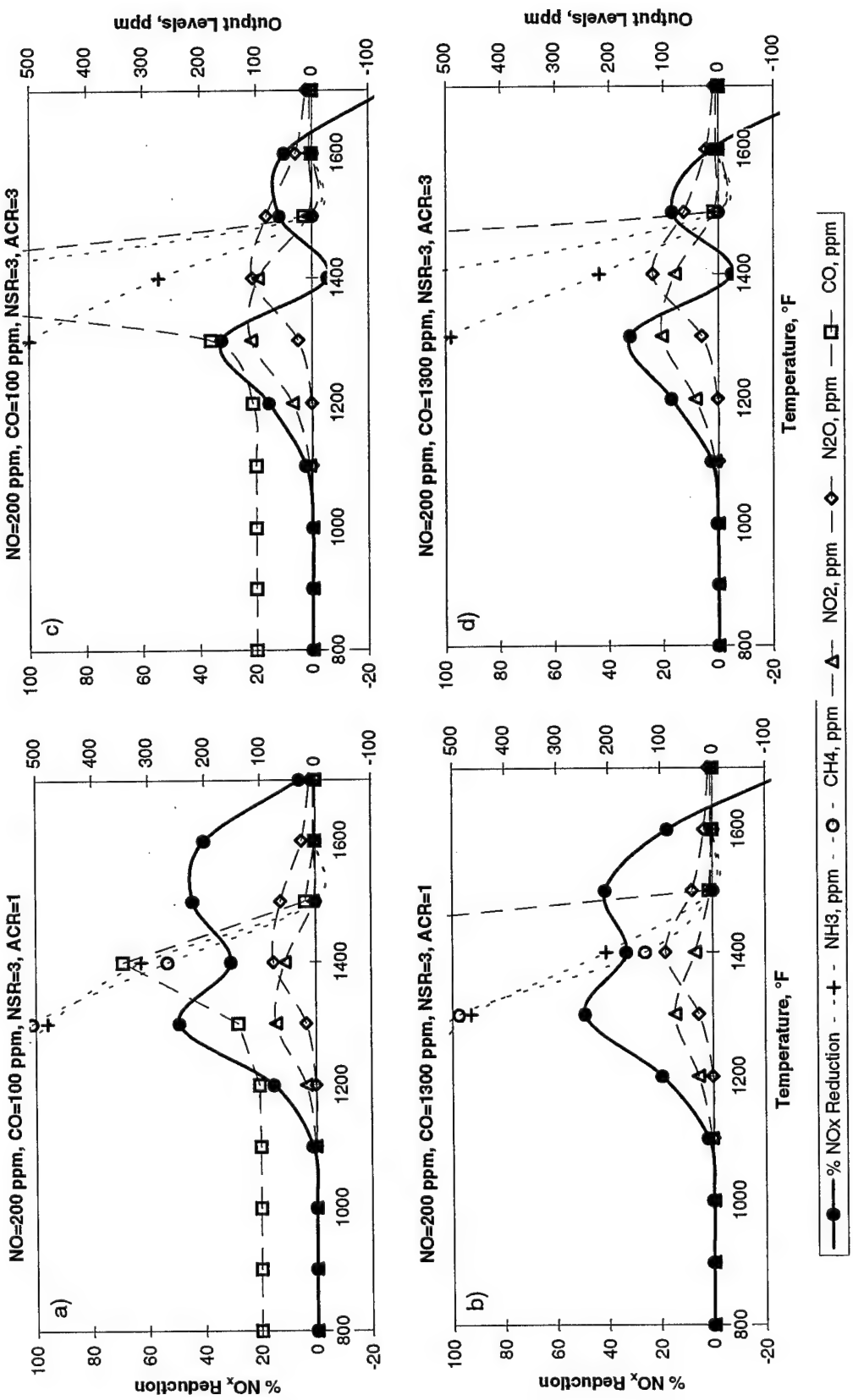

Figure E-28: Chemkin Modeling Results using Ammonia with Methane Additive.

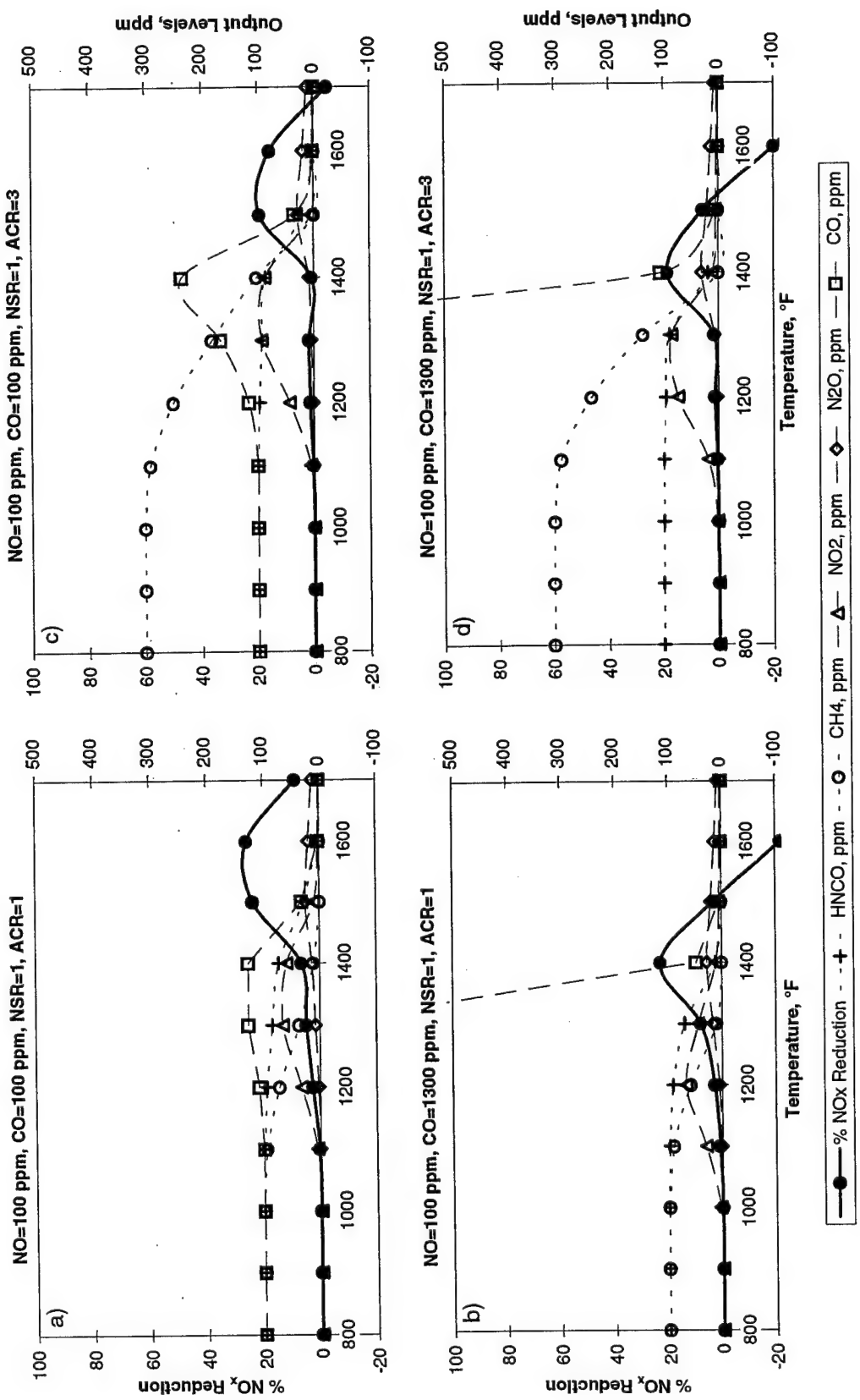

Figure E-29: Chemkin Modeling Results using Cyanuric Acid with Methane Additive.

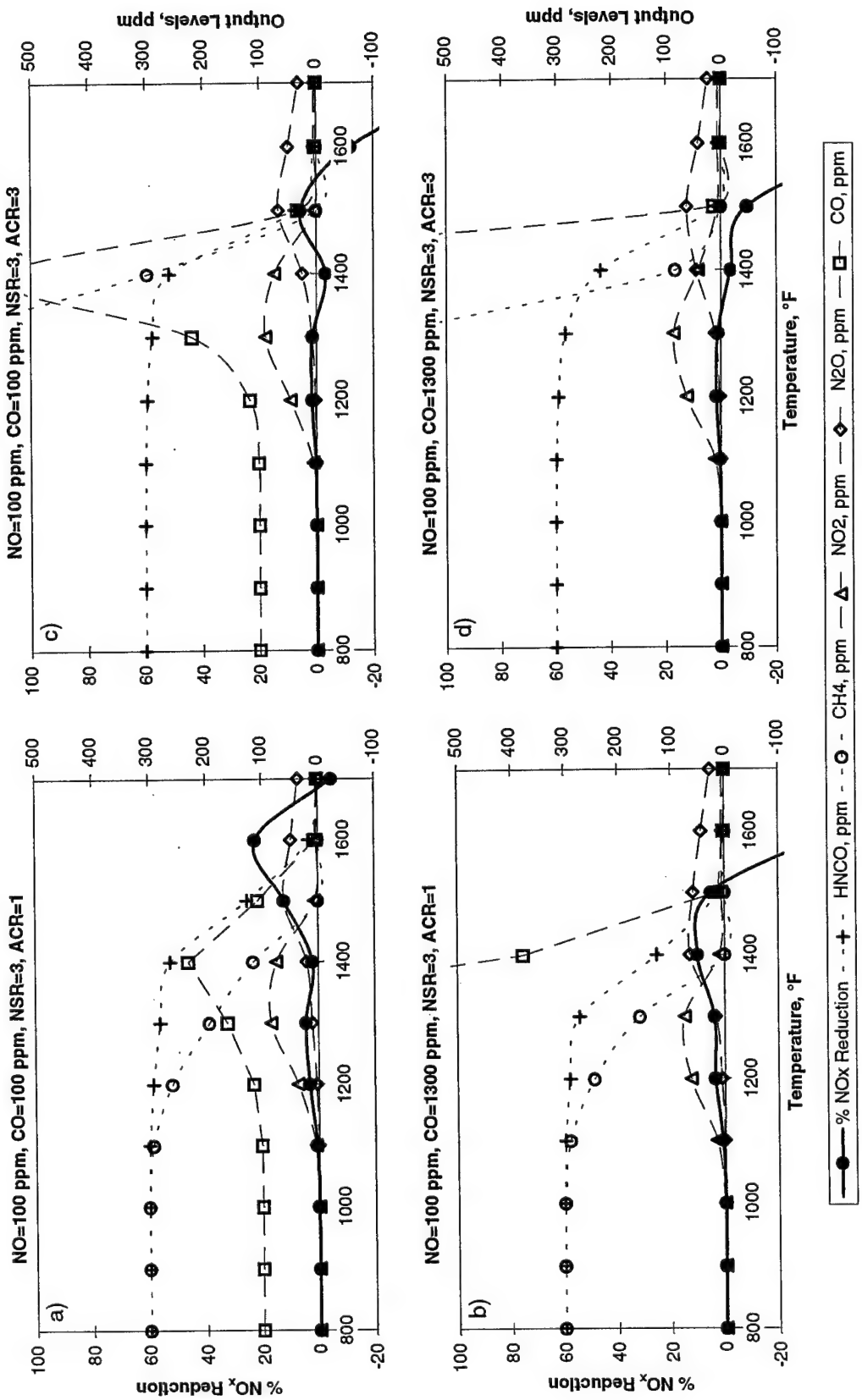

Figure E-30: Chemkin Modeling Results using Cyanuric Acid with Methane Additive.

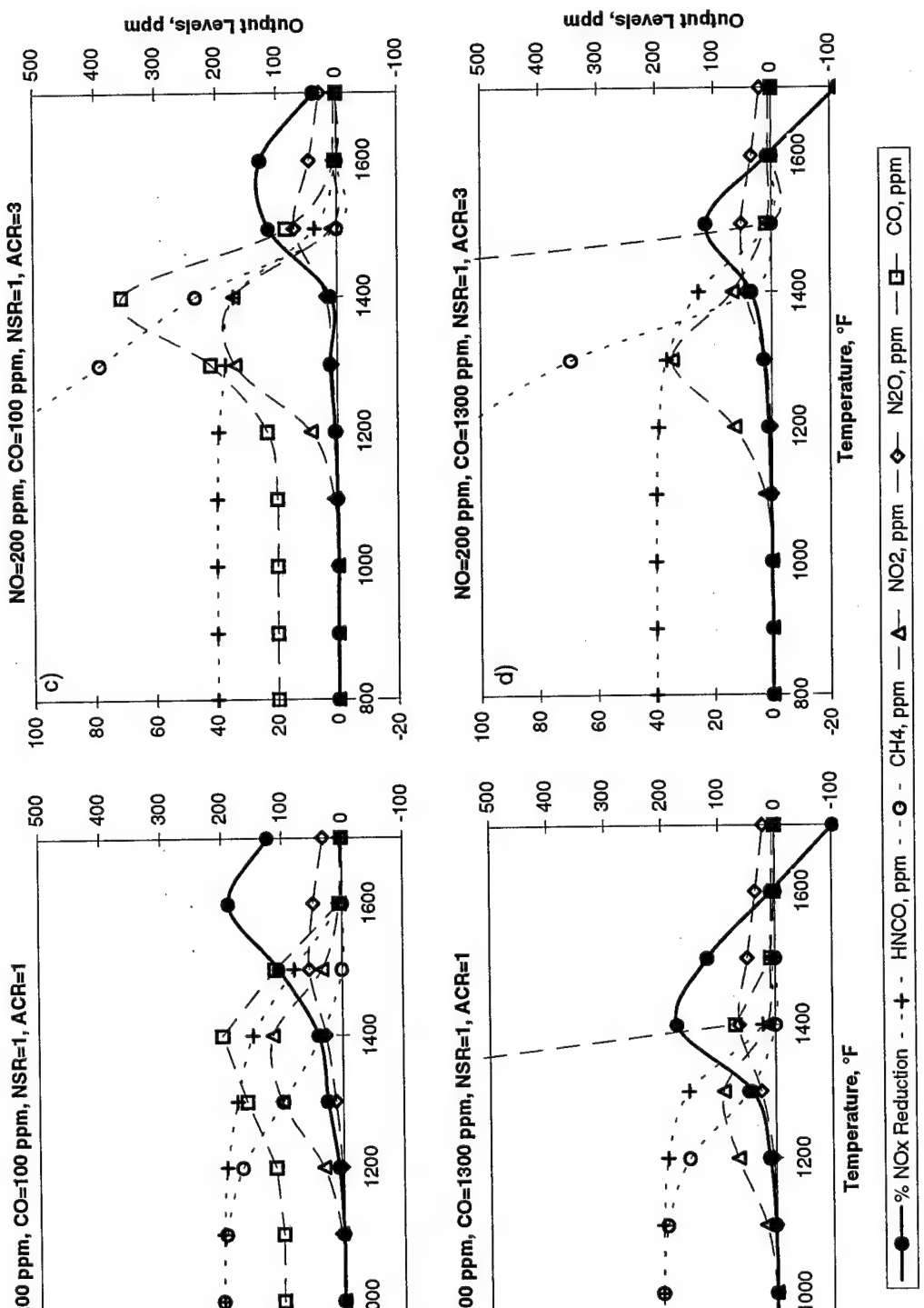

Figure E-31: Chemkin Modeling Results using Cyanuric Acid with Methane Additive.

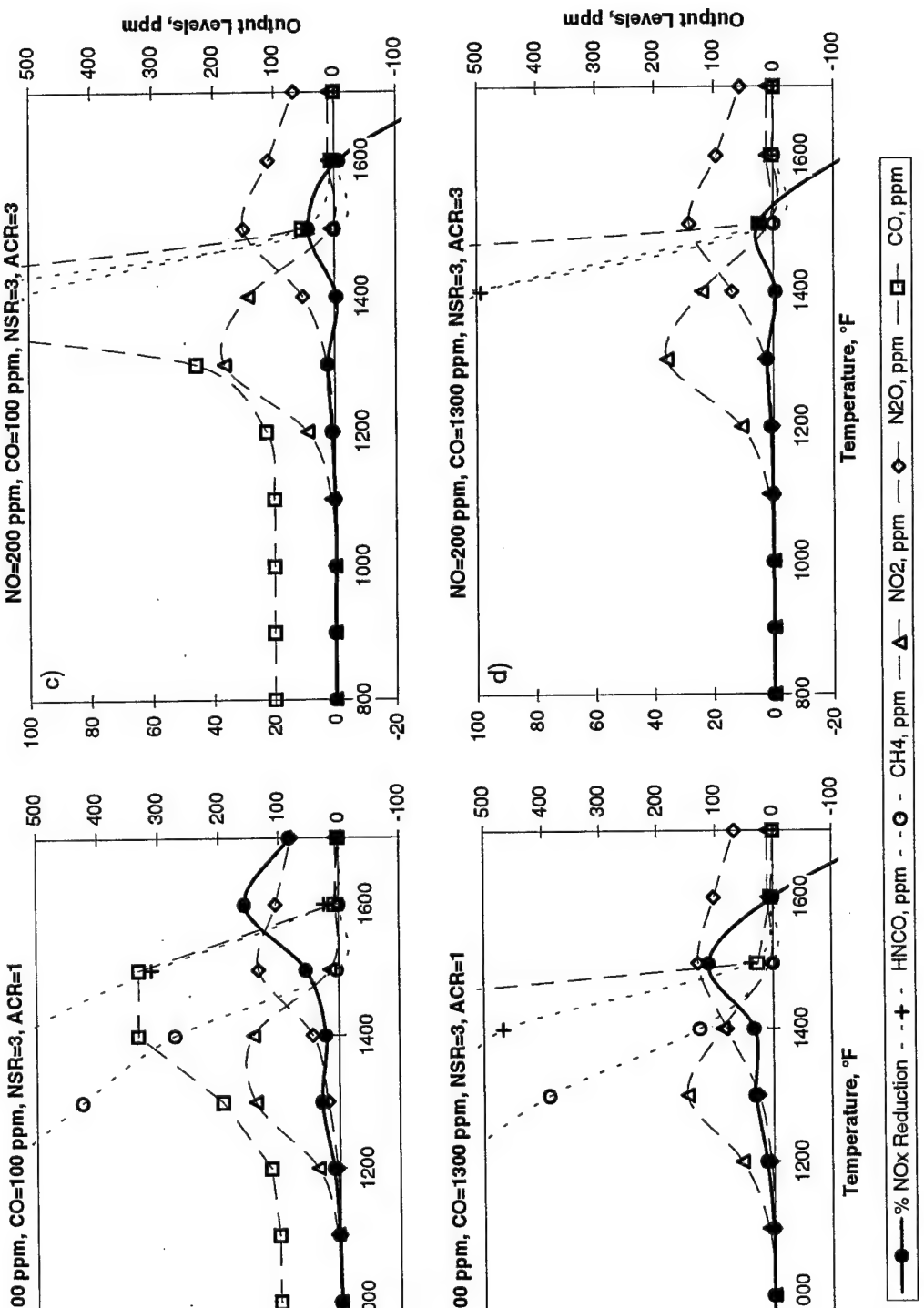

Figure E-32: Chemkin Modeling Results using Cyanuric Acid with Methane Additive.

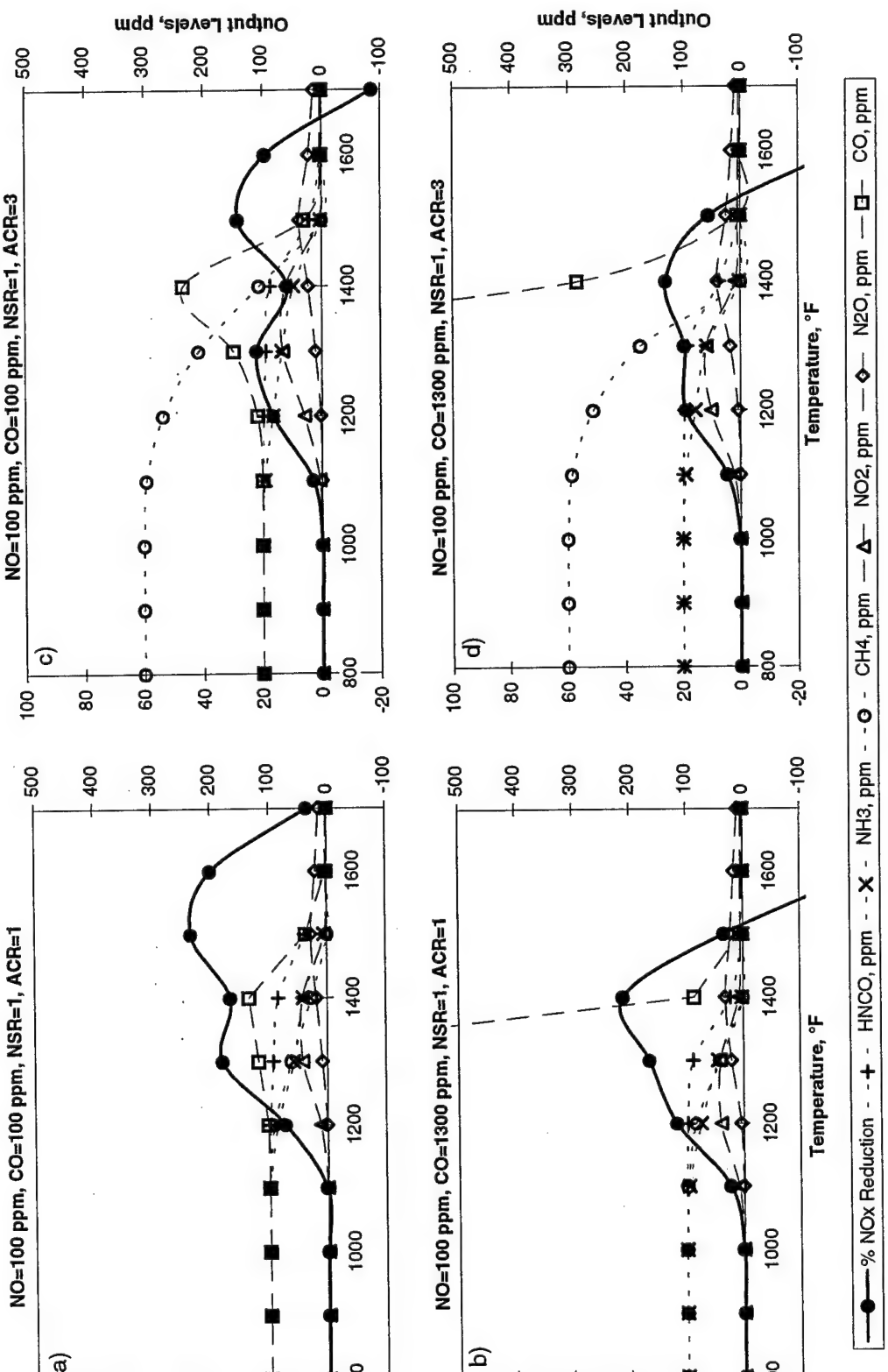

Figure E-33: Chemkin Modeling Results using Urea with Methane Additive.

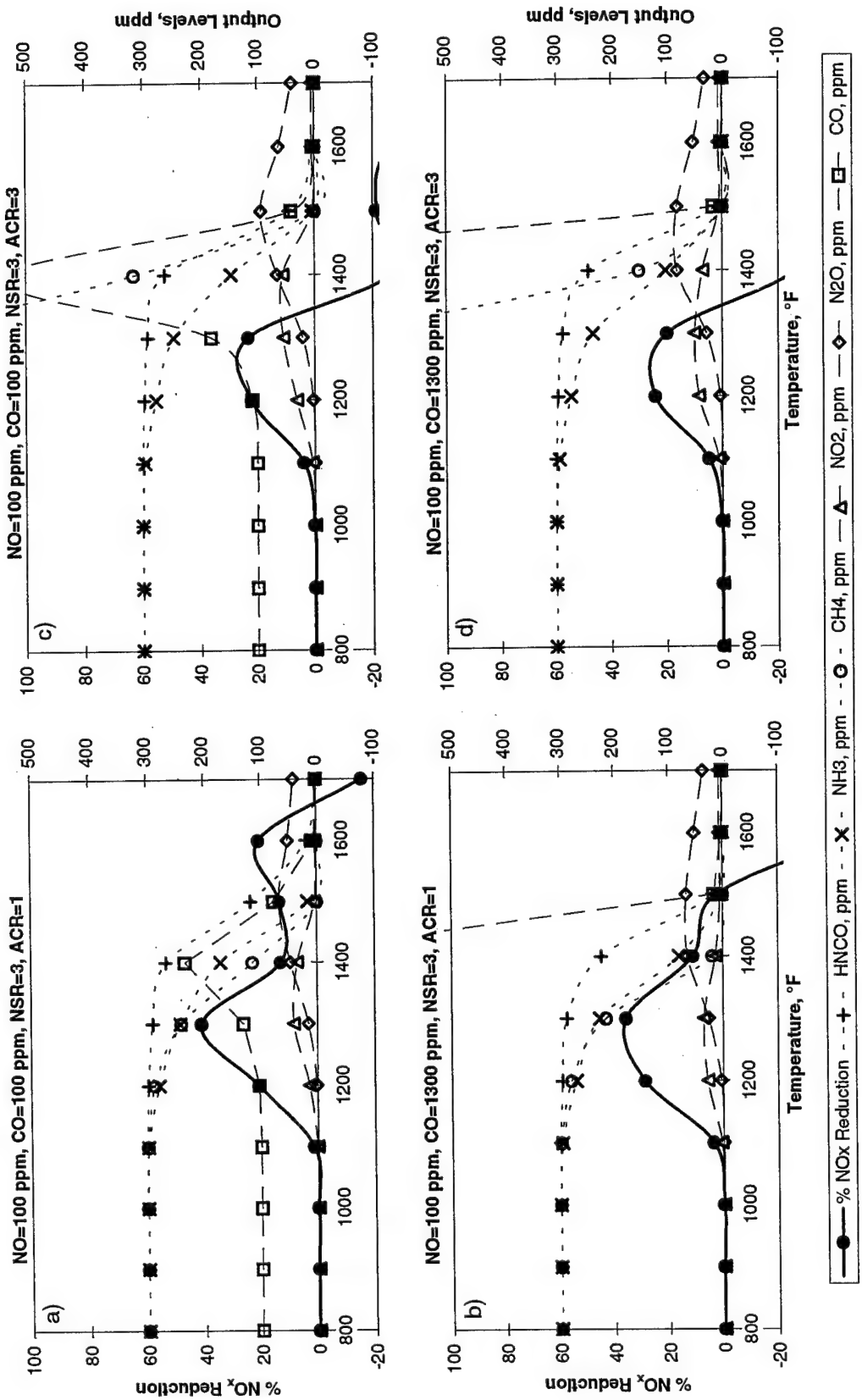

Figure E-34: Chemkin Modeling Results using Urea with Methane Additive.

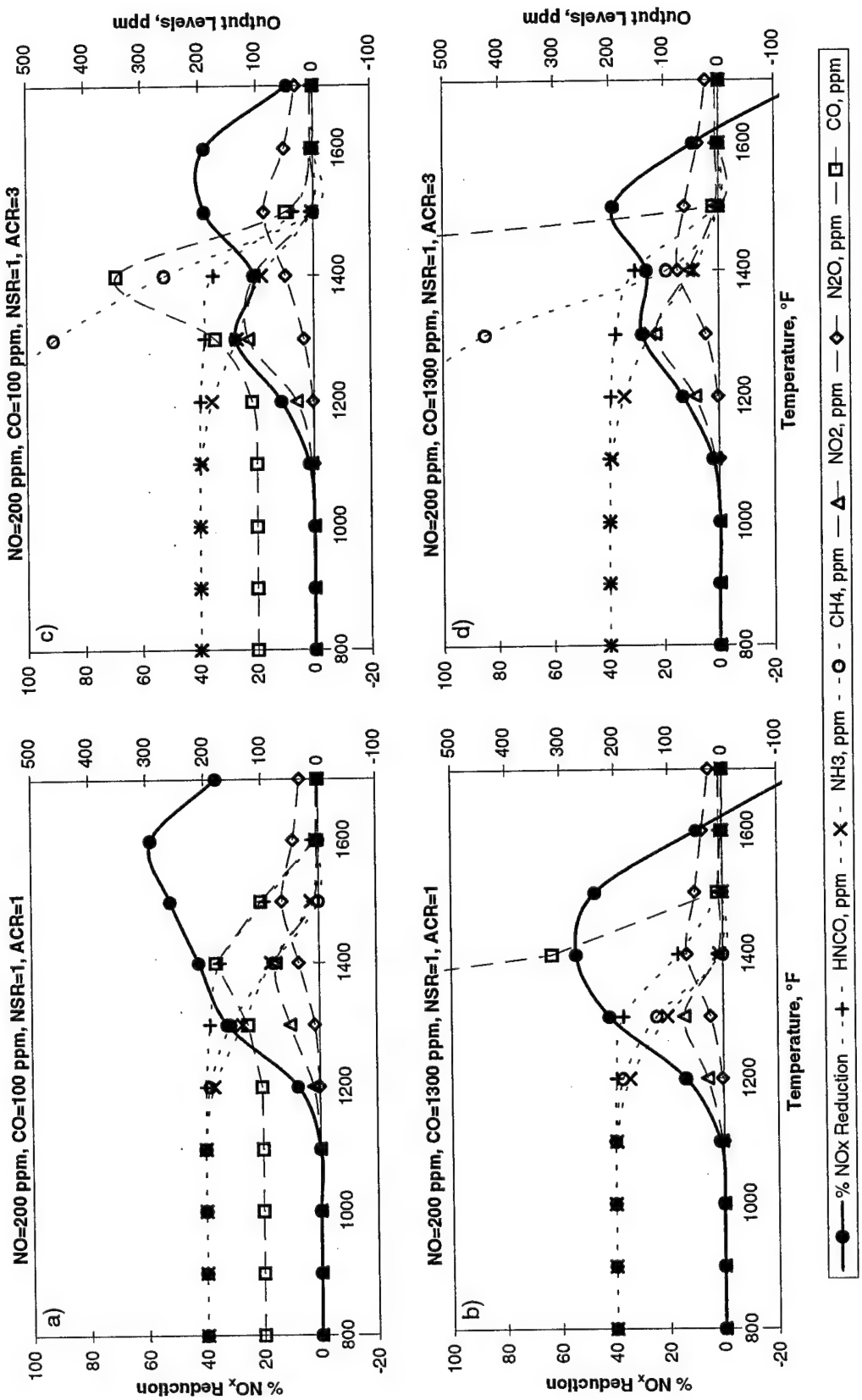

Figure E-35: Chemkin Modeling Results using Urea with Methane Additive.

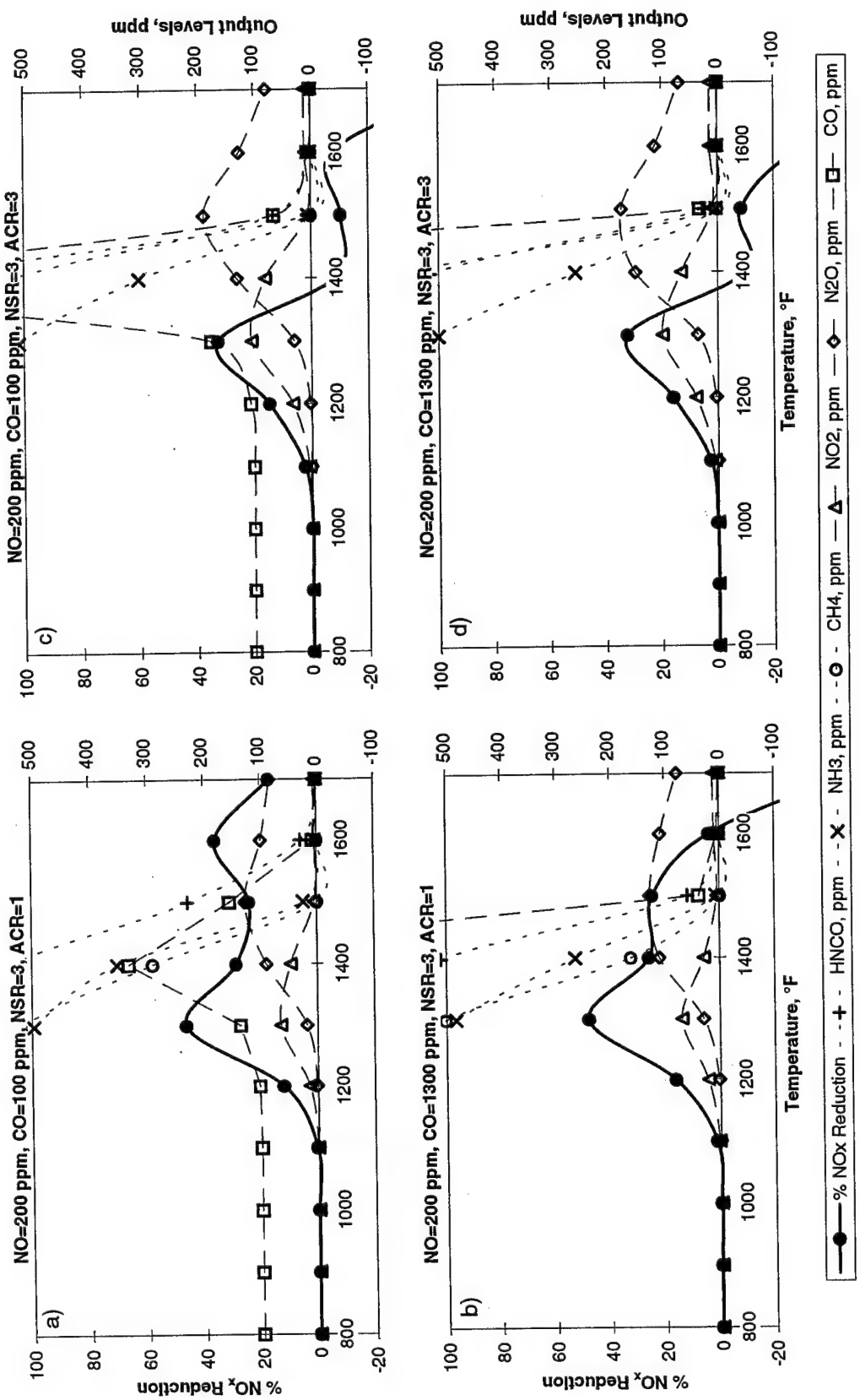

Figure E-36: Chemkin Modeling Results using Urea with Methane Additive.

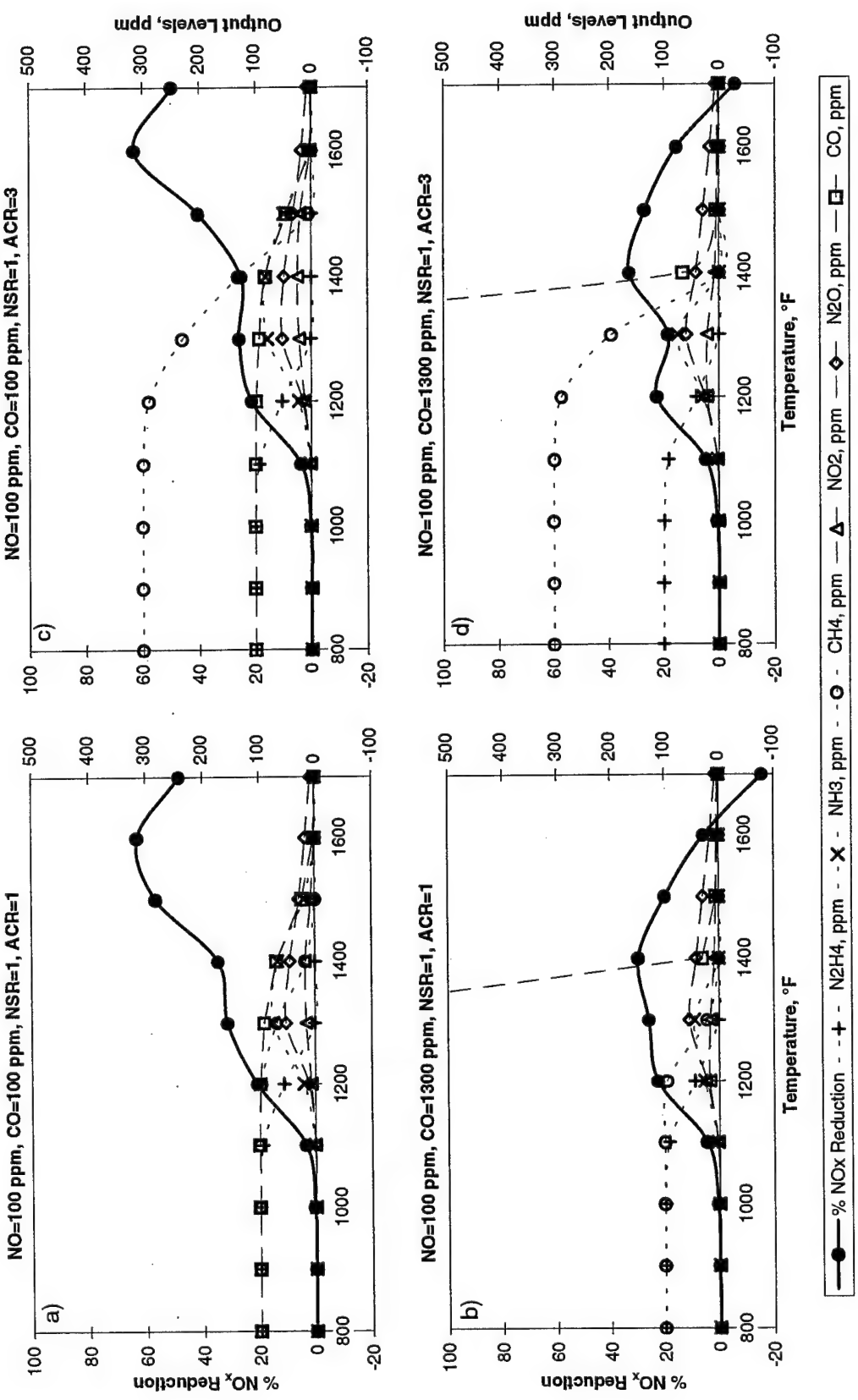

Figure E-37: Chemkin Modeling Results using Hydrazine with Methane Additive.

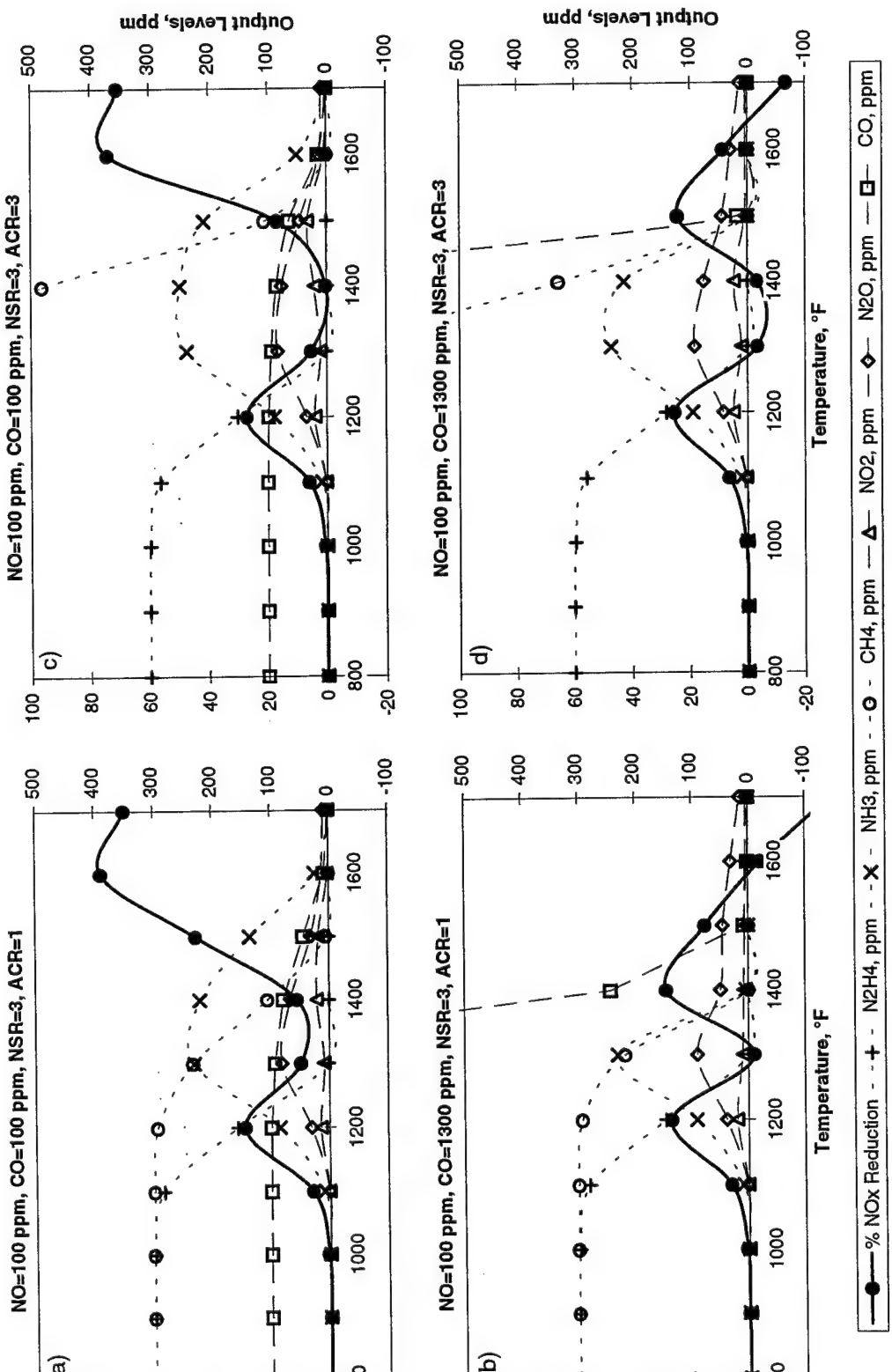

Figure E-38: Chemkin Modeling Results using Hydrazine with Methane Additive.

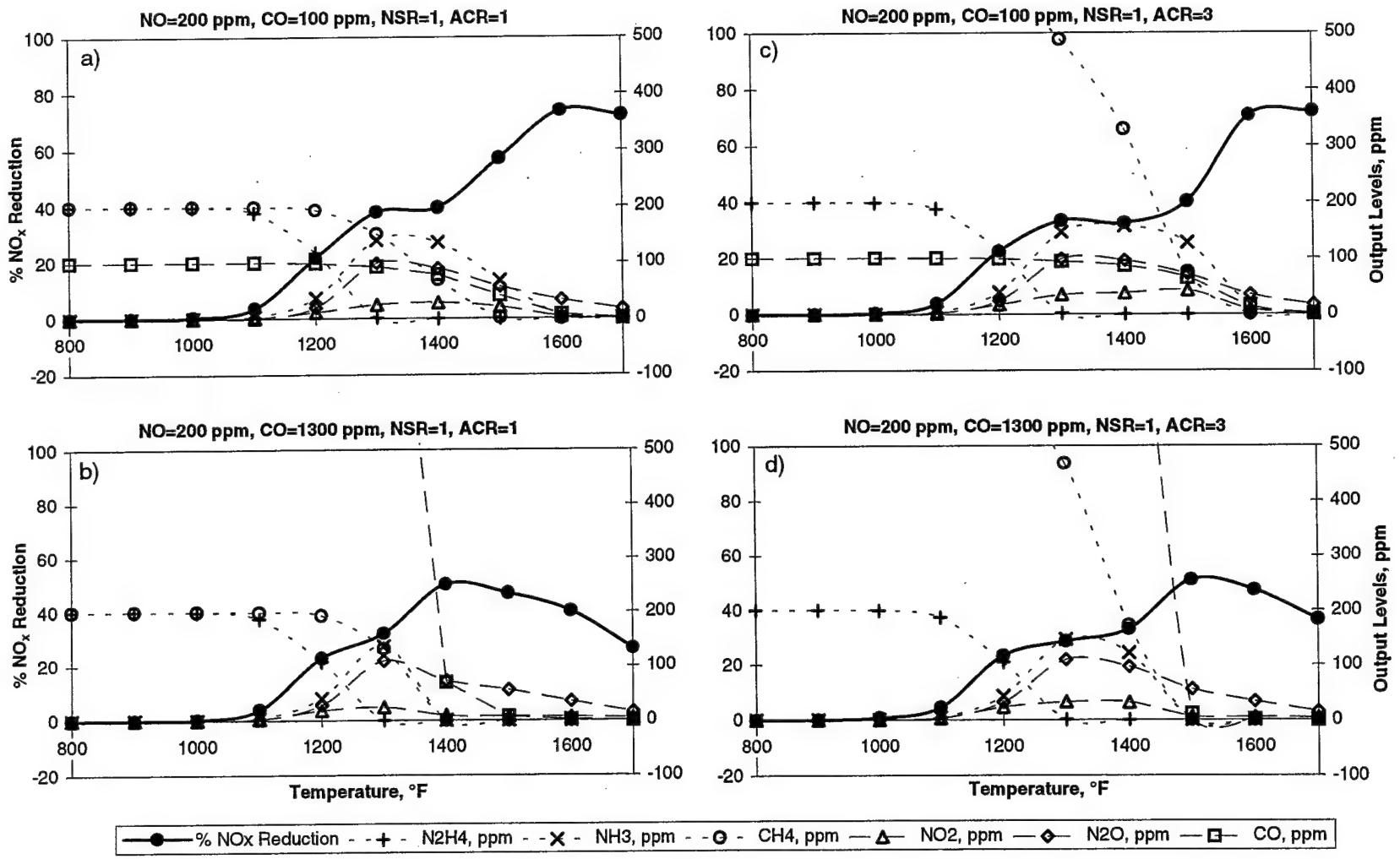

Figure E-39: Chemkin Modeling Results using Hydrazine with Methane Additive.

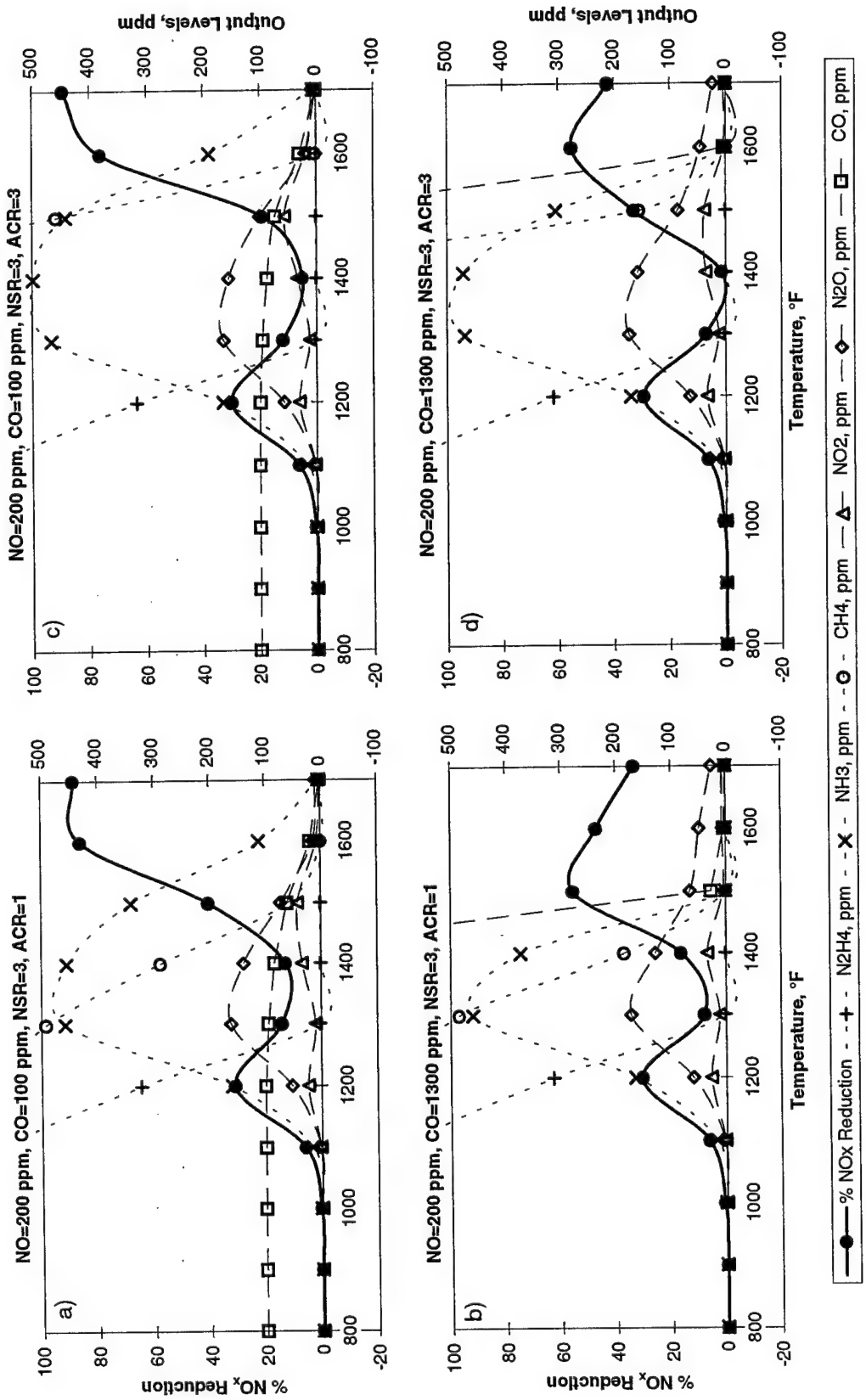

Figure E-40: Chemkin Modeling Results using Hydrazine with Methane Additive.

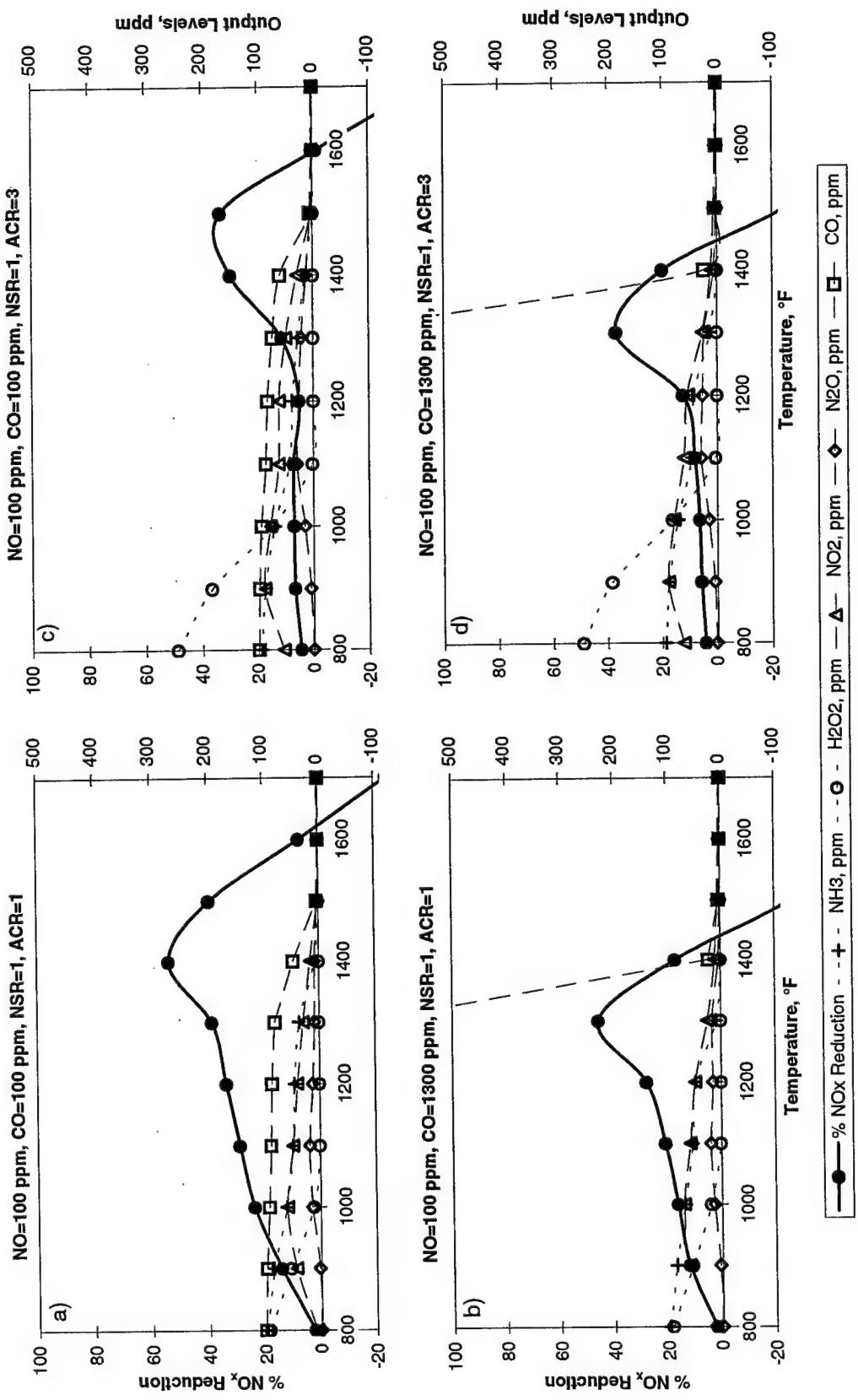

Figure E-41: Chemkin Modeling Results using Ammonia with Hydrogen Peroxide Additive.

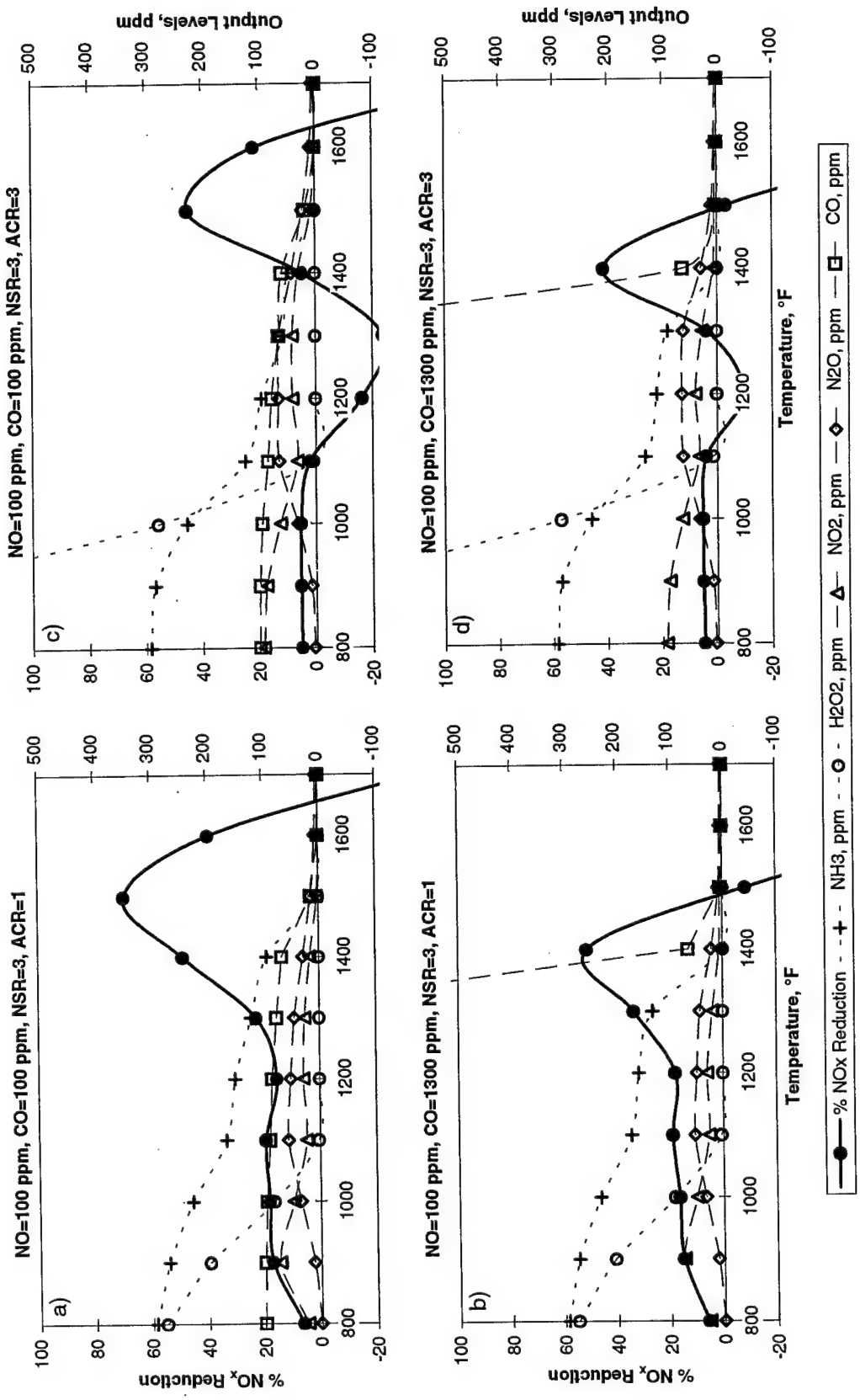

Figure E-42: Chemkin Modeling Results using Ammonia with Hydrogen Peroxide Additive.

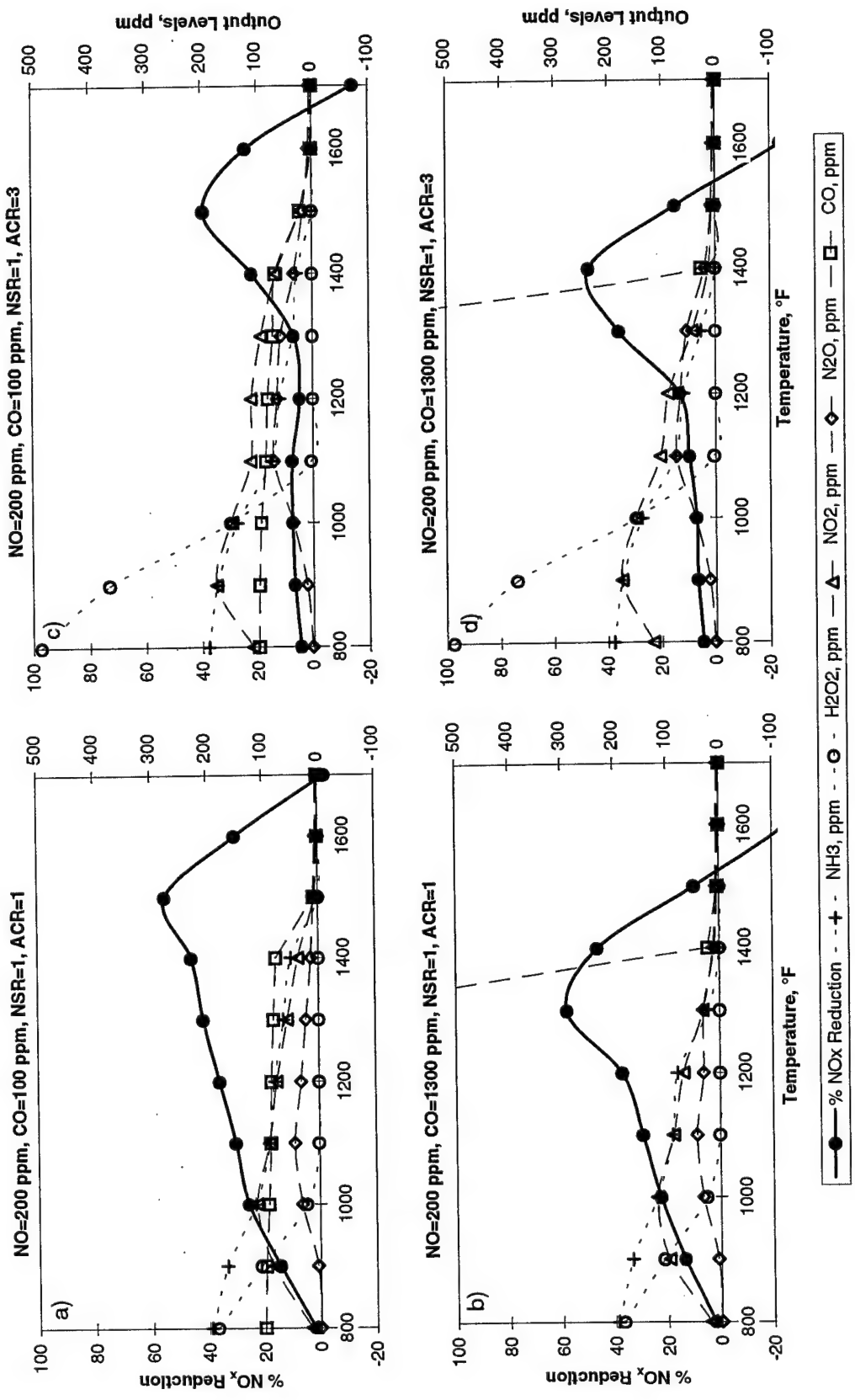

Figure E-43: Chemkin Modeling Results using Ammonia with Hydrogen Peroxide Additive.

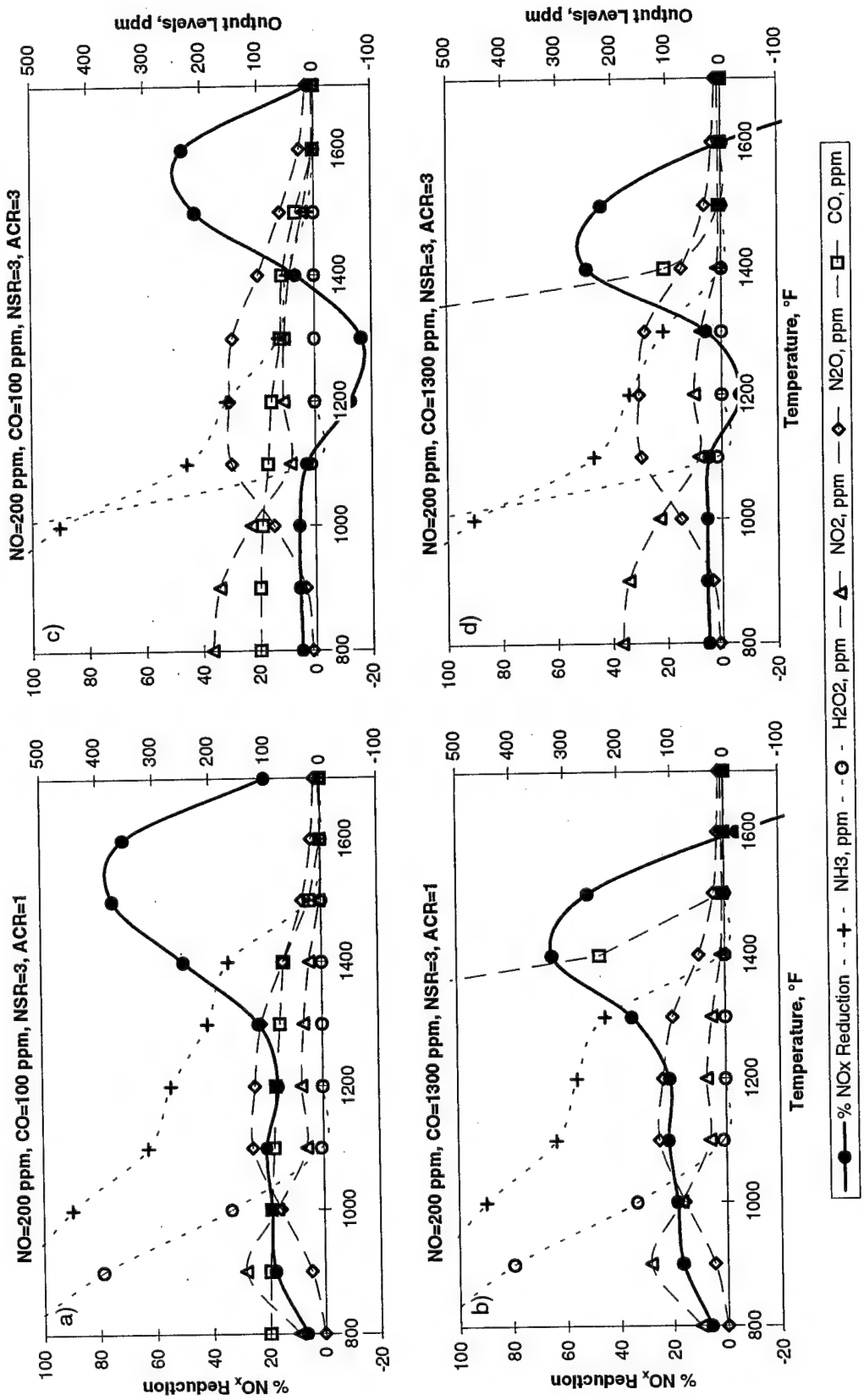

Figure E-44: Chemkin Modeling Results using Ammonia with Hydrogen Peroxide Additive.

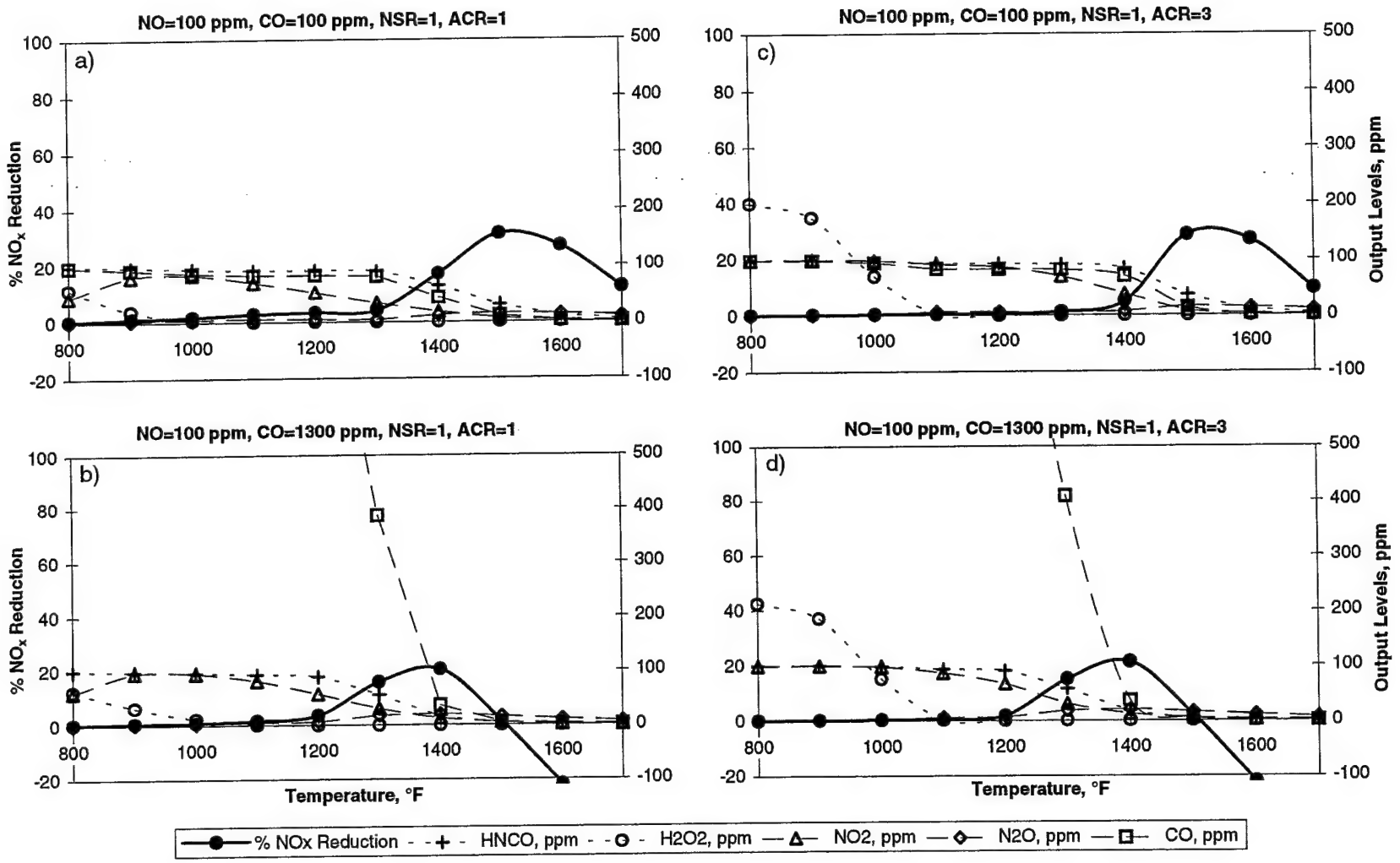

Figure E-45: Chemkin Modeling Results using Cyanuric Acid with Hydrogen Peroxide Additive.

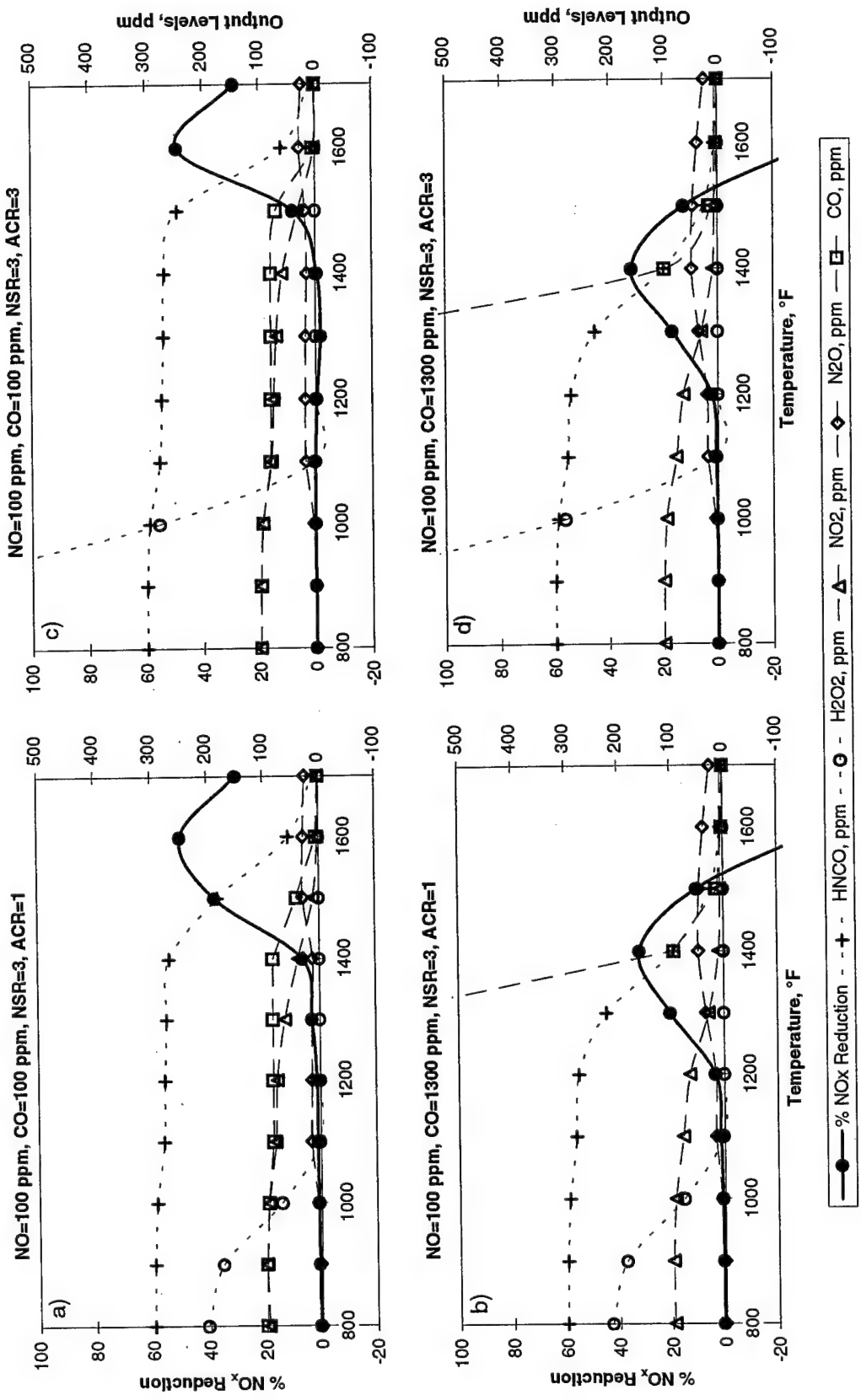

Figure E-46: Chemkin Modeling Results using Cyanuric Acid with Hydrogen Peroxide Additive.

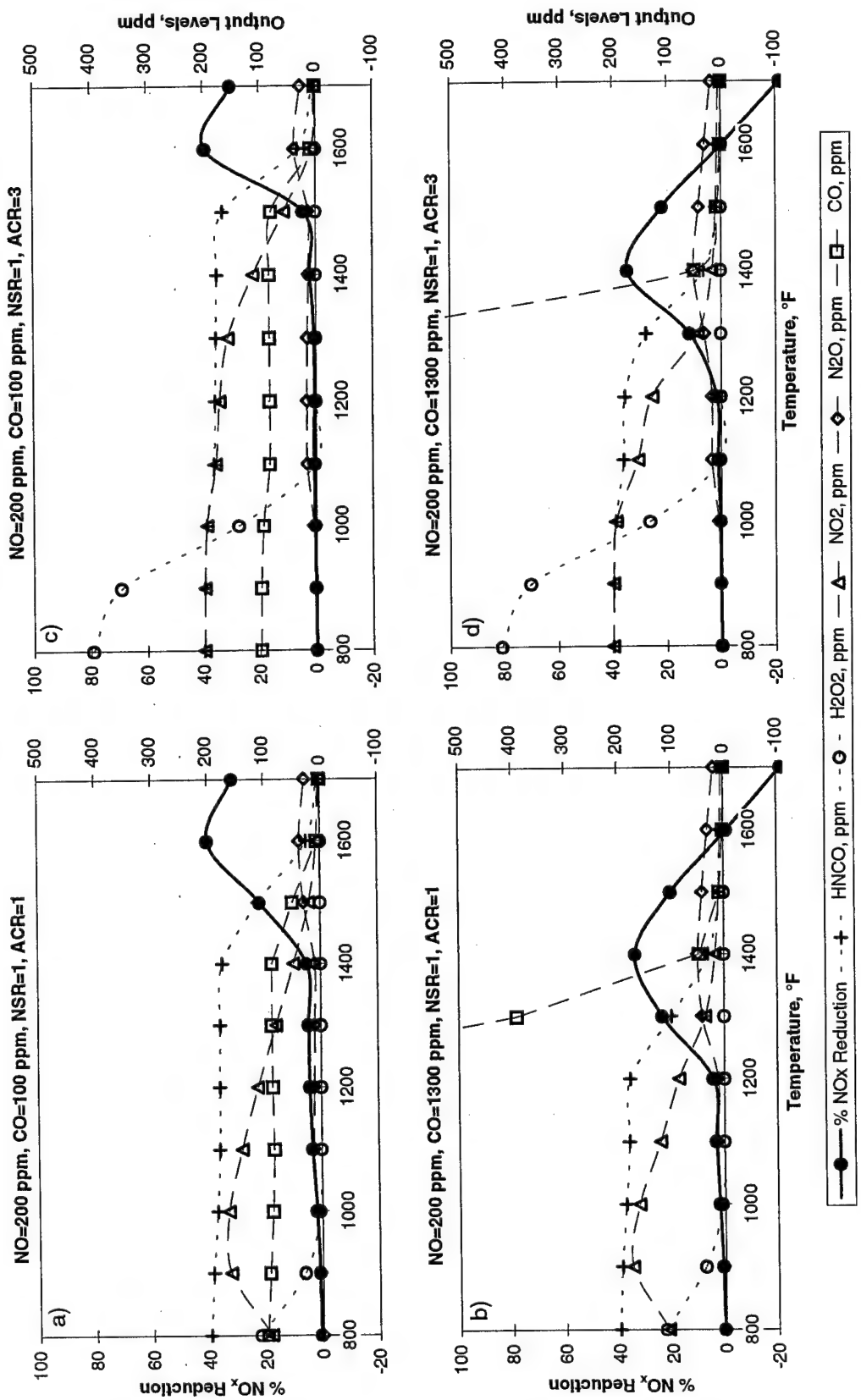

Figure E-47: Chemkin Modeling Results using Cyanuric Acid with Hydrogen Peroxide Additive.

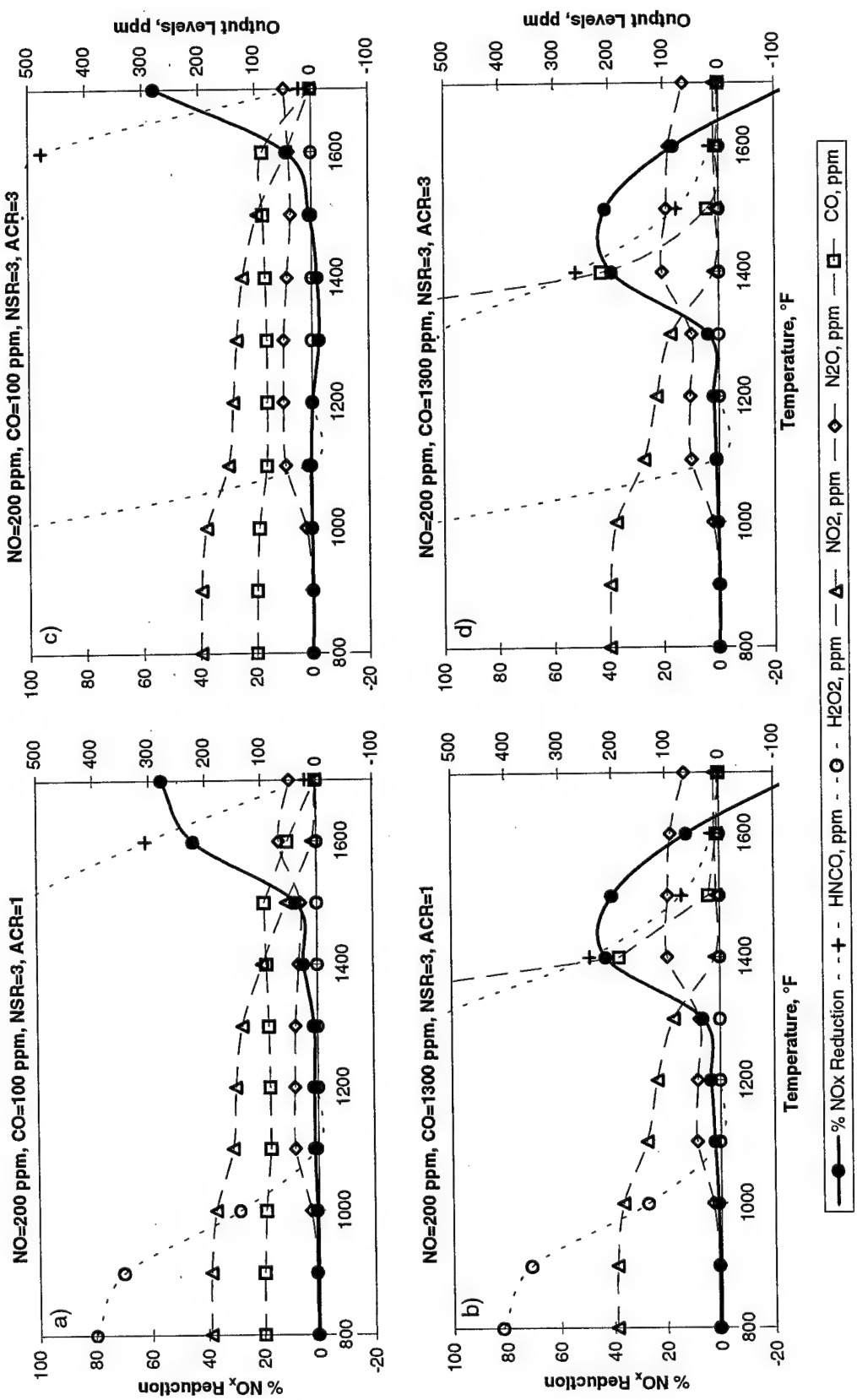

Figure E-48: Chemkin Modeling Results using Cyanuric Acid with Hydrogen Peroxide Additive.

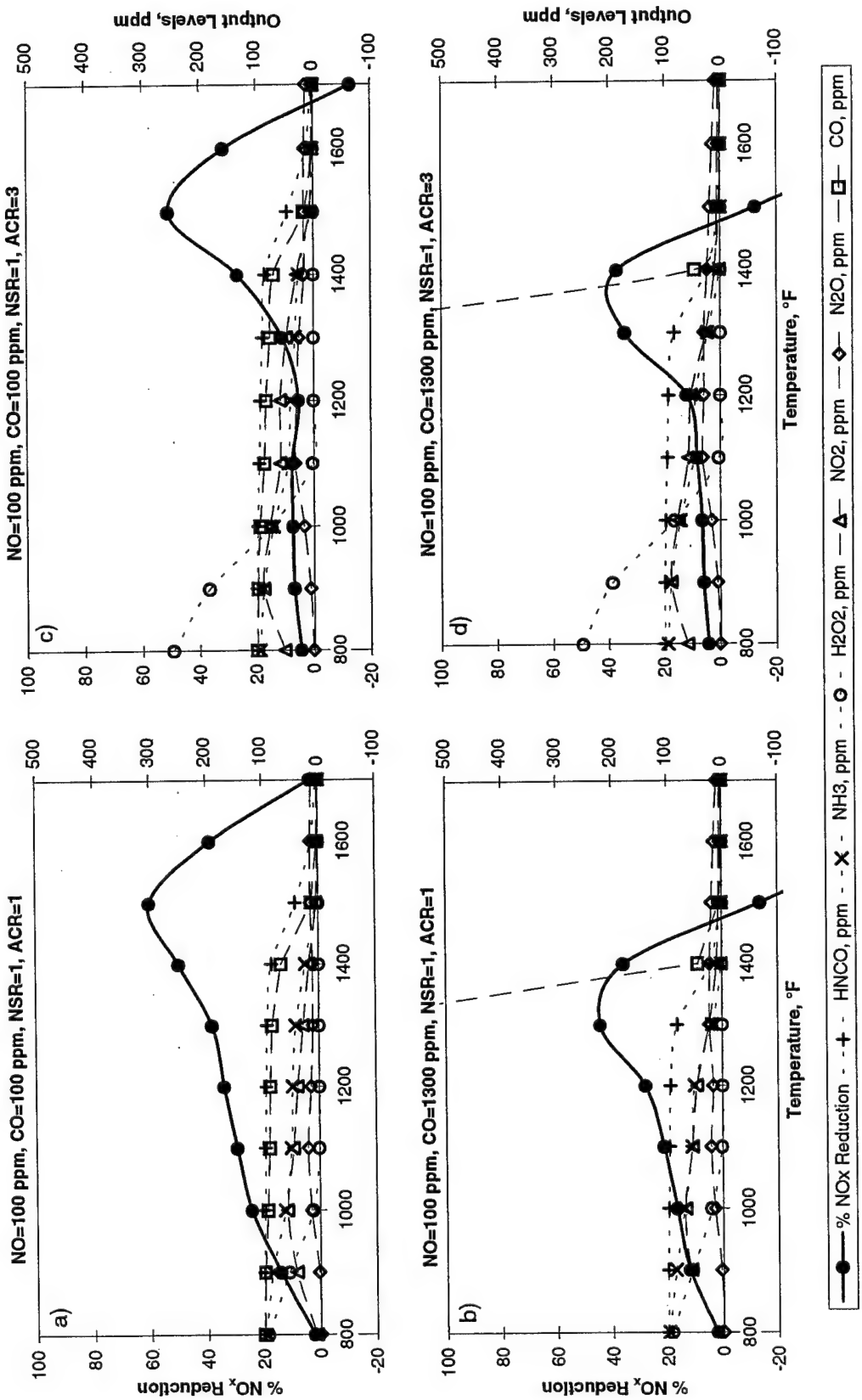

Figure E-49: Chemkin Modeling Results using Urea with Hydrogen Peroxide Additive.

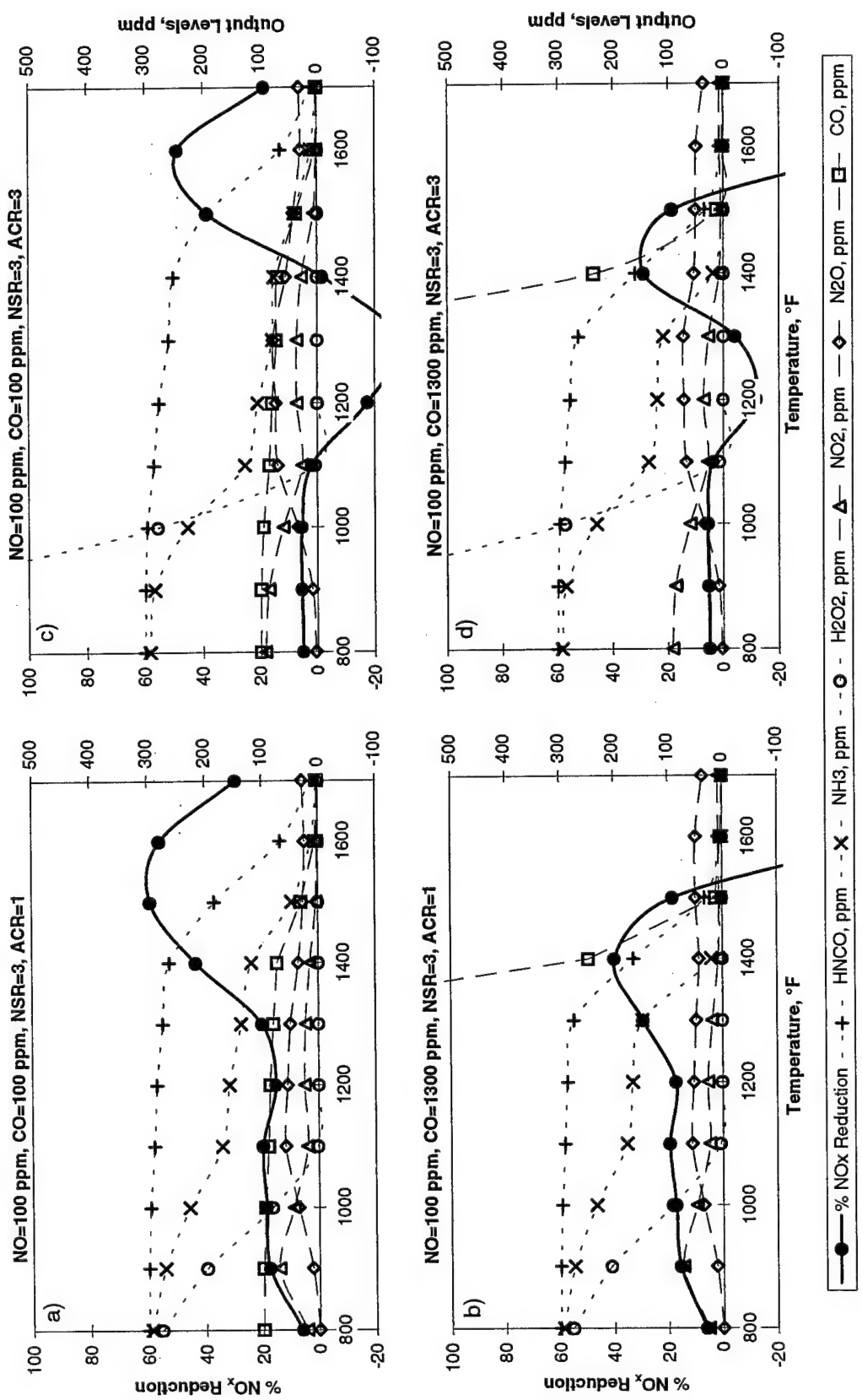

Figure E-50: Chemkin Modeling Results using Urea with Hydrogen Peroxide Additive.

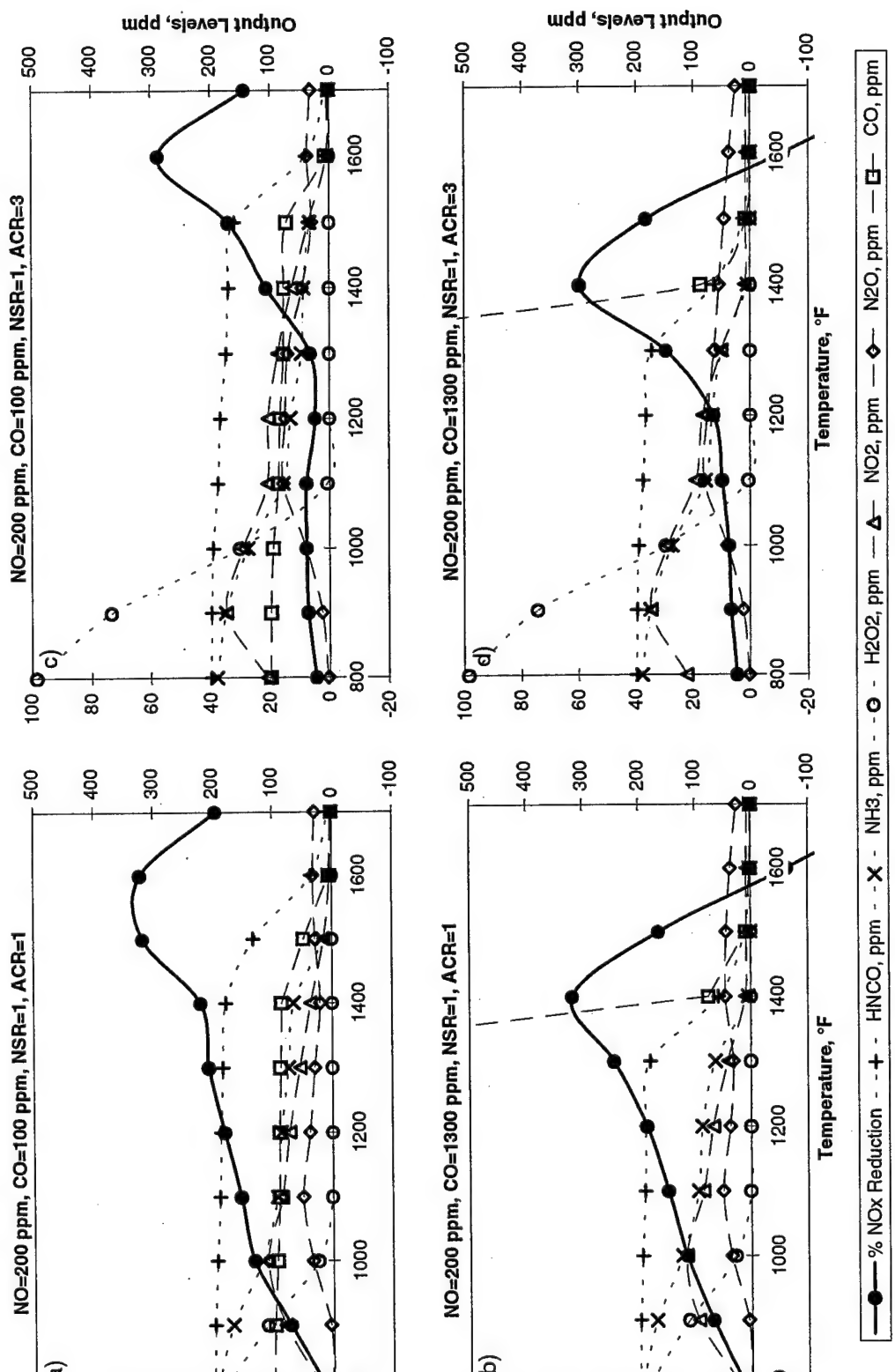

Figure E-51: Chemkin Modeling Results using Urea with Hydrogen Peroxide Additive.

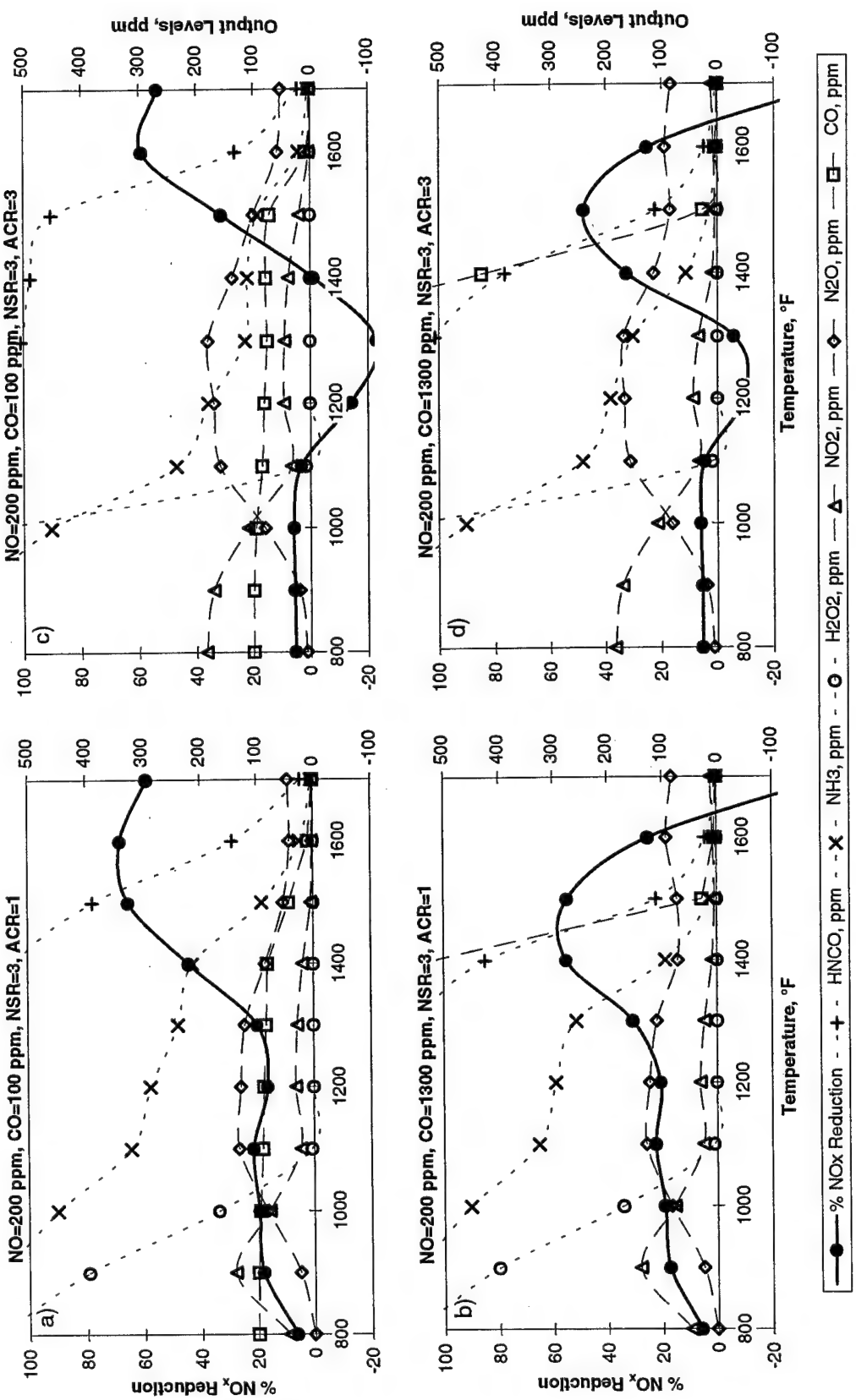

Figure E-52: Chemkin Modeling Results using Urea with Hydrogen Peroxide Additive.

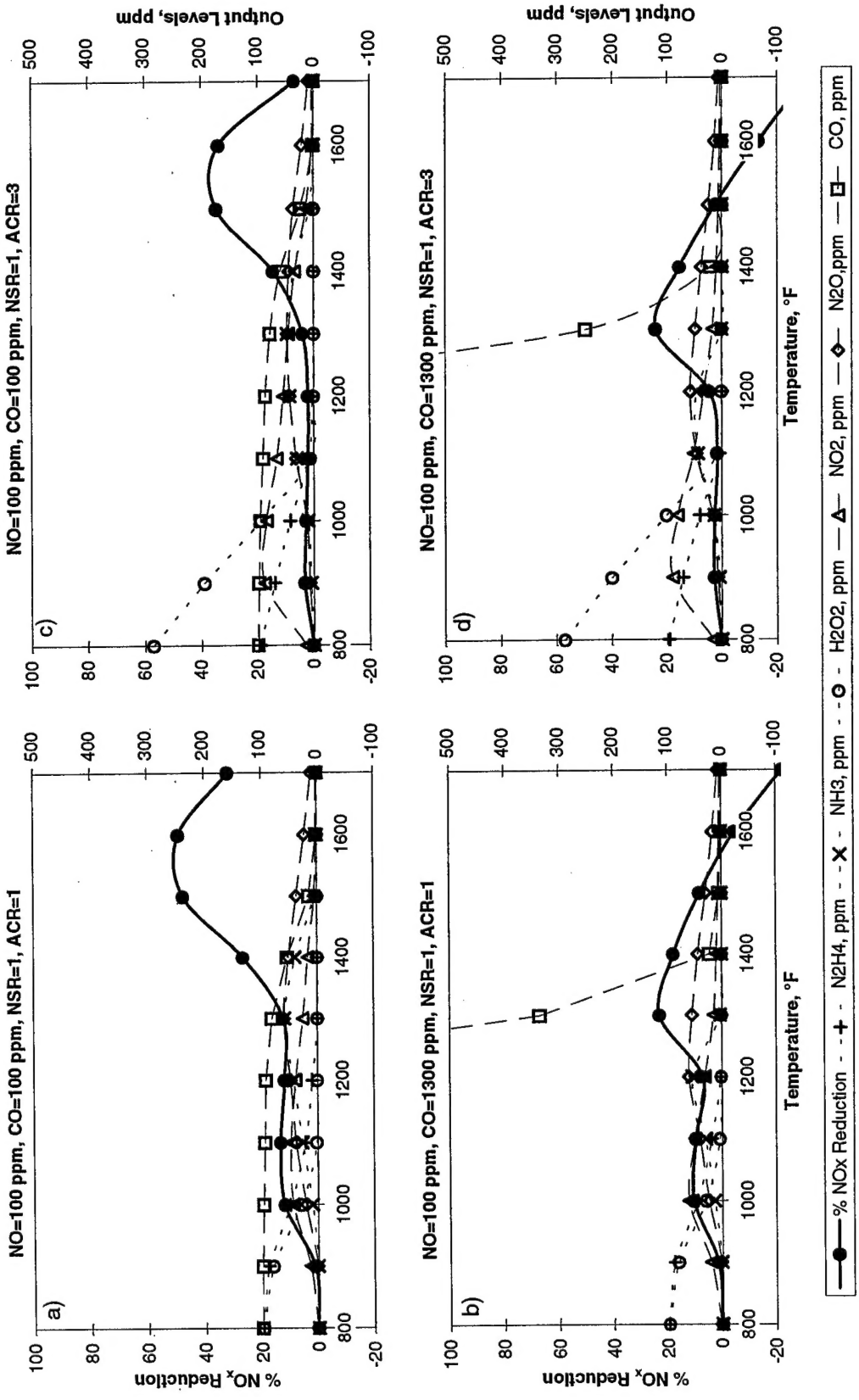

Figure E-53: Chemkin Modeling Results using Hydrazine with Hydrogen Peroxide Additive.

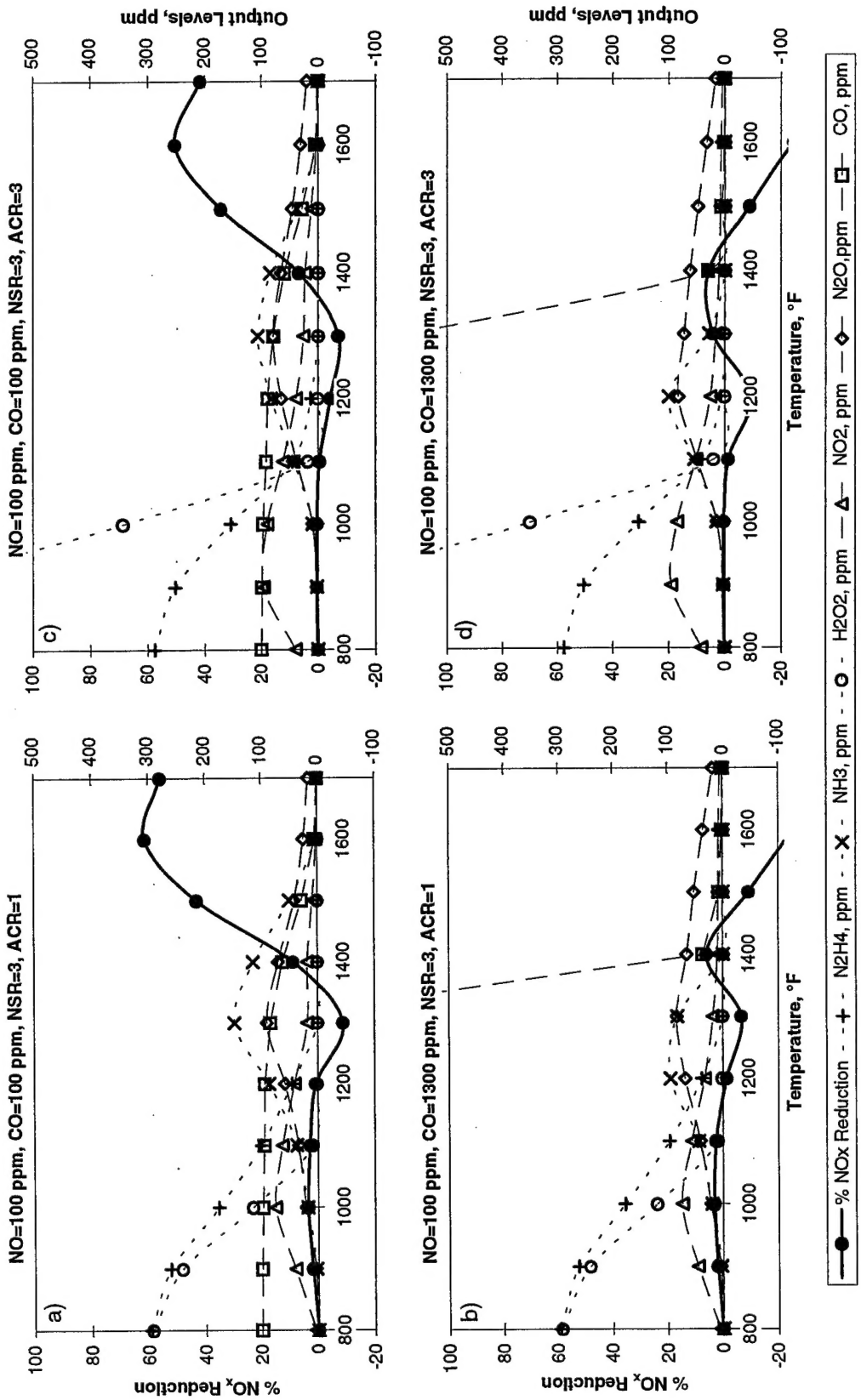

Figure E-54: Chemkin Modeling Results using Hydrazine with Hydrogen Peroxide Additive.

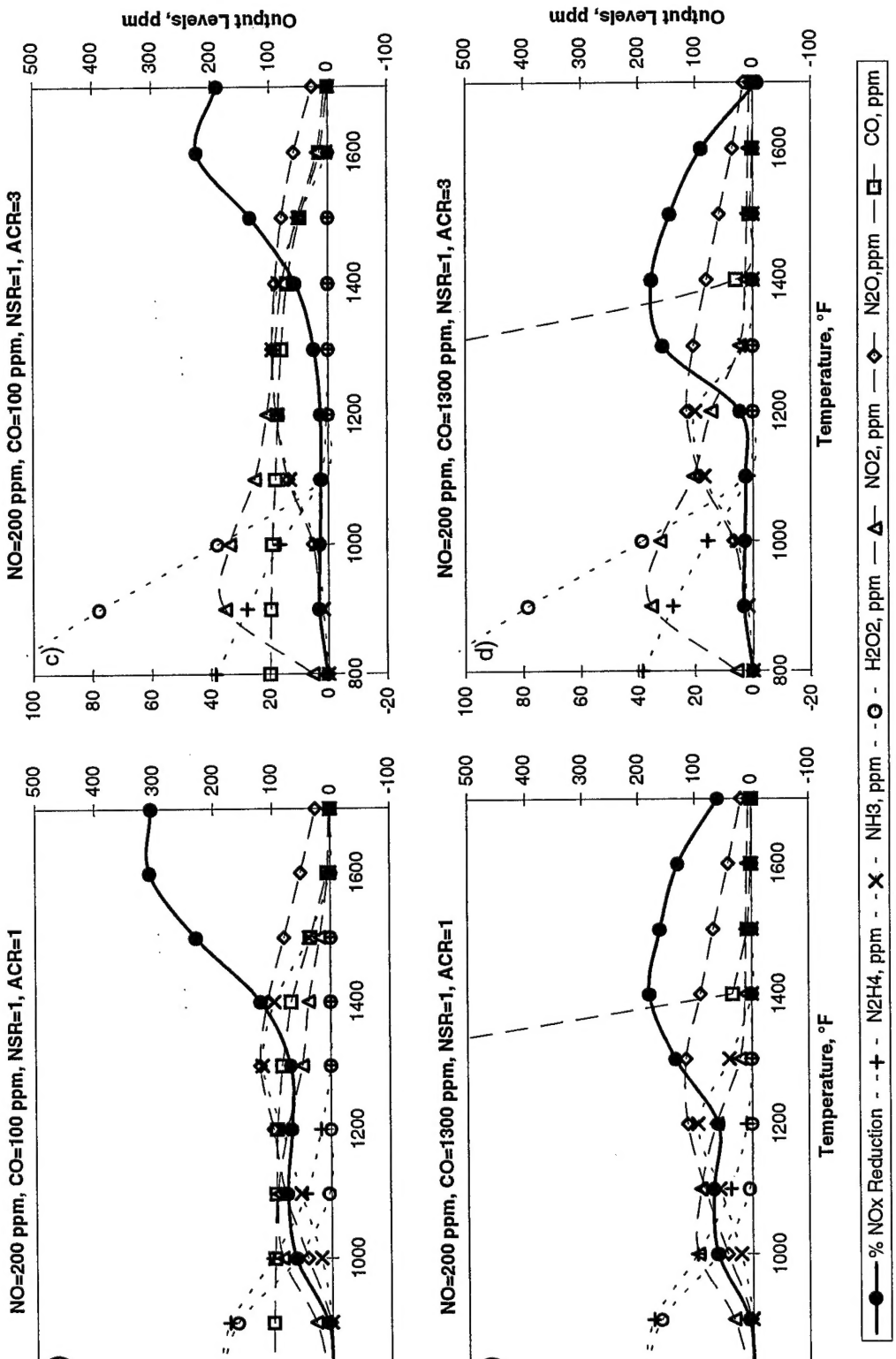

Figure E-55: Chemkin Modeling Results using Hydrazine with Hydrogen Peroxide Additive.

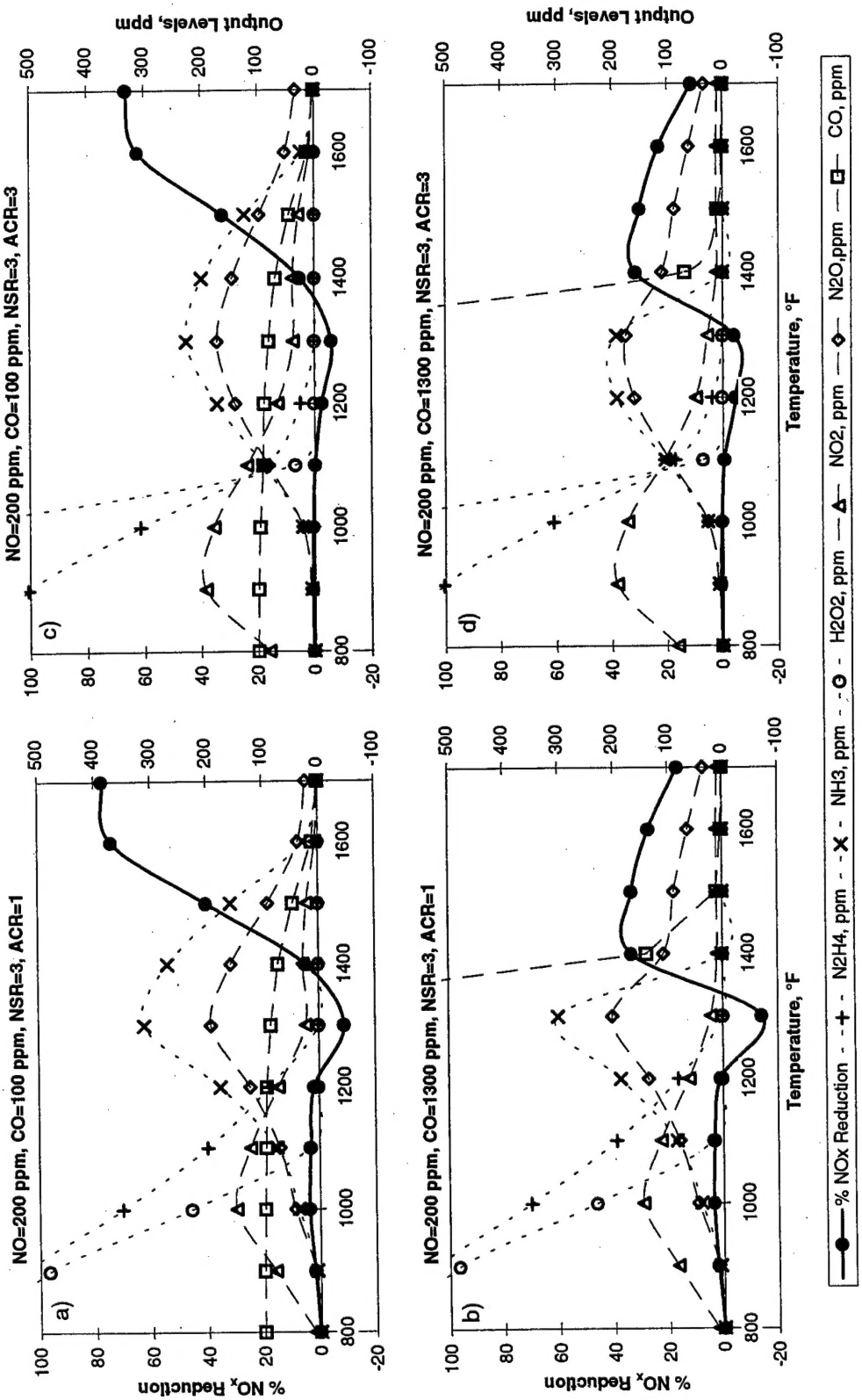

Figure E-56: Chemkin Modeling Results using Hydrazine with Hydrogen Peroxide Additive.